

Palaeoenvironmental Reconstruction and Geoarchaeology of the Cuatro Ciénegas Basin, NE Mexico, from the Late Pleistocene to the Present

Nicholas James Felstead

**A thesis submitted in partial fulfilment of the requirements of
Liverpool John Moores University for the degree of
Doctor of Philosophy**

**This research was carried out in collaboration with the NERC Isotope Geoscience
Laboratory, Keyworth, Nottinghamshire**

April 2012

UNIVERSITY HAVE REQUESTED THE FOLLOWING ITEMS TO BE REDACTED

FIG 1.2 P7

FIG 1.3 P8

FIG 2.1 P14

FIG 2.2 P15

FIG2.3 p19

FIG 2.4 P20

FIG 2.5 P21

FIG 2.7 P22

FIG 2.9 P26

FIG 2.36 P76

FIG 2.37 P77

FIG 3.4 P87

FIG 4.1A P123

FIG 4.4 P128

FIG 4.5 P129

FIG 4.12 P143

FIG 5.2 P148

FIG 6.1 P221

**THESIS
CONTAINS
CD/DVD**

"We'll fall off that bridge when we come to it"

Professor Alan Turner

Abstract

With over 200 pools, lakes and rivers supporting over 70 species of endemic flora and fauna, the Cuatro Ciénegas Basin, Coahuila, NE Mexico is an extremely important and extensively studied area in terms of conservation. The palaeoenvironment, however, is relatively understudied with only two reconstructions published to date – Meyer [1973] and Minckley and Jackson [2008]. This project has analysed a 15 m carbonate sediment core for multi-proxy palaeoenvironmental information and combined this with stable isotope, modern hydrological and geoarchaeological information in the Cuatro Ciénegas Basin.

This study has analysed water samples from 26 of the >200 pools, lakes and rivers in the Cuatro Ciénegas Basin suggesting an evaporative through-flow system, buffered by groundwater reservoirs. Analysis of stable $\delta^{18}\text{O}_{\text{CARB}}$, $\delta^{13}\text{C}_{\text{DIC}}$ and $\delta^{13}\text{C}_{\text{ORGANIC}}$ isotopes as well as pollen analysis, ^{14}C AMS and U-series dating techniques has allowed a chronologically well constrained palaeoenvironmental reconstruction of the Cuatro Ciénegas Basin. The results of this study suggest the Cuatro Ciénegas Basin contains palaeoenvironmental information spanning at least the Late Pleistocene (~85 ka BP) to the present and has undergone extensive environmental and climatic change, controlled by stadial-interstadial cycles. Data analysed in this study suggest that stadial conditions are climatically wetter, increasing the presence of temperate vegetation types and moisture availability from groundwater discharge. Interstadial conditions are climatically variable, punctuated by high variability in groundwater discharge and increased presence of arid vegetation species.

This study reports a new *in situ* human footprint trackway, combining the use of stable isotopes and U-series dating, placing the footprint locality at 7.24 ka BP during a climatically wetter period of the Holocene (Unit 7). The results of this study suggest the importance of temperate vegetation types e.g. *Carya* during this wetter period of the Holocene. The presence of nut and seed bearing vegetation would have provided sustenance to the Coahuilan Indians and also emphasises the importance of a groundwater reservoir in this arid region of northern Mexico, effectively buffering the hydrological system in climatically variable interstadial conditions

Acknowledgements

Firstly, I would like to thank NERC for their funding and support of my travel to Mexico to conduct field work for my project. The NERC steering committee, without whom I would not have had the support to conduct the isotope and U-series work within this thesis, are also thanked. Thanks also goes to LJMU who have assisted my work by providing funds, when needed, and access to rooms and laboratories from which to conduct my research work.

I would like to thank my project supervisors Prof. Silvia Gonzalez, Dr. Jason Kirby and Prof. Melanie Leng for their continued support and guidance, not only during the field work phase of my project but also during laboratory work, discussion, writing up and every other aspect of the work. Prof. David Huddart is particularly thanked for his continued support and pestering throughout all aspects of my project, despite not being part of my supervisory team. Special thanks to Dr. Steve Noble and Dr. Neil Boulton for making me feel welcome at NIGL and for their help and guidance in thin section analysis, sample preparation and dating analysis during the U-series procedure. LJMU academic staff, in particular, Dr. Julien Louys, Dr. Hannah O'Regan, Dr. Siobhan Power and Dave Williams, are thanked having helped me numerous times throughout my studies, providing informal discussions and sanity that has improved my work no end. Dr. Tom Minckley from the University of Wyoming, United States is thanked for the pollen analysis conducted on the sediment core and his unsurpassed knowledge of the Cuatro Ciénegas Basin that has assisted me throughout the process of writing this thesis. Prof. Sarah Metcalfe from Nottingham University, UK is thanked for her assistance during field work in Mexico and for her knowledge of isotopes in water and helping with the analysis and discussion of water samples from Cuatro Ciénegas. Dr. Dean Hendrickson and his son, Jacob, are also thanked for their knowledge and discussions regarding all aspects of the Cuatro Ciénegas Basin.

A special mention must go to Prof. Alan Turner (1947-2012) who sadly passed away in January 2012, following a short period of ill health. I was fortunate enough to have shared a laboratory with Alan for four years of my research and, I must say, it was pleasure. It is sad that he will never know how much his help, advice, good nature and humour has influenced my life and he will be sadly missed.

I have been fortunate enough to have visited the Cuatro Ciénegas Basin on four occasions, none of which would have been possible without permission from the APFFCC (Área de Protección de la Flora y Fauna Cuatro Ciénegas). Ivo Garcia Gutierrez is particularly thanked for providing permits and access to field sites within the Cuatro Ciénegas Basin. Cuatro Ciénegas archaeologists Leticia Gonzalez and Antonio Reyes, INAH, are both thanked for their assistance in explaining the locations and significance of archaeological finds in the basin and also John Seebach from Sul Ross State University, United States with whom discussions on human occupation in N. America were vital.

I would like to especially thank my family for their continued support, both financially and motivationally, over the past four years. Without them I would not have been able to begin, and then pursue my research.

Finally, to my girlfriend Clara McGillan and best friend Bryony Vierke, both of whom have always supported me with my research and kept me sane in my most troubled moments. Thank you.

Statement of originality

All field work, sample collection, laboratory work, data analysis, data interpretation and discussion, tables, images and figures were conducted and/or produced by Nicholas Felstead unless otherwise stated within this thesis. Below is a statement of co-workers and their individual contributions towards the research conducted within this thesis.

The NERC Isotope Geosciences Laboratory (NIGL) conducted all mass spectrometric analysis of samples (water and carbonates) for stable isotopic studies within this thesis. The NIGL produced all the raw isotopic data which was then forwarded to myself for analysis and interpretation.

Dr. Thomas Minckley (University of Wyoming, USA) assisted me during the four weeks field work in March 2008. During the field work Dr. Minckley helped with core logging, sediment description and sediment sampling, and was responsible for laboratory analysis and identification of pollen, and raw pollen data production used in chapter 5.

Prof. Sarah Metcalfe (University of Nottingham, UK) was present in the field for one week during the field work in March 2008. Prof. Metcalfe assisted in the identification and sampling of water bodies for isotopic analysis. The NERC Isotope Geosciences Laboratory (NIGL) prepared and analysed water samples and produced the raw data used in chapter 2.

Dr. Steve Noble (NERC Isotope Geosciences Laboratory, UK) produced the U-series dates used in chapters 4 and 5. Dr. Noble conducted all U-series dating laboratory preparation and analysis (with assistance in sample preparation from myself), and produced raw data used in chapters 4 and 5.

Dr. Bruce Albert (Durham University, UK) conducted laboratory analysis and identification of pollen from tufa carbonates used in chapter 4. Dr. Albert also produced raw pollen data used in chapter 4.

Dr. Gilbert Price (The University of Queensland) produced the two U-series dates used in chapter 3. Dr. Price provided the preliminary dates used in the chapter although no raw data was provided.

Preface

To achieve the aim of this research, extensive collection of raw data was necessary. Field work was carried out in the Cuatro Ciéneas Basin (CCB) over a four week period in March 2008. The main focus during the first field work season was to collect two lake sediment cores; this was conducted in conjunction with the *Technología en Control de Suelos y Concreto, S. A. de C. V.* drilling company. In total, seven days were spent collecting core samples including drilling, sedimentary analysis, sample identification and sub-sampling. The remaining three weeks involved detailed geomorphological mapping and observations of carbonate formations, including the sampling of an *in situ* human footprint trackway for carbonate characterisation, stable isotopic and U-series dating analysis. Sampling of a large (10 m) perched terrace was also carried out and involved the use of professional climbing apparatus to obtain the samples. All the work conducted in the CCB was carried out in close collaboration with the *Área de Protección de la Flora y Fauna Cuatro Ciéneas (APFFCC)* who allowed access to all areas of the CCB, also facilitating the collection of 26 water samples from springs, pools, rivers etc. within the basin. Whilst collecting water samples the opportunity was taken to sample modern flora and fauna for stable isotopic characterisation to assist in planned dietary reconstructions on human samples. Additional field work seasons were conducted in January 2009 and 2010, for three and two weeks respectively. Further geomorphological observations and measurements were conducted during these trips with additional help from Level 3 Geology and Physical Geography students at LMU.

Unfortunately, because of permit restrictions from INAH (*Instituto Nacional de Antropología e Historia*), collection and sampling of archaeological artefacts as well as sampling of human remains, both bone and hair, was not possible. These restrictions have limited the discussion and conclusions of this thesis in relation to the material culture and dietary patterns of the Coahuilan Indians. Human hair samples were obtained from the Peabody Museum of Archaeology and Ethnology, Cambridge, USA but because of the limited sample size, the results obtained only provided a basis for future research rather than expanding current knowledge. Problems experienced during U-series dating of tufa samples also limited the chronological control of the palaeoenvironmental reconstruction of the CCB. Tufas had to be re-sampled because

of contamination of original samples and subsequent changes applied to the chemistry methodology of U-series analysis. A further 6 month setback to the dating of samples was encountered between May and November 2009, as a result of the failure of the mass spectrometer at NIGL, Keyworth, Nottinghamshire.

Contents	Page
Abstract	iii
Acknowledgements	iv
Statement of originality	vi
Preface	vii
Contents	ix
List of figures	xv
List of tables	xxxii
Chapter 1: Introduction	
1.1 Scientific background and justification	1
1.2 Project aim	4
1.3 Introduction to the Cuatro Ciénegas Basin study site	5
1.3.1 Pre-Quaternary geology of the Cuatro Ciénegas Basin	6
1.4 Chapter overview	9
1.4.1 Chapter 2: Reconnaissance isotope hydrology of the Cuatro Ciénegas Basin	10
Basin	
1.4.2 Chapter 3: Terrestrial carbonate environments of the Cuatro Ciénegas Basin	10
Basin	
1.4.3 Chapter 4: Human occupation in the CCB and the depositional context for the <i>in situ</i> human footprint trackway	10
1.4.4 Chapter 5: Multi-proxy palaeoenvironmental reconstruction of the Cuatro Ciénegas Basin	11

Chapter 2: Reconnaissance isotope hydrology of the Cuatro Ciénegas Basin

2.1 Introduction	12
2.1.1 Stable isotope geochemistry	13
2.1.1.1 Stable isotopes in arid-zone hydrology	14
2.1.2 Current topography and surface stream network	20
2.1.3 Hydrogeology of the Cuatro Ciénegas Basin	22
2.2 Methods	27
2.2.1 Water sampling strategy	27
2.2.2 $\delta^{18}\text{O}$ and δD method	32
2.2.3 Carbonate (Dissolved Inorganic Carbon) method	32
2.3 Results	33
2.3.1 Stable $\delta^{18}\text{O}$ and δD	33
2.3.1.1 Water body temperature vs. $\delta^{18}\text{O}$ and δD	41
2.3.2 $\delta^{18}\text{O}$ vs. $\delta^{13}\text{C}_{\text{DIC}}$ from water carbonate	47
2.4 Discussion	57
2.4.1 $\delta^{18}\text{O}$ vs. $\delta^{13}\text{C}_{\text{DIC}}$	57
2.4.2 $\delta^{18}\text{O}$ vs. δD	58
2.4.2.1 Independent system	61
2.4.2.2 Main through-flow system	62
2.4.2.3 Secondary through-flow system	66
2.4.3 Evaporation and brine evolution across the CCB	72
2.4.4 Modern human influence	75
2.5 Conclusions and future work	77

Chapter 3: Terrestrial carbonate environments of the Cuatro Ciénegas Basin

3.1 Introduction	80
3.1.1 Tufa and travertine formation	80
3.2 Calcium carbonate formation within the CCB	86
3.2.1 Rim-stone pool/dam complex	87
3.2.1.1 Study site	88
3.2.1.2 Preliminary research and methods	88
3.2.2 Perched terrace	93
3.2.2.1 Study site	94
3.2.2.2 Preliminary research and methods	97
3.3 Discussion	110
3.3.1 Calcium carbonate deposition within the modern hydrological system	110
3.3.2 Calcium carbonate deposition away from the modern hydrological system	113
3.3.2.1 Perched tufa terrace of fluvial, spring and paludal origin	113
3.3.2.2 Raised pluvial lake shoreline	116
3.3.3 Complexity of the CCB hydrology	117
3.4 Conclusions and future work	119

Chapter 4: Human occupation in the CCB and the depositional context for the

***in situ* human footprint trackway**

4.1 Introduction	122
4.1.1 Human occupation and the CCB cultural tradition	123
4.2 Study site	126
4.2.1 Tierra Blanca spring mound	127
4.3 Description of <i>in situ</i> human footprint trackway	128

4.4 Methods	131
4.4.1 Tufa sample description	131
4.4.2 U-series dating	131
4.4.3 Stable isotopes	132
4.4.4 Pollen	132
4.5 Results	133
4.5.1 U-series dating	133
4.5.2 $\delta^{13}\text{C}_{\text{DIC}}$ and $\delta^{18}\text{O}_{\text{CARB}}$ isotopes	134
4.5.3 Pollen	137
4.6 Discussion	138
4.6.1 Palaeoenvironment	138
4.6.2 Southward migration and activity of hunter-gatherers	141
4.7 Conclusions and future work	143

Chapter 5: Multi-proxy palaeoenvironmental reconstruction of the Cuatro

Ciénegas Basin

5.1 Introduction	146
5.1.1 Climate of the Cuatro Ciénegas Basin	146
5.2 Previous palaeoenvironmental studies	149
5.3 Stable isotopes in lacustrine and wetland sediments	152
5.3.1 Oxygen	152
5.3.2 Inorganic carbon	154
5.3.3 Carbon isotopes in organic matter	155
5.4 Study site	157
5.5 Laboratory methods	159

5.5.1 Stable $\delta^{18}\text{O}_{\text{CARB}}$, $\delta^{13}\text{C}_{\text{DIC}}$ and $\delta^{13}\text{C}_{\text{ORGANIC}}$ analysis	159
5.5.1.1 Organic and carbonate content by loss on ignition (LOI)	162
5.5.2 U-series dating	163
5.5.3 ^{14}C AMS dating	164
5.5.4 Pollen	164
5.6 Results	164
5.6.1 Core PTB chronology	165
5.6.1.1 Potential problems in age/depth modelling of core PTB	165
5.6.1.2 ^{14}C AMS and U-series dating	166
5.6.1.3 Linear interpolation	169
5.6.1.4 Smooth spline interpolation using 'classical' age modelling (CLAM)	173
5.6.2 Stable $\delta^{18}\text{O}_{\text{CARB}}$ and $\delta^{13}\text{C}_{\text{ORGANIC}}$ isotopes and stratigraphy	175
5.6.3 $\delta^{13}\text{C}_{\text{DIC}}$ vs. C/N ratio	188
5.6.4 $\delta^{13}\text{C}_{\text{ORGANIC}}$ vs. C/N ratios	191
5.6.5 $\delta^{18}\text{O}_{\text{CARB}}$ and $\delta^{13}\text{C}_{\text{DIC}}$ isotopic covariance	193
5.6.6 Pollen	195
5.7 Interpretation and discussion	200
5.7.1 Unit 1. $84,900 \pm 8,500 - 56,400 \pm 2,600$ cal yr BP	203
5.7.2 Unit 2. $56,400 \pm 2,600 - 54,300 \pm 2,500$ cal yr BP	205
5.7.3 Unit 3. $54,300 \pm 2,500 - 37,500 \pm 2,500$ cal yr BP	207
5.7.4 Unit 4. $37,500 \pm 2,500 - 31,200 \pm 2,200$ cal yr BP	208
5.7.5 Unit 5. $31,200 \pm 2,200 - 28,051 \pm 417$ cal yr BP	210
5.7.6 Unit 6. $28,051 \pm 417 - 12,200 \pm 400$ cal yr BP	211
5.7.7 Unit 7. $12,200 \pm 400$ cal yr BP - present	212

5.8 Regional and global climate change or environmental stability in the CCB?	213
5.9 Conclusions and future work	215
Chapter 6: Discussion	
6.1 Hydrology and palaeoenvironment of the Cuatro Ciénegas Basin	219
6.1.1 Climatically wet environments in the Cuatro Ciénegas Basin	221
6.1.2 Climatically variable environments in the Cuatro Ciénegas Basin	224
6.2 Terrestrial carbonate formation, hydrology and environment	227
6.3 Palaeoenvironment and archaeology	230
6.4 Regional and global controls of hydrology and endemism	234
Chapter 7: Conclusion	
7.1 Aims	236
7.2 Future work	239
7.3 Concluding remarks	240
References	242
Appendices (CD-ROM)	
Appendix 1	
1.1 Fissure ridge complex (PDF document)	
1.2 Perched tufa terrace log descriptions (PDF document)	
Appendix 2	
2.1 Core PTB Loss on Ignition (Excel spreadsheet)	

2.2 Core PTB description and stratigraphy

2.2.1 Core PTB stratigraphy (PDF document)

2.2.2 Full Core PTB stratigraphy with C/N ratios and LOI (.TIF Image)

List of Figures

Page

All images and figures within this thesis were produced by Nicholas Felstead unless otherwise stated.

Fig. 1.1 (a) Location of the Cuatro Ciénegas Basin within Mexico (b) Coahuila state borders the USA to the north, separated by the Rio Grande (c) Black line shows the limit of the CCB, the area enclosed has been declared a protected area [image from google.co.uk/earth]. 6

Fig. 1.2 Contemporary geological map of Mexico and southern USA. 7
TMVB-Trans Mexican Volanic Belt; CT-Cayman Transform; MzTT-Tehuantepec Transform; CAS-Collision Acretion Suture; C-CT-California-Coahuila Transform; CTT-Coahuila-Tamaulipas Transform; O-MS-Ouachita-Marathon Suture; Be-Belize; Cz-Cenozoic; Gu-Guatemala; Ho-Honduras; Mz-Mesozoic; Pz-Palaeozoic; Sa-El Salvador [modified after Dickinson and Lawton, 2001].

Fig. 1.3 Geological map of Cuatro Ciénegas showing the major limestone outcrops and CCB recharge zone [modified after Badino *et al.*, 2004; Rodriguez *et al.*, 2005]. 8

Fig. 2.1 Schematic model of the hydrological cycle and the major sinks and fluxes of water within it (100 units constitutes the marine sink) [modified after Gat, 1996]. 14

Fig. 2.2 Schematic model of the carbon cycle in lake water with the major sources of carbon and the effect of each source on $\delta^{13}\text{C}$ isotope value of the water [modified after Gat, 1996]. 15

- Fig. 2.3** Ranges of $\delta^{13}\text{C}$ values from natural compounds represented in lake water isotope values [modified after Clark and Fritz, 1997]. 19
- Fig. 2.4** Topography of the Cuatro Ciénegas Basin. Elevations of the major limestone outcrops and CCB recharge zone are shown [modified after Wolaver *et al.*, 2005]. 20
- Fig. 2.5** Topography of the Cuatro Ciénegas Basin with possible stream locations from the high peaks of the surrounding mountains. Black lines are roads and tracks. Blue lines are proposed water flow paths [modified after Wolaver *et al.*, 2005]. 21
- Fig. 2.6** Alluvial fan deposits at the base of the Sierra Madera, the northern most boundary of the CCB. Incised channels on the alluvial fan deposits suggest they are long standing features [image from www.google.co.uk/earth]. 22
- Fig. 2.7** Schematic of water inputs within the basin and flow within the carbonate strata [modified after Badino *et al.*, 2004 and Rodriguez *et al.*, 2005]. 22
- Fig. 2.8** Locations of the Bolson de Mapimi, CCB and Monterrey City in NE Mexico. The proposed hydrologic gradient of the Cupido-Aurora aquifer in the direction of the Gulf of Mexico can be seen [image from www.google.co.uk/earth]. 24

Fig. 2.9 Water body temperature map for the CCB. Greater densities of hot pools (25°C - 35°C) are located around the piedmont of the Sierra San Marcos y Pinos suggesting fault controls. Ambient pools (20°C - 25°C) cluster in a similar area to hot pools suggesting the possibility of mixing with colder pools. Ambient pools <20°C appear to cluster in areas with alluvial fan deposits (see Fig. 2.4 also). Circles represent the temperature of the pools sampled – larger circles represent higher temperatures. Overall map colours are a spatial representation of water temperatures on the CCB floor, based on data collected [modified after Minckley, 1969 and Evans, 2005]. 26

Fig. 2.10a Water isotope sample locations were separated into four areas (I, II, III and IV) within the Cuatro Ciénegas Basin. Sample codes are as follows: SM – San Marcos; PC – Poza Churince; LC – Laguna Churince; LG – Laguna Grande; B – Poza Becerra; G – Poza Garrabatal; 30-1 – Mex 30-1; JS – Poza Juan Santos; PS – Palm Spring; RP – Rim Pond; FS – Fast Stream; TB – Poza Tierra Blanca; YP – Yucca Pond; BS - Bone Site; 30-2 – Mex 30-2; A – Poza Anteojo; RM1 – Rio Mesquites; AzII – Poza Azul II; Az I – Poza Azul I; Az – Poza Azul; RM2 – Rio Mesquites 2; Q – Poza Quintero; P – Poza Pronatura; LH – Los Hundidos; LS – Las Salinas; CR – Charco Rojo 29

[image from www.google.co.uk/earth]. See also enlarged images from figures 2.9b to 2.9e.

Fig. 2.10b Enlarged map of location I (Fig. 2.10a). SM – San Marcos; PC – Poza Churince; LC – Laguna Churince; LG – Laguna Grande; B – Poza Becerra [image from www.google.co.uk/earth]. 30

Fig. 2.10c Enlarged map of location II (Fig. 2.10a). G – Poza Garrabatal; 30-1 – Mex 30-1; JS – Poza Juan Santos; PS – Palm Spring; RP – Rim Pond; FS – Fast Stream; TB – Poza Tierra Blanca; YP – Yucca Pond; BS - Bone Site; 30-2 – Mex 30-2; A – Poza Anteojo; RM1 – Rio Mesquites; AzII – Poza Azul II; Az I – Poza Azul I; Az – Poza Azul; RM2 – Rio Mesquites 2 [image from www.google.co.uk/earth]. 30

Fig. 2.10d Enlarged map of location III (Fig. 2.10a). Q – Poza Quintero; P – Poza Pronatura; LH – Los Hundidos [image from www.google.co.uk/earth].	31
Fig. 2.10e Enlarged map of location IV (Fig. 2.10a). LS – Las Salinas; CR – Charco Rojo [image from www.google.co.uk/earth].	31
Fig. 2.11 $\delta^{18}\text{O}$ vs. δD water isotope values within the Cuatro Ciénegas Basin for location I (Fig. 2.10b).	36
Fig. 2.12 $\delta^{18}\text{O}$ vs. δD water isotope values within the Cuatro Ciénegas Basin for location II (Fig. 2.10c).	37
Fig. 2.13 $\delta^{18}\text{O}$ vs. δD water isotope values within the Cuatro Ciénegas Basin for location III (Fig. 2.10d).	38
Fig. 2.14 $\delta^{18}\text{O}$ vs. δD water isotope values within the Cuatro Ciénegas Basin for location IV (Fig. 2.10e).	39
Fig. 2.15 $\delta^{18}\text{O}$ vs. δD water isotope values within the Cuatro Ciénegas Basin, plotted by location (Fig. 2.10a). The GMWL [Craig, 1961] and LMWL [Cortés <i>et al.</i> , 1997] are displayed with CCB residual water plotting to the right as a Local Evaporation Line (LEL) $\delta D = 4.4\delta^{18}\text{O} - 19.5$. The inset shows the main cluster of data points in more detail so map areas (I-IV) are more easily interpreted.	40
Fig. 2.16 $\delta^{18}\text{O}$ vs. δD water isotope values within the Cuatro Ciénegas Basin plotted by hot water body temperature (25°C - 35°C).	42
Fig. 2.17 $\delta^{18}\text{O}$ vs. δD water isotope values within the Cuatro Ciénegas Basin plotted by ambient water body temperature (20°C - 25°C).	43

Fig. 2.18 $\delta^{18}\text{O}$ vs. δD water isotope values , with high $\delta^{18}\text{O}$ value samples, within the Cuatro Ciénegas Basin plotted by ambient water body temperature (<20°C).	44
Fig. 2.19 $\delta^{18}\text{O}$ vs. δD water isotope values , without high $\delta^{18}\text{O}$ value samples, within the Cuatro Ciénegas Basin plotted by ambient water body temperature (<20°C).	45
Fig. 2.20 $\delta^{18}\text{O}$ vs. δD water isotope values within the Cuatro Ciénegas Basin, plotted by water body temperature. The GMWL [Craig, 1961] and LMWL [Cortés <i>et al.</i> , 1997] are displayed with CCB residual water plotting to the right as a Local Evaporation Line (LEL) $\delta D = 4.4\delta^{18}\text{O} - 19.5$.	46
Fig. 2.21 $\delta^{18}\text{O}$ vs. $\delta^{13}\text{C}_{\text{DIC}}$ water isotope values within the Cuatro Ciénegas Basin for location I (Fig. 2.10b).	48
Fig. 2.22 $\delta^{18}\text{O}$ vs. $\delta^{13}\text{C}_{\text{DIC}}$ water isotope values within the Cuatro Ciénegas Basin for location II (Fig. 2.10c).	49
Fig. 2.23 $\delta^{18}\text{O}$ vs. $\delta^{13}\text{C}_{\text{DIC}}$ water isotope values within the Cuatro Ciénegas Basin for location III (Fig. 2.10d).	50
Fig. 2.24 $\delta^{18}\text{O}$ vs. $\delta^{13}\text{C}_{\text{DIC}}$ water isotope values within the Cuatro Ciénegas Basin for location IV (Fig. 2.10e).	51
Fig. 2.25 $\delta^{18}\text{O}$ vs. $\delta^{13}\text{C}_{\text{DIC}}$ water isotope values within the Cuatro Ciénegas Basin, plotted by location (Fig. 2.10a).	52
Fig. 2.26 $\delta^{18}\text{O}$ vs. $\delta^{13}\text{C}_{\text{DIC}}$ water isotope values within the Cuatro Ciénegas Basin plotted by hot water body temperature (25°C - 35°C).	53
Fig. 2.27 $\delta^{18}\text{O}$ vs. $\delta^{13}\text{C}_{\text{DIC}}$ water isotope values within the Cuatro Ciénegas Basin plotted by ambient water body temperature (20°C - 25°C).	54

- Fig. 2.28** $\delta^{18}\text{O}$ vs. $\delta^{13}\text{C}_{\text{DIC}}$ water isotope values within the Cuatro Ciénegas Basin plotted by ambient water body temperature (<20°C). 55
- Fig. 2.29** $\delta^{18}\text{O}$ vs. $\delta^{13}\text{C}_{\text{DIC}}$ water isotope values within the Cuatro Ciénegas Basin, plotted by water body temperature. 56
- Fig. 2.30** $\delta^{18}\text{O}$ vs. δD water isotope values within the Cuatro Ciénegas Basin, plotted by hydrologic 'system'. The GMWL [Craig, 1961] and LMWL [Cortés *et al.*, 1997] are displayed with CCB residual water plotting to the right as a Local Evaporation Line (LEL) $\delta D = 4.4\delta^{18}\text{O} - 19.5$. 60
- Fig. 2.31** Main hydrologic through-flow system. Las Salinas and Charco Rojo have been excluded from the plot due to their location at the end of the hydrologic system, after the main and secondary systems have converged. 63
- Fig. 2.32** a) Subterranean exchanges between ambient subterranean water and hydrothermal groundwater at a depth of 1.5 m below surface level, highlighting the complexity of the CCB hydrologic system. b) Aerial photograph showing surface flow from Poza Churince into Laguna Grande (prior to complete drying of the lake) before flowing from Laguna Churince to Poza Becerra [image from google.co.uk/earth]. 64
- Fig. 2.33** Secondary through-flow system in the CCB. Las Salinas and Charco Rojo have been excluded from the plot due to their location at the end of the hydrologic system, after the main and secondary systems have converged. 68
- Fig. 2.34a** Comparable maps showing water flow patterns. Top – Water body locations in the CCB. Arrows mark the major flow patterns between water bodies, inferred from changes in isotopic composition of water. Names and locations of water bodies are as figure 2.10a [image from www.google.co.uk/earth]. Bottom – Elevation map of water body locations, shown by hydrologic system, in the CCB [elevation map after Wolaver, 2005]. 69

Fig. 2.34b Comparable maps showing water flow patterns of location I 70
(Fig. 2.34a). Left – Water body locations in the CCB. Arrows mark the major flow patterns between water bodies, inferred from changes in isotopic composition of water. Names and locations of water bodies are as figure 2.10a [image from www.google.co.uk/earth]. Right – Elevation map of water body locations, shown by hydrologic system, in the CCB with the $\delta^{18}\text{O}$ value of the water displayed next to each water body [elevation map after Wolaver, 2005].

Fig. 2.34c Comparable maps showing water flow patterns of location II 70
(Fig. 2.34a). Left – Water body locations in the CCB. Arrows mark the major flow patterns between water bodies, inferred from changes in isotopic composition of water. Names and locations of water bodies are as figure 2.10a [image from www.google.co.uk/earth]. Right – Elevation map of water body locations, shown by hydrologic system, in the CCB with the $\delta^{18}\text{O}$ value of the water displayed next to each water body [elevation map after Wolaver, 2005].

Fig. 2.34d Comparable maps showing water flow patterns of location III 71
(Fig. 2.34a). Left – Water body locations in the CCB. Arrows mark the major flow patterns between water bodies, inferred from changes in isotopic composition of water. Names and locations of water bodies are as figure 2.10a [image from www.google.co.uk/earth]. Right – Elevation map of water body locations, shown by hydrologic system, in the CCB with the $\delta^{18}\text{O}$ value of the water displayed next to each water body [elevation map after Wolaver, 2005].

- Fig. 2.34e** Comparable maps showing water flow patterns of location IV (Fig. 2.34a). Left – Water body locations in the CCB. Arrows mark the major flow patterns between water bodies, inferred from changes in isotopic composition of water. Names and locations of water bodies are as figure 2.10a [image from www.google.co.uk/earth]. Right – Elevation map of water body locations, shown by hydrologic system, in the CCB with the $\delta^{18}\text{O}$ value of the water displayed next to each water body [elevation map after Wolaver, 2005]. 71
- Fig. 2.35** Brine evolution and mineral deposition from west to east across the CCB. Red – shows gypsum precipitation at Laguna Grande with a representative photograph (taken facing north). Green – shows tufa deposition at the piedmont of the Sierra San Marcos y Pinos with a representative photograph (taken facing south). Blue – shows salt deposition in the endorheic, east side of the CCB with a representative photograph (taken facing north east) [aerial photograph from www.google.co.uk/earth]. 74
- Fig. 2.36** Poza Baño Escobedo prior to canalization in the 1960's (left) and 30 years later in the 1990s (right) [image from Minckley, 1992]. 76
- Fig. 2.37** Poza Becerra prior to canalization in the 1960s (top) and 30 years later in the 1990s (bottom) [image from Minckley, 1992]. 77
- Fig. 3.1** Schematic model showing E-W cross section across the CCB - from the meteoric water source in the limestone sierra (San Marcos y Pinos) to the basin floor. Local thrust faulting in the sierra provides a route for water heated deep underground to surface due to increased head pressure in the mountain. This recharge during climatically wetter periods causes water to not only recharge in pozas but also as calcium carbonate depositing springs. 83

- Fig. 3.2** Photographs of CCB calcium carbonate deposits; a) Laminar tufa deposits, with a hammer for scale; b) Microbially deposited tufa displaying characteristic annual laminations, with a coin for scale; c) reed and palm frond encrustations *in situ*, with a lens cap for scale. 85
- Fig. 3.3** Location of studied tufa deposits within the CCB; (a) a rim stone pool complex, (b) a spring mound containing human footprints (see chapter 4), (c) a fissure ridge complex (see appendix 1), (d) a perched terrace where previous quarrying activity has occurred showing the sequence in detail [image from *google.co.uk/earth*]. 86
- Fig. 3.4** Model for terraced “rim-stone pool” complex to the NW of the piedmont of the Sierra San Marcos y Pinos [modified after Pentecost, 2005]. 87
- Fig. 3.5** Location of the rim-stone pool complex. The red line highlights the depositional area and line A-B represents the transect across the rim-stone pools in Figure 3.8 [image from *google.co.uk/earth*]. 88
- Fig. 3.6** Large rim-stone pool complex. Although now inactive, no fissure ridge or spring mound is present to have provided source waters. 89
- Fig. 3.7** Photographs of vegetation preserved at the rim-stone pool complex; a) bryophytic microfabric in the form of algal encrustations, preserved algae is at the base of photo presented alongside modern day living algae; b) bryophytic mesofabric preserved in a dam structure. 90
- Fig. 3.8** Topographic transect of the rim-stone pool/dam complex. Vertical scale is exaggerated so up-walls and drop-walls are more prominent. Samples S1 and S2 were taken for U-series dating but subsequently not used. 91

- Fig. 3.9** Schematic showing perched terrace deposition [modified after Pedley *et al.*, 2003]. Fluvial tufa deposition at the base of the terrace is succeeded by springline and paludal tufa deposition. Incised fluvial channels and bryophyte curtains are characteristic of these types of deposits. 94
- Fig. 3.10** Location of the perched terrace in the CCB. The typical lobate plain view is highlighted by the dashed red line and the extent of the quarrying activity can be clearly seen with access tracks on the north, east and south faces. Numbers 1-8 show where stratigraphic logs were taken (Figs. 3.17, 3.18, 3.19, 3.20, 3.21) [aerial photograph provided by Dean Hendrickson]. 95
- Fig. 3.11** Original photograph of the perched terrace taken by W. L. Minckley in the 1960s [Minckley, 1969]. The original geomorphology of the terrace can be seen (in comparison with the heavily quarried modern view in Fig. 3.12). 96
- Fig. 3.12** Annotated photograph of the perched terrace in the CCB. The Sierra San Marcos y Pinos to the left (east) of the terrace is heavily karstified. The black dashed line shows the extent of the flat terrace top before quarrying began. 96
- Fig. 3.13** Annotated photograph of the perched terrace north face. The black dashed line shows the extent of the flat terrace top before quarrying began. The parallel red lines show the exposed studied section through the underlying stratigraphy due to the construction of the upper north face access road. * shows the location of figure 3.14. + shows the location of figure 3.15. ~ shows the location of figure 3.16. 97
- Fig. 3.14** Red colouration suggesting hot fluid circulation and deposition of FeO within the laminated limestone bedrock. 98

- Fig. 3.15** Photograph of ‘jigsaw puzzle’ clast observed in the perched terrace conglomerate. The clast maintains its sub-rounded shape despite extensive fracturing. 99
- Fig. 3.16** Annotated photograph of inter-bedded conglomerate and laminated calcium carbonate. Incised laminated tufa and poorly sorted, sub-rounded conglomerate at the base suggest fluvial/flash flood deposition. A change from clast supported to tufa matrix supported conglomerate up the section suggests intermittent fluvial and spring activity at the perched terrace. 99
- Fig. 3.17** Annotated photograph showing the locations of measured stratigraphic logs 1, 2, 3, 7 and 8 (Fig. 3.18). 101
- Fig. 3.18** Stratigraphic logs 1, 2, 3, 7 and 8. Location of the stratigraphic logs can be seen in Figures 3.10 and 3.17. Full stratigraphic descriptions can be seen in appendix 1.2. 102
- Fig. 3.19** Stratigraphic log 4 presented alongside an annotated photograph of the logged section. Full stratigraphic descriptions can be seen in appendix 1.2. See Figure 3.10 for exact log location. 103
- Fig. 3.20** Stratigraphic log 5 presented alongside an annotated photograph of the logged section. Full stratigraphic descriptions can be seen in appendix 1.2. See Figure 3.10 for exact log location. 104
- Fig. 3.21** Stratigraphic log 6 presented alongside an annotated photograph of the logged section. Full stratigraphic descriptions can be seen in appendix 1.2. See Figure 3.10 for exact log location. 105
- Fig. 3.22** Annotated photograph showing the steeply dipping macrophyte curtain on the front (west face) of the perched terrace. The red box is enlarged in figure 3.23. 106

- Fig. 3.23** Enlarged photograph of figure 3.22. Steeply dipping macrophytic stem structures with subsequent stalactite growth. Stalactite growth is indicative of a waterfall type structure. 106
- Fig. 3.24** Abundant palm frond impressions towards the base of the tufa sequence, hammer is presented as scale. 107
- Fig. 3.25** Preliminary $\delta^{18}\text{O}_{\text{CARB}}$ and $\delta^{13}\text{C}_{\text{DIC}}$ isotopes for the perched tufa terrace. Samples were taken at 16 intervals down the sequence. Photograph of the sampled section is also presented alongside isotopic data. 108
- Fig. 3.26** Annotated map of the locations of the three tufa areas and their proximity to each other. Red circles show the locations of each area. Black arrows show the modern surface water flow direction within the main through-flow system in the CCB (see chapter 2). 111
- Fig. 3.27** Possible direction of water flow from rivers or flash floods originating at the peak of the Sierra San Marcos y Pinos. The combination of this and local faulting could have resulted in episodic river/spring tufa precipitation during the Pleistocene. 115
- Fig. 3.28** Possible direction of fluvial outflow from Sierra San Marcos y Pinos into Laguna Grande. Red line highlights the position of the gypsum playa flats. The aerial photo was taken in 2008 and shows the final location of Laguna Grande before complete drying up in 2009 [image from google.co.uk/earth]. 119
- Fig. 4.1** a) The two footprints preserved in tufa currently on display at the Museo del Desierto, Saltillo [Gonzalez *et al.*, 2007] b) Example of a modern poza where impressions of horse prints can be seen in the centre, preserved under water in the fine carbonate sediment. 123

- Fig. 4.2** Locations of archaeological cave sites in Coahuila state, in particular within the Cuatro Ciénegas Basin shown by green squares. Red squares represent towns and cities and black squares represent cave localities. 125
- Fig. 4.3** Location of the *in situ* human footprint trackway in the Tierra Blanca quarry within the Cuatro Ciénegas Basin and proximity to the Mex-30 highway where the museum footprints were discovered [image from google.co.uk/earth]. 126
- Fig. 4.4** Schematic showing development of a spring mound. a-d) Growth of a mound where alternating (yellow and brown) layers of calcium carbonate are deposited, initially down slope before the mound builds to a higher elevation, depositing calcium carbonate upslope also; f) example of Tierra Blanca spring mound – a fault controlled flowing artesian spring; g) Tierra Blanca spring mound facies [modified after Pentecost, 2005]. 128
- Fig. 4.5** 3D Laser scanned map of the *in situ* human footprint trackway located at Tierra Blanca. Well preserved prints are designated 1-5 on the diagram whilst eroded prints are not numbered. Three prints (L-R-L sequence) are missing between prints 1 and 2 and a further three (R-L-R sequence) are missing after print 5 [image courtesy of Prof. Matthew Bennett, Bournemouth University, UK]. 129
- Fig. 4.6** Examples of the footprint trackway tufa a) Filamentous structure observed within the tufa where the carbonate can be seen formed around organic matter (dark areas are true pore spaces). b) Black surface contamination observed in the upper most layer of the sampled footprint tufa [images courtesy of Steve Noble, NIGL]. 131
- Fig. 4.7** Alternating porous/non-porous layers sampled for age profiling within tufa sample 036521-7 with $^{230}\text{Th}/\text{U}$ ages representative of adjacent layer [image courtesy of Steve Noble, NIGL]. Arrow indicates orientation of the sample - base to surface. 134

Fig. 4.8 $\delta^{18}\text{O}_{\text{CARB}}$ and $\delta^{13}\text{C}_{\text{DIC}}$ isotope values for Tierra Blanca tufa samples. Pit stratigraphy is presented in the photograph with depths. Samples for pollen analysis were taken from the surface and 0-9cm levels.	135
Fig. 4.9 Annotated stratigraphic log of the Tierra Blanca footprint site tufa. The log was taken at N 26°54'52.60" W 102°09'11.70 in a small pit 5 m from the footprint locality.	136
Fig. 4.10 Preliminary pollen data for Tierra Blanca tufa stratigraphy. TB Print 1 was taken at the surface so is plotted at 0 cm and 1-9 cm is plotted at 9 cm to accentuate the stratigraphic change in pollen with such a low resolution (two samples).	137
Fig. 4.11 Example of <i>Carya</i> (Hickory/Pecan) pollen present in the Tierra Blanca footprint top level tufa.	140
Fig. 4.12 Stride length against speed for adult humans (circle), dogs (square) and camels (triangle). Red line represents data for the human footprint trackway in the CCB [modified after Alexander, 1989].	143
Fig. 5.1 Location of the Cuatro Ciénegas Basin in Mexico (A and B) with the Tierra Blanca Quarry site (C). Core Poza Tierra Blanca (PTB) location is marked with a star [image from google.co.uk/earth].	147
Fig. 5.2 The major circulation patterns over Mexico in (a) winter (DJF) and (b) summer (JJA). Dominant seasonal moisture sources are shown with bold arrows. The CCB location is displayed as a red star [modified after Metcalfe <i>et al.</i> , 2000].	148
Fig. 5.3 Previous palaeoenvironmental studies conducted in the north of Mexico and southern United States.	149
Fig. 5.4 Locations of cores PTB and CCM taken within the CCB.	157

- Fig. 5.5** The location of core PTB. Poza Tierra Blanca can be seen in the foreground of the photograph. The Tierra Blanca footprint site can also be seen as a small mound to the left of the photograph. 158
- Fig. 5.6** The fragmented basal tufa of core CCM. The fragmented nature of the tufa meant it was unreliable for dating due to the possible mixing of older and younger stratigraphic layers. 161
- Fig. 5.7** Alternating peat – marl – tufa stratigraphy of core PTB. Displayed in the photograph is 2.4 m to 1.6 m in the core with well humified peat, marl, organic marl and tufa all present. 161
- Fig. 5.8** Thin sections of tufas from core PTB (taken at x40 magnification under bright field illumination). Showing: (a) PTB 317-318 - Quartz grain in the centre of the slide (b) PTB 317-318 - True pore space in-filled with organic detritus (c) PTB 339-341 - True pore space where calcite crystals can be seen surrounding organic carbonate matter (d) PTB 355-356 - Mollusc sp. where no detrital calcite can be seen (e) PTB 355-356 – Possible pollen grain where organic matter has been replaced by calcite during tufa formation (f) Possible contamination where darker carbonate has in-filled tufa pore space. 169
- Fig. 5.9** Linear age/depth model constructed using only the ^{14}C AMS dates – 241 ± 26 cal yr BP (36 cm), $9,467 \pm 68$ cal yr BP (160 cm) and $28,051 \pm 417$ cal yr BP (368 cm). 171
- Fig. 5.10** Linear age/depth model constructed using the ^{14}C AMS dates – 241 ± 26 cal yr BP (36 cm), $9,467 \pm 68$ cal yr BP (160 cm) and $28,051 \pm 417$ cal yr BP (368 cm) – and U-series dates - 22130 ± 880 cal yr BP (317-356 cm) and 56180 ± 2250 cal yr BP (1013-1020 cm). 172
- Fig. 5.11** Calibrated ^{14}C AMS and U-series dates versus depth using CLAM [Blaauw, 2010]. Black line represents best mid-calibrated age and the grey shaded areas represent a 95% confidence interval range. 174

Fig. 5.12 Enlarged view of unit 1 $\delta^{13}\text{C}_{\text{ORGANIC}}$ and $\delta^{18}\text{O}_{\text{CARB}}$ isotope trends with C/N ratios, and organic content and CaCO_3 content by LOI (see appendix 2.2.2).	181
Fig. 5.13 Enlarged view of unit 2 $\delta^{13}\text{C}_{\text{ORGANIC}}$ and $\delta^{18}\text{O}_{\text{CARB}}$ isotope trends with C/N ratios, and organic content and CaCO_3 content by LOI (see appendix 2.2.2).	182
Fig. 5.14 Enlarged view of unit 3 $\delta^{13}\text{C}_{\text{ORGANIC}}$ and $\delta^{18}\text{O}_{\text{CARB}}$ isotope trends with C/N ratios, and organic content and CaCO_3 content by LOI (see appendix 2.2.2).	183
Fig. 5.15 Enlarged view of unit 4 $\delta^{13}\text{C}_{\text{ORGANIC}}$ and $\delta^{18}\text{O}_{\text{CARB}}$ isotope trends with C/N ratios, and organic content and CaCO_3 content by LOI (see appendix 2.2.2).	184
Fig. 5.16 Enlarged view of unit 5 $\delta^{13}\text{C}_{\text{ORGANIC}}$ and $\delta^{18}\text{O}_{\text{CARB}}$ isotope trends with C/N ratios, and organic content and CaCO_3 content by LOI (see appendix 2.2.2).	185
Fig. 5.17 Enlarged view of unit 6 $\delta^{13}\text{C}_{\text{ORGANIC}}$ and $\delta^{18}\text{O}_{\text{CARB}}$ isotope trends with C/N ratios, and organic content and CaCO_3 content by LOI (see appendix 2.2.2).	186
Fig. 5.18 Enlarged view of unit 7 $\delta^{13}\text{C}_{\text{ORGANIC}}$ and $\delta^{18}\text{O}_{\text{CARB}}$ isotope trends with C/N ratios, and organic content and CaCO_3 content by LOI (see appendix 2.2.2).	187
Fig. 5.19 Variations in C/N ratios and $\delta^{13}\text{C}_{\text{DIC}}$ values in the core PTB sediment column. Changes in sediment type to carbonate rich marl or tufa appears to coincide with higher $\delta^{13}\text{C}_{\text{DIC}}$ values with organic rich sediments coinciding with much lower $\delta^{13}\text{C}_{\text{DIC}}$ values.	190
Fig. 5.20 $\delta^{13}\text{C}_{\text{ORGANIC}}$ vs. C/N ratios of organic sediments in core PTB. Ranges of the four major $\delta^{13}\text{C}$ contributors – C_4 , C_3 , CAM and aquatic – are set according to Leng [2005] and Minckley <i>et al.</i> [2009] after Meyers [1994].	192
Fig. 5.21 Units 1 to 7 $\delta^{18}\text{O}_{\text{CARB}}$ and $\delta^{13}\text{C}_{\text{DIC}}$ isotope data for core PTB with R^2 covariance displayed. Linear regression is shown by a trend line through the data.	193

- Fig. 5.22** $\delta^{18}\text{O}_{\text{CARB}}$ and $\delta^{13}\text{C}_{\text{DIC}}$ isotope data for core PTB with R^2 covariance displayed. Overall R^2 covariance is shown by linear regression through the data. Unit specific linear regressions have been omitted from the data graph for ease of analysis although unit specific R^2 covariance is shown. 195
- Fig. 5.23** $\delta^{13}\text{C}_{\text{ORGANIC}}$ and $\delta^{18}\text{O}_{\text{CARB}}$ isotope data for core PTB. Key upland wooded pollen taxa are displayed, highlighting the mesic (temperate) taxa; xeric (arid) taxa and continual (present throughout the whole sequence) taxa (the presence of a particular species is displayed as a '+'). The chronology – three ^{14}C AMS and two U-series dates – is also presented. 198
- Fig. 5.24** Percentage pollen data for mesic (temperate), xeric (arid) and wetland taxa in core PTB presented alongside the chronology and a simplified stratigraphy. Major upland and lowland species are displayed with high resolution (5 cm intervals) analysis having been conducted on the upper 700 cm of the core. Below 700 cm samples were taken at 50 cm intervals. Where <300 terrestrial pollen grains were counted, crosses (+) indicate the presence of an individual pollen taxa based on 100 grains to 1000 tracers. 199
- Fig. 5.25** Classical age/depth model (CLAM) applied to units 1-7. Top and bottom dates are applied to each unit based on the cm scale age point estimates predicted by CLAM. Hydrology of the CCB (open vs. closed system) is also displayed based on $\delta^{18}\text{O}_{\text{CARB}}$ vs. $\delta^{13}\text{C}_{\text{DIC}}$ linear covariance (Figs. 5.21 and 5.22). 202
- Fig. 5.26** Alternating bands of marl and peat within unit 1 of core PTB. Soft sediment deformation can be seen within the peat banding which is a process of percussion coring. 204
- Fig. 5.27** Modern peat formation in a marsh (ciénega) area of the CCB. Peat formation is the product of the drying process whereby grasses and mosses populate the marshland, increasing biomass and creating peat. 205

Fig. 6.1 Geology of the Cuatro Ciénegas Basin with transect (A – B) used in Figures 6.2 and 6.3 [modified after Badino <i>et al.</i> , 2004; Rodriguez <i>et al.</i> , 2005].	221
Fig. 6.2 Schematic model of stadial conditions in the CCB during units 2, 4 and 6. Dominance of winter monsoon climate with hydrologically open basin characteristics provided a stable basis for woodland expansion down to the bajada level and wetlands suitable for mesic vegetation on the CCB floor.	223
Fig. 6.3 Schematic model of non-stadial, high aridity conditions in the CCB during units 1, 3, 5 and 7. These conditions currently prevail in the CCB. Dominance of summer monsoon climate with hydrologically closed basin characteristics caused by complex interplay between the NAM and ITCZ. Decreased groundwater flow coupled with increased evaporation caused the formation of salt flats and endorheic pools.	226
Fig. 6.4 Photograph displaying abundant <i>Acoelorrhaphe wrightii</i> palm frond impressions and encrustations, towards the base of the perched tufa sequence.	228
Fig. 6.5 Well preserved Sotol grass impressions in what is now a completely dry area in the CCB.	229
Fig. 6.6 Locations of archaeological cave sites in Coahuila state, in particular within the Cuatro Ciénegas Basin (marked with green squares).	233
List of Tables	Page
Table 2.1 Stable isotope ($\delta^{18}\text{O}$, $\delta^{13}\text{C}$ and δD) values, facies and location for samples taken in the CCB.	35
Table 4.1 U-Th isotope data, calculated ages and initial $^{234}\text{U}/^{238}\text{U}$ activity ratios for the <i>in situ</i> footprint trackway.	133

Table 5.1 U-series and ^{14}C AMS dates obtained for core PTB. #PTB 317-318, 321-322, 339-341 and 355-356 give an average age of 22.13 cal kyr BP for the 317-356 tufa within core PTB which is used as a minimum age for this tufa. 168

Table 6.1 Summary table comparing the palaeoenvironmental interpretation obtained from this study with previous published studies from the Chihuahuan Desert and southern United States region. 220

Chapter 1: Introduction

1.1 Scientific background and justification

The arid or semi-arid zone covers the majority of the Earth's land surface between latitudes 18° and 40° north and south of the equator, including northern and southern Africa, the Middle East, southern South America and parts of central Asia and Europe [NOAA, 2011]. This arid region of the world also includes Mexico, lying in the northern hemisphere tropics, between latitudes 16° and 32° north.

Although there is clearly an opportunity for the study of climatic change in this arid region of the Earth, very little work has been conducted, particularly when compared to the arid regions of the United States of America, including the Great Basin [Bryant, 1977; Bryant and Holloway, 1985; Van Devender, 1990; Winograd *et al.* 1992; Wright *et al.* 1993; Fawcett *et al.* 2011], and other arid or semi-arid regions around the world [Brook *et al.* 1990; Schwalb *et al.* 1999; Kent-Corson *et al.* 2009; Ortiz *et al.* 2009].

Palaeoenvironmental work that has been conducted in Mexico has, however, primarily focussed on records from central Mexico, particularly the Trans Mexican Volcanic Belt (TMVB). There is a wide range of palaeoclimatic data available for this region with well dated pollen sequences spanning as far back as the Late Pleistocene (~44 ka BP) [Watts and Bradbury, 1982; Gonzalez Quintero, 1986; Straka and Ohngemach, 1989], as well as detailed records covering the Holocene [Brown, 1985; Xelhuantzi Lopez, 1994; Park *et al.* 2010]. The majority of palaeoenvironmental studies focussing on fossil freshwater diatoms also come from the TMVB. Detailed studies [Bradbury, 1971, 1989; Caballero Miranda, 1997; Caballero Miranda and Ortega Guerrero, 1998] have yielded long spanning (~46 ka BP) records, comparable with pollen records from the same region [Metcalf *et al.* 2000].

Pollen and diatom proxy data are, however, susceptible to diagenetic effects [Hobbs *et al.* 2010; Shimokawara *et al.* 2010] and are only abundant in certain sediment deposits: pollen is generally confined to organic deposits and diatoms to minerogenic deposits. The paucity of these deposits in arid Mexico coupled with diagenetic effects has limited the palaeoenvironmental work and as a result, it is not

uncommon to encounter palaeoenvironmental records containing discontinuous proxy data.

The palaeoenvironmental record for arid northern Mexico, in comparison to the TMVB, is relatively neglected. Packrat midden records for the Late Pleistocene/Holocene have provided a basis for detailed palaeoenvironmental records in North America [Betancourt *et al.* 1990], particularly the desert region of Sonora [Van Devender, 1990; Anderson and Van Devender, 1995], which straddles northern Mexico and the American Southwest. Despite these midden studies providing an opportunity for climatic reconstruction in northern Mexico, the proxy bearing deposits are scarce in this arid region, leading to limited work having been conducted [Van Devender, 1990].

However, natural wetlands in arid to semi-arid regions across the American Southwest, southern United States and northern Mexico are well documented, providing a valuable resource for native flora, fauna and human populations [Haynes and Agogino, 1966; Minckley, 1969; Davis *et al.* 2002; Haynes, 2008; Minckley *et al.* 2009]. These desert wetlands, or *ciénegas*, can contain sediment deposits holding an array of valuable information regarding both natural and human induced changes in the terrestrial environment [Minckley and Brunelle, 2007]. These, often lengthy, unconsolidated sequences of intercalated minerogenic and organic sediments may provide information regarding climatic and environmental changes [Last and Smol, 2001; Leng and Marshall, 2004]. The sediment deposits from arid wetlands have been shown to be the same as lacustrine sediment deposits [Minckley and Brunelle, 2007; Minckley *et al.* 2009], which have been used to reconstruct past climate change on both regional [e.g. Castiglia and Fawcett, 2006] and global scales [e.g. Yu *et al.* 1997], and when combined with present day lake studies has elucidated the response of lake systems to past and future climate changes [e.g. Johnson *et al.* 1991].

The use of oxygen and carbon isotope ratios ($^{18}\text{O}/^{16}\text{O}$ and $^{13}\text{C}/^{12}\text{C}$ expressed as $\delta^{18}\text{O}$ and $\delta^{13}\text{C}$ respectively) of bulk carbonate lacustrine sediment have become successful tools for palaeoenvironmental reconstructions. They have provided information about atmospheric moisture and organic matter sources entering a lake system, and thus any climatic and vegetation changes through time [e.g. Schwalb *et al.* 1999; Huang *et al.* 2001; Holmes *et al.* 2010]. Arid wetland deposits, being the same as

lacustrine sediment deposits, should represent the same climatic and vegetation changes through time and are thus an under-utilized repository of palaeoenvironmental information. First, understanding the modern hydrology of a lake or wetland system is important for the interpretation of any palaeoenvironmental archives obtained, as any interpretation must take into account any likely changes to hydrology that may have occurred in the past. The degree of hydrological 'closure', determined through $\delta^{18}\text{O}$ and $\delta^{13}\text{C}$ co-variance, is a useful tool in the determination of hydrology, and thus palaeoenvironmental change [Leng and Marshall, 2004], and has been used to good effect in showing past changes in hydrology [e.g. Talbot, 1990; Johnson *et al.* 1991; Winter and Rosenberry, 1995; Li and Ku, 1997] and the various sources for $\delta^{18}\text{O}$ and $\delta^{13}\text{C}$ in sediments.

Proxy bearing deposits are, however, relatively scarce in many arid/semi-arid regions around the world. Therefore, even though there may be clear evidence that many of these regions have undergone significant environmental changes in the past, poor preservation of proxy data means there is still great uncertainty surrounding these changes. This thesis explores the potential of pollen, $\delta^{18}\text{O}$ and $\delta^{13}\text{C}$ for a multi-proxy research approach to reconstruct the palaeoenvironment of an arid wetland region of northern Mexico. This is achieved by utilizing a study of modern hydrology using $\delta^{18}\text{O}$ and $\delta^{13}\text{C}$ isotopic values of water and comparing this study with, principally, the $\delta^{18}\text{O}$ and $\delta^{13}\text{C}$ record from a wetland sediment core, but also the pollen record. Comparing high resolution isotopic studies with pollen records will allow the detection of small scale, as well as large scale hydrological and palaeoenvironmental changes. This thesis also addresses the use of terrestrial carbonate formations as geomorphological indicators of past climate change in this arid wetland. A study of how any inferred palaeoenvironmental change has affected human populations during the Holocene is also an important component of this thesis.

Meyer [1973] conducted the only palaeoenvironmental reconstruction of the Cuatro Ciénegas Basin (CCB), analysing pollen from a 13 m sediment core to conclude that no environmental change had occurred from ~31 ka BP to present, leading to a high degree of endemism in the CCB associated with a long period of biogeographic isolation and apparent environmental stability. This interpretation was first proposed by Minckley [1969] and later supported by the pioneering pollen work of Meyer [1973].

However, the high degree of floral and faunal endemism does not necessarily imply environmental stability as is previously thought. The high mountain ranges surrounding the CCB and presence of deep groundwater reservoirs and subsequent groundwater discharge into the CCB's pools, lakes and rivers create riparian, marsh and aquatic habitats that have the potential to create a unique desert wetland refugium in a region that is known to have experienced environmental change through the Late Pleistocene and Holocene [Metcalf *et al.* 1997; Musgrove *et al.* 2001; Metcalfe *et al.* 2002; Castiglia and Fawcett, 2006]. The discovery of a human footprint trackway in the CCB in 2006 [Gonzalez *et al.* 2007] triggered a reinvestigation of Meyer's original pollen data by Minckley and Jackson [2008]. They concluded that the CCB had undergone extensive climatic and environmental change from at least 16 ka BP to the present. The contradictory nature of the only two palaeoenvironmental studies in the CCB leaves a distinct gap in the understanding of climatic and environmental change in northern Mexico on both a regional and global scale.

Multi-proxy environmental data has the potential of ensuring a robust palaeoenvironmental record [e.g. Hammarlund *et al.* 2002], and the contradictory palaeoenvironmental reconstructions and availability of arid wetland sediment in the Cuatro Ciénegas Basin, located in the Chihuahuan Desert region of northern Mexico provides a valuable opportunity to apply a multi-proxy approach to palaeoenvironmental reconstructions in an arid region. Understanding how climatic and environmental changes affect the CCB in the modern day, as well as on Quaternary timescales, will increase understanding of this arid region in the context of global climate change and also elucidate the response of human populations to climatic and environmental change in an important, and little understood, archaeological region of the Americas.

1.2 Project aim

The aim of this research is to examine the palaeoenvironmental evidence of climate change and associated human responses in the Cuatro Ciénegas Basin (Fig. 1.1) from the Late Pleistocene to the present and to obtain a clear picture of the palaeoclimate, hydrology and geoarchaeology, placing it within a regional and global context. The Cuatro Ciénegas Basin provides a unique desert oasis with the potential

to contain a long palaeoenvironmental record, back to and possibly beyond 30 ka BP [Meyer, 1973]. Extraction of water for industry is currently threatening this fragile desert ecosystem, making studies of hydrology and environmental change of the utmost importance. The aim of this research is achieved with the following objectives:

- To investigate the palaeoenvironment of the Cuatro Ciénegas Basin from the Late Pleistocene/Holocene to the present through stable isotope and palynological analysis of a 15 m sediment core located in the basin.
- To investigate modern hydrogeology and water flow patterns by stable isotope analysis to obtain a conceptual hydrologic model, applicable to palaeohydrological regimes.
- To explore the relationship between terrestrial tufa formations and previous environmental and hydrological regimes within the Cuatro Ciénegas Basin.
- To explore the relationship between palaeoenvironmental change and consequent human response through integrating archaeological excavations of human footprints with published studies of Coahuilan Indians.

1.3 Introduction to the Cuatro Ciénegas Basin study site

The Cuatro Ciénegas Basin (CCB) is a 1400 km² basin located in the state of Coahuila, NE Mexico (Fig. 1.1). Designated an “Área de Protección de la Flora y Fauna” (area of protection for flora and fauna) by the Comisión Nacional de Áreas Protegidas in 1994, the CCB is now recognised as unique and one of the most biodiverse wetland ecosystems in the World.

Located in the Sierra Madre Oriental mountain range, the CCB lies approximately 742 m a.s.l, surrounded on all sides by Cretaceous Limestone mountains, with peaks reaching over 3000 m. Over 200 pools (known locally as pozas), lagoons and rivers exist in the CCB, fed by the surrounding karst environment and a deep underground aquifer - the Cupido-Aurora aquifer – feeding hydrothermal groundwater into over 70 of the pools [Johannesson *et al.*, 2004; Rodriguez *et al.* 2005].

Earliest human presence in the basin, first documented by Palmer [1882], dates from the Late Pleistocene/Early Holocene (12 ka BP) to the present based on well stratified archaeological cave deposits in the mountains around the basin [Gonzalez *et al.* 2007; Taylor, 2003; Turpin, 2003]. The early inhabitants were nomadic hunter-

gatherers who were well adapted to the desert conditions and highly dependent on the local environment for their subsistence.

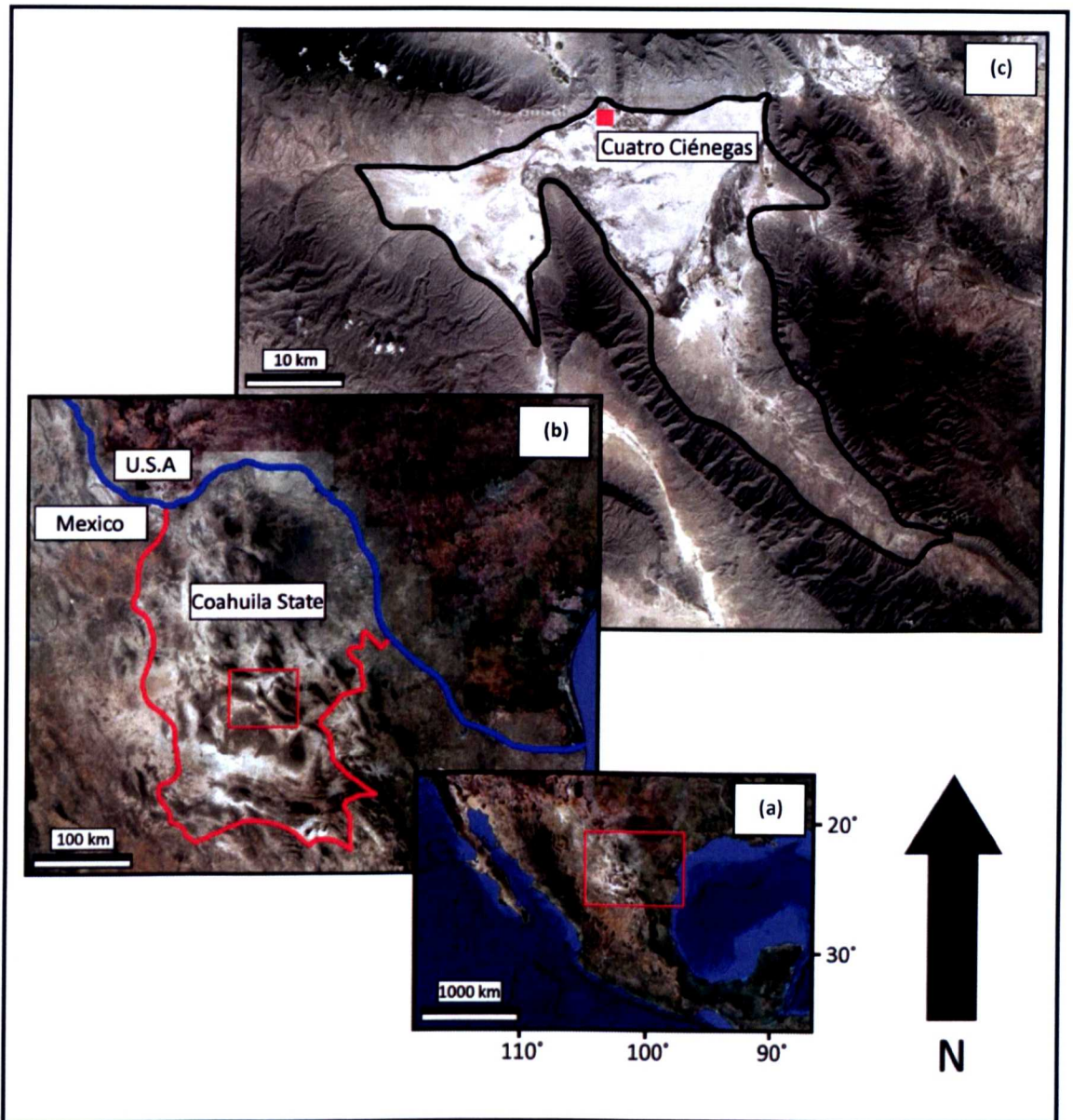


Figure 1.1. (a) Location of the Cuatro Ciénegas Basin within Mexico (b) Coahuila state borders the USA to the north, separated by the Rio Grande (c) Black line shows the limit of the CCB, the area enclosed has been declared a protected area [image from google.co.uk/earth].

1.3.1 Pre-Quaternary geology of the Cuatro Ciénegas Basin

The CCB forms part of the Coahuila Block in north-eastern Mexico and southern Texas (Fig. 1.2). The “basement block” of the Coahuila Block is of Gondwanan origin after the collision with the north-American continent (Laurentia) during the Taconic-Ocloyic orogenic event (280 Mya) [Lehmann *et al.* 1999]. Lying south of the Ouachita-Marathon suture, created during this event, and north of the California-Coahuila

transform, the Coahuila Block is composed of granite and granodiorite, of Permian-Triassic age, intruded into Permian orogenic sediments [Lehmann *et al.*, 1999; Dickinson and Lawton, 2001].

Figure 1.2. Contemporary geological map of Mexico and southern USA. TMVB-Trans Mexican Volcanic Belt; CT-Cayman Transform; MzTT-Tehuantepec Transform; CAS-Collision Accretion Suture; C-CT-California-Coahuila Transform; CTT-Coahuila-Tamaulipas Transform; O-MS-Ouachita-Marathon Suture; Be-Belize; Cz-Cenozoic; Gu-Guatemala; Ho-Honduras; Mz-Mesozoic; Pz-Palaeozoic; Sa-El Salvador [modified after Dickinson and Lawton, 2001].

The rift phase of the opening of the Gulf of Mexico is linked to the formation of the Coahuila Block at the beginning of the Cretaceous [Badino *et al.*, 2004]. Shifting of the more southern “Tampico Block” towards the east c.175 Mya created the Coahuila-Tamaulipas transform. At the same time dislocation inside the Coahuila Block, created by the shifting Tampico Block, was compensated by extension (enlargement by bulging), with the resultant faults from the extension allowing the intrusion of plutons which in turn led to smaller fault blocks emerging within the Coahuila Block. One of these fault blocks was the “Coahuila Peninsula” – now known as the Sierra El Granizo, Sierra Australia and Sierra La Fragua (Fig. 1.3).

Figure 1.3. Geological map of Cuatro Ciénegas showing the major limestone outcrops and CCB recharge zone [modified after Badino *et al.*, 2004; Rodriguez *et al.*, 2005].

At the time of the Coahuila-Tamaulipas transform formation, the fault blocks surrounding the Coahuila Peninsula dropped below sea level, forming a carbonate platform, which would later become the Sierra San Marcos y Pinos, Sierra Menchaca, Sierra La Purisma and Sierra Madera (Fig. 1.3) [Badino *et al.*, 2004]. Between 160 Mya and 130 Mya the rift phase of the Gulf of Mexico was complete by which time the region had begun to subside, with over 1000 m of carbonates deposited; these can be seen today as the mountain ridges surrounding the CCB. The “Cupido” carbonate platform began to form c.130 Mya from, what is now modern day Louisiana, south to the Gulf of Mexico and also west - flanking the southern-most edge of the Coahuila Peninsula. This platform composing the “Cupido Formation” limestone formed in shallow lagoons where at the same time the “Lower Tamaulipas Formation” (mudstones) formed beyond the margins of the Cupido platform in the deeper, oxygen scarce waters [Lehmann *et al.*, 2001]. Deposition of the Cupido Formation up to a thickness of 500 m continued until 115 Mya when sea levels began to rise once more, thus creating deep anoxic waters from which the marls of the “La Peña Formation” were deposited up to a thickness of 20 m.

The relative sinking of the Cupido platform, associated with the start of the subduction in the west, resulted in the sea moving inland, covering the platform and creating an eastward carbonate slope and a new Cupido platform margin 100 km west of the original margin. Large lagoons formed beyond the new Cupido platform margin to the east, where the “Acatita Formation” was deposited – a series of evaporate sediments reaching up to 500 m thickness. Around 108 Mya, when the lagoons had fully established the eastward carbonate slope, the “Aurora Formation” of limestone muds began to sediment. The carbonate slope gradually reached further east, meeting the open sea and enabling the “Upper Tamaulipas Formation” to form in the Gulf of Mexico. The Cupido platform and Aurora Formation now form the Cupido-Aurora aquifer, a deep lying confined aquifer flowing from the Bolson de Mapimi in the west to the Gulf of Mexico [Badino *et al.* 2004].

The Laramide orogeny affected northern Mexico during the Eocene (55-35 Mya) [Badino *et al.*, 2004; Molina-Garza *et al.*, 2008] allowing the formation of the Sierra Madre Oriental (including the Coahuila fold ridge) and marking the eastern most limits of the deformation. The Coahuila fold ridge was created as a result of décollement (sliding plane between surfaces) between the Cupido platform and the basement block, creating the characteristic NW axial thrust-fold anticlines seen today in the CCB limestone mountains (e.g. Sierra San Marcos y Pinos), whilst the basement block remained unaltered. Tectonic activity during the Oligocene, Miocene and Pliocene (35-2.5 Mya), as a result of the Laramide orogeny, reactivated the San Marcos Fault, raising the northern block and creating strong thermal activity. These hydrothermal fluids resulted in deposits of mixed metal sulphurs and mineral deposits such as fluoride that can today be seen at the base levels of the limestone deposits in the area [McKee, 1990].

1.4 Chapter overview

The following chapters are split into individual studies, each providing an experimental focus supported with available documentary evidence. Below is a brief overview of the topics covered by each chapter.

1.4.1 Chapter two: Reconnaissance isotope hydrology of the Cuatro Ciénegas Basin

A reconnaissance stable isotopic study of the waters of the Cuatro Ciénegas Basin has been undertaken utilizing stable $\delta^{18}\text{O}$, $\delta^{13}\text{C}$ and δD isotopes to determine the modern day water sources and subsequent flow regime. Modern water samples and flow regime determination provide a conceptual hydrologic model for the Cuatro Ciénegas Basin, applicable to previous hydrological regimes in the basin. Samples of 26 pools, lakes and rivers from both the west and east sides of the Cuatro Ciénegas Basin have been analysed and discussed, providing a flow model to complement the palaeoenvironmental chapter.

1.4.2 Chapter three: Terrestrial carbonate environments of the Cuatro Ciénegas Basin

This chapter describes, for the first time, the terrestrial carbonate formations observed within the Cuatro Ciénegas Basin and their individual depositional facies. These carbonate formations have not been previously described in the Cuatro Ciénegas Basin and the origins of each carbonate formation are proposed, based on the evidence observed compared with analogous carbonate formations from locations around the world. In particular, a perched terrace, first described by W. L. Minckley [1969] as a pluvial lake shoreline, is discussed in detail with comparisons drawn between recent local and regional hydrologic models and climate reconstructions. This chapter complements the hydrology and palaeoenvironmental chapters, providing more detailed discussions and conclusions of the overall thesis.

1.4.3 Chapter four: Human occupation in the CCB and the *in situ* human footprint trackway

This chapter investigates the ancient Coahuilan Indians of the Cuatro Ciénegas Basin. A report of a new *in situ* human footprint trackway is synthesised with Holocene palaeoenvironmental records, archaeological excavations and archaeological reports. The last formal archaeological excavations were conducted in the 1940s by Walter Taylor with artefacts including sandals, arrow points and vegetal fibres categorized and studied in detail over the last 60 years [Taylor, 2003; Turpin, 2003]. Preliminary stable $\delta^{18}\text{O}$ and $\delta^{13}\text{C}$ isotope values of calcium carbonate sediments have been analysed alongside U-series dating techniques allowing synthesis of the new isotopic palaeoenvironmental record into the known, chronologically well constrained pollen

record. The most important archaeological sites are discussed within the palaeoenvironmental and material culture records.

1.5.4 Chapter five: Multi-proxy palaeoenvironmental reconstruction of the Cuatro Ciénegas Basin

A multi-proxy study involving the use of stable $\delta^{18}\text{O}_{\text{CARB}}$, $\delta^{13}\text{C}_{\text{DIC}}$ and $\delta^{13}\text{C}_{\text{ORGANIC}}$ isotopes, C/N ratios, sediment LOI, pollen and radiometric dating techniques sampled from a 15 m sediment core has been undertaken in the Cuatro Ciénegas Basin. The obtained dataset is brought into the modern context of climate and hydrology in the Cuatro Ciénegas Basin so that the palaeoenvironment can be reconstructed. The chapter tests the null hypothesis: has the Cuatro Ciénegas Basin (CCB) provided an area of unique desert refuge, unresponsive to regional climatic and environmental change, from the Late Pleistocene to the present? It is demonstrable that the Cuatro Ciénegas Basin displays evidence of climate and environmental change from the Late Pleistocene to the present, complementing regional and global proxy data.

Chapter 2: Reconnaissance isotope hydrology of the Cuatro Ciénegas Basin

2.1 Introduction

The aim of this chapter is to investigate aspects of the hydrology, in particular the flow regime, of the Cuatro Ciénegas Basin (CCB). By studying reconnaissance stable oxygen ($\delta^{18}\text{O}$), hydrogen (δD) and carbon ($\delta^{13}\text{C}$) isotopes, insight into the flow regime in the modern day basin can be obtained, which may shed light on potential Palaeo-flow regimes.

Very little is known about the hydrology of the CCB with few studies to date [Cortés *et al.*, 1997; Johannesson *et al.*, 2004; Rodriguez *et al.*, 2005; Wolaver *et al.*, 2008]. It is, however, well established that groundwater flow systems are incredibly important in arid to semi-arid regions, particularly in the Southern U.S. [Eakin, 1966; Maxey, 1968; Gates *et al.*, 1980; Ragab and Prudhomme, 2002; Hibbs and Darling, 2005; Scanlon *et al.*, 2006; Herczeg and Leaney, 2011]. Human populations and associated biota in arid regions rely on available water systems to survive. Such systems are also often home to endemic populations that are remnants of previous pluvial environments. The CCB is home to over 70 species of endemic flora and fauna [Minckley, 1969] including fresh water stromatolites – the only ones of their kind in the World [Badino *et al.*, 2004]. This high degree of endemism in the CCB suggests a long period of biogeographic isolation and such endemic species are highly sensitive to slight changes in their habitat such as temperature change and decreases in water quality and groundwater flow. Changes can be highly detrimental to species populations and in an area closely linked with human dispersal throughout the Americas, groundwater flow regime can both affect and be affected by human populations. In the modern day environment there is a fine balance between conservation of the natural environment, eco-tourism and the need for survival – irrigation of farmland, drinking water and sanitation. Understanding the flow regime and water sources becomes paramount in such an economically poor region, as overuse of the hydrologic system could lead to irreversible water table changes. This

would not only be to the detriment of the current human inhabitants of the basin, but could also lead to the breakdown of a very fragile and long standing ecosystem.

Such changes are particularly interesting for studies of palaeoenvironment as modern conceptual hydrogeologic models can identify possible precursors to past changes that may have effected human and faunal populations.

2.1.1 Stable isotope geochemistry

Research into the measurement of isotopes began as early as the 1920's [e.g. Briscoe and Robinson, 1925]. Early research was, however, crude and the technical development of stable isotope geochemistry, particularly the measurement of oxygen, hydrogen and carbon didn't begin until the 1950's and 1960's [e.g. Craig, 1953 and 1961; Dansgaard, 1964]. Since the developmental research of the 1950's and 1960's the use of stable isotope geochemistry has increased, leading to a greater understanding of the subject area and allowing the interpretation of proxy hydrological and environmental data [e.g. Gat and Issar, 1974; Carillo-Rivera *et al.*, 1992; Winograd *et al.*, 1992; Andrews *et al.*, 1992; Love *et al.*, 1994; Andrews *et al.*, 1997; Harrington *et al.*, 2002; Guendouz *et al.*, 2003; Andrews, 2006; Bernal *et al.*, 2011; Fawcett *et al.*, 2011].

Lighter (less neutrons) and heavier (more neutrons) isotopes exist for each element and are conventionally written as the ratio of the heavy (rarer neutrons) isotope to the light (more abundant) isotope e.g. $^{18}\text{O}/^{16}\text{O}$, $^{13}\text{C}/^{12}\text{C}$. Delta (δ) is the standard notation for reporting the ratio of the abundance of the heavy isotope to the light isotope and is displayed in parts per mil (‰). Higher δ values or lower δ values mean that the ratio of the heavier isotope to the light isotope is higher or lower respectively, in the sample than the standard [Clark and Fritz, 1997; Leng, 2005; Sharp, 2007]. For example, a $\delta^{13}\text{C}$ value of -3‰ has a $^{13}\text{C}/^{12}\text{C}$ ratio that is 3 per mil, or 0.3 percent lower than the standard. The most commonly used standards from which $\delta^{18}\text{O}$ and $\delta^{13}\text{C}$ deviations are measured are: the PDB (PeeDee Belemnite) scale for terrestrial carbonate sediments and the VSMOW (Vienna Standard Mean Ocean Water) scale for water samples [for use of other reference standards see Sharp, 2007].

2.1.1.1 Stable isotopes in arid-zone hydrology

Reviews of the isotope systematics used in isotope hydrology have been conducted in great detail [see Fritz and Fontes, 1980, 1986; Clark and Fritz, 1997; Leng, 2005; Aggarwal *et al.*, 2005; Sharp, 2007], and as such this section is presented as an overview of the main hydrological processes and controls on stable $^{18}\text{O}/^{16}\text{O}$, $^2\text{H}/^1\text{H}$ (*D*) and $^{13}\text{C}/^{12}\text{C}$ isotopes, with a focus on arid/semi-arid zone hydrology.

Arid and semi-arid zones constitute the majority of the Earth's land surface between 18 and 40° North and South with low and intermittent rainfall, leaving groundwater as the only reliable water source [Herczeg and Leaney, 2011]. Stable isotopic compositions of these water sources are affected by a number of processes e.g. evaporation, and it is the affect of these processes on the most active parts of the hydrological cycle that must be considered when interpreting isotopic data (Fig. 2.1). Large, well mixed water bodies e.g. oceans, vary little in isotopic composition whereas waters of a meteoric origin, derived from the oceans through evaporation e.g. precipitation, can vary widely [Gat, 1996; Sharp, 2007].

Figure 2.1. Schematic model of the hydrological cycle and the major sinks and fluxes of water within it (100 units constitutes the marine sink) [modified after Gat, 1996].

In essence, Ocean water is evaporated and condenses into precipitation and, in turn, precipitation is transformed into three basic 'terrestrial reservoirs' that influence the oxygen ($\delta^{18}\text{O}$) and hydrogen (δD) isotopic ratio (composition) of lake water: 1) soil-zone moisture, 2) groundwater and 3) surface waters [Leng and Marshall, 2004].

The carbon isotope ratio (composition) of lake water, however, is more complicated as carbon is in the form of an anion in alkaline systems and as such the controls of the carbon cycle are not completely climate related [Leng, 2005]. The incorporation of carbon into lake water is affected by many processes e.g. interaction with atmospheric CO_2 (Fig. 2.2), so is not simply controlled by the contents of environmental water [Atekwana and Krishnamurthy, 1998; Myrbo and Shapley, 2006].

Figure 2.2. Schematic model of the carbon cycle in lake water with the major sources of carbon and the effect of each source on $\delta^{13}\text{C}$ isotope value of the water [modified after Gat, 1996].

In essence, the $\delta^{18}\text{O}$ and δD value of any lake water will be sourced from atmospheric moisture, and thus precipitation, and the $\delta^{13}\text{C}$ value of any lake water will most likely be sourced from the total dissolved inorganic carbon (TDIC) from the surrounding catchment, via interactions with soil and the atmosphere [Leng, 2005].

Oxygen and hydrogen

Meteoric water, or atmospheric water, is water that has fallen from the atmosphere, including rain, hail and snow, and is the most important influencing factor on the $\delta^{18}\text{O}$ and δD values of lake water. Craig [1961] outlined the baseline Global Meteoric Water Line (GMWL) from which regional precipitation isotopic values can be determined. Regression of meteoric water data resulted in the expression $\delta D = 8\delta^{18}\text{O} + 10$, applicable to the isotopic composition of the majority of the worlds climates [Craig, 1961]. Deviations from the GMWL are observed with regional variations in atmospheric moisture and therefore precipitation; responsible for the formations of Local Meteoric Water Lines (LMWL) [Rozanski *et al.*, 1993]. The isotopic composition of precipitation in any given region is controlled, often by a combination of, six physical processes:

- 1) Temperature: Dansgaard [1964] first noticed that surface temperature, particularly in temperate regions, is strongly correlated with the isotopic composition of meteoric water. This is termed Rayleigh fractionation; an open system whereby condensate is continually removed from the vapour of an air mass in under a fixed fractionation factor [see Gat, 1996 for further discussion of Rayleigh fractionation in open, closed and steady state conditions]. In arid/semi-arid zones, the air mass is less readily condensed because of higher temperatures so $\delta^{18}\text{O}$ and δD values of the air mass will more closely reflect the isotopic value of the parent water: ocean water ($\delta^{18}\text{O}$ value 0‰) [Gat, 1996; Sharp, 2007].
- 2) Continentality: precipitation from an air mass moving over a land mass, or continent, will become isotopically lighter because it will experience more cycles of precipitation, preferentially raining out the heavier ^{18}O isotope [e.g. Kent-Corson *et al.*, 2009]. Arid regions will exhibit higher δ values due the continual recirculation of ^{16}O through preferential evaporation.
- 3) Latitude: $\delta^{18}\text{O}$ and δD values of precipitation will be lower with increasing latitude due to decreasing temperature and the air mass experiencing more cycles of precipitation, preferentially removing the heavier ^{18}O .
- 4) Altitude: Colder temperatures are experienced at higher elevations, intensifying Rayleigh fractionation and lowering the isotopic composition of the

water [Sharp, 2007]. As an air mass is deflected up by a mountain it cools, increasing rainout and decreasing the vapour content of the remaining air mass, thereby lowering the $\delta^{18}\text{O}$ and δD values of the precipitation. The altitude of precipitation that is the source for a recharging water body can often be calculated by the oxygen isotopic composition of that water [e.g. Johannesson *et al.*, 2004].

- 5) The Amount effect: mean $\delta^{18}\text{O}$ and δD values of precipitation negatively correlate with the amount of precipitation in tropical regions [Dansgaard, 1964]. More cycles of precipitation and flash flooding will lead to isotopic ratios being highly depleted in the heavy isotope in each subsequent rainfall, so δ values are higher in months with low rainfall and lower in months with high rainfall [e.g. Rozanski *et al.*, 1993]. However, in convecting arid/semi-arid air masses, four further processes that can affect the isotopic composition of precipitation must be considered: 1) falling droplets can exchange with rising air vapour; 2) falling droplets incorporate more vapour as they fall, becoming larger; 3) droplets can evaporate upon exiting the cloud; 4) droplets can exchange with each other within the air mass [see Sharp, 2007, for further discussion].
- 6) Seasonality: all of the aforementioned processes are affected by seasonality. Changes in the dominant moisture source between summer and winter will affect the isotopic composition of precipitation e.g. winter Pacific air mass vs. summer Gulf of Mexico air mass [Metcalf *et al.*, 2000]. Also, due to the tendency for more rainfall to be lost to the atmosphere in summer than in winter, isotopic ratios may become more depleted in the heavier isotope [Herczeg and Leaney, 2011 after Fontes, 1994].

In the arid/semi arid zone, groundwaters in karst and other unconfined aquifers usually display isotopic ratios that represent the weighted mean of meteoric water inputs, displaying isolation from temperature, seasonality and amount effects e.g. Carrillo-Rivera [1993] and Clark and Fritz [1997 after Rank *et al.*, 1992]. A decrease in the $\delta^{18}\text{O}$ variability in water is observed with increasing depth and temperature, with surface water bodies usually displaying isotopic ratios within 0.5‰ of the source precipitation [e.g. Carrillo-Rivera, 1993]. However, groundwater sourced from deep

lying aquifers may display a different isotopic composition to that of modern precipitation in any given area if the recharge region is far away from the sample site, with a different catchment altitude or residence time [e.g. Johannesson *et al.*, 2004], or if the aquifer contains palaeo-water. In the case of palaeo-water, Gat and Issar [1974] showed groundwater isotope compositions are observably more negative than that of the weighted mean precipitation. Further studies have since shown that the stable isotopic composition of groundwater decreases with age along an inferred flow path [Love *et al.*, 1994; Guendouz *et al.*, 2003; Abdalla, 2009], leading to the possible formation of palaeo-water.

Although groundwater is the primary water resource in arid/semi-arid zones [Herczeg and Leaney, 2011], water-air interactions (evaporation) from soil in the unsaturated zone and surface waters remain the most influential processes that can affect $\delta^{18}\text{O}$ and δD values of lake water. Studies of soil pore water in the unsaturated zone [Allison, 1982; Allison and Barnes, 1985; Fontes *et al.*, 1986; Barnes and Allison, 1988; Song *et al.*, 2009] have shown up to 1-2 m depth in a soil zone will be affected by evaporative enrichment before any precipitation infiltrates down to the water table before mixing with lake water. However, Allison [1982] observed mixing between evaporated soil water and subsequent rainfall events, displacing the residual soil water downward, results in groundwater isotopic values that can be $\sim 2\%$ and $\sim 15\%$ enriched in ^{18}O and ^2H (D) respectively, relative to the isotopic composition of local precipitation.

It is not just soil water that can be affected by kinetic isotope effects, if two or more lakes are joined by a surface flow system, progressively higher $\delta^{18}\text{O}$ and δD isotope values of the water are observed the greater distance the water flows, as increased contact with the warm, dry air increases preferential evaporation of ^{16}O [Allison and Barnes, 1985; Gat, 1996]. This progressive enrichment can lead to a Local Evaporation Line [LEL] from which to base hydrological models [Leng, 2005].

Carbon

Groundwaters originate as meteoric water and infiltrate the soil and rocks gaining dissolved inorganic carbon (DIC) along the way. The dissolution of CO_2 through acid-base weathering of carbonate rock and soil results in groundwater rich in

bicarbonate (HCO_3^-) and carbonate (CO_3^{2-}) species. As well as DIC, groundwater will invariably dissolve organic matter from the soil in the form of dissolved organic matter (DOC). In ground and lake water, microbiological activity degrades the organic compounds resulting in the evolution of redox conditions and methanogenic reactions. All sources of carbon are linked through these acid-base and redox reactions but DIC will give a better understanding of hydrologic pathways than DOC as there are various sources for DIC: atmospheric CO_2 , soil CO_2 and organic/biogenic interactions (Fig. 2.2), whereas DOC is derived from parent organic matter or fossil organic material [Clark and Fritz, 1997; Atekwana and Krishnamurthy, 1998; Leng, 2005]. $\delta^{13}\text{C}_{\text{DIC}}$ is the dominant precursor for carbon bearing proxies e.g. carbonates, and is present in terrestrial water bodies e.g. lakes and groundwaters [Leng, 2005]. $\delta^{13}\text{C}_{\text{DIC}}$ values of lake water (Fig. 2.3), when used with other measurements, can be used to evaluate the sources, sinks and fluxes of carbon in an environment and for any given water body will reflect contributions from groundwater, streams, biogenic CO_2 uptake and/or release and atmospheric CO_2 invasion/evasion [Atekwana and Krishnamurthy, 1998].

Figure 2.3. Ranges of $\delta^{13}\text{C}$ values from natural compounds represented in lake water isotope values [modified after Clark and Fritz, 1997].

However, in a groundwater sourced recharge system the $\delta^{13}\text{C}_{\text{DIC}}$ value of the water body (or bodies) will mirror that of the groundwater and significant run-off events can lead to dilution of the $\delta^{13}\text{C}_{\text{DIC}}$ value [Taylor and Fox, 1996; Yang *et al.*, 1996; Atekwana and Krishnamurthy, 1998; Leng, 2005].

See chapter 5 for more detail of controls on oxygen, hydrogen and carbon isotopic composition of carbonate sediments.

2.1.2 Current topography and surface stream network

As discussed in Chapter 1, the CCB forms part of the Sierra Madre Oriental mountain range, of which the elevation model for the current topography of the CCB can be seen in Figure 2.4. The CCB floor has an average elevation of 742 m a.s.l although the west of the basin is on average 50 m higher in elevation than the east of the basin [Badino *et al.*, 2004].

Figure 2.4. Topography of the Cuatro Ciénegas Basin. Elevations of the major limestone outcrops and CCB recharge zone are shown [modified after Wolaver *et al.*, 2005].

Despite not being topographically closed, as deep canyons exist between the Sierra Madera and Sierra la Fragua in the NW of the basin; Sierra Menchaca and Sierra Sacramento in the NE of the basin and the Sierra Granizo and Sierra San Marcos y

Pinos in the SW of the basin (Figs. 2.4 and 2.5), the CCB currently acts as a hydrologically closed basin system (endorheic) [Badino *et al.*, 2004]. The CCB displays a high degree of karstification with no surface hydrologic links between the basin and any of the surrounding basins with the exception of streams originating on the high peaks of the surrounding mountains (Fig. 2.5) [Badino *et al.*, 2004; Rodriguez *et al.*, 2005; Wolaver *et al.*, 2008]. Precipitation falls on the high mountain peaks before either evaporating or entering the karst system. The topography observed today in the CCB has been created by precipitation eroding water courses through weaknesses in the natural lithological structures of the Cretaceous limestone ridges. The effect of this erosion, since the Laramide Orogeny in the Eocene (c.55 million years), can be seen as deep canyons directly on the relief of the mountains and accumulation of alluvium on the valley floor (Figs 2.4 and 2.5).

Figure 2.5. Topography of the Cuatro Ciénegas Basin with possible stream locations from the high peaks of the surrounding mountains. Black lines are roads and tracks. Blue lines are proposed water flow paths [modified after Wolaver *et al.*, 2005].

Build up of thick alluvium sequences on the CCB floor due to erosion is well documented [Guzmán, 2001; Badino *et al.*, 2004; Rodriguez *et al.*, 2005; Wolaver *et al.*, 2008], the exact depth is largely unknown, although it is estimated to be in the region

of 200 m [Rodriguez *et al.*, 2005]. As well as alluvium, the effects of erosion can be seen by the large alluvial fans that have deposited at the base of canyons (Fig. 2.6).



Figure 2.6. Alluvial fan deposits at the base of the Sierra Madera, the northern most boundary of the CCB. Incised channels on the alluvial fan deposits suggest they are long standing features [image from www.google.co.uk/earth].

2.1.3 Hydrogeology of the Cuatro Ciénegas Basin

The CCB contains over 200 pools, lakes, springs and rivers. The water bodies are highly variable in origin (e.g. groundwater, hydrothermal, precipitation) and as a result can exhibit extreme variability in salinity (up to hyper saline), temperature (ranging between 18°C and 35°C), water chemistry and spring discharge over small spatial areas [Minckley, 1969; Johannesson *et al.*, 2004; Evans, 2005; Rodriguez *et al.*, 2005; Wolaver *et al.*, 2008].

Figure 2.7. Schematic of water inputs within the basin and flow within the carbonate strata [modified after Badino *et al.*, 2004 and Rodriguez *et al.*, 2005].

The main types of water body in the CCB are source springs (e.g. Poza Becerra, Poza Escobedo), fed directly from upwelling water (Fig. 2.7); pools fed from surface flow and lake systems [Minckley, 1969].

The Cupido-Aurora carbonate aquifer is known to recharge in the CCB and gives rise to the hydrothermal pools, lakes and rivers [Johannesson *et al.*, 2004; Rodriguez *et al.*, 2005; Wolaver *et al.*, 2008]. Early groundwater flow models for the Cupido-Aurora aquifer [Lesser Jones, 1967; Lesser and Lesser, 1988] show that in the vicinity of Monterrey, Nuevo León, Mexico, water recharge occurs through exposed carbonate platforms up to 150 km west of the city, within the Sierra Madre Oriental mountain range, including the CCB, and north-west in the Bolson de Mapimi (Fig. 2.8). It is hypothesised that water flows down the hydrologic gradient, created around 108 Mya (see Chapter 1) from the Bolson de Mapimi in an east-southeast direction towards the Gulf coastal plain. The hydrostatic pressures created by this flow in the limestone of the aquifer have produced flowing artesian wells around the city of Monterrey and coastal plains. Early flow models failed to explain large discharge springs located in the Sierra Madre Oriental and although fractures in the aquifer gives rise to springs in this discharge zone the exact flow regime remains unknown [Johannesson *et al.*, 2004; Rodriguez *et al.*, 2005; Wolaver *et al.*, 2008]. More recent groundwater flow models [Johannesson *et al.*, 2004; Rodriguez *et al.*, 2005; Evans, 2005; Wolaver, 2005; Wolaver *et al.*, 2008] suggest that a significant component of groundwaters in the CCB are recharged in the local mountain ranges surrounding the basin but the hydrothermal pools located predominantly on the western flank, but also on the eastern flank, of the Sierra San Marcos and Pinos recharge from sources outside of the basin, thought to be the Cupido Aurora aquifer.

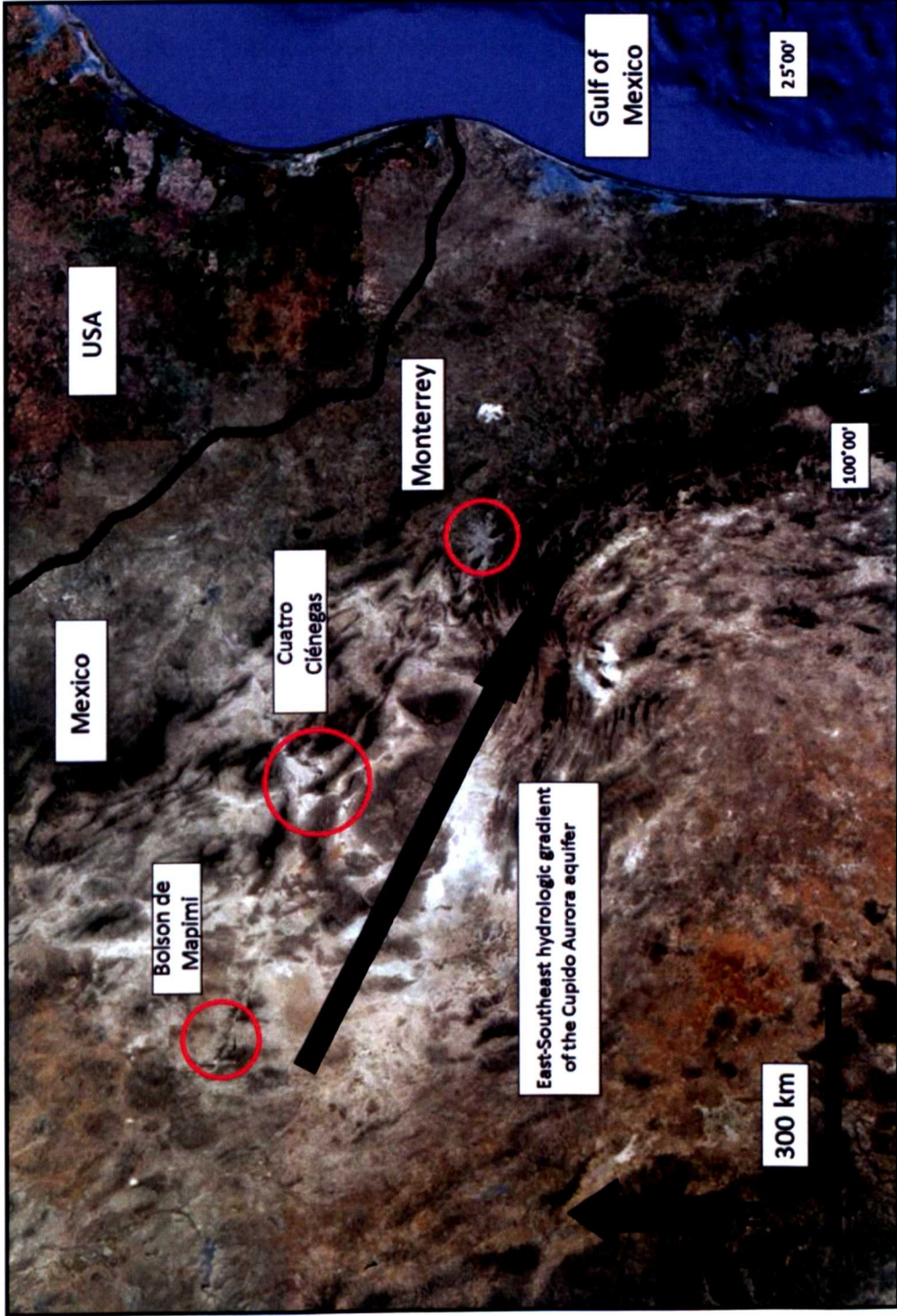


Figure 2.8. Locations of the Bolson de Mapimi, CCB and Monterrey City in NE Mexico. The proposed hydrologic gradient of the Cupido-Aurora aquifer in the direction of the Gulf of Mexico can be seen [image from www.google.co.uk/earth].

The pools within the CCB vary in morphology and depth and can be explained by their geographical position. The basin is effectively split in the middle (N-S axis) by the Sierra San Marcos y Pinos with the basin floor west of this lying approximately 50 m higher than the floor to the east (Fig. 2.4). The hot pools at the piedmont and to the west of the Sierra San Marcos y Pinos are on the sub-vertical side of the Sierra and generally exhibit higher water temperatures, +26.7 to +32.4°C (Fig. 2.9) [Minckley, 1969; Johannesson *et al.*, 2004; Evans, 2005]. These are fed directly from hydrothermal sources, uprising through faults (e.g. Poza Becerra) and natural fissures in the carbonate strata (Fig. 2.7). Hot pools to the east of the Sierra San Marcos are on the less sloping side of the Sierra and group nearer to the centre of the CCB; where the relief is lower (Fig. 2.9). Hydrothermal pools evident on the east side of the basin (Poza Escobedo, +32°C) are fed through a mix of deep hot water rising and meteoric water from interstratal karst (Fig. 2.7) [Minckley, 1969; Badino *et al.*, 2004].

It is interesting to note that pools <20°C appear to group more densely further south on the eastern flank of the Sierra San Marcos y Pinos (Fig. 2.9). No faults or fracture zones are thought to be located in this region of the CCB with the pools forming through subsidence of the basin floor as underground sinkholes (created by karstic flow) collapse e.g. Los Hundidos [Badino *et al.*, 2004]. Wolaver [2005] suggests alluvial fans could be acting as reservoirs for interstratal karst, releasing captured precipitation gradually throughout the year, creating <20°C water bodies. Similarly, alluvial fans may also be preventing upwelling of hydrothermal groundwaters, causing the low density of hot pools observed in the same area (Fig. 2.9).

Figure 2.9. Water body temperature map for the CCB. Greater densities of hot pools (25°C - 35°C) are located around the piedmont of the Sierra San Marcos y Pinos suggesting fault controls. Ambient pools (20°C - 25°C) cluster in a similar area to hot pools suggesting the possibility of mixing with colder pools. Ambient pools <20°C appear to cluster in areas with alluvial fan deposits (see Fig. 2.4 also). Circles represent the temperature of the pools sampled – larger circles represent higher temperatures. Overall map colours are a spatial representation of water temperatures on the CCB floor, based on data collected [modified after Minckley, 1969 and Evans, 2005].

The CCB borders the physiographic boundary between the Sierra Madre Oriental and the Bolson de Mapimi and therefore the groundwater flow regime adheres to the proposed dominant east-southeast direction. However, the differing water bodies of the CCB appear to suggest a very complex mixture of local and regional karst water and groundwater recharge.

2.2 Methods

2.2.1 Water sampling strategy

Water samples were collected for stable oxygen, hydrogen and carbon isotope analysis from 14/3/08 – 17/3/08, using 26 pre-sterilized 250 ml polyethylene terephthalate (PET) plastic bottles.

Water samples for analysis were collected from: 15 pools (Mex 30-2, Poza Churince, Poza Tierra Blanca, Poza de Quintero, Poza Pronatura, Poza Azul 1, Poza Azul 2, Los Hundidos, Yucca Pond, Rim Pond, Poza Juan Santos, Poza Garrabatal, Poza Anteojo, Poza Azul and Poza la Becerra); 3 springs (Mex 30-1, 'Bone Site' and Palm Spring), 2 lakes (Laguna Grande and Laguna Churince); 2 rivers (Rio Mesquites and Rio Mesquites 2), 2 streams (San Marcos and 'Fast Stream'); and 2 salt pools (Charco Rojo and Las Salinas) (Table 2.1; and Figs. 2.10a, 2.10b, 2.10c, 2.10d and 2.10e).

To obtain the best possible range of water sources to best understand the reconnaissance flow regime, locations of water bodies sampled were chosen for their distribution in both the east and west areas of the CCB with GPS coordinates logged. Due to the CCB being a protected area, sampling localities were limited and as such water body samples from the east of the CCB were taken from two main localities: 1) cold pools in close proximity to the Sierra San Marcos y Pinos (Poza Quintero, Poza Pronatura and Los Hundidos) and 2) cold salt pools in the centre of the eastern basin of the CCB (Las Salinas and Charco Rojo). Water body samples from the west of the CCB were again focused around two main localities: 1) a mixture of hot pools (San Marcos, Poza Churince, Laguna Churince and Poza Becerra) and a cold lake (Laguna Grande) in close proximity to the fault zone of the Sierra San Marcos y Pinos and 2) a mixture of hot pools (Poza Juan Santos, Poza Anteojo and Poza Azul), ambient pools (Mex 30-1, Mex 30-2, Poza Azul I and Poza Azul II), ambient rivers (Rio Mesquites 1 and Rio Mesquites 2) and cold pools (Poza Garrabatal, Palm Spring, Rim Pond, Fast Stream, Bone Site, Poza Tierra Blanca and Yucca Pond) centred around the ciénega (marsh) area of the piedmont of the Sierra San Marcos y Pinos.

Calibration problems with the Hanna pH, ORP and temperature meter meant that exact pH and temperature measurements were not taken. Instead qualitative assessments of water body temperature ranges were made on-site using published

water temperature data, sampled in April [Minckley and Cole, 1968; Winsborough, 1990; Minckley, 1992; Johannesson *et al.* 2004], and also with the help of APFFCC staff who have an in-depth knowledge of the CCBs pools, lakes and rivers. The decision to not re-sample water for temperature and pH from the 26 localities on subsequent visits to the CCB was taken. This was due to the later visits taking place in January, as opposed to March when the original samples were taken, where differences in seasonality, flow relatedness, source water, atmospheric temperature, wind and evaporation flux could have adversely affected any repeated lab based analyses [Hirsch *et al.* 1982; Michel, 1992; Vega *et al.* 1998; Bade *et al.* 2004].

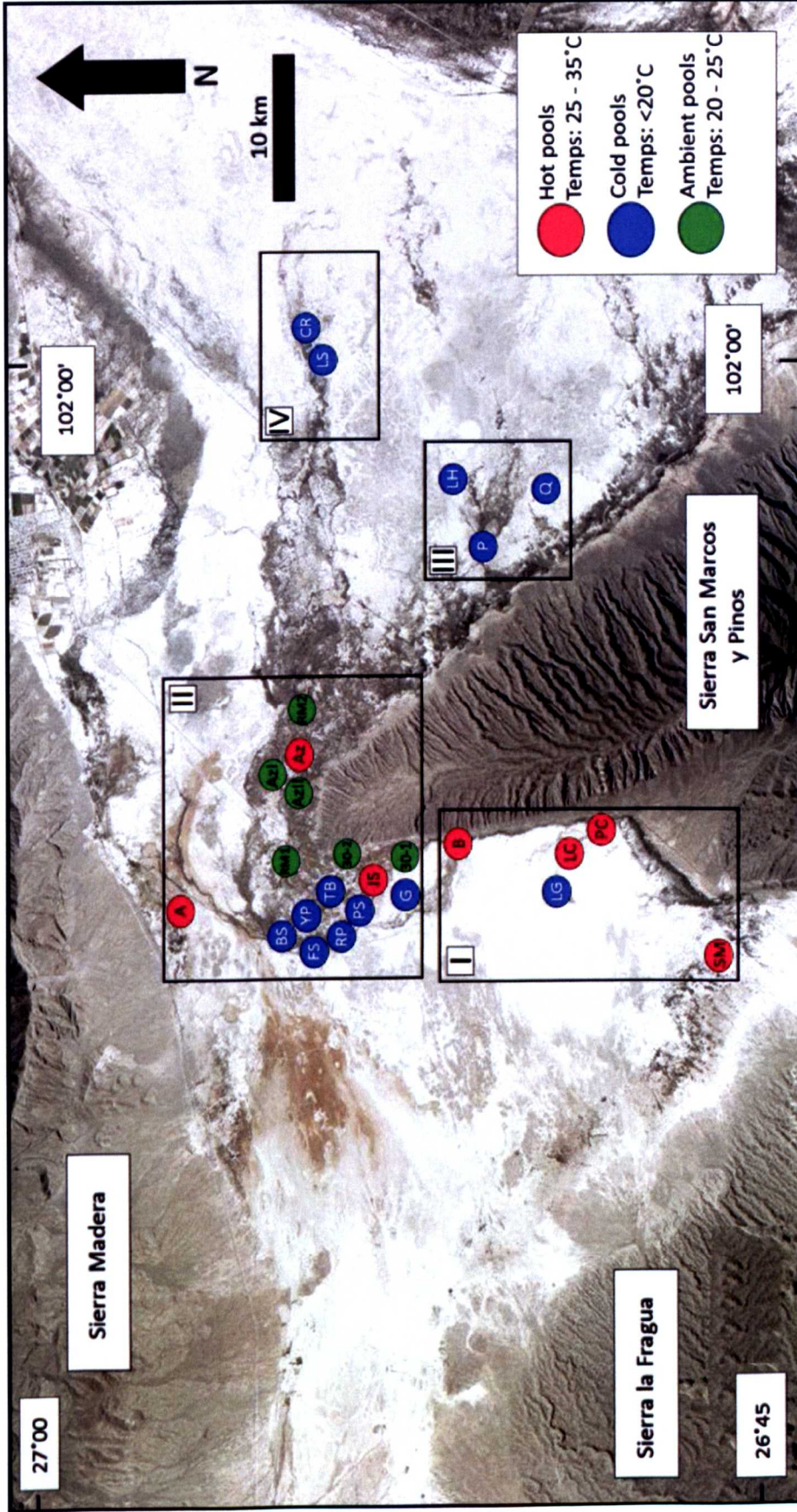


Figure 2.10a. Water isotope sample locations were separated into four areas (I, II, III and IV) within the Cuatro Ciénegas Basin. Sample codes are as follows: SM – San Marcos; PC – Poza Churince; LC – Laguna Churince; LG – Laguna Grande; B – Poza Becerra; G – Poza Garrabatal; 30-1 – Mex 30-1; JS – Poza Juan Santos; PS – Palm Spring; RP – Rim Pond; FS – Fast Stream; TB – Poza Tierra Blanca; YP – Yucca Pond; BS - Bone Site; 30-2 – Mex 30-2; A – Poza Anteojo; RM1 – Rio Mesquites; AzII – Poza Azul II; Az I – Poza Azul I; Az – Poza Azul; RM2 – Rio Mesquites 2; Q – Poza Quintero; P – Poza Pronatura; LH – Los Hundidos; LS – Las Salinas; CR – Charco Rojo [image from www.google.co.uk/earth]. See also enlarged images from figures 2.9b to 2.9e.

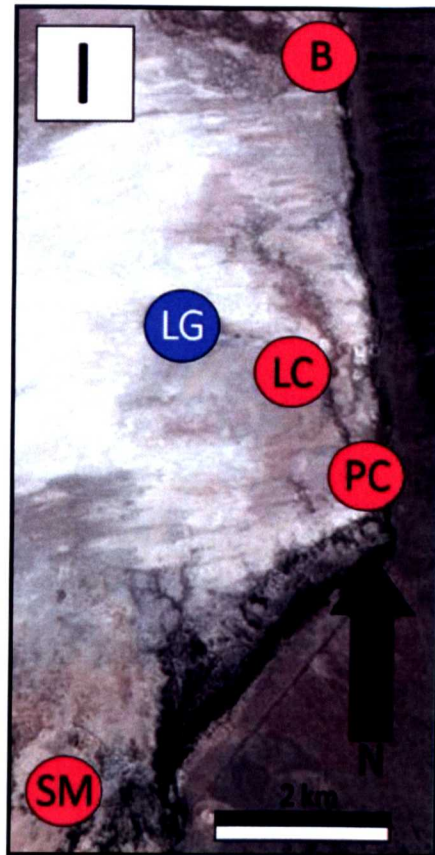


Figure 2.10b. Enlarged map of location I (Fig. 2.10a). SM – San Marcos; PC – Poza Churince; LC – Laguna Churince; LG – Laguna Grande; B – Poza Becerra [image from www.google.co.uk/earth].

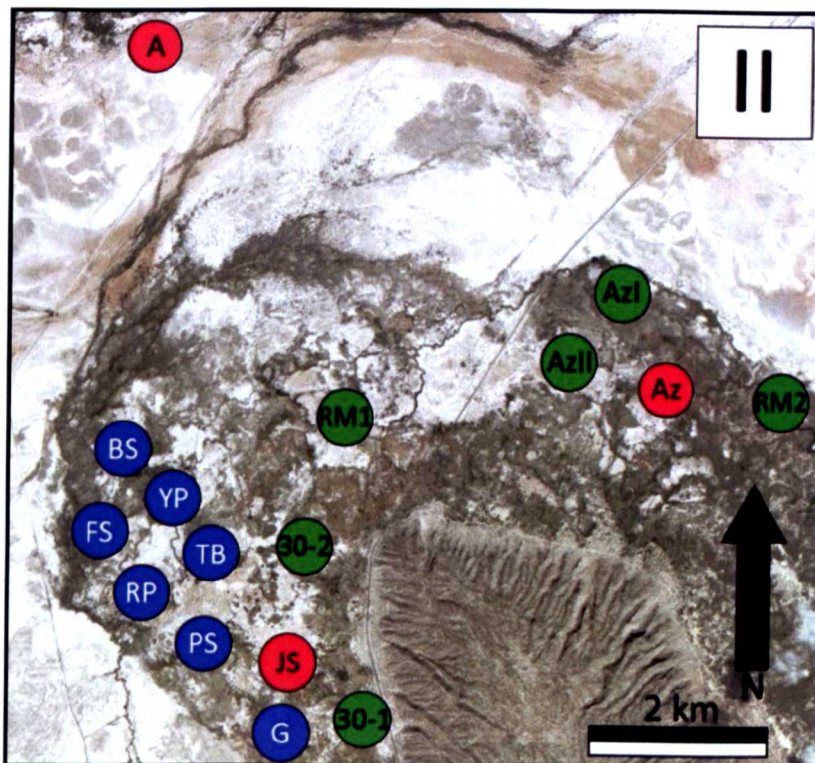


Figure 2.10c. Enlarged map of location II (Fig. 2.10a). G – Poza Garrabatal; 30-1 – Mex 30-1; JS – Poza Juan Santos; PS – Palm Spring; RP – Rim Pond; FS – Fast Stream; TB – Poza Tierra Blanca; YP – Yucca Pond; BS - Bone Site; 30-2 – Mex 30-2; A – Poza Anteoyo; RM1 – Rio Mesquites; AzII – Poza Azul II; Az I – Poza Azul I; Az – Poza Azul; RM2 – Rio Mesquites 2 [image from www.google.co.uk/earth].

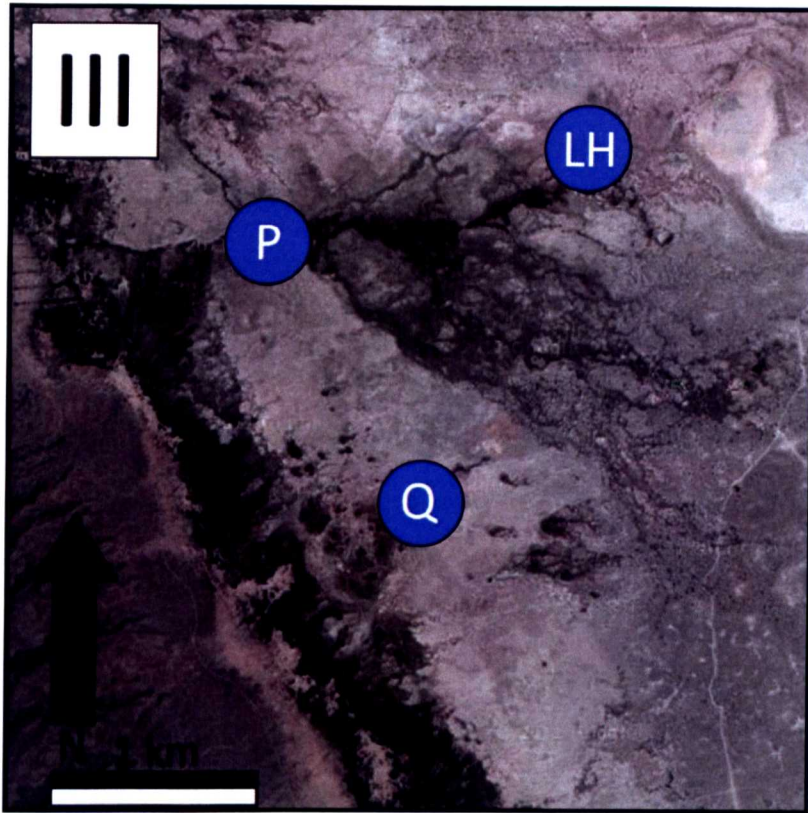


Figure 2.10d. Enlarged map of location III (Fig. 2.10a). Q – Poza Quintero; P – Poza Pronatura; LH – Los Hundidos [image from www.google.co.uk/earth].

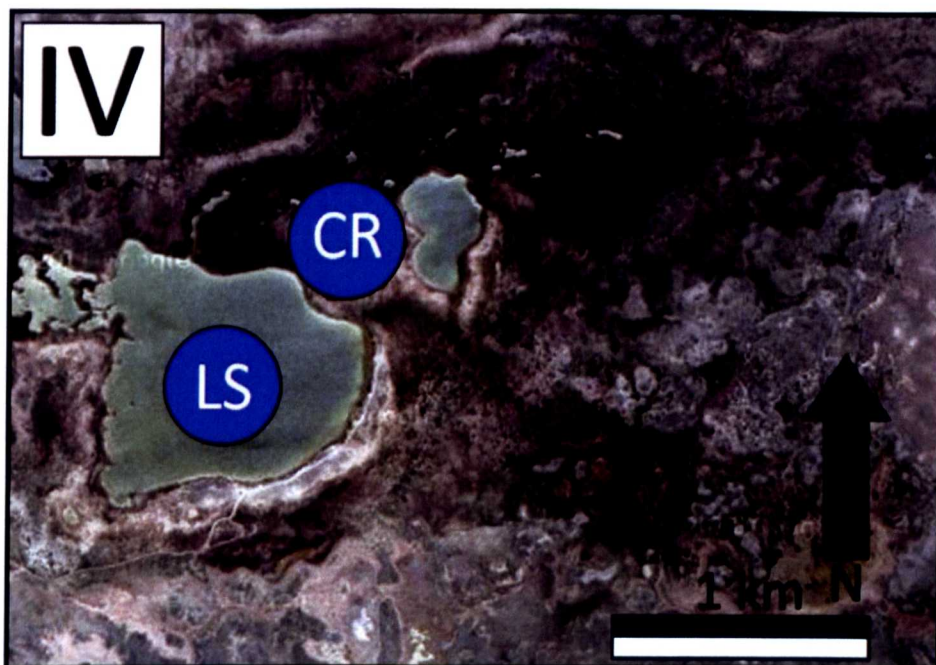


Figure 2.10e. Enlarged map of location IV (Fig. 2.10a). LS – Las Salinas; CR – Charco Rojo [image from www.google.co.uk/earth].

2.2.2 $\delta^{18}\text{O}$ and δD method

Sample bottles were flushed and overfilled in the collection water three times prior to collection. Samples were collected from the epilimnion (30 cm below the air-water interface) and capped tightly before being stored in cooler box, in the dark until they could be stored in a fridge. Samples were transported back from Mexico in a refrigerated box and subsequently kept in a refrigerator at the NERC (Natural Environment Research Council) Isotope Geosciences Laboratory, Keyworth, Nottingham until they were analysed at the same location (within 1 to 2 weeks of sampling). The 250 ml water samples were equilibrated with CO_2 using an Isoprep 18 device for oxygen isotope analysis with mass spectrometry performed on a VG SIRA. For hydrogen isotope analysis, an on-line Cr reduction method was used with a EuroPyrOH-3110 system coupled to a Micromass Isoprime mass spectrometer. Isotopic ratios ($^{18}\text{O}/^{16}\text{O}$ and $^2\text{H}/^1\text{H}$) are expressed in delta units, $\delta^{18}\text{O}$ and δD (‰, parts per mil), and defined in relation to the international standard, VSMOW (Vienna Standard Mean Ocean Water). NIGL analytical precision (reproducibility) for water samples is $\pm 0.08\text{‰}$ for $\delta^{18}\text{O}$ and $\pm 1.0\text{‰}$ for δD (2σ).

2.2.3 Carbonate (Dissolved Inorganic Carbon) method

Dissolved Inorganic Carbon (DIC) analysis was conducted at the NERC Isotope Geoscience Laboratory (NIGL), Keyworth, Nottingham. After precipitation of the bicarbonate from the water samples, the bicarbonate was filtered to leave only fine fraction material, before being washed with deionised water and dried at 40°C and ground in agate. The carbonate was reacted with anhydrous phosphoric acid *in vacuo* overnight at a constant 25°C . The CO_2 liberated was separated from water vapour under vacuum and collected for analysis. Measurements were made on a VG Optima mass spectrometer. Isotope values ($\delta^{13}\text{C}$) are reported as per mil (‰) deviations of the isotopic ratio ($^{13}\text{C}/^{12}\text{C}$) calculated to the VPDB scale using a within-run laboratory standard calibrated against NBS standards. NIGL analytical precision (reproducibility) for bicarbonate samples is normally better than $\pm 0.1\text{‰}$ for $\delta^{13}\text{C}$ (2σ).

2.3 Results

2.3.1 Stable $\delta^{18}\text{O}$ and δD

$\delta^{18}\text{O}$ and δD isotope data for the 26 locations in the CCB are presented in Table 2.1 and are plotted by map area (Figs. 2.10a, 2.10b, 2.10c, 2.10d and 2.10e) on figures 2.11, 2.12, 2.13, 2.14 with figure 2.15 showing the overall spatial distribution of $\delta^{18}\text{O}$ vs. δD in the CCB. $\delta^{18}\text{O}$ and δD isotope data are also plotted by water body temperature on Figures 2.16, 2.17, 2.18, 2.19 and 2.20 using linear regression to investigate if water body temperature has an effect on the $\delta^{18}\text{O}$ vs. δD relationship.

Figure 2.15 shows $\delta^{18}\text{O}$ and δD isotope data for the 26 locations alongside the LMWL (Local Meteoric Water Line) from Chihuahua [Cortés *et al.*, 1997] and GMLW (Global Meteoric Water Line [Craig, 1961]. $\delta^{18}\text{O}$ and δD values of precipitation in the CCB are thought to be -8.3‰ and -55.8‰ respectively, although no meteoric water line is available [Wassenaar *et al.*, 2009]. The CCB is, however, geographically bound by Monterrey and Chihuahua (Bolson de Mapimi) (Fig. 2.8) which have almost identical meteoric water lines: $\delta D = 6.8\delta^{18}\text{O} + 1.85$ and $\delta D = 7\delta^{18}\text{O} + 1.9$ respectively [Cortés *et al.*, 1997]. The strong similarity in both LMWL's for Monterrey and Chihuahua suggests that the CCB is likely to be similar, since the CCB forms part of the Chihuahuan Desert and it is thought the Cupido-Aurora aquifer, providing groundwater to the CCB, originates here [Johannesson *et al.*, 2004; Rodriguez *et al.*, 2005; Wolaver *et al.*, 2008], it is therefore reasonable to use the Chihuahuan LMWL. The similarity in LMWL also suggests that the regional meteoric water sources arise from the same precipitation sources – the Gulf of Mexico during the summer months and the Pacific Ocean during the winter months [Johannesson *et al.*, 2004].

All of the isotopic water samples plot to the right of the GMWL [Craig, 1961] and the LMWL [Cortés *et al.*, 1997] in the CCB (Fig. 2.15). Of the 26 samples, 22 of them are grouped together with $\delta^{18}\text{O}$ and δD values of the water ranging from -6.92‰ to -5.67‰ and -50.3‰ and -44‰ respectively (Fig. 2.15). Poza Anteojos water plots very closely to the LMWL with $\delta^{18}\text{O}$ and δD values of the water of -7.99‰ and -54.8‰ respectively (Figs. 2.12 and 2.15). Three main outliers are evident on Figure 2.15, all plotting with positive $\delta^{18}\text{O}$ values – Laguna Grande ($\delta^{18}\text{O}$ value of the water was $+1.17\text{‰}$, δD value of the water was -10‰), Las Salinas ($\delta^{18}\text{O}$ value of the water was

+2.98‰, δD value of the water was -2‰) and Charco Rojo ($\delta^{18}\text{O}$ value of the water was $+4.97\text{‰}$, δD value of the water was $+0.3\text{‰}$). These three samples have much higher values of both $\delta^{18}\text{O}$ and δD relative to the other 23 samples, with Laguna Grande plotting 6.84‰ and 34‰ higher than Los Hundidos (Fig. 2.15) for $\delta^{18}\text{O}$ and δD respectively.

Using a linear regression line through the data for 23 water bodies (Fig. 2.15), a Local Evaporation Line (LEL) of $\delta D = 4.4\delta^{18}\text{O} - 19.5$ is proposed. The LEL shows a high correlation coefficient ($R^2 = 0.96$) and crosses the LMWL at -8.3‰ and -55.8‰ (the modern isotopic composition of precipitation in the CCB) for $\delta^{18}\text{O}$ and δD respectively. Although Laguna Grande, Las Salinas and Charco Rojo water samples display positive $\delta^{18}\text{O}$ values, they still plot very close to the proposed LEL.

However, Map III water samples (Figs. 2.10d and 2.13) plot along the same LEL as Maps I, II and IV (Fig. 2.15). The possibility of a secondary flow system is interesting as the first pool of the secondary flow system, Poza Quintero, displays a similar $\delta^{18}\text{O}$ water value (-6.84‰) to that of Poza Churince (-6.92‰). However, Poza Quintero has low water temperature ($<20^\circ\text{C}$) whereas Poza Churince has a higher water temperature ($>25^\circ\text{C}$ - 35°C) suggesting that, despite similarity in the isotopic composition of their source waters, both pools have different sources and separate flow systems. Map III samples being taken on the east flank of the Sierra San Marcos y Pinos, as opposed to the west flank (Maps I and II), and the adherence to the LEL suggests the possibility of a secondary evaporative enrichment system.

Table 2.1. Water isotope values ($\delta^{18}\text{O}$, δD and $\delta^{13}\text{C}_{\text{DIC}}$), facies and location for samples taken in the CCB.

Code	Location	Map/Code (Fig. 2.9)	Lat (N°)/Long (W°)	Facies	Date	Temp	$\delta^{18}\text{O}$	δD	$\delta^{13}\text{C}$
cc/5	Poza Churince	I (PC)	26°50'24.76"/102°08'02.40"	pool	14.3.08	Hot (25°C - 35°)	-6.92	-50.3	-19.8
cc/4	San Marcos	I (SM)	26°48'22.51"/102°09'23.08"	pool	14.3.08	Hot (25°C - 35°)	-6.68	-49.6	
cc/26	Poza Becerra	I (B)	26°52'42.98"/102°08'17.27"	pool	17.3.08	Hot (25°C - 35°)	-6.63	-48.9	
cc/6	Laguna Churince	I (LC)	26°50'54.00"/102°08'30.03"	lake	14.3.08	Hot (25°C - 35°)	-5.71	-45.3	-15.1
cc/7	Laguna Grande	I (LG)	26°51'09.51"/102°09'05.15"	lake	14.3.08	Ambient (<20°C)	+1.17	-10.0	-13.9
cc/22	Poza Anteojo	II (A)	26°58'04.58"/102°07'38.22"	pool	16.3.08	Hot (25°C - 35°)	-7.99	-54.8	-15.7
cc/21	Poza Garrabatal	II (G)	26°53'42.71"/102°08'42.02"	pool	16.3.08	Ambient (<20°C)	-6.58	-47.9	-17.6
cc/23	Poza Azul	II (Az)	26°55'21.41"/102°07'20.84"	pool	17.3.08	Hot (25°C - 35°)	-6.51	-48.0	-13.2
cc/1	Mex30-1	II (30-1)	26°53'42.65"/102°08'31.57"	spring	14.3.08	Ambient (20°C - 25°C)	-6.37	-48.7	-12.4
cc/20	Poza Juan Santos	II (JS)	26°53'52.00"/102°08'53.82"	pool	16.3.08	Hot (25°C - 35°)	-6.35	-47.5	-11.1
cc/16	Palm spring	II (PS)	26°54'27.71"/102°09'24.41"	spring	16.3.08	Ambient (<20°C)	-6.34	-47.1	-9.2
cc/3	Rio Mesquites	II (RM1)	26°55'14.53"/102°08'21.31"	river	14.3.08	Ambient (20°C - 25°C)	-6.27	-48.3	-21.6
cc/13	Poza Azul II	II (Az II)	26°55'47.60"/102°07'30.35"	pool	15.3.08	Ambient (20°C - 25°C)	-6.24	-47.1	-10.8
cc/12	Poza Azul I	II (Az I)	26°55'52.82"/102°07'28.28"	pool	15.3.08	Ambient (20°C - 25°C)	-6.16	-47.0	-14.7
cc/24	Rio Mesquites 2	II (RM2)	26°55'23.11"/102°07'06.48"	river	17.3.08	Ambient (20°C - 25°C)	-6.14	-45.7	-11.8
cc/9	Bone site	II (BS)	26°54'59.46"/102°07'19.13"	spring	14.3.08	Ambient (<20°C)	-6.13	-46.3	-13.4
cc/19	Fast stream	II (FS)	26°54'46.38"/102°09'41.42"	stream	16.3.08	Ambient (<20°C)	-5.84	-45.3	-10.0
cc/17	Yucca pond	II (YP)	26°54'45.89"/102°09'13.89"	pool	16.3.08	Ambient (<20°C)	-5.79	-45.1	-10.2
cc/18	Rim pond	II (RP)	26°54'38.16"/102°09'38.48"	pool	16.3.08	Ambient (<20°C)	-5.75	-45.5	-18.8
cc/2	Mex30-2	II (30-2)	26°54'19.04"/102°09'12.56"	pool	14.3.08	Ambient (20°C - 25°C)	-5.75	-45.2	-10.4
cc/8	Poza Tierra Blanca	II (TB)	26°54'38.24"/102°09'10.30"	pool	14.3.08	Ambient (<20°C)	-5.68	-44.5	-18.0
cc/10	Poza de Quintero	III (Q)	26°51'09.31"/102°03'09.70"	pool	15.3.08	Ambient (<20°C)	-6.84	-50.1	-13.3
cc/11	Poza Pronatura	III (P)	26°51'47.53"/102°02'31.15"	pool	15.3.08	Ambient (<20°C)	-6.80	-49.4	-16.2
cc/14	Los Huididos	III (LH)	26°51'59.35"/102°01'54.77"	pool	15.3.08	Ambient (<20°C)	-5.67	-44.0	-14.8
cc/25	Las Salinas	IV (LS)	26°54'42.90"/102°00'50.64"	salt pool	17.3.08	Ambient (<20°C)	+2.98	-2.0	-17.5
cc/15	Charco Rojo	IV (CR)	26°54'53.40"/102°00'33.23"	salt pool	15.3.08	Ambient (<20°C)	+4.97	0.3	

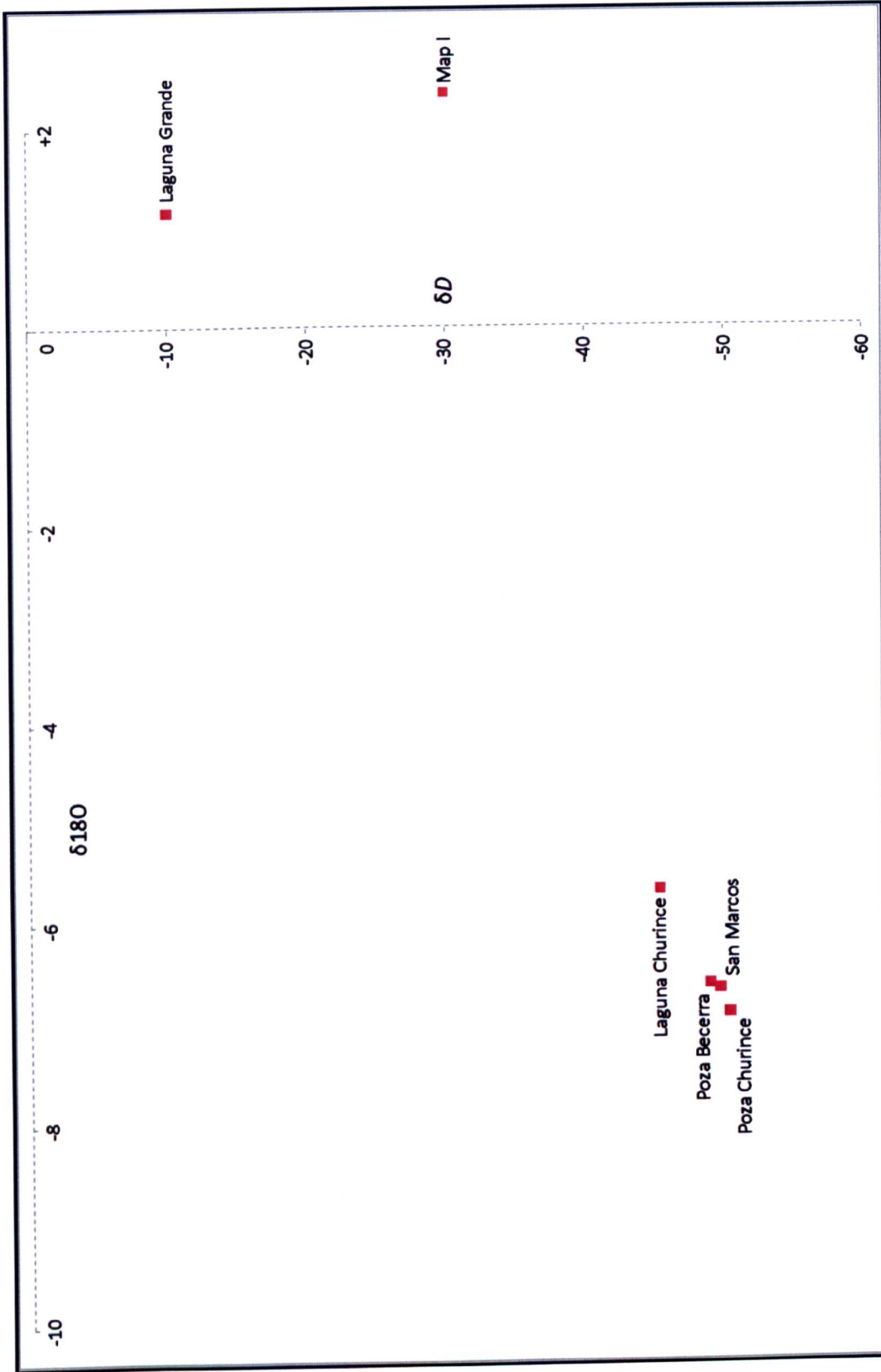


Figure 2.11. $\delta^{18}O$ vs. δD water isotope values within the Cuatro Ciénegas Basin for location I (Fig. 2.10b).

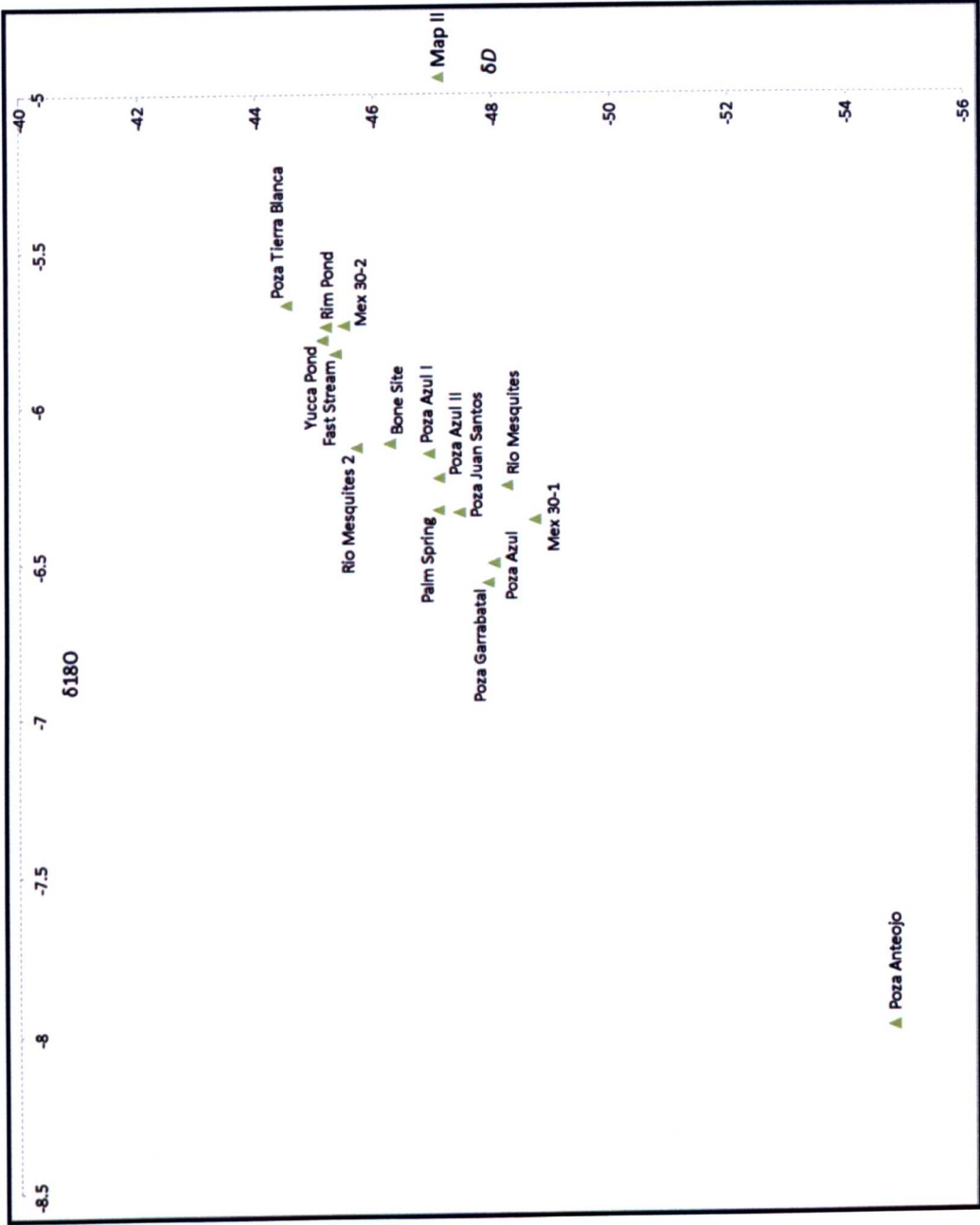


Figure 2.12. δ¹⁸O vs. δD water isotope values within the Cuatro Ciénegas Basin for location II (Fig. 2.10c).

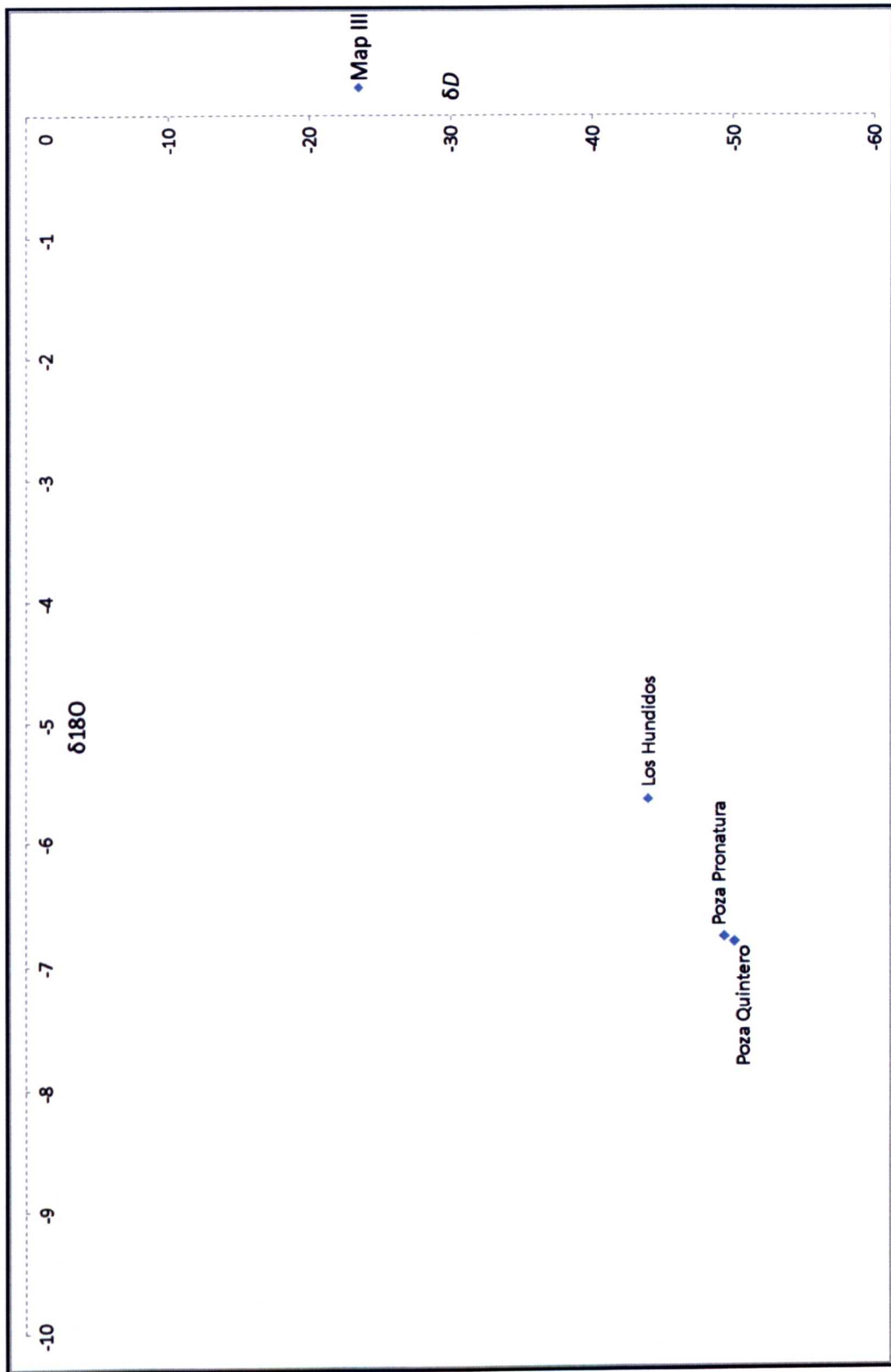


Figure 2.13. $\delta^{18}\text{O}$ vs. δD water isotope values within the Cuatro Ciénegas Basin for location III (Fig. 2.10d).

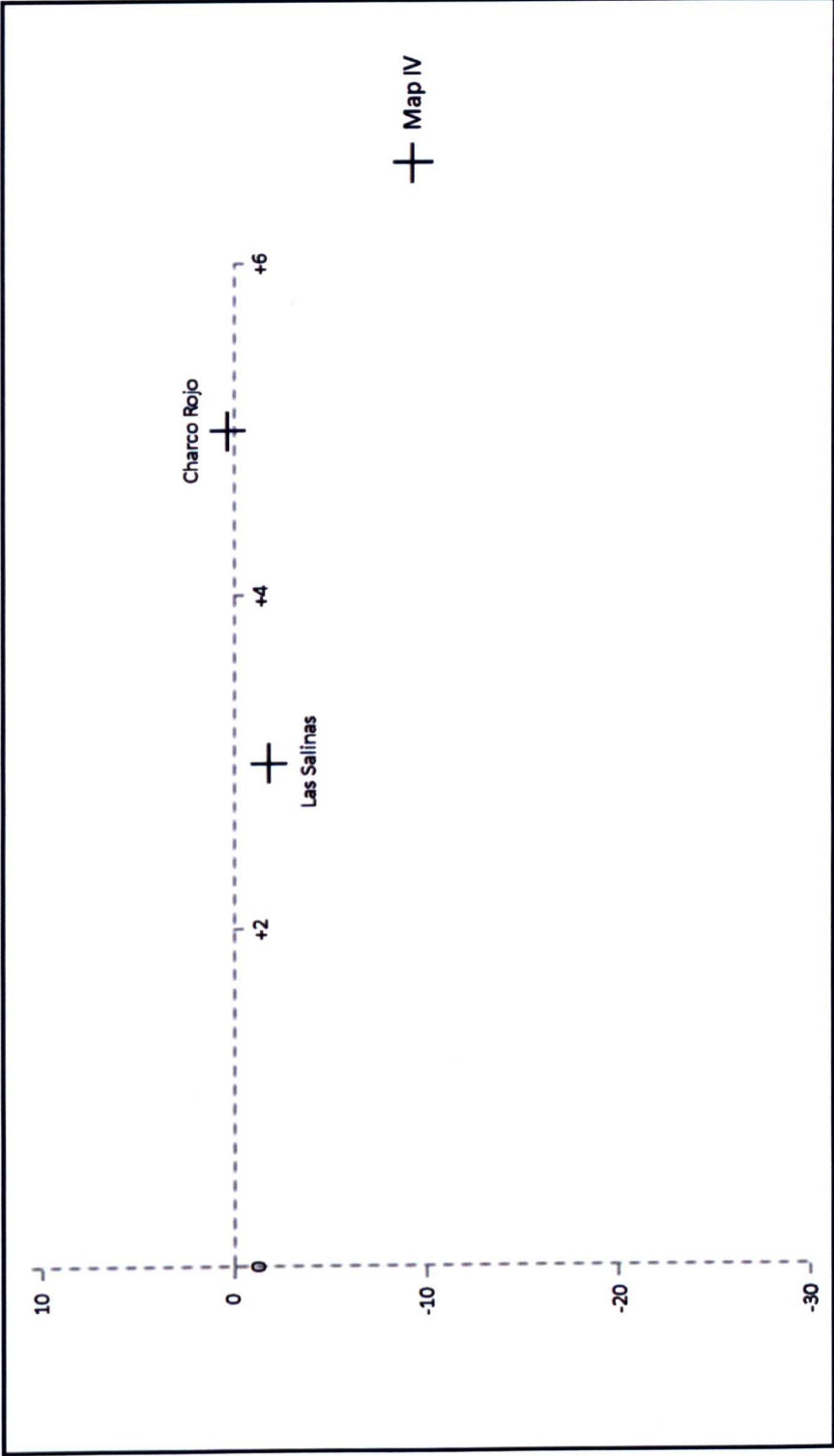


Figure 2.14. $\delta^{18}\text{O}$ vs. δD water isotope values within the Cuatro Ciénegas Basin for location IV (Fig. 2.10e).

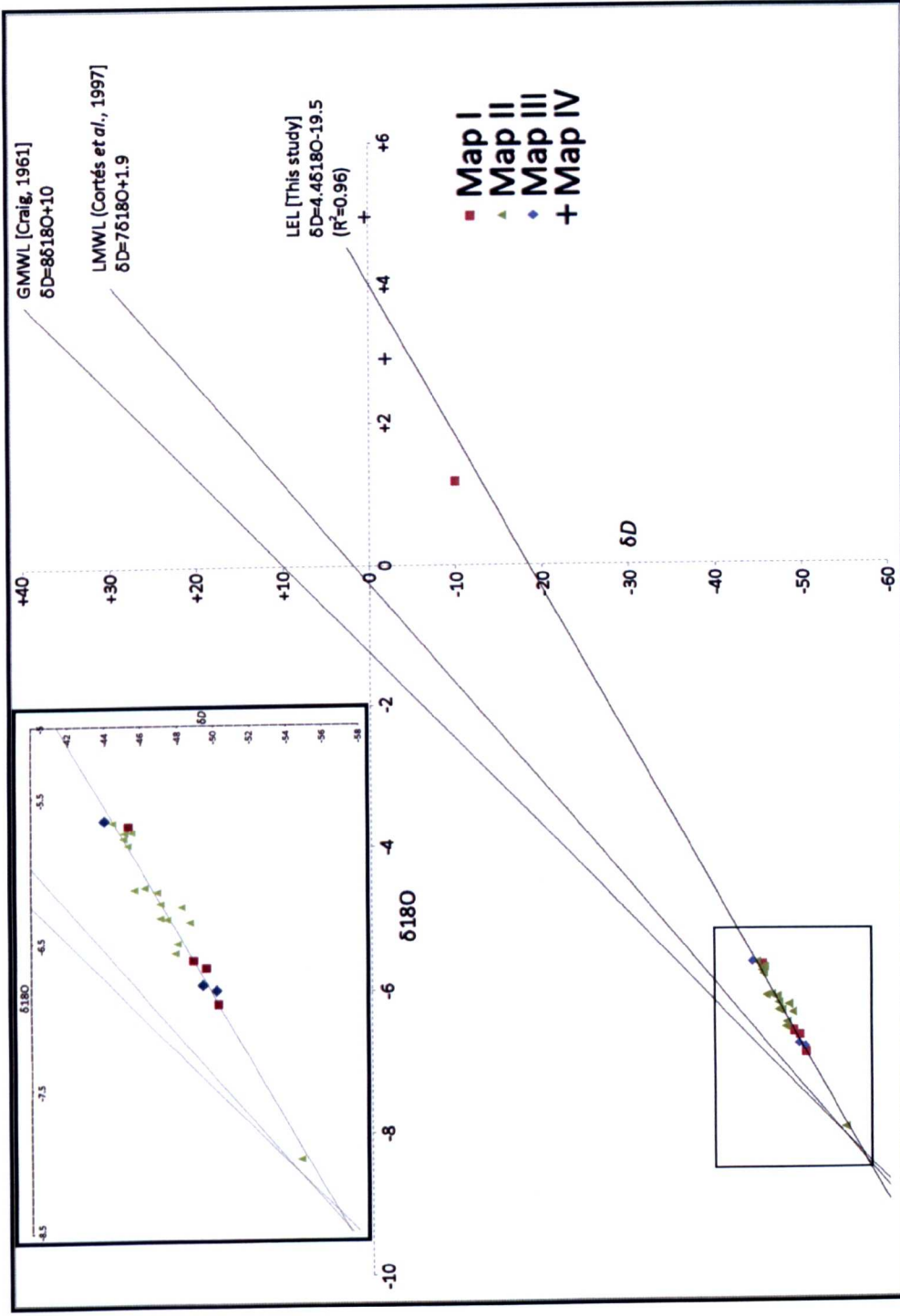


Figure 2.15. $\delta^{18}\text{O}$ vs. δD water isotope values within the Cuatro Ciéngas Basin, plotted by location (Fig. 2.10a). The GMWL [Craig, 1961] and LMWL [Cortés *et al.*, 1997] are displayed with CCB residual water plotting to the right as a Local Evaporation Line (LEL) $\delta D = 4.46^{18}\text{O} - 19.5$. The inset shows the main cluster of data points in more detail so map areas (I-IV) are more easily interpreted.

2.3.1.1 Water body temperature vs. $\delta^{18}\text{O}$ and δD

$\delta^{18}\text{O}$ and δD values of the water bodies are plotted by water body temperature on Figures 2.16 (25°C - 35°C), 2.17 (20°C - 25°C), 2.18 (<20°C), 2.19 (<20°C minus outliers) and 2.20.

Hot water bodies (25°C - 35°C) $\delta^{18}\text{O}$ values range from -7.99‰ to -5.71‰ (Table 2.1; Fig. 2.16) with a mean value of -6.68‰ ($n = 7$). Taking away the main outlier (Poza Anteojó) gives a $\delta^{18}\text{O}$ range of -6.92‰ to -5.71‰, producing a slightly higher mean value of -6.45‰ ($n = 6$). Ambient water bodies (20°C - 25°C) $\delta^{18}\text{O}$ values range from -6.37‰ to -5.75‰ (Table 2.1; Fig. 2.17) with a mean value of -6.15‰ ($n = 6$). Cold water bodies (<20°C) $\delta^{18}\text{O}$ values range from -6.84‰ to +4.97‰ (Table 2.1; Fig. 2.18) with a mean value of -4.02‰ ($n = 13$). Taking away the three main outliers (Laguna Grande, Las Salinas and Charco Rojo) gives a $\delta^{18}\text{O}$ range of -6.84‰ to -5.67‰ (Table 2.1; Fig. 2.19), producing a much lower mean value of -6.14‰ ($n = 10$).

Hot and <20°C ambient water bodies (Figs. 2.16 and 2.18 respectively) display very similar, good linear relationships ($R^2 = 0.99$), adhering to the LEL (Fig. 2.20). The three samples displaying the most ^{18}O enriched water (Laguna Grande, Las Salinas and Charco Rojo with $\delta^{18}\text{O}$ of +1.17‰, +2.98‰ and +4.97‰ respectively) are all <20°C and the one sample displaying the most ^{18}O depleted water (Poza Anteojó with $\delta^{18}\text{O}$ of -7.99‰) is hot (25°C - 35°C). Figures 2.18 and 2.19 show <20°C water bodies with and without the most ^{18}O enriched waters respectively, the similar linear regression lines ($R^2 = 0.99$ and 0.96 respectively) suggest high $\delta^{18}\text{O}$ values are not water body temperature related as including them does not significantly change the correlation of the samples. The similarity of the data between the two extremes of temperature (25°C - 35°C vs. <20°C) also suggests water temperature of an individual water body does not have a direct effect on the isotopic composition of that water body.

20°C - 25°C ambient water bodies (Fig. 2.17) display a less strong linear relationship ($R^2 = 0.74$) than hot and <20°C ambient water bodies (both $R^2 = 0.99$). All the 20°C - 25°C ambient water bodies plot within the -7.99‰ to +4.97‰ $\delta^{18}\text{O}$ isotopic range for 25°C - 35°C and <20°C water bodies (Fig. 2.20).

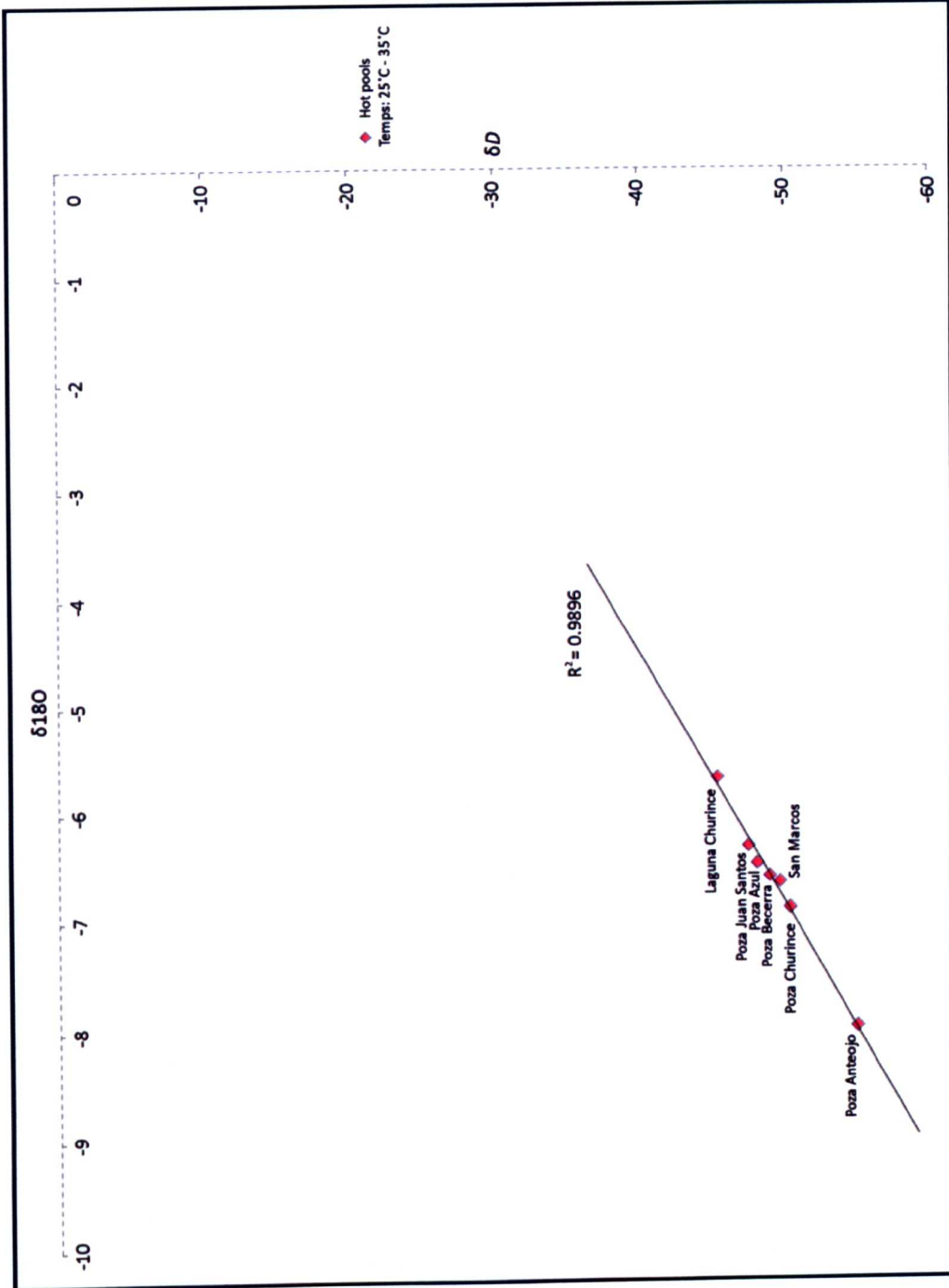


Figure 2.16. $\delta^{18}\text{O}$ vs. δD water isotope values within the Cuatro Ciénegas Basin plotted by hot water body temperature (25°C - 35°C).

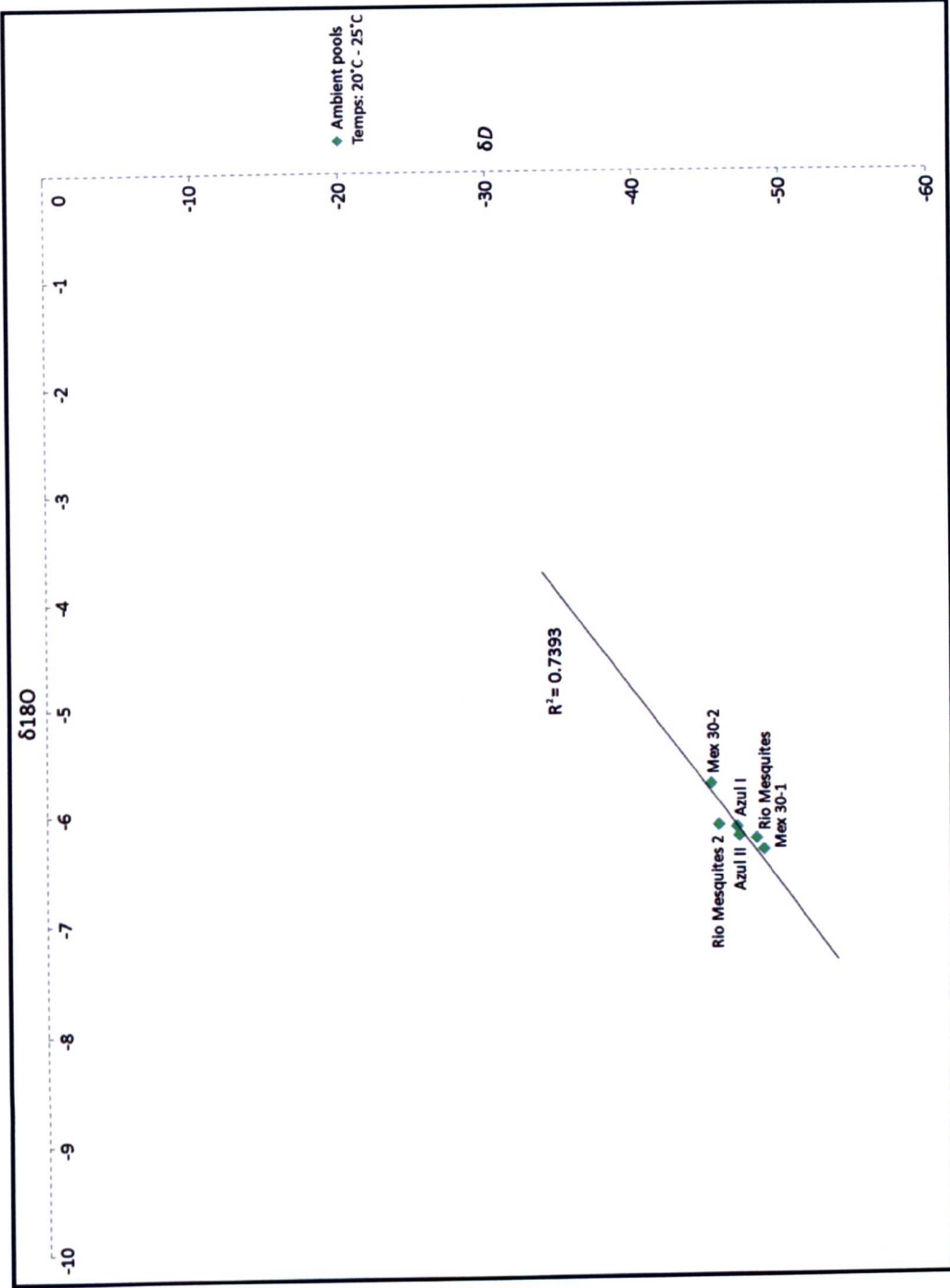


Figure 2.17. $\delta^{18}\text{O}$ vs. δD water isotope values within the Cuatro Ciénegas Basin plotted by ambient water body temperature (20°C - 25°C).

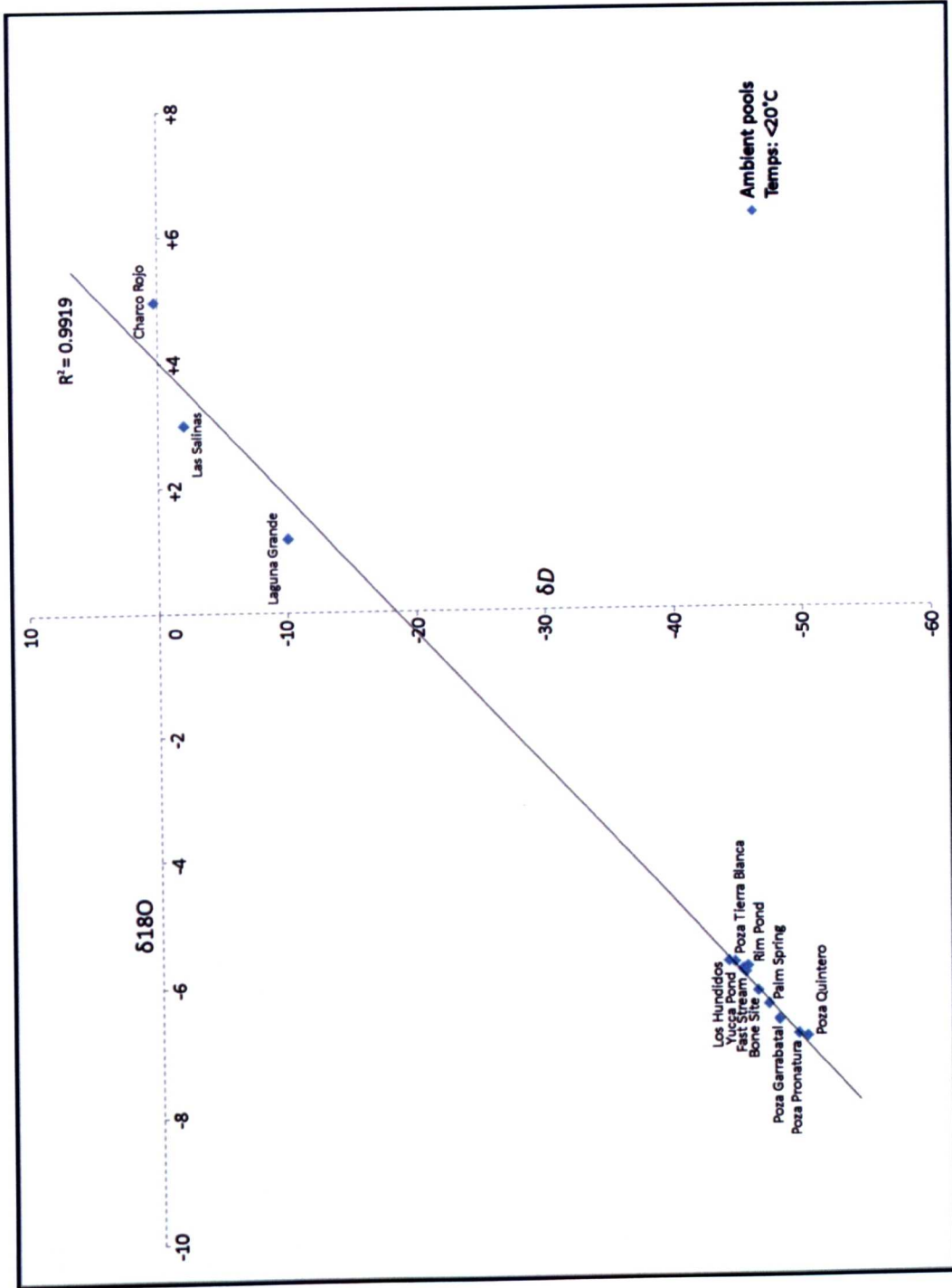


Figure 2.18. $\delta^{18}O$ vs. δD water isotope values, with high $\delta^{18}O$ value samples, within the Cuatro Ciénegas Basin plotted by ambient water body temperature (<20°C).

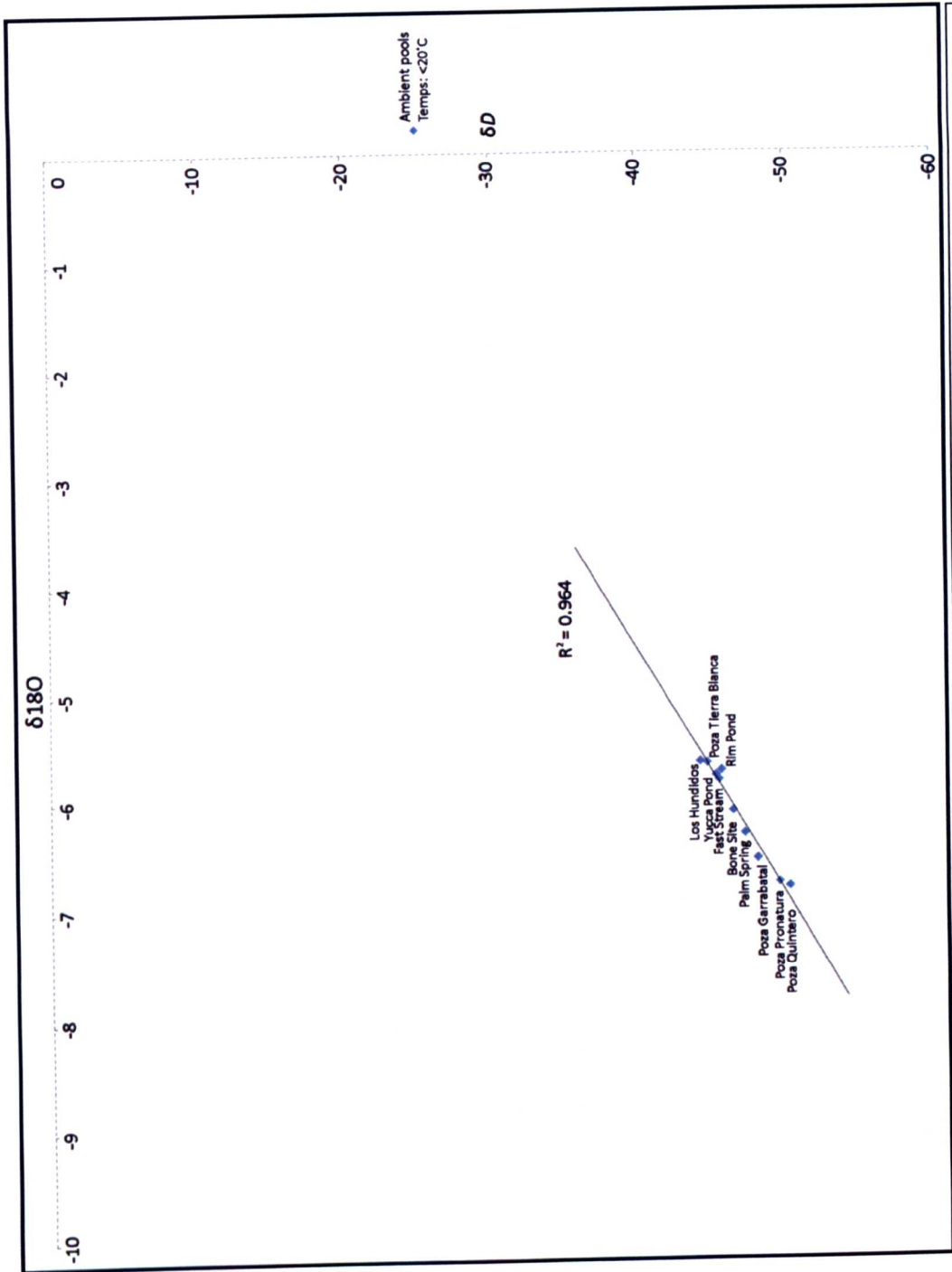


Figure 2.19. $\delta^{18}\text{O}$ vs. δD water isotope values, without high $\delta^{18}\text{O}$ value samples, within the Cuatro Ciénegas Basin plotted by ambient water body temperature (<20°C).

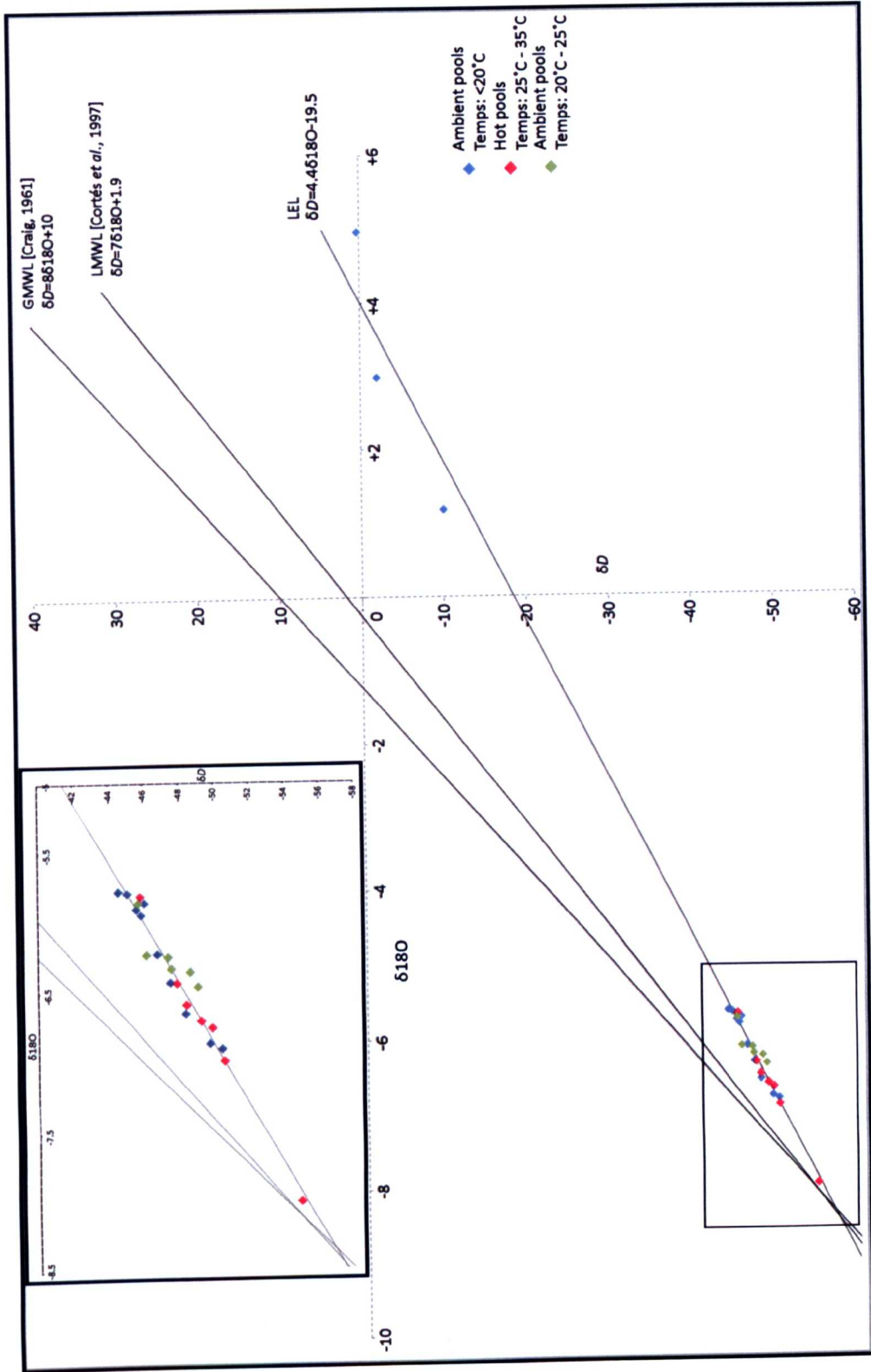


Figure 2.20. $\delta^{18}\text{O}$ vs. δD water isotope values within the Cuatro Ciénegas Basin, plotted by water body temperature. The GMWL [Craig, 1961] and LMWL [Cortés et al., 1997] are displayed with CCB residual water plotting to the right as a Local Evaporation Line (LEL) $\delta\text{D} = 4.46^{18}\text{O} - 19.5$.

2.3.2 $\delta^{18}\text{O}$ vs. $\delta^{13}\text{C}_{\text{DIC}}$ from water carbonate

$\delta^{18}\text{O}$ vs. $\delta^{13}\text{C}_{\text{DIC}}$ isotope data for the 26 locations in the CCB are presented in Table 2.1 and are plotted by map area (Figs. 2.10a, 2.10b, 2.10c, 2.10d and 2.10e) on Figures 2.21, 2.22, 2.23 and 2.24 with Figure 2.25 showing the overall spatial distribution of $\delta^{18}\text{O}$ vs. $\delta^{13}\text{C}_{\text{DIC}}$ in the CCB. $\delta^{18}\text{O}$ vs. $\delta^{13}\text{C}_{\text{DIC}}$ isotope data are also plotted by water body temperature on Figures 2.26, 2.27, 2.28 and 2.29 using linear regression to investigate if water body temperature has an effect on the isotopic composition of the water samples. Pozas San Marcos, Becerra and Charco Rojo did not contain sufficient amounts of bicarbonate for $\delta^{13}\text{C}_{\text{DIC}}$ analysis so do not plot on any of the figures.

$\delta^{18}\text{O}$ vs. $\delta^{13}\text{C}_{\text{DIC}}$ from modern water samples are plotted in figure 2.26, 2.27, 2.28 and 2.29. They do not display a strong relationship with each other, ranging from -21.6‰ to -9.2‰ (mean -14.8‰ , $n = 23$). Hot water body ($25^{\circ}\text{C} - 35^{\circ}\text{C}$) $\delta^{13}\text{C}_{\text{DIC}}$ values range from -19.8‰ to -13.2‰ (Table 2.1; Fig. 2.26) with a mean value of -15‰ ($n = 5$). Linear regression through the hot water data indicates no relationship between samples ($R^2 = 0.1$). Ambient water body ($20^{\circ}\text{C} - 25^{\circ}\text{C}$) $\delta^{13}\text{C}_{\text{DIC}}$ values range from -21.6‰ to -10.4‰ (Table 2.1; Fig. 2.27) with a mean value of -13.6‰ ($n = 6$). Rio Mesquites (RM1) appears to be an outlier with the lowest $\delta^{13}\text{C}_{\text{DIC}}$ value (-21.6‰). Without this water sample included, $\delta^{13}\text{C}_{\text{DIC}}$ values range from -14.7‰ to -10.4‰ with a higher mean value of -12‰ ($n = 5$). Linear regression through the ambient ($20^{\circ}\text{C} - 25^{\circ}\text{C}$) water data indicates no relationship between samples ($R^2 = 0.1$). Cold water body ($<20^{\circ}\text{C}$) $\delta^{13}\text{C}_{\text{DIC}}$ values range from -18.8‰ to -9.2‰ (Table 2.1; Fig. 2.28) with a mean value of -14.4‰ ($n = 12$). Linear regression through the cold ($<20^{\circ}\text{C}$) water data indicates no relationship between samples ($R^2 = 0.04$).

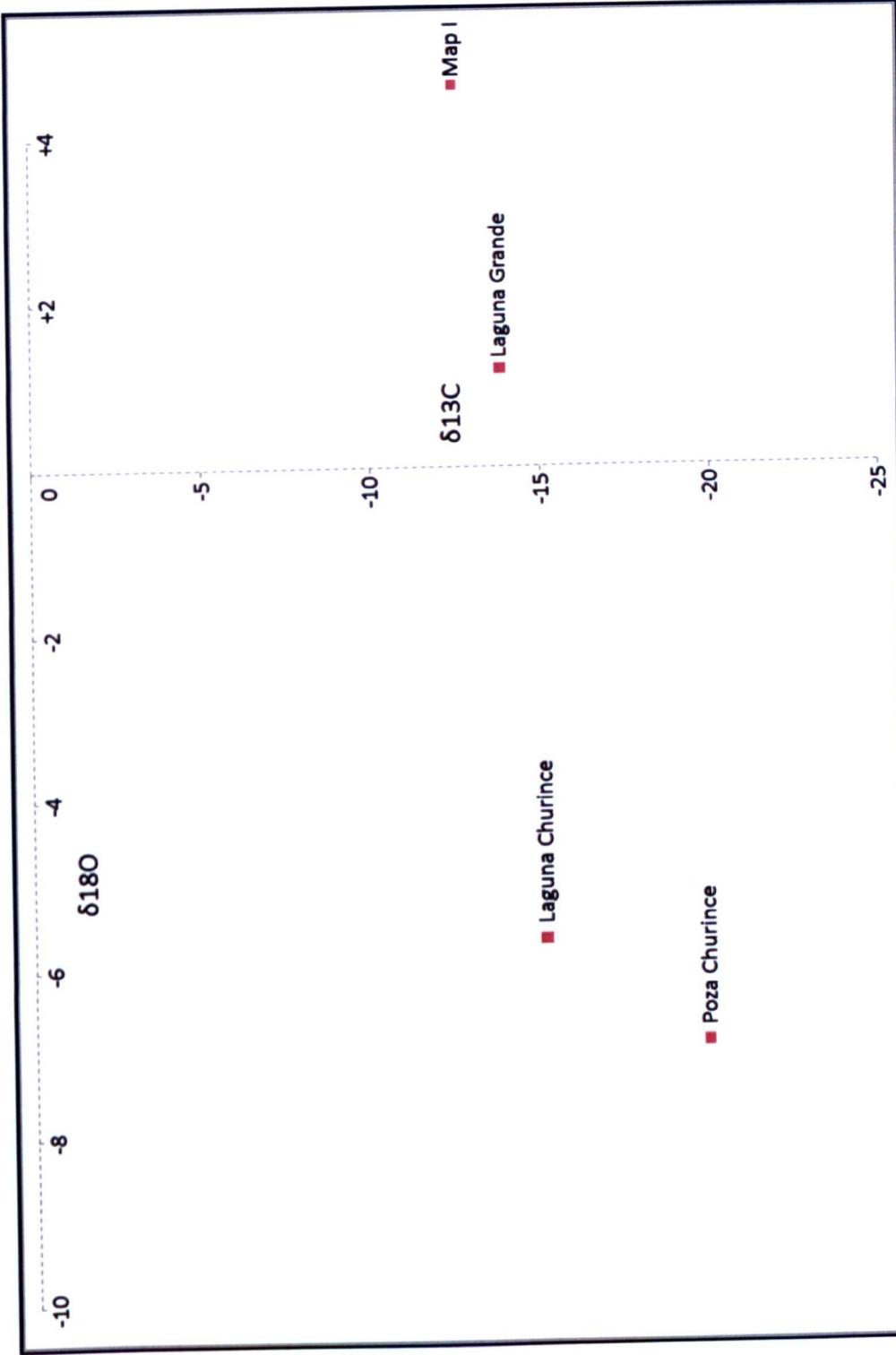


Figure 2.21. $\delta^{18}\text{O}$ vs. $\delta^{13}\text{C-DIC}$ water isotope values within the Cuatro Ciénegas Basin for location I (Fig. 2.10b).

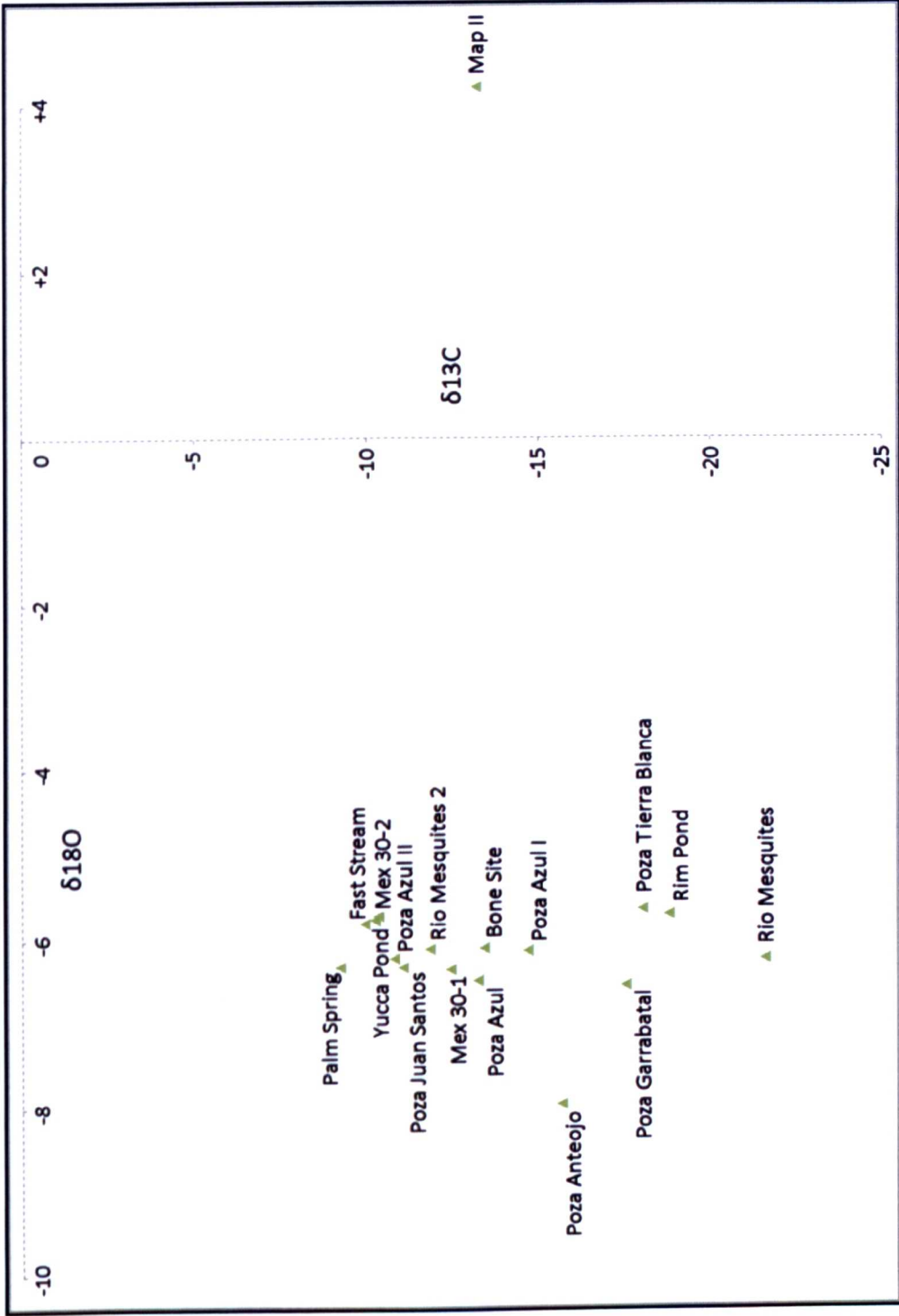


Figure 2.22. $\delta^{18}\text{O}$ vs. $\delta^{13}\text{C}_{\text{DIC}}$ water isotope values within the Cuatro Ciénegas Basin for location II (Fig. 2.10c).

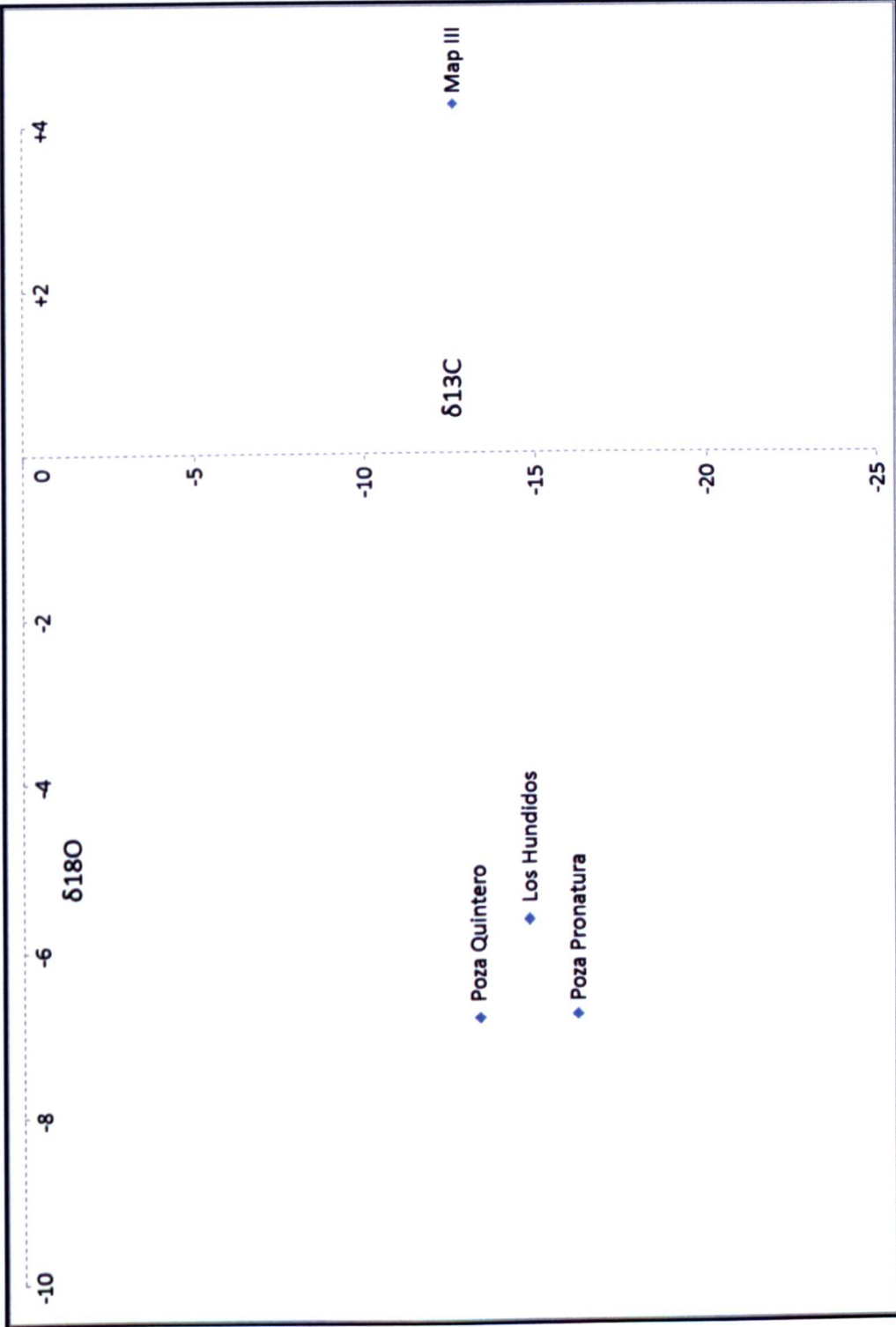


Figure 2.23. $\delta^{18}\text{O}$ vs. $\delta^{13}\text{C}_{\text{DIC}}$ water isotope values within the Cuatro Ciénegas Basin for location III (Fig. 2.10d).

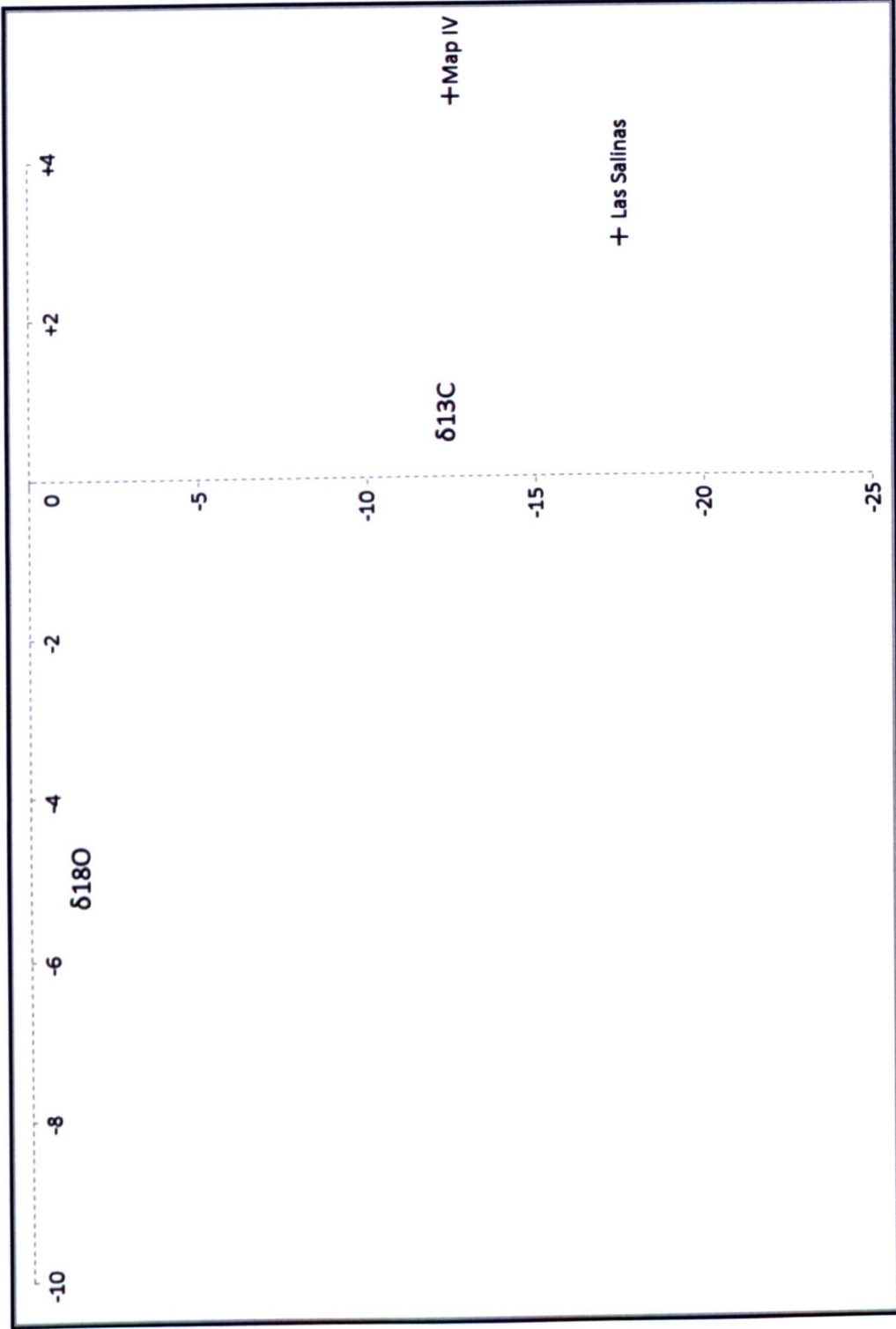


Figure 2.24. $\delta^{18}\text{O}$ vs. $\delta^{13}\text{C}_{\text{DIC}}$ water isotope values within the Cuatro Ciénegas Basin for location IV (Fig. 2.10e).

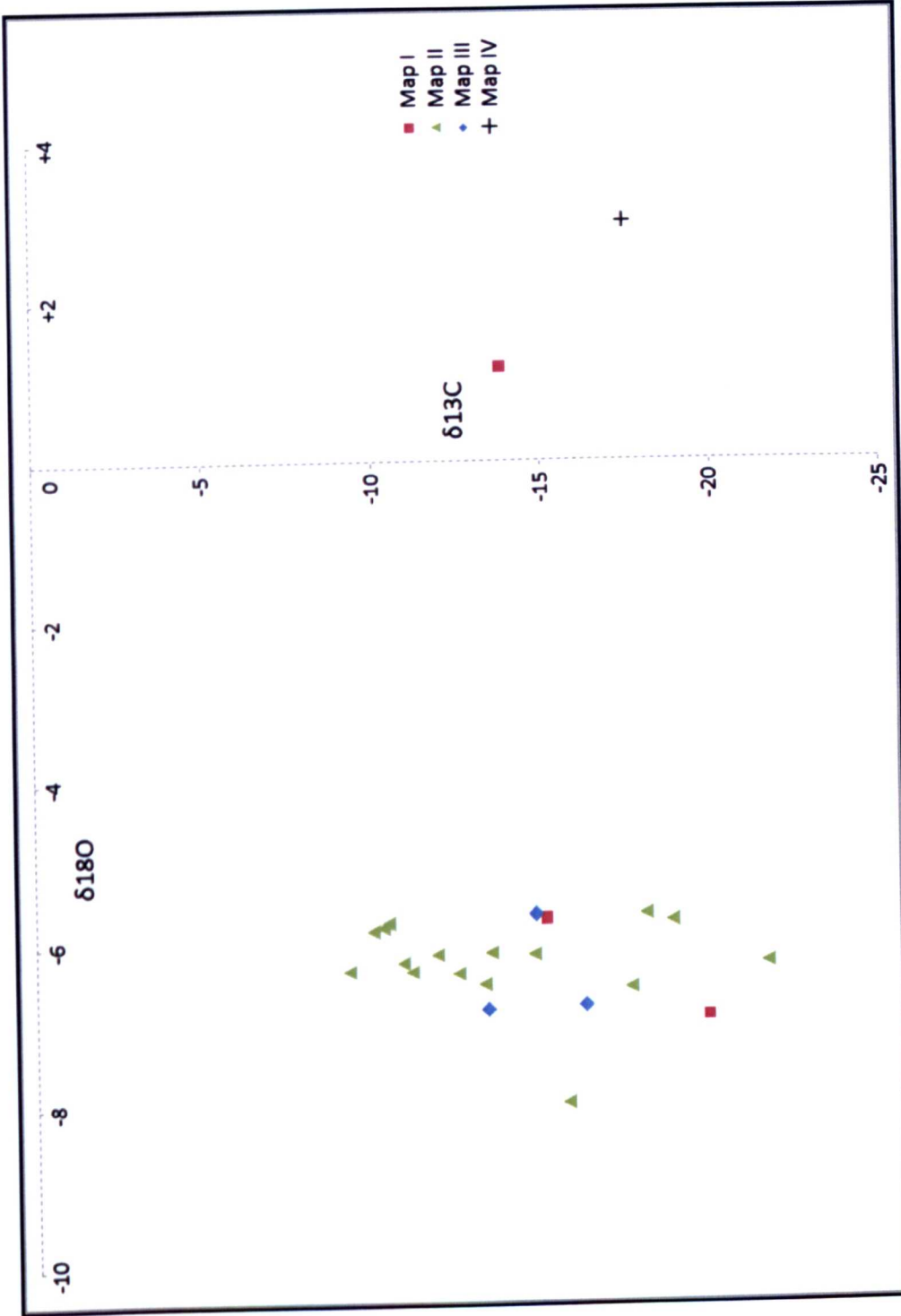


Figure 2.25. $\delta^{18}\text{O}$ vs. $\delta^{13}\text{C}_{\text{DIC}}$ water isotope values within the Cuatro Ciénegas Basin, plotted by location (Fig. 2.10a).

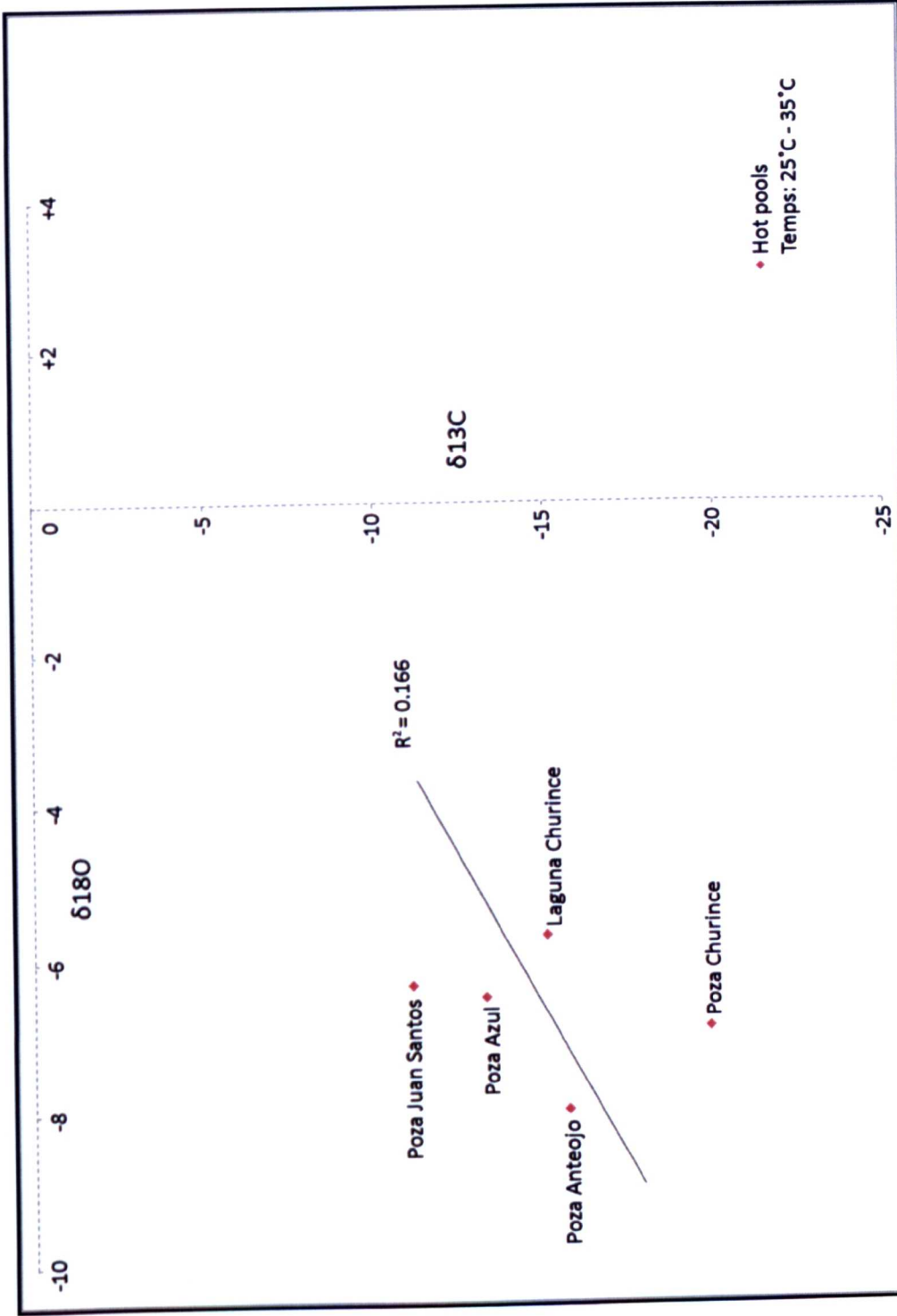


Figure 2.26. $\delta^{18}\text{O}$ vs. $\delta^{13}\text{C}_{\text{DIC}}$ water isotope values within the Cuatro Ciénegas Basin plotted by hot water body temperature (25°C - 35°C).

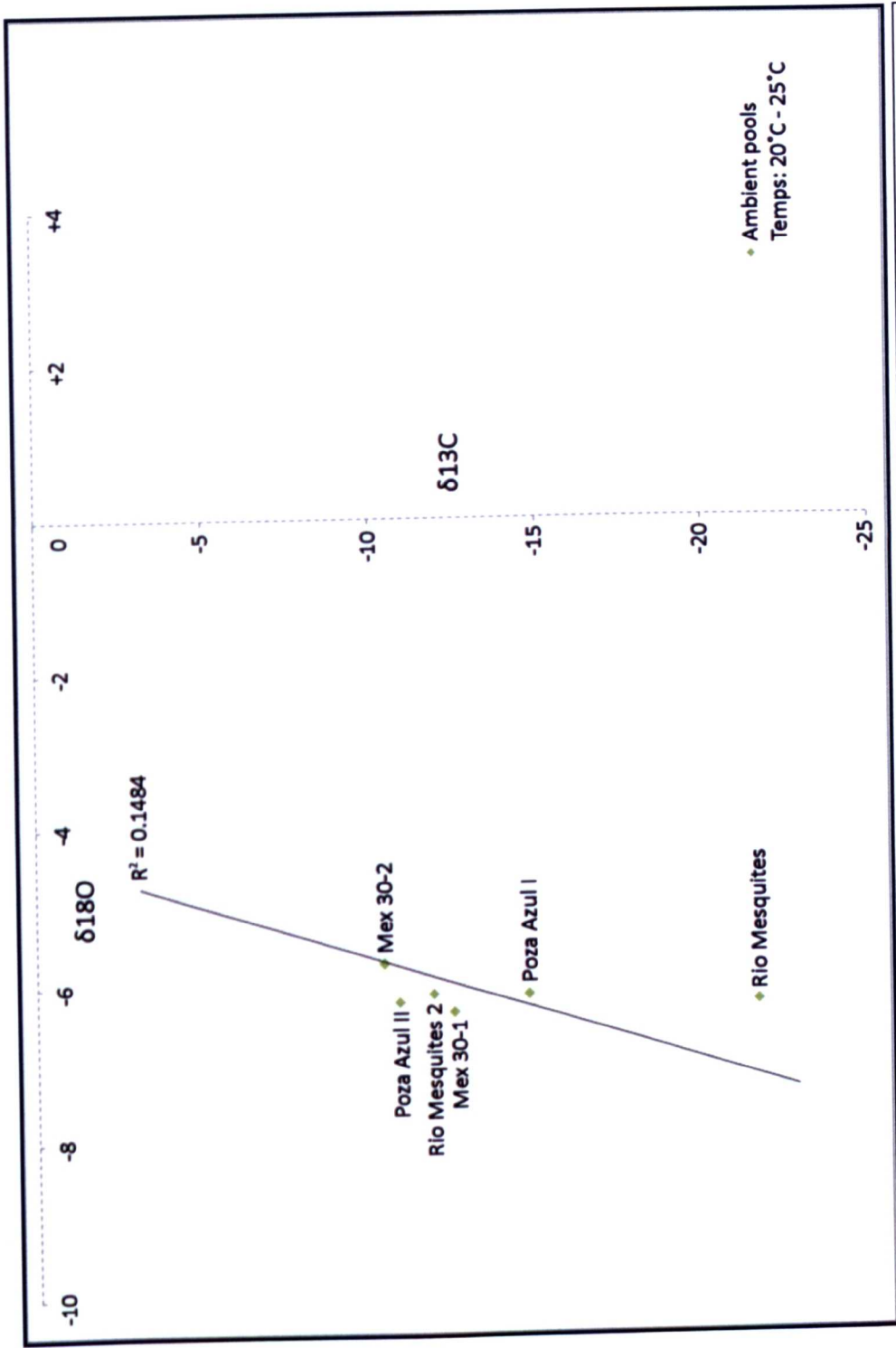


Figure 2.27. $\delta^{18}\text{O}$ vs. $\delta^{13}\text{C}_{\text{DIC}}$ water isotope values within the Cuatro Ciénegas Basin plotted by ambient water body temperature (20°C - 25°C).

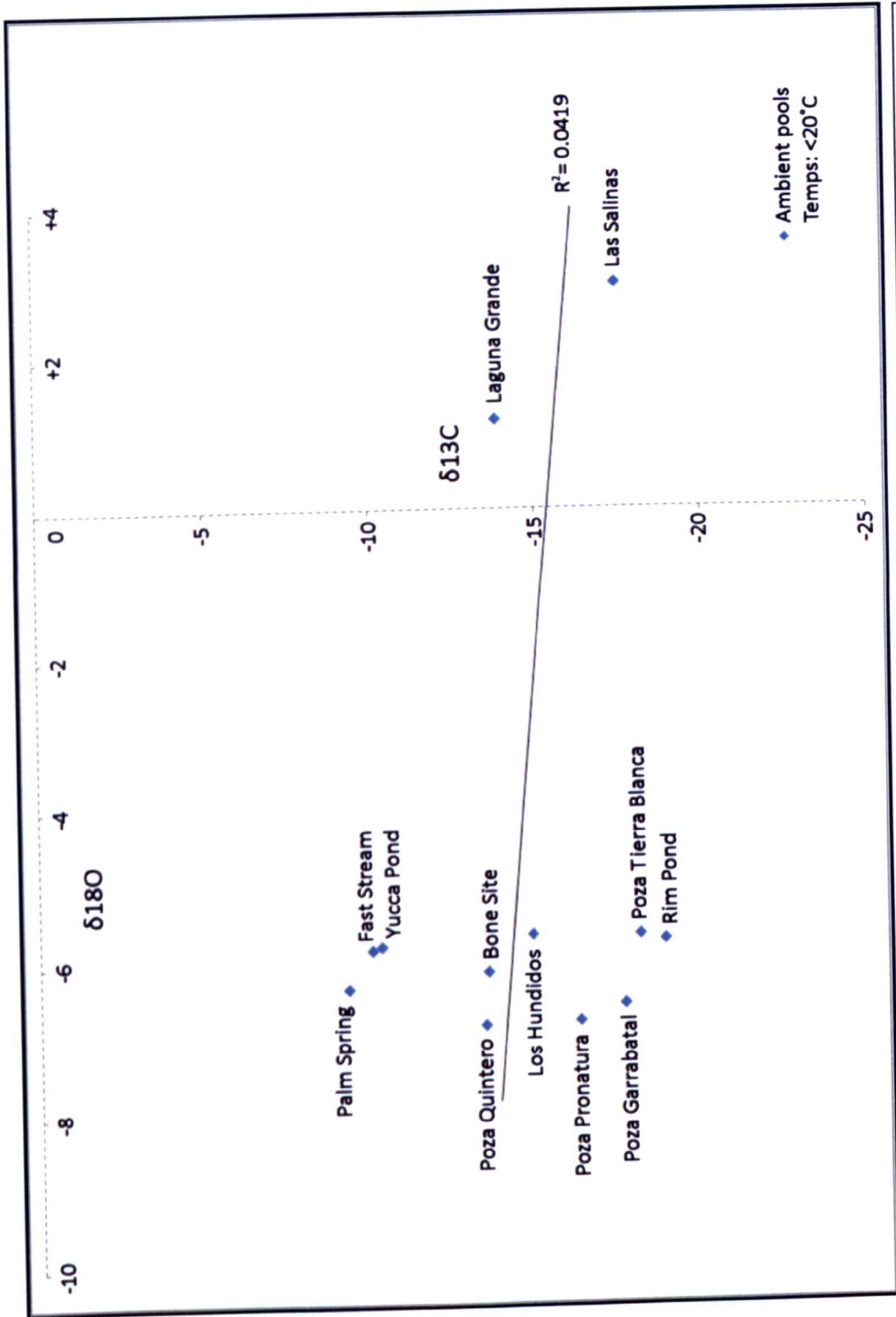


Figure 2.28. $\delta^{18}\text{O}$ vs. $\delta^{13}\text{C}_{\text{DIC}}$ water isotope values within the Cuatro Ciénegas Basin plotted by ambient water body temperature (<20°C).

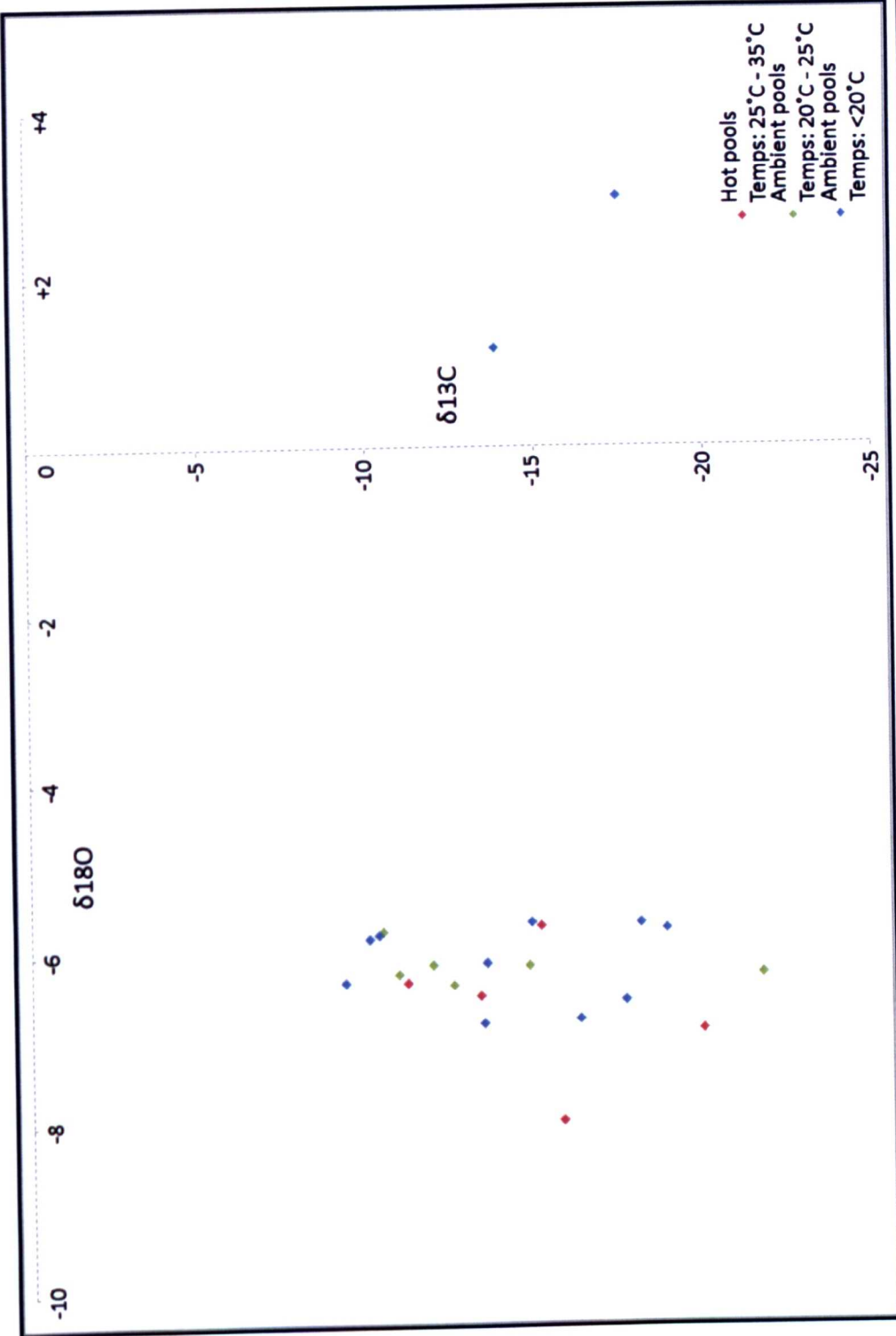


Figure 2.29. $\delta^{18}\text{O}$ vs. $\delta^{13}\text{C}_{\text{DIC}}$ water isotope values within the Cuatro Ciénegas Basin, plotted by water body temperature.

2.4 Discussion

2.4.1 $\delta^{18}\text{O}$ vs. $\delta^{13}\text{C}_{\text{DIC}}$

Without precise pH, temperature, water body morphology, soil carbon content and $\delta^{13}\text{C}_{\text{DIC}}$ of regional groundwater from the CCB, it is hard to make exact determinations as to the origin of $\delta^{13}\text{C}_{\text{DIC}}$ of the 26 sampled water bodies. However, the range of $\delta^{13}\text{C}_{\text{DIC}}$ values (-21.6‰ to -9.2‰) from the 26 water bodies samples in the CCB suggest each water body may experience an individual microclimate with varying degrees of biogenic input, plant respiration, CO_2 invasion from the atmosphere, CO_2 degassing and groundwater input, all of which can affect the $\delta^{13}\text{C}_{\text{DIC}}$ value of water bodies [Eakin, 1966; Taylor and Fox, 1996; Yang *et al.*, 1996; Atekwana and Krishnamurthy, 1998; Leng, 2005]. Water bodies with lower $^{13}\text{C}_{\text{DIC}}$ values, in the range of -22‰ to -16‰ (Table 2.1; Fig. 2.10a), most likely reflect increased CO_2 invasion from plant respiration and/or a higher degree of carbon isotope input from CAM vegetation. Water bodies with higher $^{13}\text{C}_{\text{DIC}}$ values, in the range of -16‰ to -8‰ (Table 2.1; Fig. 2.10a) most likely reflect increased groundwater aquifer discharge into the CCB and/or a higher production of CO_2 in the catchment soils.

It is likely that all water bodies in the CCB will reflect some degree of groundwater input and mixing of surface waters. Increased aquifer discharge into the CCB could affect $^{13}\text{C}_{\text{DIC}}$ values of water bodies from increased input of ^{13}C enriched water from carbonate dissolution. However, it is thought the regional Cupido-Aurora aquifer has a relatively short residence time of water, in the region of 20 to 1500 years [Badino *et al.*, 2004; Johannesson *et al.*, 2004; Wolaver, 2008], suggesting very little dissolution of the aquifer limestone occurs. Bralower [1999] estimates the Cupido-Aurora limestones to have $^{13}\text{C}_{\text{DIC}}$ values of $+2\text{‰}$ to $+4.5\text{‰}$ which suggests dissolution of the Cupido-Aurora limestone would result in ^{13}C enriched groundwater. The highest $^{13}\text{C}_{\text{DIC}}$ value recorded from the 23 samples was -9.2‰ so short residence time of groundwater and increased aquifer discharge into the CCB could be supported by this data.

The CCB is currently considered to be a hydrologically closed basin [Badino *et al.*, 2004; Johannesson *et al.*, 2004; Evans, 2005; Rodriguez *et al.*, 2005; Wolaver *et al.*, 2008]. Leng [2005, after Leng and Marshall, 2004] suggests hydrologically closed lakes

will display some degree of $\delta^{18}\text{O}_{\text{LAKEWATER}}$ vs. $\delta^{13}\text{C}_{\text{DIC}}$ covariance, thought to be where $R^2 > 0.7$. The 23 available water bodies sampled from the CCB display very little covariance, where $R^2 \leq 0.1$ (Figs. 2.26, 2.27 and 2.28), suggesting the CCB may be of open lake hydrology. However, the complexity of the CCB hydrology, with the basin having over 200 water bodies, suggests the possibility of a larger closed basin flow system rather than a typical over flowing open lake [e.g. Li and Ku, 1997; Li *et al.*, 1997].

2.4.2 $\delta^{18}\text{O}$ vs. δD

All 26 samples plot to the right of the GMWL and LMWL, suggesting they have undergone some degree of evaporation, creating the LEL (Fig. 2.15). Poza Anteojo ($\delta^{18}\text{O} = -7.99\text{‰}$, $\delta D = -54.8\text{‰}$) plots very close to the GMWL and LMWL, closely reflecting modern precipitation $\delta^{18}\text{O}$ value of -8.3‰ for the CCB [Wassenaar, 2009], predominantly rained out on the high peaks (>3000 m a.s.l) of the surrounding mountains [Badino *et al.*, 2004]. Poza Anteojo is the only water body that plots so close to the GMWL and LMWL suggesting the other 25 water bodies may be of a different origin.

Poza Churince displays the lowest $\delta^{18}\text{O}$ value (-6.92‰) of the remaining 25 water bodies (Table 2.1) which is very similar to the precipitation value of Chihuahua (-7.1‰ [Wassenaar, 2009]) where the Cupido-Aurora aquifer originates in the Bolson de Mapimi, so the oxygen isotope composition of the Cupido-Aurora aquifer water should reflect that of the Bolson de Mapimi. The Bolson de Mapimi has an average elevation of 1200 m a.s.l [Van Devender and Burgess, 1985] so precipitation recharging the Cupido-Aurora aquifer may be less subject than the CCB to the altitude effect, whereby ^{18}O is progressively rained out at increasing elevations creating a lower $\delta^{18}\text{O}$ precipitation value at higher elevations. The Bolson de Mapimi has a lower rainout elevation (1200 m a.s.l) relative to the CCB (> 3000 m a.s.l) so therefore has a higher $\delta^{18}\text{O}$ precipitation value of -7.1‰ , compared to -8.3‰ respectively. Johannesson *et al.* [2004] calculated an approximate groundwater recharge elevation of 1200 – 1400 m a.s.l for the CCB groundwaters, placing the Bolson de Mapimi within this range. The similarity in oxygen isotope composition and calculated recharge elevation of 1200 – 1400 m a.s.l of CCB groundwater, like that of Poza Churince, suggests the Cupido-

Aurora aquifer provides a significant component of the CCB water. The difference in water oxygen isotope composition between Poza Anteojo and the remaining 25 water body samples suggests they are of separate origins. Based on the extrapolated LEL from the 26 water body samples and modern precipitation values, three separate hydrologic 'systems' are evident in the CCB:

- 1) The first 'system' is independent of the through-flow systems and consists of independent pools such as Poza Anteojo that are fed directly from the interstratal karst and closely reflect the isotopic signature of local meteoric water (Figs. 2.30, 2.34a and 2.34c).
- 2) The first of two evaporative through-flow systems seen in the CCB possibly closely related to the Cupido-Aurora aquifer. The main through-flow system begins at Poza Churince on the western flank of the Sierra San Marcos y Pinos before flowing around the piedmont towards the furthest pools with higher $\delta^{18}\text{O}$ - Las Salinas and Charco Rojo - in the centre of the eastern side of the CCB, consistent with progressive evaporation across the basin (Figs. 2.30, 2.31, 2.34a, 2.34b, 2.34c and 2.34e).
- 3) The secondary evaporative through-flow system occurs on the eastern flank of the Sierra San Marcos y Pinos, beginning at Poza de Quintero. The water here flows north to Poza Pronatura before reaching Los Hundidos and joining with the first through flow system at Las Salinas and Charco Rojo (Figs. 2.30, 2.33, 2.34a, 2.34d and 2.34e).

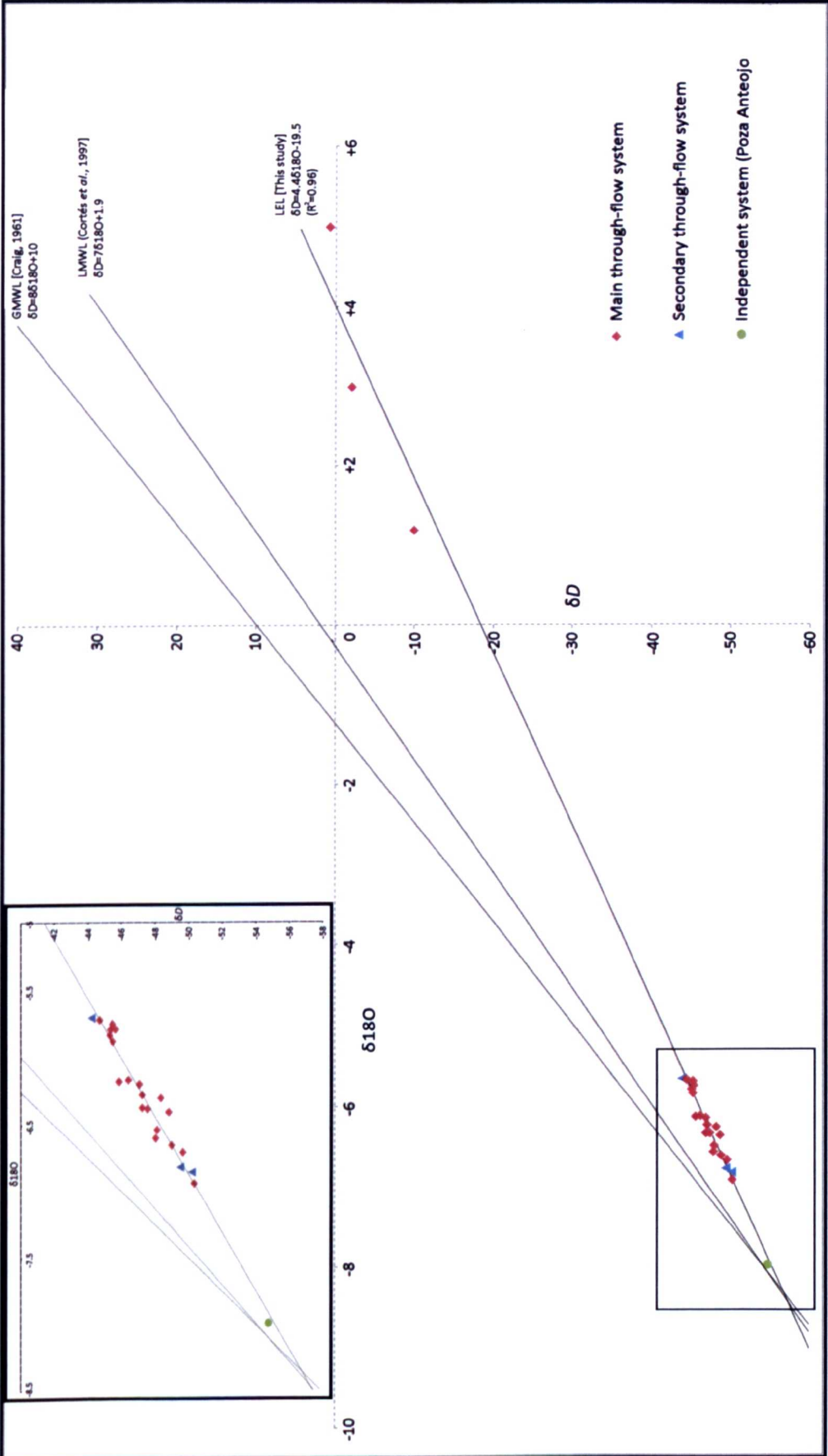


Figure 2.30. $\delta^{18}\text{O}$ vs. δD water isotope values within the Cuatro Ciénegas Basin, plotted by hydrologic 'system'. The GMWL [Craig, 1961] and LMWL [Cortés et al., 1997] are displayed with CCB residual water plotting to the right as a Local Evaporation Line (LEL) $6\text{D} = 4.46^{18}\text{O} - 19.5$.

2.4.2.1 Independent system

Poza Anteojo discharges towards the north of the CCB and has the lowest $\delta^{18}\text{O}$ of the 26 samples ($\delta^{18}\text{O} -7.99\text{‰}$) suggesting that it most closely reflects the high elevation, low $\delta^{18}\text{O}$ precipitation of the basin. Poza Anteojo lies within modern precipitation values for the Chihuahuan desert [Cortés *et al.*, 1997; Johannesson *et al.*, 2004; Wassenaar *et al.*, 2009] and also plots on the LEL (Fig. 2.30). This suggests that it is fed from similar regional meteoric sources but is separate from the main or secondary through-flow systems. Poza Anteojo could be fed directly from the limestone karst system, arising from Sierra la Madera, but the warm temperature of the water, $+26.2^{\circ}\text{C}$ [Johannesson *et al.*, 2004], is higher than the CCB average mean annual air temperature of 21.2°C [Badino *et al.*, 2004] suggesting Poza Anteojo water has some degree of deep thermal action or possible influence from the Cupido-Aurora aquifer.

Rodriguez *et al.* [2005], suggest the Sierra Madera has a meteoric water (precipitation) sourced karst reservoir which suggests the $+26.2^{\circ}\text{C}$ Poza Anteojo water may be a process of focused channel recharge [e.g. Blasch *et al.*, 2008]. Precipitation occurs on the high > 3000 m a.s.l Sierra Madera, providing Poza Anteojo with water that more closely reflects the oxygen isotope composition of CCB precipitation that is stored in a karst reservoir [Badino *et al.*, 2004; Rodriguez *et al.*, 2005]. This karst reservoir may form a part confined aquifer, specific to the CCB, heated by insolation and geothermal activity, similar to arid groundwater recharge areas in Arizona and Texas [Kastning, 1983; Hogan *et al.*, 2004; Blasch *et al.*, 2008]. The Trinity aquifer of the Edwards Plateau, Texas provides a model from which to base the CCB with three separate, self contained aquifers within the carbonates feeding the groundwater system [Kastning, 1983]. The CCB may possibly have a similar system with two aquifers, the regional Cupido-Aurora aquifer and a possible part confined aquifer. The movement of water through the porous limestone by gravity creates a hydrostatic head pressure, like those of Mammoth Hot springs, Wyoming and the American Southwest [Barger, 1978; Guo and Riding, 1999; Blasch *et al.*, 2008] resulting in recharge at the base of the Sierra Madera from the part confined aquifer. Poza Anteojo may be the result of this recharge, whereby the thermally heated CCB meteoric water surfaces as an independent, self contained pool.

2.4.2.2 Main through-flow system

The isotopic data suggests the main hydrologic feature in the CCB to be a through-flow system originating to the west of the basin before flowing towards the east (Figs. 2.30, 2.31, 2.34a, 2.34b, 2.34c and 2.34e). Pozas San Marcos, Churince and Becerra are where the main flow system originates (Figs. 2.34a and 2.34b), most closely reflecting the oxygen isotope composition of the Cupido-Aurora aquifer water, although Poza San Marcos does not appear to form part of the through-flow system. The waters on west side of the CCB originate from the local faulting (Fig. 2.7) [Badino *et al.*, 2004; Johannesson *et al.*, 2004], where deep water enriched in dissolved ions (i.e. Laguna Grande - 588mg/kg Ca, 262mg/kg Mg [Johannesson *et al.*, 2004]) up wells through the local faulting to the surface, resulting in gypsum precipitation (see section 2.4.3).

Pozas Becerra and Churince and Laguna Churince are very closely linked with Laguna Grande by surface flow (Fig. 2.32b) with Pozas Churince and Becerra both fed directly from the fault line. Poza Churince ($\delta^{18}\text{O}$ -6.92‰) flows to Laguna Churince ($\delta^{18}\text{O}$ -5.71‰), before flowing into Laguna Grande ($\delta^{18}\text{O}$ $+1.17\text{‰}$), which is much more ^{18}O enriched, possibly due to a high degree of evaporation (Fig. 2.34b). Laguna Grande, despite being located at the beginning of the main through-flow system (Fig. 2.34b), has a much more ^{18}O enriched water, so is further along the LEL (Figs. 2.11 and 2.15). Laguna Grande is much larger and shallower than Poza Churince and Laguna Churince and may experience a much larger degree of evaporative enrichment relative to the water bodies in close proximity, resulting in a higher $\delta^{18}\text{O}$ value (Fig. 2.31 and 2.34b). Without studying exact water body size and depth, exact amounts of evaporation are unknown, so it is hard to substantiate exactly why Laguna Grande displays a much higher $\delta^{18}\text{O}$ value. Surface flow from Poza Churince and Laguna Churince reaches Poza Becerra ($\delta^{18}\text{O}$ -6.63‰), the 0.29‰ enrichment observed between Pozas Churince and Becerra can possibly be accounted for by mixing of the evaporatively enriched Laguna Churince water with the groundwater fed Poza Becerra (Fig. 2.32b). However, discharge from the Cupido-Aurora aquifer in the CCB has recently decreased with the observed disappearance of Laguna Grande in 2009 [APFFCC], possibly changing the isotopic composition of both the pool itself and also

the through-flow system observed across the CCB since this reconnaissance study was conducted.

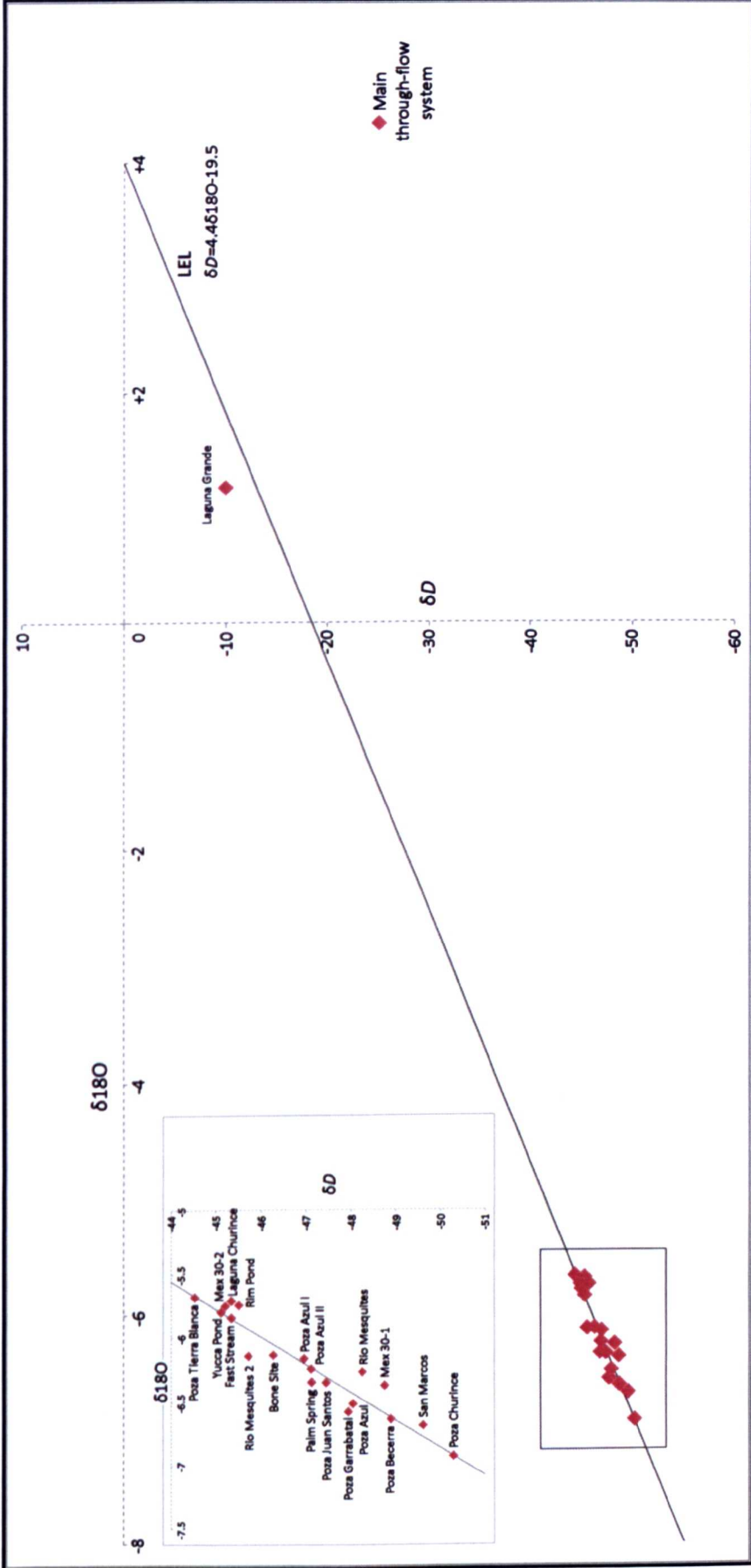


Figure 2.31. Main hydrologic through-flow system. Las Salinas and Charco Rojo have been excluded from the plot due to their location at the end of the hydrologic system, after the main and secondary systems have converged.

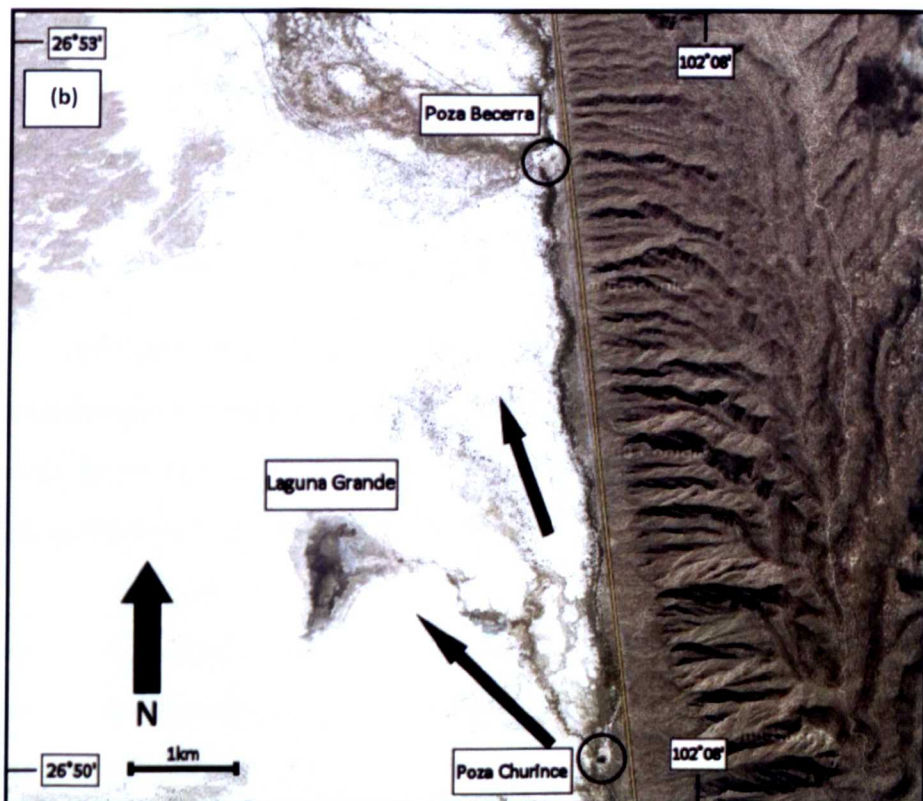
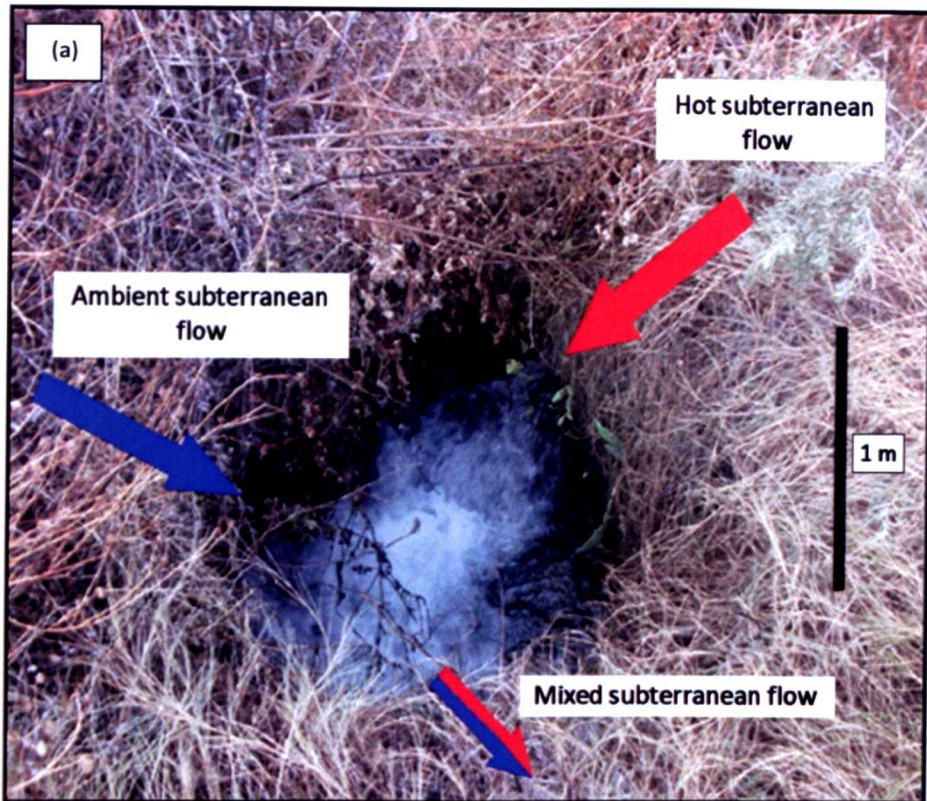


Figure 2.32. a) Subterranean exchanges between ambient subterranean water and hydrothermal groundwater at a depth of 1.5 m below surface level, highlighting the complexity of the CCB hydrologic system. b) Aerial photograph showing surface flow from Poza Churince into Laguna Grande (prior to complete drying of the lake) before flowing from Laguna Churince to Poza Becerra [image from google.co.uk/earth].

As the main through-flow system reaches the piedmont of the Sierra San Marcos y Pinos (Figs. 2.34a and 2.34c) the specific flow pattern across the CCB becomes a complex mix of ambient surface, ambient subterranean and hydrothermal groundwater flow with a great deal subterranean exchanges between different flow processes as is seen in ciénegas (marshes) of the Sonoran desert [Minckley and Brunelle, 2007; Minckley *et al.*, 2009] (Figs. 2.32a and 2.34c). This complex hydrology makes it particularly difficult to trace flow patterns between pools at the piedmont of the Sierra San Marcos y Pinos. The close cluster of pools, including the Rio Mesquites, are linked together by a complex ciénega (marsh) flow system, first documented by Minckley [1969] and later summarised in more detail by Badino *et al.*, [2004]. The ciénega (marsh) displays high spatial variability of environments, water bodies and sediments, ranging from carbonate muds to peats, allowing interchange of water between the many pools in this area (Fig. 2.34c). The complex flow in this area of the CCB creates mixed isotopic values of the water as the Rim Pond, Yucca Pond, Fast Stream and Poza Tierra Blanca sites (Fig. 2.34c) appear further along the LEL than expected in the main through-flow system (Fig. 2.31). The additional enrichment of these sites, in particular Poza Tierra Blanca, is similar to that of Laguna Grande where relative size and shallow depth of the water body coupled with further surface flow possibly increases evaporation, increasing the $\delta^{18}\text{O}$ value of each water body.

Ambient (20°C to 25°C) water temperature of the ciénega (marsh) system (Fig. 2.17) complements the isotopic data, however, when combined with some available water body temperatures from Minckley [1969]. The Map B (Fig. 2.34c) system originates at Poza Juan Santos ($\delta^{18}\text{O}$ -6.35‰, +32.4°C) and Poza Garrabatal ($\delta^{18}\text{O}$ -6.58‰, +18.6°C) with hydrothermal and cold water inputs respectively. The hydrothermal water flows subsurface toward the Rio Mesquites ($\delta^{18}\text{O}$ -6.27‰, +24°C), mixing with colder Poza Garrabatal, decreasing in temperature from +32.4°C to +24°C. This decrease in water body temperature combined with higher $\delta^{18}\text{O}$ values towards the east of the piedmont (Fig. 2.34c) suggests that the water also surfaces with some degree of mixing and evaporation through the ciénega (marsh) area before discharging directly into the Rio Mesquites. Cooler surface water flow from Poza Garrabatal also flows toward Poza Tierra Blanca and the smaller water bodies (Fig. 2.34c), resulting in ^{18}O enriched water with no discernable temperature changes, +18.6°C to +18.4°C, as

the cooler water has already equilibrated with the air temperature. This mixing of hot (25°C to 35°C) and cold (<20°C) water may create the ambient (20°C to 25°C) water bodies, explaining the weaker correlation coefficient ($R^2 = 0.74$) observed in ambient water bodies (Fig. 2.17).

Poza Azul ($\delta^{18}\text{O} -6.51\text{‰}$, +32°C) water data suggests it is sourced from the Cupido-Aurora aquifer by a similar process to Poza Baño Escobedo (Fig. 2.7). Poza Azul artificially flows into Pozas Azul I and II so both exhibit slightly higher $\delta^{18}\text{O}$ values of -6.16‰ and -6.24‰ respectively, before flowing into the Rio Mesquites 2 which terminates at the Las Salinas and Charco Rojo endorheic pools (Fig. 2.34e)

2.4.2.3 Secondary through-flow system

The secondary through-flow system evident in the CCB originates on the east side of the Sierra San Marcos y Pinos at Poza de Quintero before flowing to Poza Pronatura and towards Los Hundidos (Figs. 2.33, 2.34a and 2.34d). The water bodies plot on the CCB LEL, similar to the main through-flow system in figure 2.30, but are located on the east flank of the Sierra San Marcos y Pinos creating a second similar system. Poza de Quintero ($\delta^{18}\text{O} -6.84\text{‰}$) has a very similar isotopic composition to that of Poza Churince suggesting that it is sourced from the same Cupido-Aurora aquifer groundwaters. However, unlike the hydrothermal water bodies sourced from the Cupido-Aurora aquifer, Poza Quintero is a cold water body (<20°C) suggesting the secondary through-flow system may be sourced from a karst reservoir, similar to that of Poza Anteojo.

Wolaver [2005] suggests alluvial fans in this area of the CCB may be preventing the upwelling of deep, thermal water and no faults are evident in the limestone strata to suggest any direct upwelling. Johannesson *et al.*, [2004] suggest pools with a $\delta^{18}\text{O}$ value between -6.7‰ and -7‰ may be recharged at elevations of 1600 to 1800 m a.s.l which is the elevation of the Sierra San Marcos y Pinos in the Map C area (Fig. 2.34a). The alluvial fans may be acting as reservoirs for precipitation falling at 1600 to 1800 m a.s.l, creating a more 'classic' cold water karst environment [Palmer, 1991; Kaufmann and Braun, 2000; Gabrovsek and Dreybrodt, 2010] rather than the hot water karst aquifer proposed for Poza Anteojo.

The secondary through-flow system could also form part of a larger, eastern CCB flow system. Figure 2.9 shows greater numbers of water body formation, both hot (25°C to 35°C) and cold (<20°C), further south on the eastern flank of the Sierra San Marcos y Pinos. A limited number of hot water bodies e.g. Poza Baño Escobedo (Fig. 2.7) form on the eastern flank of the Sierra San Marcos through upwelling of hot water where alluvial fans are not located [Badino *et al.*, 2004; Wolaver *et al.*, 2008]. These may be a process of Cupido-Aurora aquifer water upwelling or focused channel recharge at the beginning of a larger through-flow system, possibly similar to the main through-flow system due to the similarity of the three sampled water bodies on the LEL (Fig. 2.30).

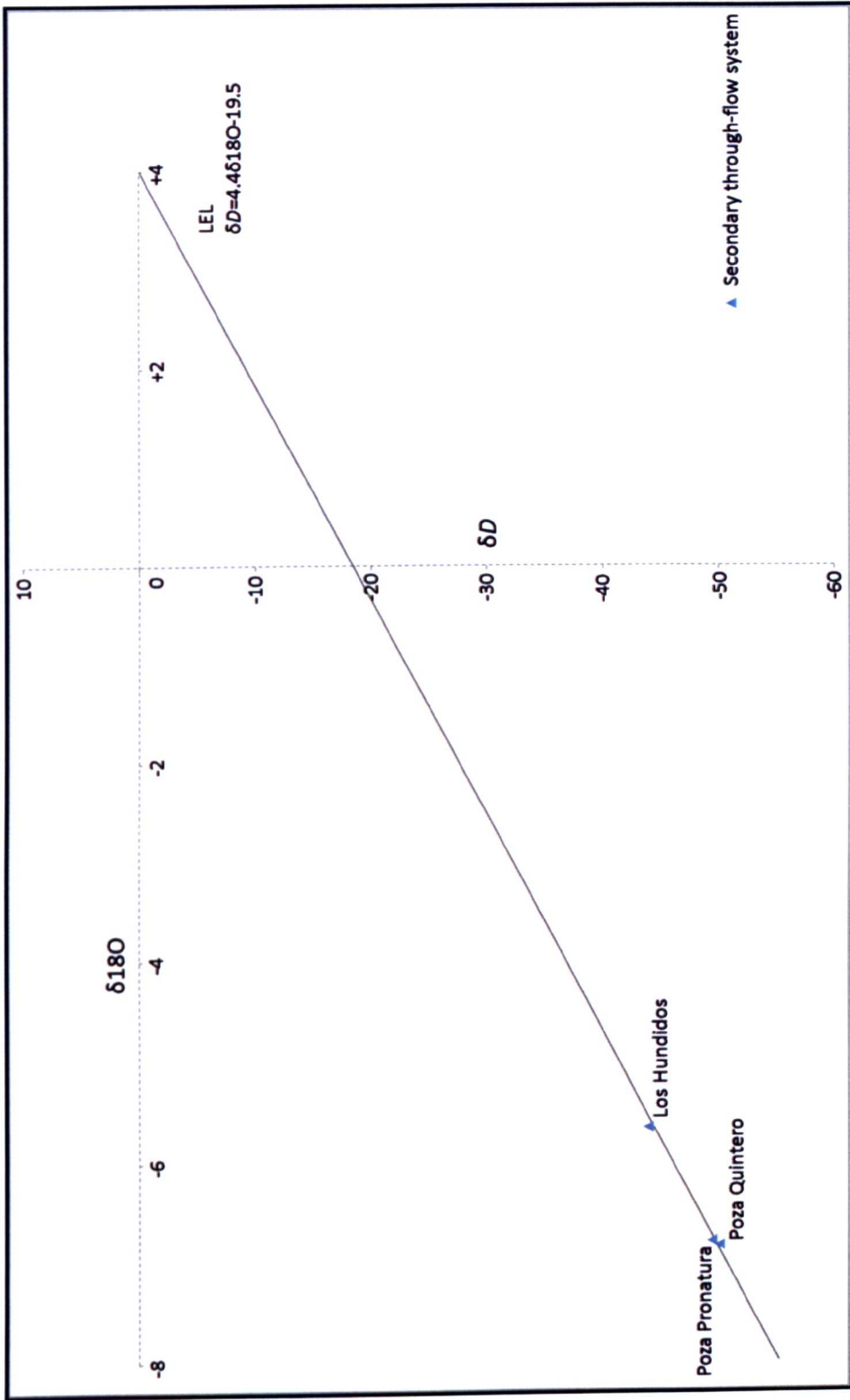


Figure 2.33. Secondary through-flow system in the CCB. Las Salinas and Charco Rojo have been excluded from the plot due to their location at the end of the hydrologic system, after the main and secondary systems have converged.

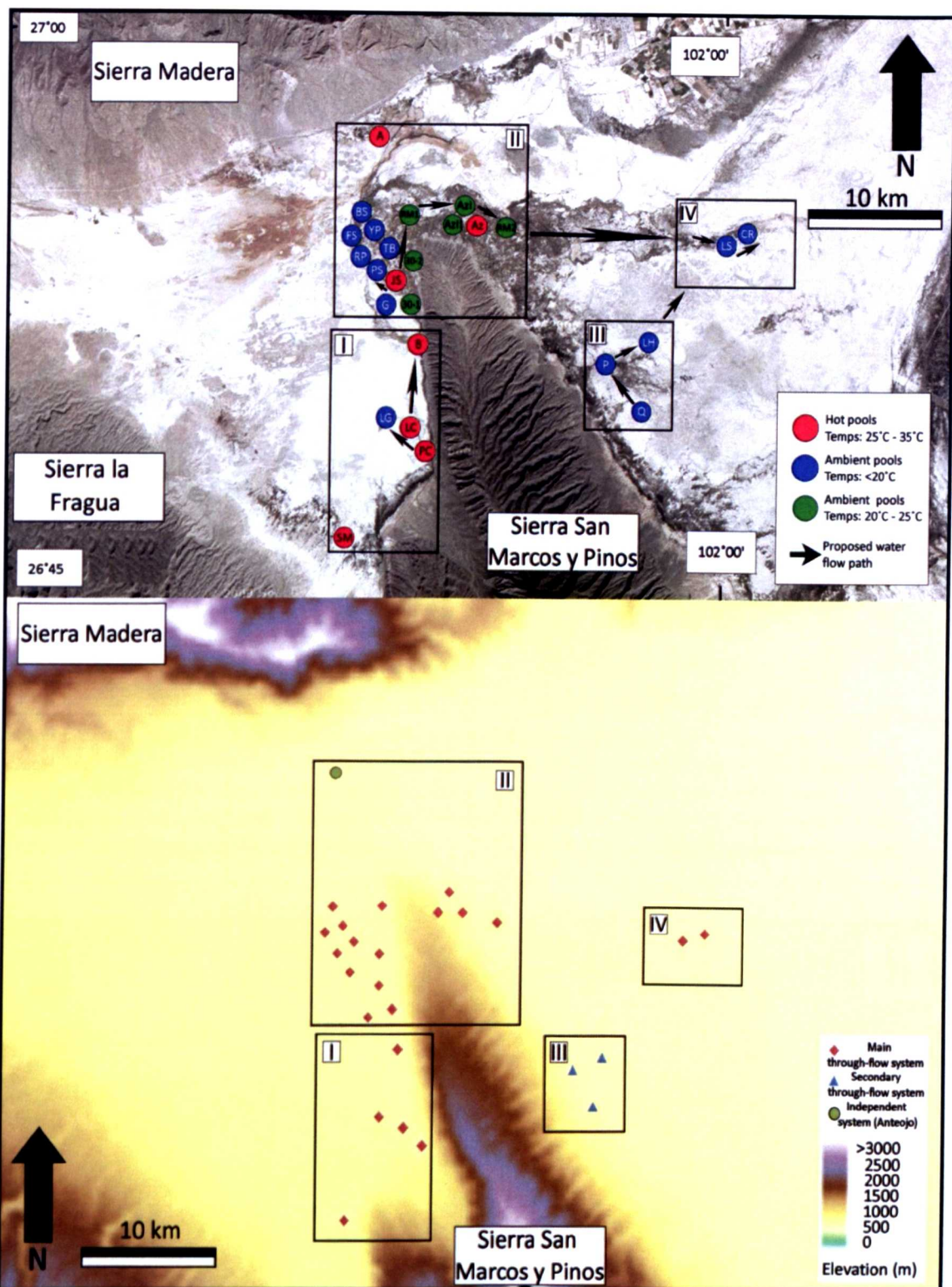


Figure 2.34a. Comparable maps showing water flow patterns. Top – Water body locations in the CCB. Arrows mark the major flow patterns between water bodies, inferred from changes in isotopic composition of water. Names and locations of water bodies are as figure 2.10a [image from www.google.co.uk/earth]. Bottom – Elevation map of water body locations, shown by hydrologic system, in the CCB [elevation map after Wolaver, 2005].

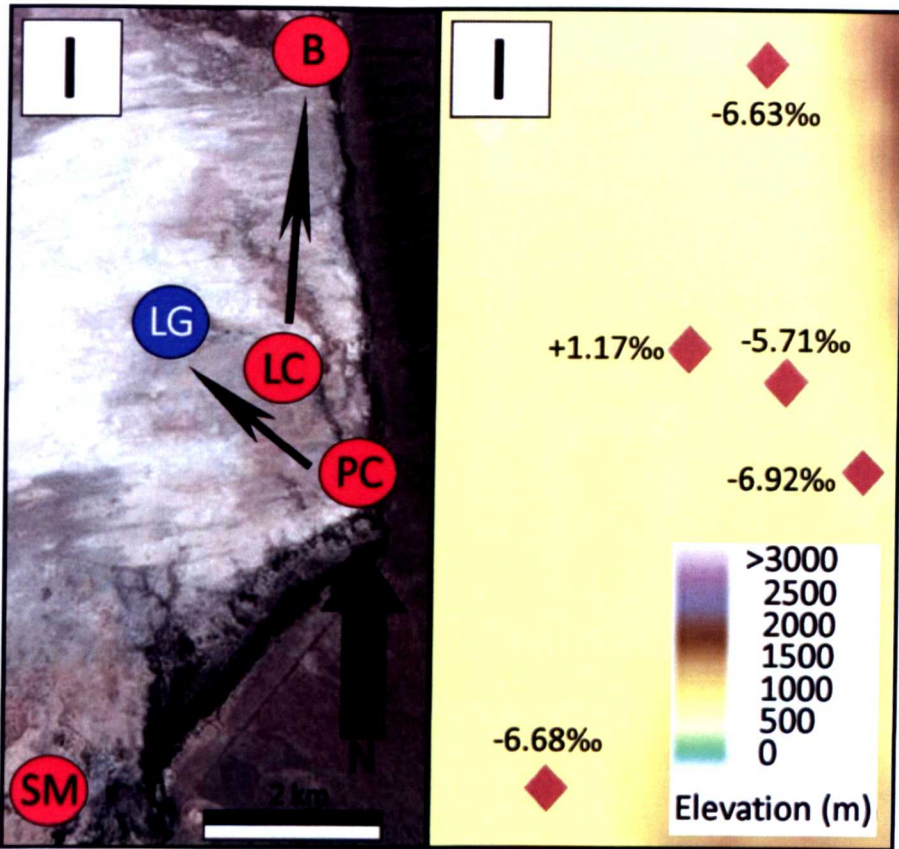


Figure 2.34b. Comparable maps showing water flow patterns of location I (Fig. 2.34a). Left – Water body locations in the CCB. Arrows mark the major flow patterns between water bodies, inferred from changes in isotopic composition of water. Names and locations of water bodies are as figure 2.10a [image from www.google.co.uk/earth]. Right – Elevation map of water body locations, shown by hydrologic system, in the CCB with the $\delta^{18}\text{O}$ value of the water displayed next to each water body [elevation map after Wolaver, 2005].

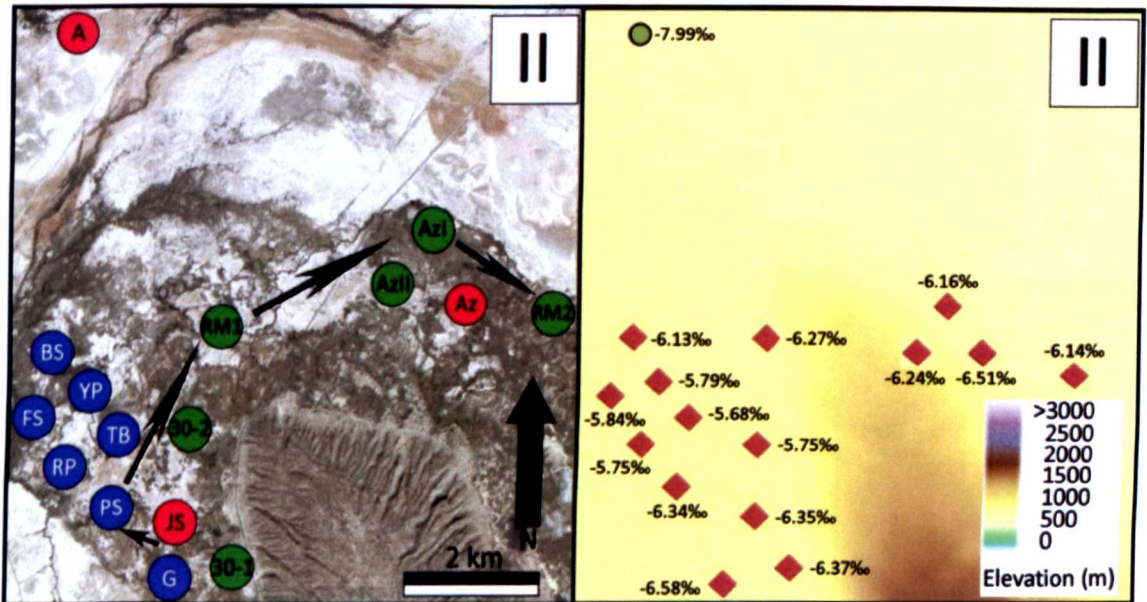


Figure 2.34c. Comparable maps showing water flow patterns of location II (Fig. 2.34a). Left – Water body locations in the CCB. Arrows mark the major flow patterns between water bodies, inferred from changes in isotopic composition of water. Names and locations of water bodies are as figure 2.10a [image from www.google.co.uk/earth]. Right – Elevation map of water body locations, shown by hydrologic system, in the CCB with the $\delta^{18}\text{O}$ value of the water displayed next to each water body [elevation map after Wolaver, 2005].

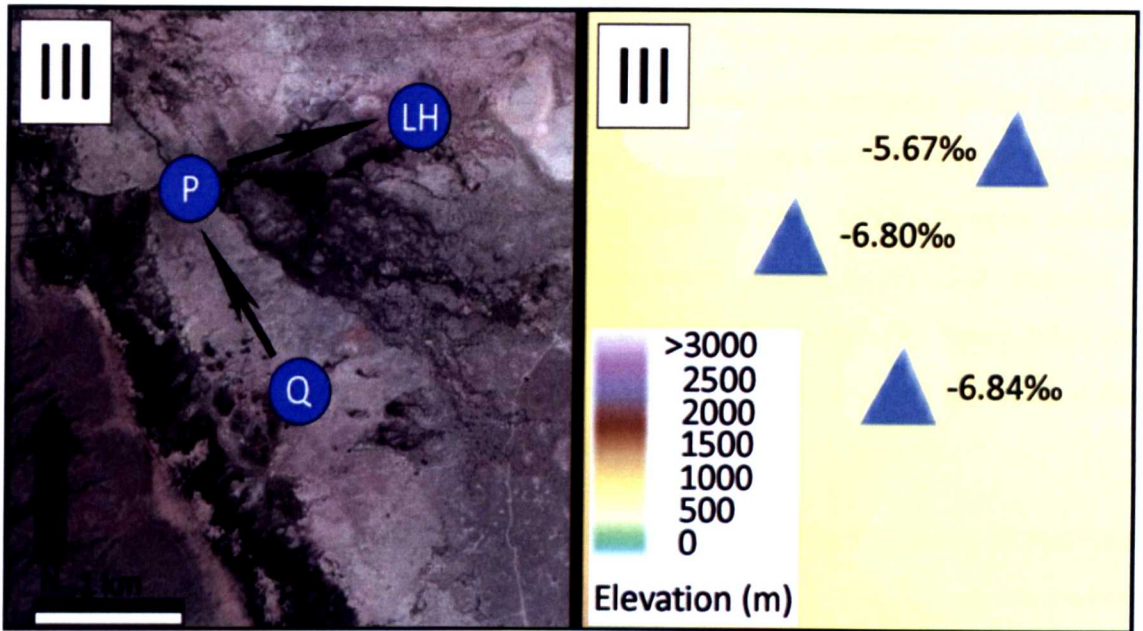


Figure 2.34d. Comparable maps showing water flow patterns of location III (Fig. 2.34a). Left – Water body locations in the CCB. Arrows mark the major flow patterns between water bodies, inferred from changes in isotopic composition of water. Names and locations of water bodies are as figure 2.10a [image from www.google.co.uk/earth]. Right – Elevation map of water body locations, shown by hydrologic system, in the CCB with the $\delta^{18}\text{O}$ value of the water displayed next to each water body [elevation map after Wolaver, 2005].



Figure 2.34e. Comparable maps showing water flow patterns of location IV (Fig. 2.34a). Left – Water body locations in the CCB. Arrows mark the major flow patterns between water bodies, inferred from changes in isotopic composition of water. Names and locations of water bodies are as figure 2.10a [image from www.google.co.uk/earth]. Right – Elevation map of water body locations, shown by hydrologic system, in the CCB with the $\delta^{18}\text{O}$ value of the water displayed next to each water body [elevation map after Wolaver, 2005].

2.4.3 Evaporation and brine evolution across the CCB

Brine evolution is a process of surface water flow evaporation, particularly in closed basin arid regions [Jones *et al.*, 2008; Lowenstein and Risacher, 2008; Risacher and Fritz, 2008; Kilic and Kilic, 2010], leading to progressive enrichment of dissolved ions, precipitating differing minerals [Tucker and Wright, 1990]. Oxygen isotope composition of the main through-flow system water bodies in the CCB suggests a progressive evaporative enrichment of surface flow occurs as water flows from the west, across the piedmont of the Sierra San Marcos Y Pinos, towards the east of the basin (Figs. 2.30, 2.34a, 2.34b, 2.34c and 2.34e).

Laguna Grande lies on the west area of the basin at the beginning of the main through-flow system with a $\delta^{18}\text{O}$ value of +1.17‰ (Table 2.1). The ^{18}O enriched water of Laguna Grande is possibly a consequence of its large size and relative shallow depth and, as previously discussed, may experience increased evaporation relative to the other water bodies in that area. The water in Laguna Grande originates from Poza Churince and has low alkalinity (116 mg/kg HCO_3) and high dissolved ions (588 mg/kg Ca, 262 mg/kg Mg) [Johannesson *et al.*, 2004]. As a result of this low ratio, where $\text{HCO}_3 \ll \text{Ca}$ and Mg, gypsum is precipitated – as can be seen by gypsum dune formation north and west of Laguna Grande (Fig. 2.35).

Water then proceeds to flow north towards Poza Becerra and into the ciénega (marsh) system, experiencing further evaporation of surface waters, increasing alkalinity (200 mg/kg HCO_3) and reducing dissolved ions (360 mg/kg Ca, 105 mg/kg Mg) [Johannesson *et al.*, 2004] due to them being precipitated as the brine evolves. As the ratio equilibrates, where $\text{HCO}_3 \geq \text{Ca}$ and Mg, precipitation of carbonates occurs – as can be seen towards the piedmont of Sierra San Marcos y Pinos (Fig. 2.35). Figures 2.34a and 2.34c show the close relationship of the pools in this area with carbonate rich tufas being precipitated (Fig. 2.35).

The main through-flow system gradually reaches higher alkalinity in the eastern area of the basin, towards the endorheic water bodies (Las Salinas and Charco Rojo) known locally as Las Playitas (meaning beach or plains) because of salt flat deposition. These pools are known to experience high levels of evaporation, precipitating salts and minerals such as trona and nahcolite [Badino *et al.*, 2004]. As the surface water flows

towards the eastern area of the CCB, alkalinity increases (317 mg/kg HCO_3) with very low dissolved ion concentrations (168 mg/kg Ca, 44 mg/kg Mg) [Johannesson *et al.*, 2004]. The high ratio, where $\text{HCO}_3 \gg \text{Ca}$ and Mg, results in salt mineral precipitation (Fig. 2.35). The eastern area of the CCB is where the western (main) through-flow system confluences with the eastern (secondary) through-flow system, before becoming terminal where waters are evaporated, with the exception of a small man made river, used for irrigation, flowing to the NE of the CCB.

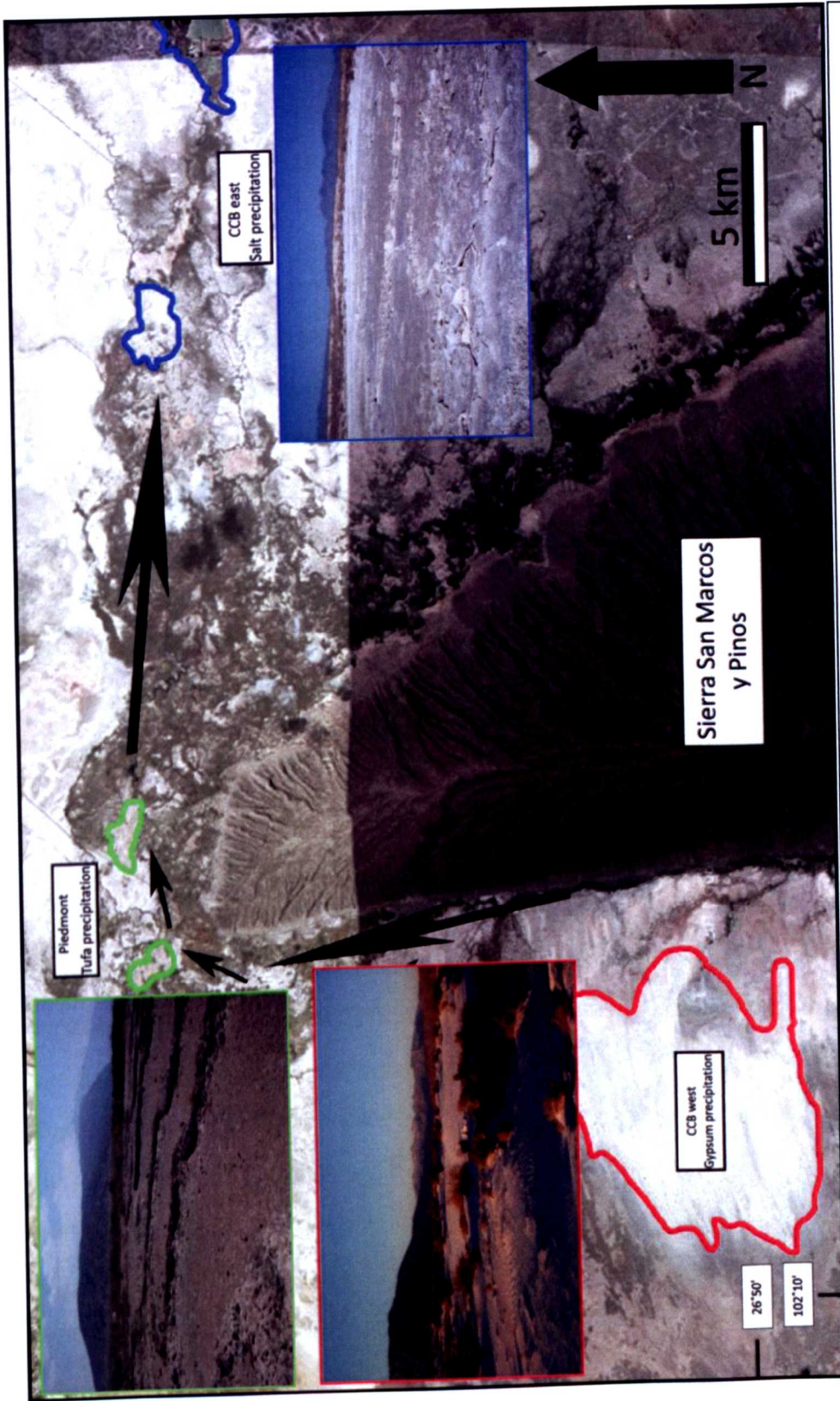


Figure 2.35. Brine evolution and mineral deposition from west to east across the CCB. Red – shows gypsum precipitation at Laguna Grande with a representative photograph (taken facing north). Green – shows tufa deposition at the piedmont of the Sierra San Marcos y Pinos with a representative photograph (taken facing south). Blue – shows salt deposition in the endorheic, east side of the CCB with a representative photograph (taken facing north east) [aerial photograph from www.google.co.uk/earth].

2.4.4 Modern human influence

Further to the isotopic data, human water exploitation within the CCB has a considerable influence on the water table and systematics of both the hydrothermal and freshwater springs, pools, lakes and rivers. The main extraction of water from the CCB is for irrigation of over 3,983 hectares of pastureland [Badino *et al.*, 2004] in the Ocampo and Hundido Basins, north and west of the CCB respectively, used to grow alfalfa (*Medicago sativa*) – a very water demanding crop used to feed cattle.

Other extractions of water within the CCB are for the purposes of sanitation and drinking, after cleansing. Canals are used in the CCB to transport this water away from the hydrologic system and have been in use for since the early 1900s [Minckley, 1969]. Four main canals are used in the CCB for the extraction and transport water – 1) Saca de Fuente 2) Becerra 3) Santa Tecla 4) Ejido El Venado. The Saca de Fuente (Saca Salada) Canal is the largest, draining water from the eastern through flow system in the CCB - Poza de Quintero, Poza Pronatura and Los Hundidos as well Poza Baño Escobedo, Poza Tio Candido and Rio Mesquites. Saca de Fuente was completed in 1902 and is 80km in length, extracting 1500L/s through the NE exit of the CCB, towards Nadadores.

The extraction of such large amounts of water has led to dramatic water level drops in the past 40 years [Minckley, 1992; APFFCC] (Figs. 2.36 and 2.37), suggested to be up to 4m in some pools [PRONATURA] but generally accepted to be around 0.5m [Hendrickson and Minckley, personal comms.]. Rodriguez *et al.*, [2005] suggest a hypothesis that over extraction of water in the Hundido Basin, for industry, may be a significant reason for the water level drop in the west of the CCB. Extraction in the Hundido Basin is taken directly from the Cupido-Aurora aquifer, so may be reducing discharge into the western, fault sourced water bodies in the CCB e.g. Poza Churince and Poza Becerra. However, Minckley [1992] and Wolaver *et al.*, [2008] suggest hypotheses that over extraction of water through canalization may have a larger contribution to water level drops in the CCB.

The Becerra Canal, completed in 1966, extracts water at a rate of 600L/s towards the town of Cuatro Ciénegas, from Poza Becerra at the start of the main through-flow system in the CCB and has subsequently led to a large drop in water level

in the pool [Minckley, 1992] (Fig. 2.36). This drop in water level has not only affected Poza Becerra but, in late 2009, also caused the complete drying up of Laguna Grande [APFFCC]. Discharge, from the Cupido-Aurora aquifer, into the CCB therefore may not have been affected as hypothesised by Rodriguez *et al.* [2005]; rather, extraction of water, through canalization, out of the hydrologic system is now exceeding discharge into the hydrologic system. Wolaver *et al.* [2008] estimated inflow discharge from the springs as approximately $3.5 \times 10^7 \text{m}^3/\text{year}$ and canal outflow discharge as approximately $5.3 \times 10^7 \text{m}^3/\text{year}$. This suggests the hypothesis of over extraction through canalization is correct but, unfortunately, with so little data as to the exact inflow/outflow (m^3/year) ratio of water in the CCB it is hard to substantiate.

Figure 2.36. Poza Baño Escobedo prior to canalization in the 1960's (left) and 30 years later in the 1990s (right) [image from Minckley, 1992].

Figure 2.37. Poza Becerra prior to canalization in the 1960s (top) and 30 years later in the 1990s (bottom) [image from Minckley, 1992].

2.5 Conclusions and future work

The Cuatro Ciénegas Basin is a unique desert oasis located in NE Mexico, supporting over 70 species of endemic flora and fauna as a direct result of groundwater discharge. Despite the ecological importance of this site, very little is currently known about the groundwater flow regime. Reconnaissance hydrological isotope data ($\delta^{18}\text{O}$, δD and $\delta^{13}\text{C}$) presented in this chapter suggests the CCB is currently functioning as a hydrologically closed basin with evaporative through-flow between water bodies. Groundwater discharge in the CCB appears to be a complex mix of hydrothermal groundwater originating from the Cupido-Aurora aquifer, ambient meteoric karst water and water originating from the deep lying karst reservoir through

focused channel recharge, culminating in a closed basin evaporative through-flow system.

The LEL slope ($\delta D = 4.4\delta^{18}O - 19.5$) indicates evaporation of surface waters is changing the isotopic composition of the CCB surface waters. Water body temperature data suggests the observed evaporation of the CCB surface water is not related to the temperature of the water sampled, however, with a relatively small sample size (26 water bodies sampled from over 200 possible) this is hard to conclusively demonstrate without further analysis. The 26 water bodies sampled within the CCB plot to the right of the GMWL and LMWL, from which the LEL has been proposed and at least three separate hydrologic systems have been identified:

- 1) Local faulting on the Sierra San Marcos y Pinos is the main control of the primary through-flow system in the CCB. Recharge from the regional Cupido Aurora aquifer is supported by the $\delta^{18}O$ and δD data and hot groundwater discharge to the west of the Sierra San Marcos, before flowing towards the terminal east of the basin consistent with previous conceptual flow models for the CCB [e.g. Johannesson *et al.*, 2004].
- 2) A similar, secondary, through-flow system is evident on the eastern flank of the Sierra San Marcos y Pinos, although hot groundwater appears to be prevented from upwelling, suggesting a greater influence of meteoric karst waters.
- 3) An independent system (Poza Anteojo), closely reflecting the isotopic composition of modern precipitation, is consistent with recharge in the Sierra Menchaca, previously suggested by Johannesson *et al.* [2004]. Focused channel recharge is supported by the warm temperature of the water issuing from Poza Anteojo.

Limited $\delta^{13}C_{DIC}$ data suggests the CCB is dominantly groundwater fed, with ^{13}C derived predominantly from soil CO_2 , however, conclusions as to the carbon source in each water body are limited due to the nature of the study; better understanding of the pools would result in better understanding of the complex sub-surface flow that is evident throughout the CCB. Further geochemical studies would also assist in better understanding the $\delta^{13}C_{DIC}$ pool in the CCB.

Future isotopic work on the waters from the CCB is certainly warranted to identify and constrain the hydrogeology of the CCB. Additional pools from both the west and east could be sampled to better understand the nature of underground mixing that is evident within the CCB, combined with detailed geochemical analysis to better understand the mineralogy of the waters, both when surfacing and flowing across the basin floor. Water balance equations coupled with flow regime from stable isotopes could give a much better understanding of exact inflow/outflow dynamics in the CCB, leading to the possible identification of specific areas in the basin from which to extract water for industry.

The complete drying of Laguna Grande, as a result of over extraction of water, is a major concern in the CCB, with water extraction becoming an increasingly large problem for the APFFCC in recent years. Observations of flow rate within the CCB suggest the processes of canalization and water extraction has, in itself, become a hydrologic flow system, disrupting the natural flow of water from the west of the basin to the east. The evaporative through-flow systems and modern hydrologically closed system identified in this chapter has provided a good model from which to base previous hydrological regimes in the CCB. If applied to the palaeoenvironmental reconstruction and terrestrial carbonate environments chapters, the current hydrological flow regime could be used to identify similar palaeo-flow regimes in the CCB, assisting in the identification of hydrological and/or climatic change. Combined with palaeoenvironmental data, the modern hydrological data could become a useful tool in the identification of ecosystem damage and response, allowing for better future management of the complex and fragile CCB ecosystem.

Chapter 3: Terrestrial carbonate environments of the Cuatro Ciénegas Basin

3.1 Introduction

The aim of this chapter is to describe preliminary observations of the terrestrial carbonate formations and depositional processes seen in the CCB and to understand the processes involved in carbonate formation and depositional modes associated with each carbonate facies described. These carbonate deposits have not been previously described from the CCB and the origins of each carbonate facies is proposed, based on the modern hydrological data presented in chapter 2 and evidence presented within this chapter.

3.1.1 Tufa and travertine formation

The terms tufa and travertine are both commonly attributed to calcium carbonate deposits of a terrestrial origin [Guo and Riding 1994; Pentecost, 1995; Ford and Pedley, 1996; Andrews *et al.*, 1997; Pedley *et al.*, 2003; Pentecost, 2005; Andrews and Brasier, 2005; Shiraishi *et al.*, 2008]. Calcium carbonates deposited from ambient (<40°) water sources such as fresh water springs and stream channels are termed tufas [Guo and Riding, 1994; 1999; Pentecost, 2005; Omelon, 2006]. Tufas are considered to be significant archives of palaeoenvironmental information as they not only record the geochemical characteristics of their source water [Andrews *et al.*, 1997, Andrews and Brasier, 2005] but can also develop outside, in sun-lit areas, promoting a macrobiological framework through photosynthesis [Pedley *et al.*, 2003; Pentecost, 2005; Brasier *et al.*, 2010]. Calcium carbonates precipitated from hydrothermal (>40°C) water sources are known as travertines [Guo and Riding 1994; 1999; Pentecost, 2005]. Travertines display less macrofacies diversity than tufas but can be distinguished by a higher diversity of bacterial and/or physico-chemical microlithologies [Ford and Pedley, 1996; Pedley *et al.*, 2003].

The terms 'meteogene' and 'thermogene' within this chapter are adopted from Pentecost [2005] and were originally used in the classification of different travertines. However, classification of tufas and travertines is much discussed [Guo and Riding,

1994; Pentecost and Viles, 1995; Pentecost, 1995; Ford and Pedley, 1996; Pedley *et al.*, 2003; Pentecost, 2005; Brasier *et al.*, 2010], so consequently, the use of the terms 'meteogene' and 'thermogene' within this chapter is to better distinguish between the component origins of tufas and travertines.

Meteogene tufas

Calcium carbonate deposits formed from cold-water springs discharging groundwater with a meteoric carrier are classed as meteogene tufas. Meteogene tufas carry CO₂ derived from meteoric sources i.e. atmospheric CO₂, soil carbon and form in regions underlain by carbonates [Pentecost, 2005]. Meteogene tufas have Ca and HCO₃⁻ water values typically ~160mg/kg and ~480mg/kg respectively and low δ¹³C_{DIC} values, ranging between -12‰ and +2‰ (mean -8.7‰). The predominantly negative δ¹³C_{DIC} values are thought to reflect the contribution of groundwater charged with soil respired CO₂ (δ¹³C_{DIC} values of around -25‰) or causing the dissolution of limestone in the case of superambient meteogenes (δ¹³C_{DIC} values of around 0 to +2‰) [Deines, 1980; Pentecost, 2005]. Higher δ¹³C_{DIC} values in meteogene tufas can be attributed to evaporation, CO₂ evasion, photosynthesis and/or dissolution of limestone [Barnes and O'Neil, 1971; Andrews *et al.*, 1997; Pentecost, 2005].

Meteogene tufas can be divided into two categories: *Invasive*, whereby invasion of atmospheric CO₂ into the carrier water leads to tufa precipitation and the more commonly occurring *Evasive*, whereby evasion of CO₂ from the carrier water leads to tufa precipitation [Pentecost, 2005]. Invasive tufas occur less commonly and are characterised by extremely low HCO₃⁻ concentrations <40mg/kg and high pH >9. These tufas will normally occur due to manmade circumstances e.g. lime burning sites, but also in serpentinite regions e.g. California, associated with the subduction of tectonic plates [Barnes and O'Neil, 1969]. Source waters leach through OH⁻ enriched soils, deposit dissolved CO₂ and HCO₃⁻ as subsurface carbonate, subsequently allowing CO₂ invasion and tufa precipitation when the water re-surfaces. Evasive tufas are more commonly occurring and can be divided into two categories based on the temperature of the source water:

a) *Ambient meteogenes*

The term 'ambient meteogene tufas' applies to tufas deposited at or below mean annual air temperature from cold water springs [Pentecost, 2005]. Ambient meteogenes have $\delta^{13}\text{C}_{\text{DIC}}$ values ranging between -12‰ and -3‰ and are characterised by a micritic, porous and often bio-rich fabric comprised of calcite.

b) *Superambient meteogenes*

The term 'superambient meteogene tufa' is tentatively applied to tufas deposited from source water that is up to 10°C above ambient air temperature (mean annual air temperature) but $<40^{\circ}\text{C}$ ($>40^{\circ}\text{C}$ would be classed as travertine) [Pedley *et al.*, 2003; Pentecost, 2005]. Superambient meteogenes have $\delta^{13}\text{C}_{\text{DIC}}$ values between -6‰ and $+2\text{‰}$, overlapping with ambient meteogene tufa and thermogene travertine values. However, superambient meteogenes are discernable from ambient meteogenes through looking at the calcium carbonate fabric and, in the case of thermogene travertine, are discernable through HCO_3^- as thermogene HCO_3^- values are significantly higher [Pentecost, 2005]. Superambient meteogenes are characterised by a micritic, porous and often bio-rich fabric comprised of mainly calcite.

Thermogene travertines

Calcium carbonate deposits formed from thermally heated source water ($>40^{\circ}\text{C}$) are classed as thermogene travertines. Thermogene travertines are formed when the source water carries high concentrations of thermally generated CO_2 (from thermal processes within or below the Earth's crust), capable of dissolving large quantities of the surrounding limestone bedrock before degassing at the surface, depositing CaCO_3 [Pentecost, 2005]. Thermogene travertines typically have Ca and HCO_3^- water values of around 80-800mg/kg and 400-4000mg/kg respectively and could have possibly formed in the CCB during wetter climatic periods where increased head pressure from the surrounding mountains may have created increased hot spring activity e.g. Pamukkale [Dilsiz *et al.*, 2004] and Central Italy [Guo and Riding, 1999] (Fig. 3.1).

Thermogene travertines are associated with localised deposition in regions with recent volcanic and/or tectonic activity and have exit temperatures at the surface of $>40^{\circ}\text{C}$ [Pentecost, 2005]. CO_2 degassing and CaCO_3 precipitation rates are elevated in thermogene travertines and consequently they contain enriched and more constant $\delta^{13}\text{C}_{\text{DIC}}$ values (-3 to $+8\text{‰}$) than meteogene tufas. The enriched $\delta^{13}\text{C}_{\text{DIC}}$ values of thermogene travertines can be partly attributed to non soil-zone carbon sources i.e. water-rock reactions and enrichments observed during rapid CO_2 evasion [Pentecost, 2005] but it is also thought a significant magmatic contribution may exist [Yoshimura *et al.*, 2004]. Thermogene travertines are characterised by a bacterial or cyanobacterial, non-porous fabric - typically of aragonite crystals

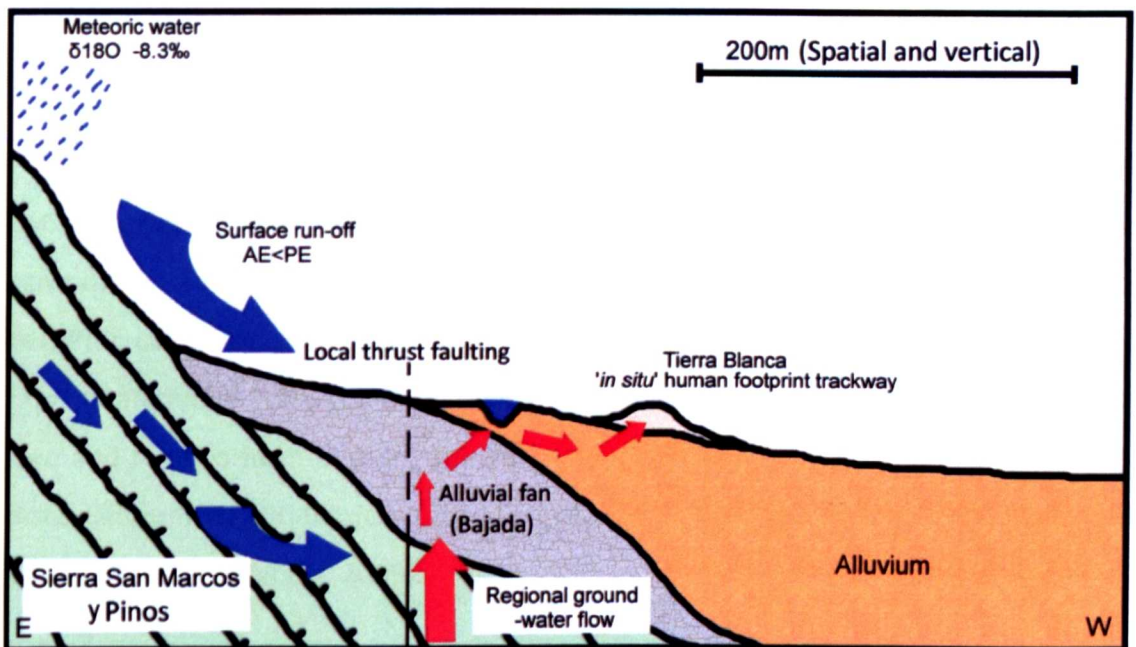


Figure 3.1. Schematic model showing E-W cross section across the CCB - from the meteoric water source in the limestone sierra (San Marcos y Pinos) to the basin floor. Local thrust faulting in the sierra provides a route for water heated deep underground to surface due to increased head pressure in the mountain. This recharge during climatically wetter periods causes water to not only recharge in pozas but also as calcium carbonate depositing springs.

Calcium carbonate fabric

Mechanisms controlling the precipitation of calcium carbonate, particularly in tufas, are related to differences in the physico-chemical (degassing of source waters) and biological (bacterial biofilm) processes acting upon the water carrying dissolved CaCO_3 in aqueous solution and are highly variable [Ford and Pedley, 1996; Pedley *et al.*, 2003; Pentecost, 2005; Brasier *et al.*, 2010]. Frequently, both processes are involved in the deposition of tufa carbonates leading to laminated microfabrics of

alternating sparry (physico-chemical) and micritic (biofilm) carbonates (Fig. 3.2) [Pedley *et al.*, 2003]. Both micritic and sparry fabrics are comprised of calcite with the former thought to be associated with biological mediation by microorganisms, particularly cyanobacteria, or physical degassing of carbon dioxide, usually as a result of high turbulence e.g. waterfall or cascade [Ford and Pedley, 1996; Pentecost, 2005]. These tufas carbonates may also display remnants of higher plant contributions e.g. bryophyte and/or phytoherm mesofabrics seen in barrage or perched springline deposits [Ford and Pedley, 1996], leaving cavities or pore space (branch and leaf moulds) within the fabric (Fig. 3.2). Sparry fabrics are thought to be associated with diagenetic infill of pore space or rapid degassing of carbon dioxide from areas of high PCO_2 to low PCO_2 , not requiring biological mediation [Pentecost, 2005; Andrews and Brasier, 2005].

As well as the physico-chemical and biological processes, temperature of the CaCO_3 carrier water can also have an effect on the calcium carbonate fabric. Travertine carbonates are deposited at temperatures $>40^\circ\text{C}$ and are commonly comprised of dendritic calcite or aragonite fabrics due to a higher calcium carbonate precipitation rate [Chafetz and Folk, 1984; Pentecost, 2005]. However, aragonite fabrics are more rare and tend to form in more sulphide-rich water under what would be considered disequilibrium conditions [Chafetz and Folk, 1984; Guo and Riding, 1994; Jones and Renaut, 1995; Pentecost, 2005].

Microbial influence on calcium carbonate formation

As previously mentioned both organic and inorganic mechanisms are involved in the formation of meteogene tufas and thermogene travertines. The role of microbes in calcium carbonate formation i.e. cyanobacteria, however, is less well understood [Andrews *et al.*, 1993; Andrews *et al.*, 1997; Pentecost, 2005; Shiraishi *et al.*, 2008]. It is generally accepted that calcium carbonate deposition by microbes can be in the form of both meteogene tufa ($<40^\circ\text{C}$) and thermogene travertine ($>40^\circ\text{C}$) and is determined by three main factors: the photosynthetic uptake of CO_2 , the presence of a polysaccharide sheath providing a favourable calcium carbonate nucleation site and favourable calcium carbonate precipitation conditions such as slow flow locations e.g. Pedley *et al.*, [2003] paludal swamp model [Pentecost and Riding, 1986; Andrews *et al.*,

1993; Andrews *et al.*, 1997; Shiraishi *et al.*, 2008]. The depositional factors, particularly photosynthetic uptake of CO₂, suggest microbial deposition of calcium carbonate to be under disequilibrium conditions, unfavourable for the recording of palaeoenvironmental data. However, photosynthetic microbial influence on δ¹⁸O values of calcium carbonate is thought to be negligible [Andrews *et al.*, 1993; Andrews and Brasier, 2005; Shiraishi *et al.*, 2008] and, other than providing a site for CaCO₃ precipitation, microbial calcification appears to adhere to equilibrium deposition in the form of annual laminations (Fig. 3.2) [Andrews and Brasier, 2005] potentially containing important climatic and palaeoenvironmental archives [e.g. Andrews *et al.*, 1993; Andrews *et al.*, 1997; Brasier *et al.*, 2010].

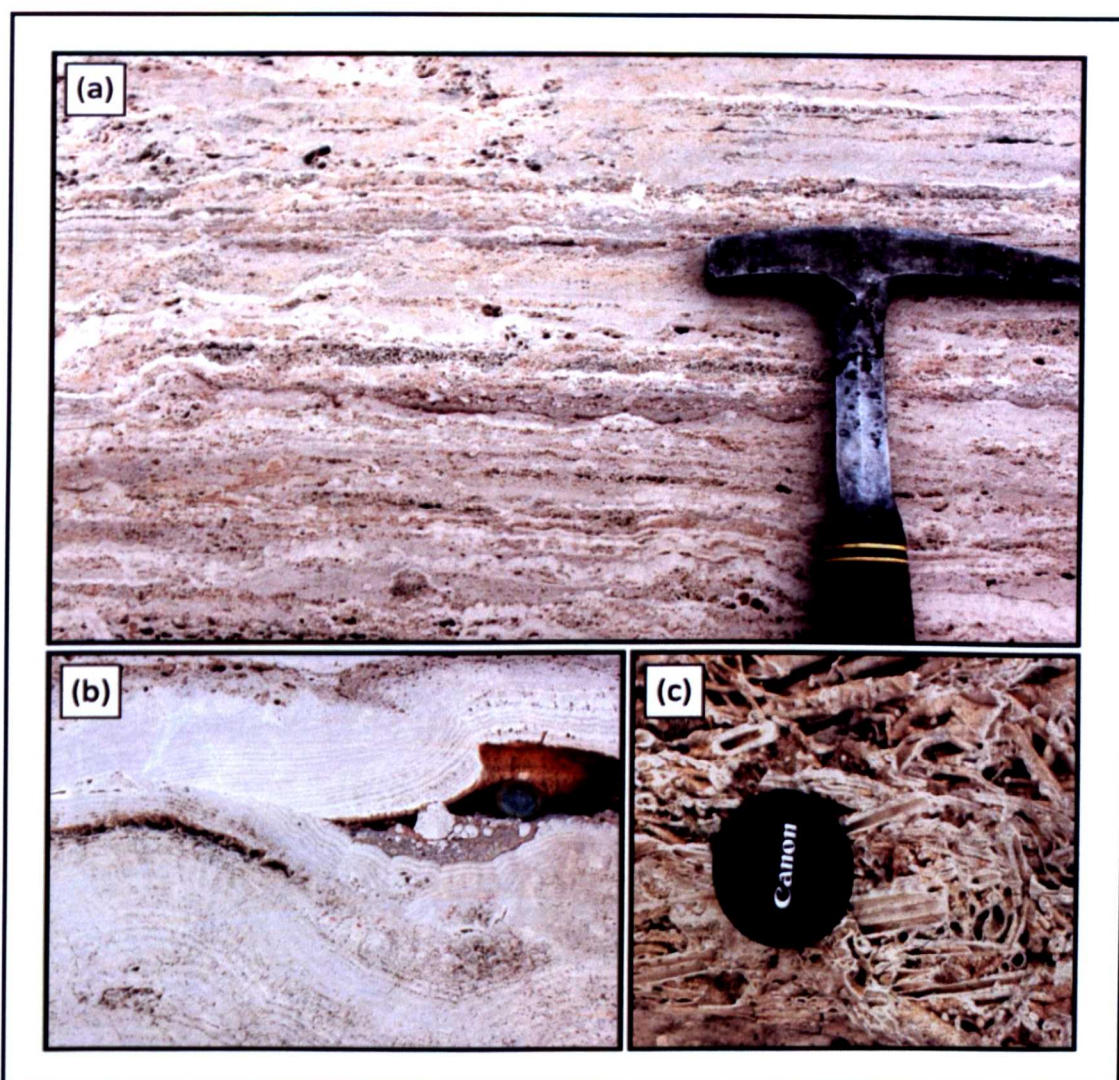


Figure 3.2. Photographs of CCB calcium carbonate deposits; a) Laminar tufa deposits, with a hammer for scale; b) Microbially deposited tufa displaying characteristic annual laminations, with a coin for scale; c) reed and palm frond encrustations *in situ*, with a lens cap for scale.

3.2 Calcium carbonate formation within the CCB

There are several sites with calcium carbonate deposits described here in the CCB (Fig. 3.3), including (a) a rim-stone pool complex, (b) the Tierra Blanca spring mound (see chapter 4), (c) a fissure ridge complex (see appendix 1.1) and (d) a perched terrace.

The hydrology of any given site is an important factor in determining what type of calcium carbonate is precipitated as differences in physical and ecological environment i.e. vegetation, can determine the tufa fabric [Pentecost, 2005]. The hydrology of the CCB is known to be extremely complicated [Johannesson *et al.*, 2004; Wolaver *et al.*, 2008; Chapter 2] and climate has not remained stable over time. The CCB is currently classed as a closed karstic system [Badino *et al.*, 2004] with surface water temperatures rarely higher than 32°C and as such it is unlikely that CO₂ within the source waters is of a thermal or magmatic origin. Circulation of meteoric water within the Cupido-Aurora aquifer, deep underground [see chapter 2], is the most likely thermal source as well as contributing, along with soil, to the carrier CO₂.

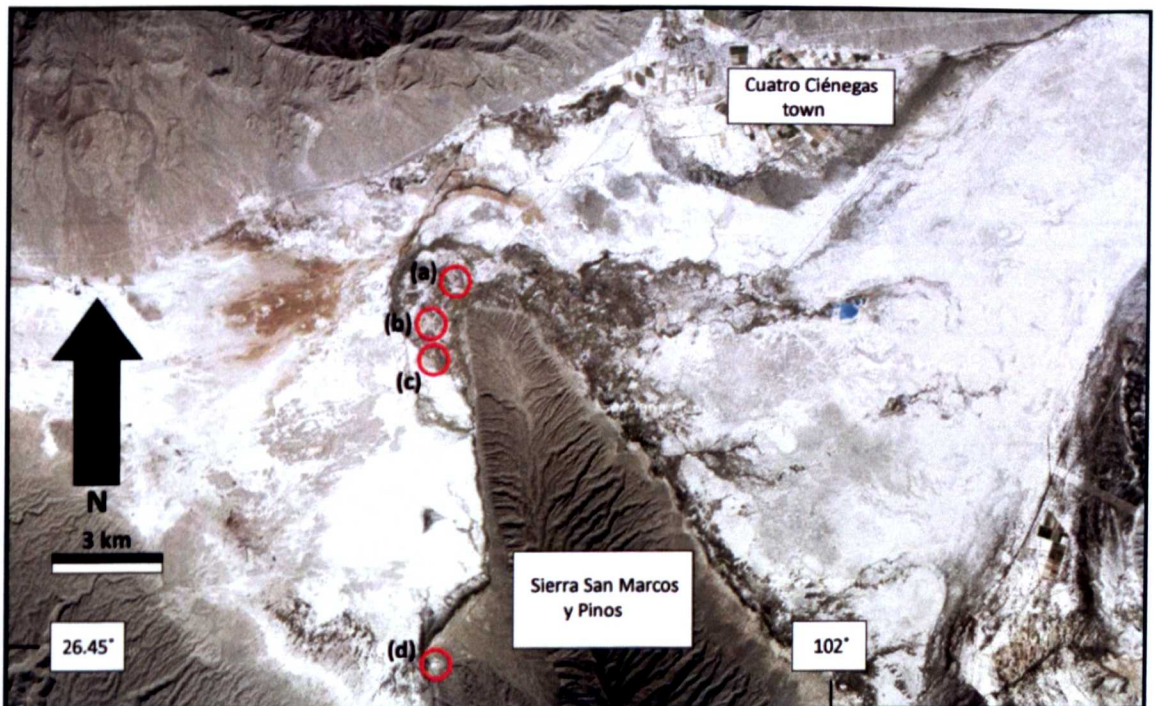


Figure 3.3. Location of studied tufa deposits within the CCB; (a) a rim stone pool complex, (b) a spring mound containing human footprints (see chapter 4), (c) a fissure ridge complex (see appendix 1.1), (d) a perched terrace where previous quarrying activity has occurred showing the sequence in detail [image from google.co.uk/earth].

3.2.1 Rim-stone pool/dam complex

Rim-stone pool complexes are meteogene tufa formations well documented around the world [Pentecost, 2005; Cruz *et al.*, 2005; Omelon *et al.*, 2006]. Within this chapter the term “rim-stone pool” is used alongside the term “dam” as definitions are dependent on the author; both terms will be adopted in this chapter. Rim-stone pools/dams are defined as vertical accretions of meteogene tufa, leading to the pooling of water (Fig. 3.4) [Pentecost, 2005].

Figure 3.4. Model for terraced “rim-stone pool” complex to the NW of the piedmont of the Sierra San Marcos y Pinos [modified after Pentecost, 2005].

The pooling of water leads to meteogene tufa precipitation *in situ* creating a succession of dam-like structures, down-gradient through a water course. The wall effectively damming the water course faces upstream and is known as the ‘up wall’. As the water eventually tops the dam, the ‘drop wall’, across which the water flows, completes the dam structure. The drop wall forms a steeper structure than the up wall and is best used for determining total dam height - ranging between <1cm to >40cm depending on factors such as source water flow speed, vegetation type (bryophyte vs. phytoherm), microbial input and mineralogy of the source water [Pentecost, 2005].

Inter-dam distance (IDD) is the distance between dams and defines the dam type. IDD's range from centimetres to kilometres depending on the slope angle of the water course and is seen as a distinguishable feature. Dams with IDD ranging 1cm-1m have slope angles typically $\leq 30^\circ$ and are termed 'minidams' whereas larger IDD's ranging from 1m->100m with slope angles typically $\leq 5^\circ$ are termed 'macrodam's' [Pentecost, 2005].

3.2.1.1 Study site

The rim-stone pool complex is located 1km NE of Tierra Blanca quarry (N $26^\circ 55' 37.1$, W $102^\circ 08' 90.6$) and 1km N of the Mex-30 highway and piedmont of the Sierra San Marcos y Pinos (Fig. 3.5).

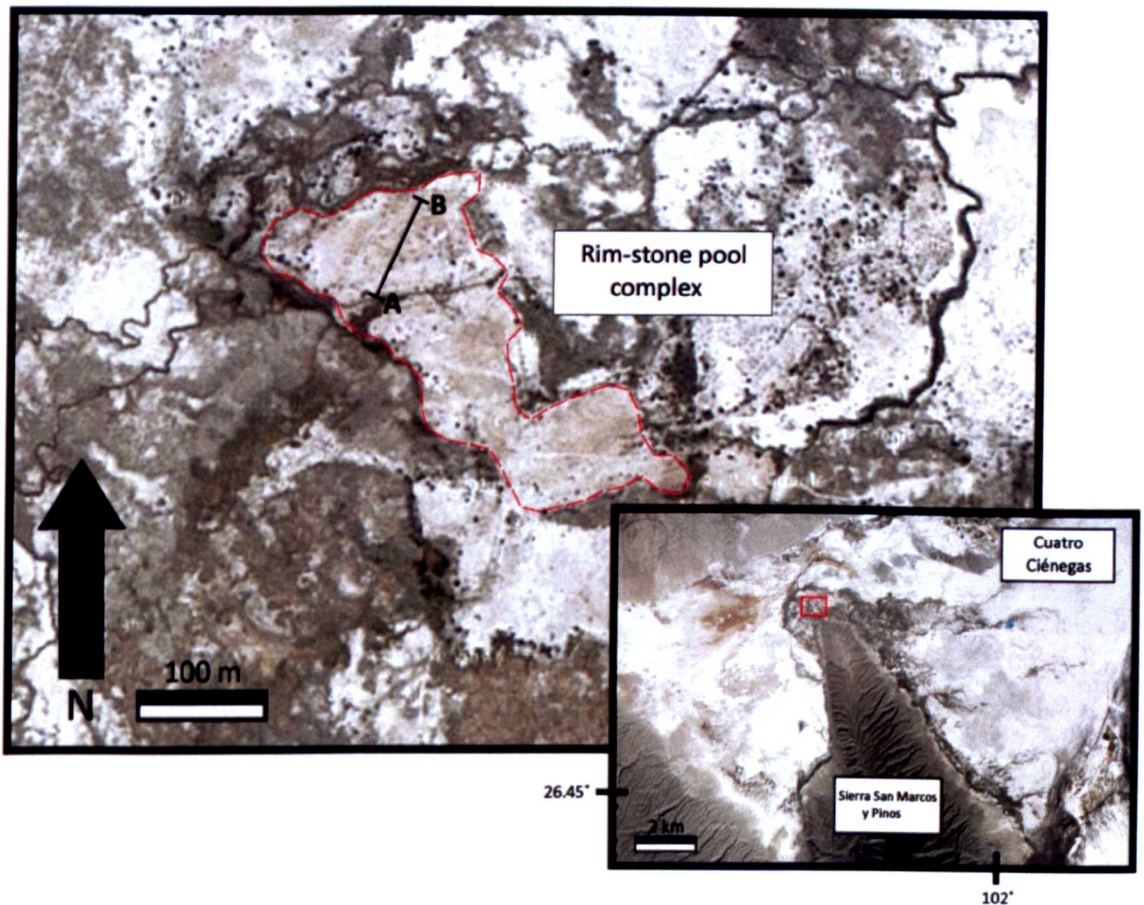


Figure 3.5. Location of the rim-stone pool complex. The red line highlights the depositional area and line A-B represents the transect across the rim-stone pools in Figure 3.8 [image from google.co.uk/earth].

3.2.1.2 Preliminary research and methods

The rim-stone pool complex in the CCB is a special facies of tufa dam in that it appears not to be directly sourced from a spring mound structure or fissure zone (Fig. 3.6) like microdams observed in Hungary [Pentecost, 2005] and macrodams observed

in Turkey [Burger, 1985]. Instead the rim-stone pool structures are sourced from a small pool at the top (highest point) of the complex. The source pool is part of the ciénega area discussed in chapter 2, forming part of the main evaporative through-flow system observed in the CCB. Increased water input appears to cause overflowing of this pool (as observed during heavy rainfalls in the CCB), the water flows down gradient building another dam and this process continues down gradient, similar to freshwater river tufa dams observed in Papua New Guinea [Humphreys *et al.*, 1995]. As water input decreases, the pools furthest down gradient will dry first as the water recedes back to the original pool.



Figure 3.6. Large rim-stone pool complex. Although now inactive, no fissure ridge or spring mound is present to have provided source waters.

A 180 m cross-section transect of the tufa dam structure in the CCB was conducted using a theodolite to investigate surface morphology and topography (Fig. 3.8). The theodolite was positioned at the edge of the contemporary pool (Fig. 3.8) at the top of the rim-stone pool complex. Elevation measurements were taken at the base of each up-wall, at the tip of each individual dam and at the base of each down-wall. The presence of the rim-stone pool complex indicates that it was deposited during a climatically wetter period as meteogene tufa is no longer being deposited.

The preservation of the complex is excellent and individual dam structures can be clearly seen, of which two samples at S1 and S2 were taken to be studied due to their location at the top and bottom of the complex respectively. S1 and S2 sample locations were chosen at the top and bottom of the complex to ascertain U-series dates for the possible advance and retreat of water through the complex as it is assumed a maximum age for the complex would be located at the top when water first over spilled and a minimum age would be located at the base of the complex as this would be the first area to become dry when the complex became inactive e.g. Moeyersons *et al.* [2006]. The dam structures also contain well preserved bryophytic microfabrics and mesofabrics (Fig. 3.7). Severe natural degrading to the tufa structures beyond 120 m has made any structures that may have been present too damaged to study, although broken fragments of tufa suggest it is likely that a continuation of the rim-stone structures was there prior to degradation.

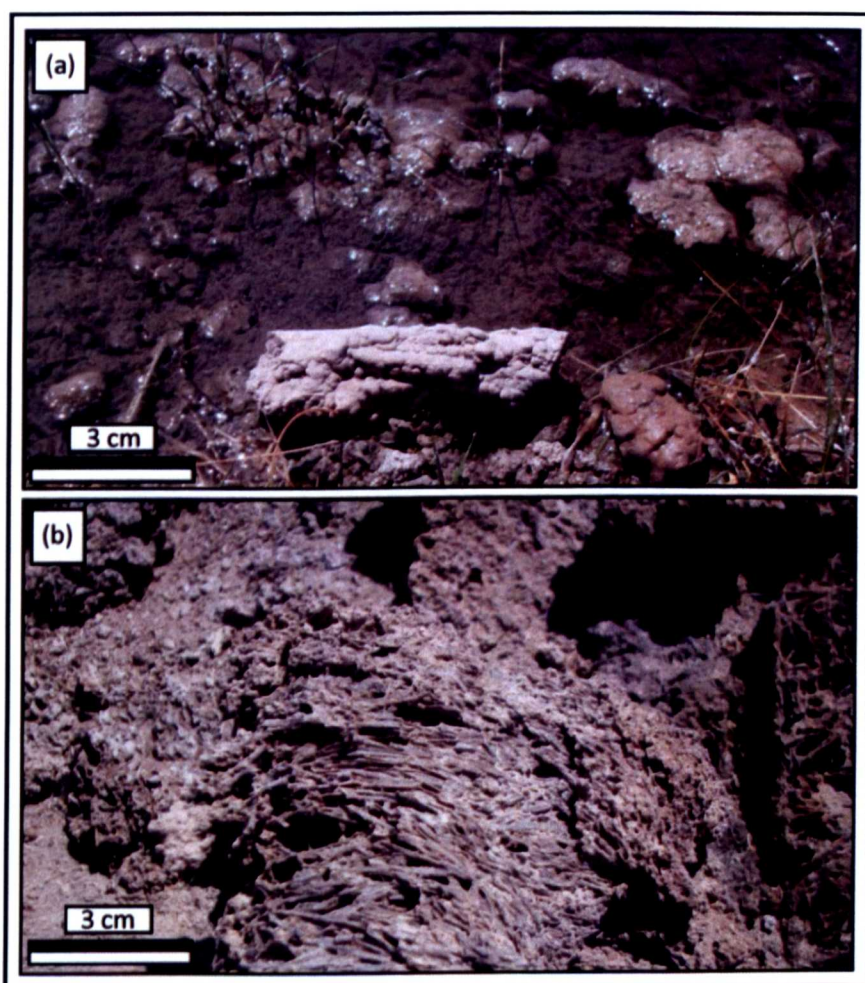


Figure 3.7. Photographs of vegetation preserved at the rim-stone pool complex; a) bryophytic microfabric in the form of algal encrustations, preserved algae is at the base of photo presented alongside modern day living algae; b) bryophytic mesofabric preserved in a dam structure.

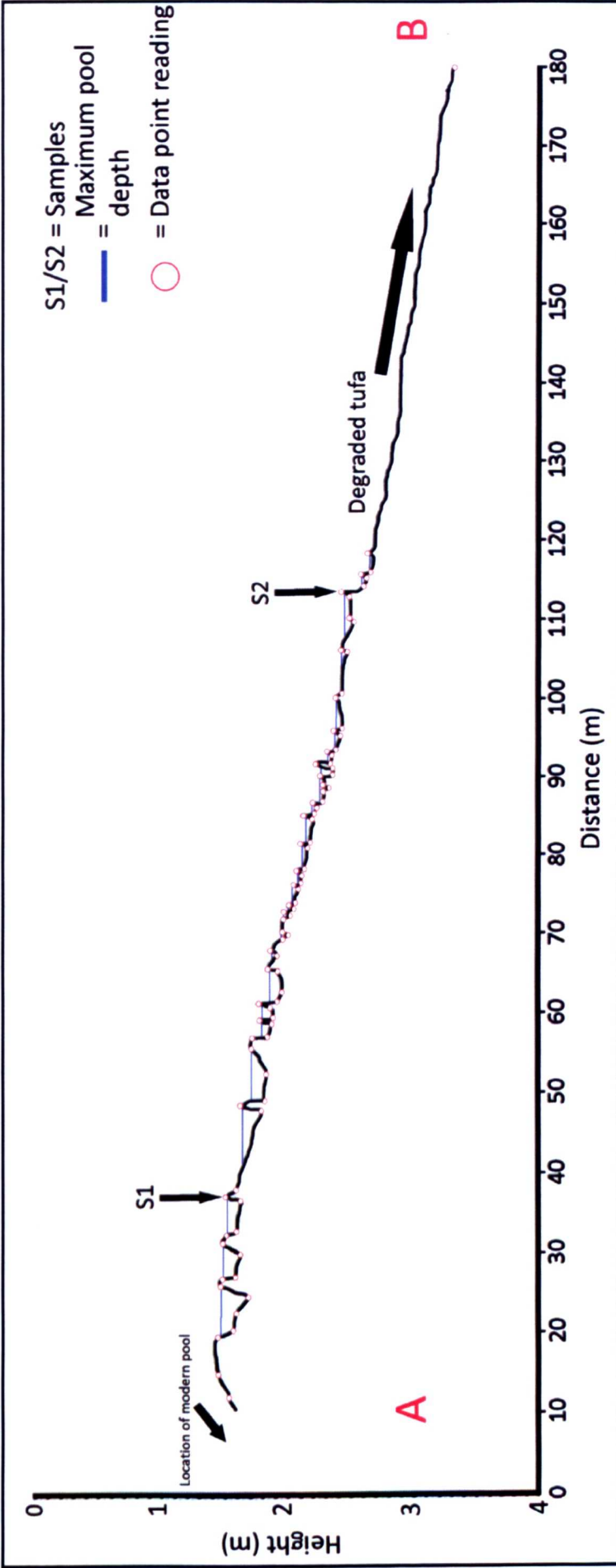


Figure 3.8. Topographic transect of the rim-stone pool/dam complex. Vertical scale is exaggerated so up-walls and drop-walls are more prominent. Samples S1 and S2 were taken for U-series dating but subsequently not used.

The dam height, IDD and slope angle determine the classification of the rim-stone pools into either microdams or macrodams [Pentecost, 2005]. The rim-stone pool complex here appears to cross both categories of dam classification with 8 pools displaying characteristics typical of microdams – IDD <1 m – and the remaining 19 pools displaying characteristics typical of macrodams – IDD >1 m. The pools formed by the series of dams seen in figure 3.8 cover 120 m of the 180 m cross-section transect with the remaining 60 m of epigean tufa being too eroded for study. 27 separate pools occur within the complex with IDDs ranging from 10 cm to 10 m in size and dam heights ranging from 5 cm to 20 cm (Fig. 3.8). The rim-stone pool complex loses a total of 1.8 m in elevation over the 120 m transect giving an approximate slope angle of 0.86°. It is interesting to note at 70 m a change from macrodam IDD structures to a cluster of 8 microdam IDD structures before changing back to macrodam structures at 94 m. Although the average slope angle for the entire transect is 0.86°, the 24 m section of microdam IDD structures has a slope of 1.19° which should still class the dam structures as macrodams.

The slope angles of 0.86° and 1.19° should constitute that of a macrodam structure (<5°) and be too shallow for that of microdams which are typically up to 35°. Definitions can be misleading however, as no definition of an intermediate dam i.e. a dam with a slope of < 5° and IDD of <1 m, exists. Therefore the terms ‘macrodam’ or ‘microdam’ would appear inappropriate to this type of dam complex in the CCB; instead the term ‘mesodam’ would be more appropriate.

A series of U-series dates will give a basis for future isotope work on the complex. A high resolution chronology would show how the water, depositing tufa, advanced and retreated. A gradual evaporative effect should be observed from the top of the complex to the bottom due to evaporation of the flowing water, a model which can then be applied on a larger scale to the whole basin.

3.2.2 Perched terrace

Perched terraces are not commonly occurring deposits and, globally, few have been studied in detail. Perched terraces typically occur along terraced rivers or valleys with steep sides [Ordonéz *et al.*, 1987; Ford and Pedley, 1996; Ortiz *et al.*, 2009] and are of a fluvial (river), spring, lacustrine or paludal (swamp) origin, although each origin type can occur with variable dominance over the course of the perched terrace depositional period [Pedley *et al.*, 2003; Ortiz *et al.*, 2009].

Calcium carbonate precipitation on perched terraces is under normal (equilibrium) circumstances of CO₂ evasion from bicarbonate rich source waters [Pedley *et al.*, 2003; Brasier *et al.*, 2010]. Although, because of the terraced valley and/or steep slopes involved with the deposition of perched terraces, source waters are generally fast flowing which can cause physical degassing of CO₂ resulting in characteristic waterfall or cascade structures (Fig. 3.9) [Pedley *et al.*, 2003]. Perched terrace deposits are commonly lobate in plain view, attributed to the fast flowing nature of the source water, and can form on a fluvial substrate that can be in the form of braided channels [e.g. Ortiz *et al.*, 2009].

These fluvial tufas can be succeeded by spring or paludal origin tufa in karstic areas: as the river bed becomes eroded leaving the fluvial tufa above the water line, the perched spring line and subsequent tufa deposition becomes raised above contemporary fluvial activity and deposition [Pedley, 1993; Pedley *et al.*, 2003; Ortiz *et al.*, 2009].

The succession of spring and paludal origin tufa can be seen in Figure 3.9 with spring activity depositing calcium carbonate in a terrace like structure. The flat top structure forms an ideal environment for shallow, paludal calcium carbonate deposition. Stromatolitic crusts form on stable substrates in shallow, slow flowing water and can be accompanied by algal mats or phytoherm cushions in the central areas of the water. Macrophytes and bryophytes can also be observed on the fringe areas of the water, the roots becoming encrusted by tufa under the water like those observed in stream crusts in the UK and Spain [Pentecost, 2005; Ortiz *et al.*, 2009].

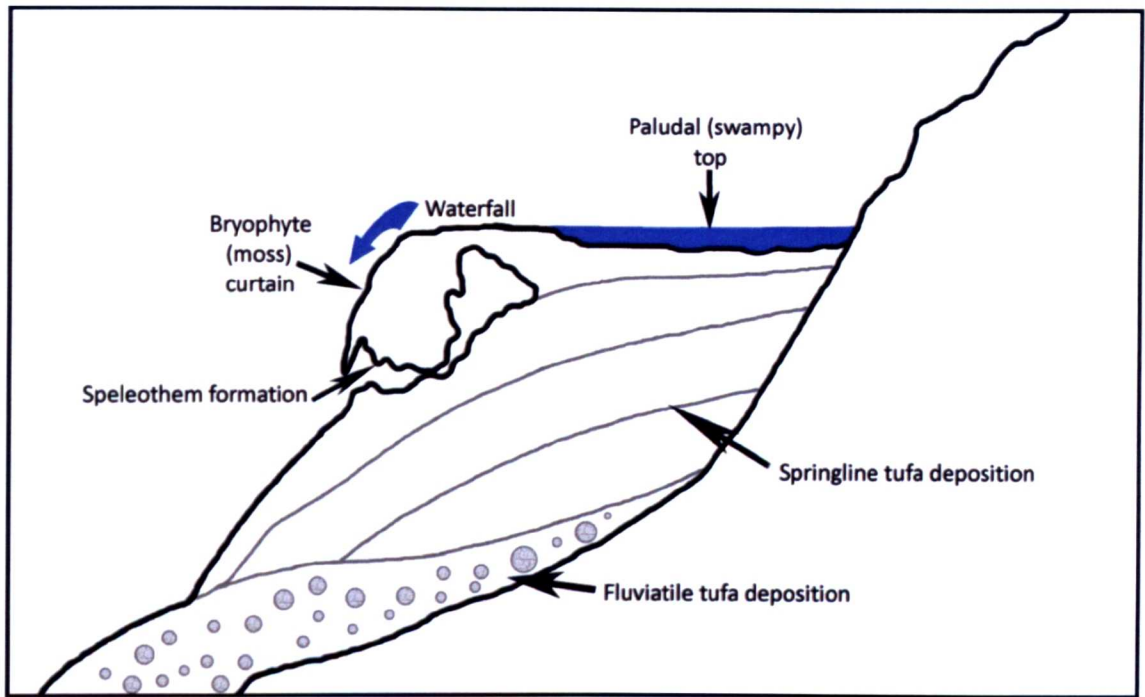


Figure 3.9. Schematic showing perched terrace deposition [modified after Pedley *et al.*, 2003]. Fluvatile tufa deposition at the base of the terrace is succeeded by springline and paludal tufa deposition. Incised fluvial channels and bryophyte curtains are characteristic of these types of deposits.

3.2.2.1 Study site

The perched terrace is located in the SW of the CCB on the west flank of the Sierra San Marcos y Pinos (N 26° 48' 61.2, W 102° 09' 05.4), approximately 100 m from the Mex-30 highway (Fig. 3.10). The site was originally described as a palaeo-shoreline of a pluvial lake [Minckley, 1969 (Fig. 3.11)] but has since remained unstudied. This isolated terrace is located 50m above the CCB floor and is the only such deposit within the CCB.

The terrace has undergone substantial change as a result of quarrying activity during the past 40 years. The consequence of this quarrying activity can be seen when comparing Figure 3.11 (Minckley, 1969) and Figure 3.12 (contemporary photograph taken in 2010). The overhang of tufa has been almost completely quarried, leaving a 10 m tufa cross-section laterally through the terrace. Because of the construction of quarry access to the east, the rear of the terrace has been almost completely removed, with two access roads cut away from the north face of the terrace (Fig. 3.10).

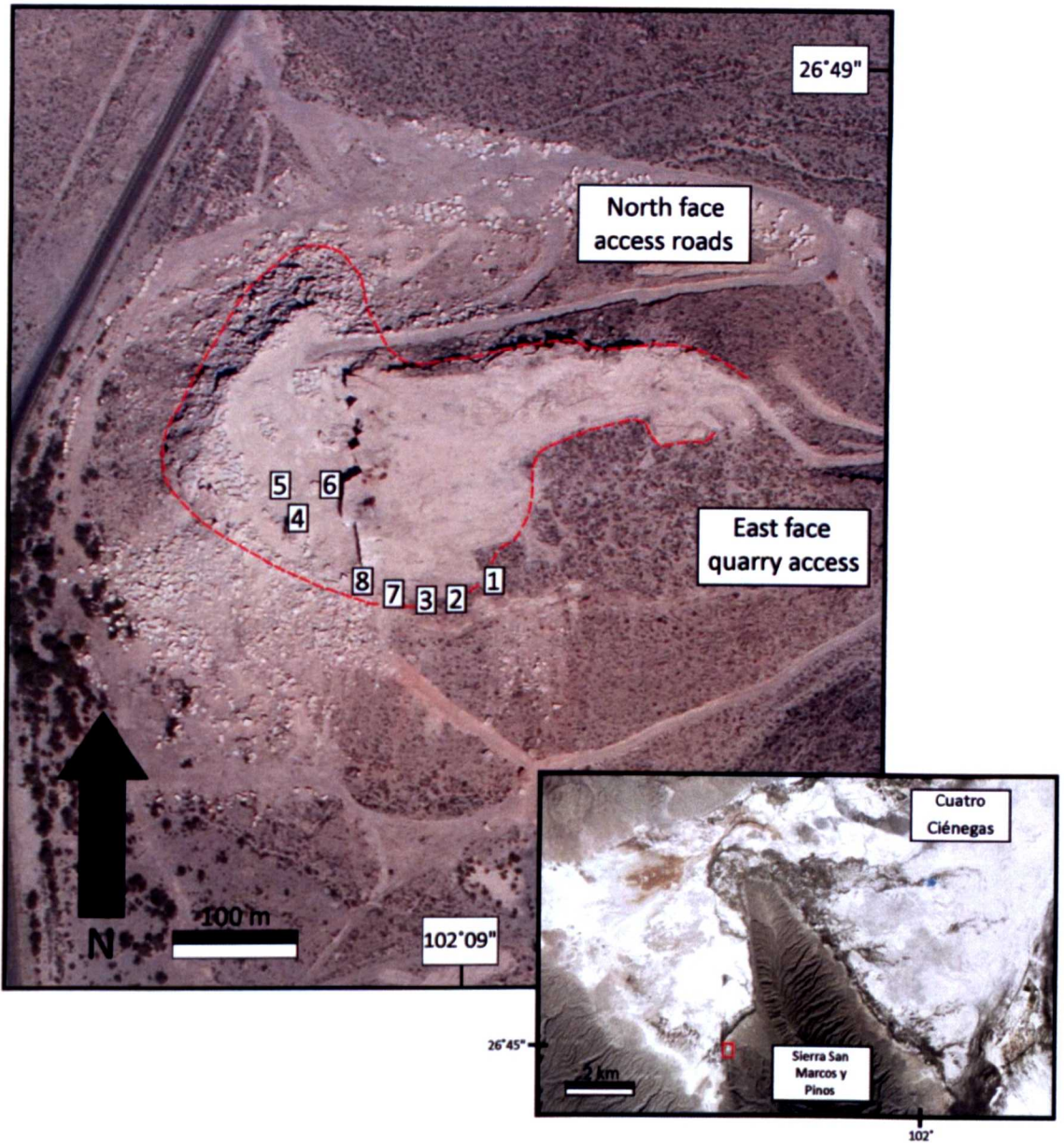


Figure 3.10. Location of the perched terrace in the CCB. The typical lobate plain view is highlighted by the dashed red line and the extent of the quarrying activity can be clearly seen with access tracks on the north, east and south faces. Numbers 1-8 show where stratigraphic logs were taken (Figs. 3.17, 3.18, 3.19, 3.20, 3.21) [aerial photograph provided by Dean Hendrickson].

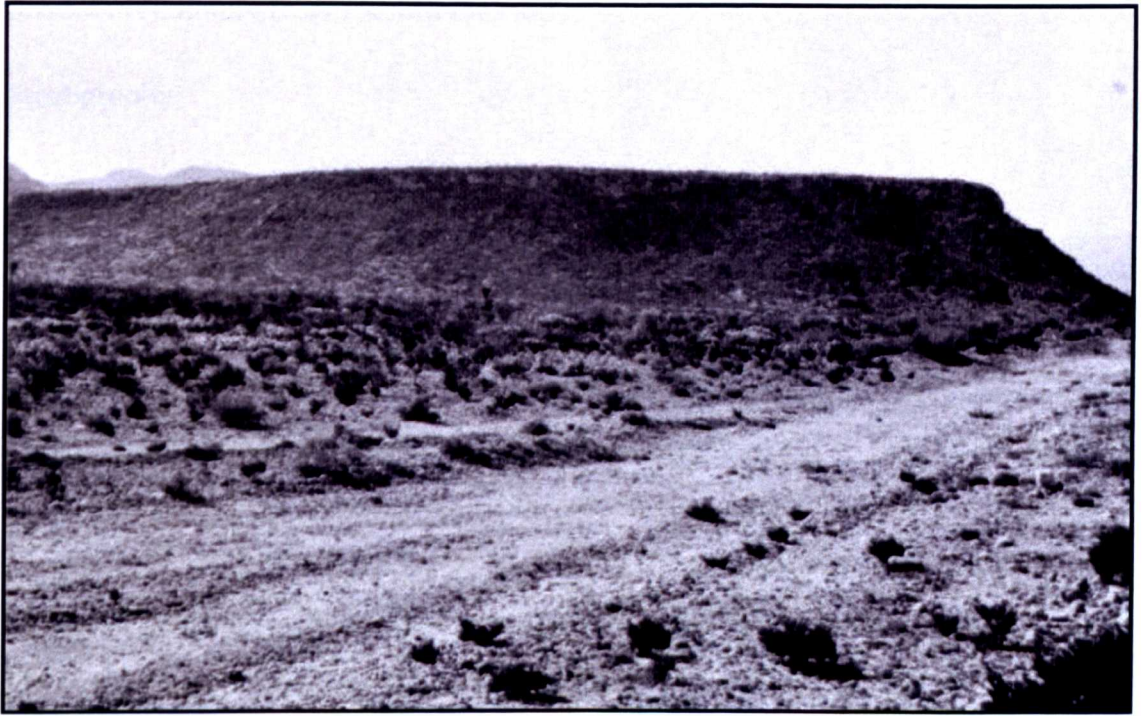


Figure 3.11. Original photograph of the perched terrace taken by W. L. Minckley in the 1960s [Minckley, 1969]. The original geomorphology of the terrace can be seen (in comparison with the heavily quarried modern view in Fig. 3.12).

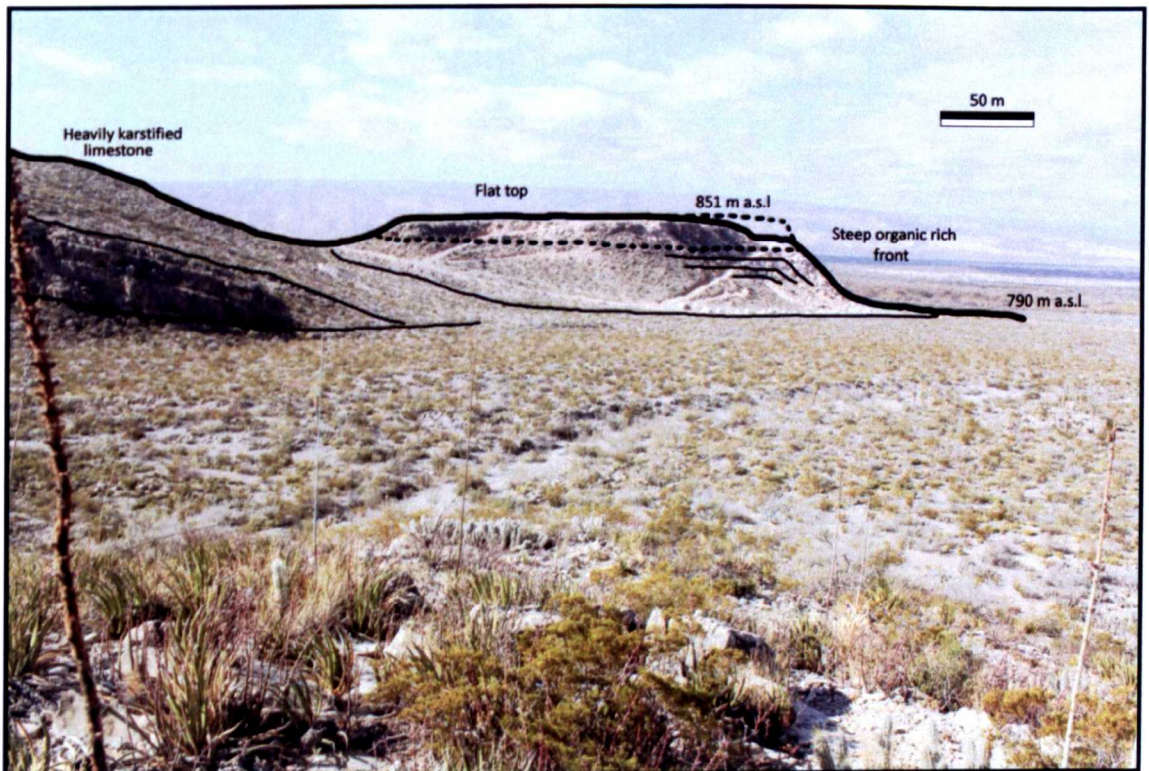


Figure 3.12. Annotated photograph of the perched terrace in the CCB. The Sierra San Marcos y Pinos to the left (east) of the terrace is heavily karstified. The black dashed line shows the extent of the flat terrace top before quarrying began.

3.2.2.2 Preliminary research and methods

Stratigraphy

a) North face

To determine the perched terrace origin, the stratigraphy of the deposit was studied. First, a 50 m section on the upper north face access road was studied to determine the underlying stratigraphy of the terrace (Fig. 3.13). The section description is compiled through a series of spatially linked observations (Figs. 3.13, 3.14, 3.15 and 3.16). At the base of the stratigraphy there is a 20 m thick section consisting of finely laminated Cretaceous limestone bedrock dipping 30° in a northerly direction, consistent with the dip direction of the plunging anticline of the Sierra San Marcos y Pinos [Badino *et al.*, 2004]. Red discolouration and alteration along the laminated planes in the limestone (Fig. 3.14) suggest the possibility of hot fluid circulation depositing FeO minerals [e.g. Pires *et al.*, 2010]. Local faulting at the rear of the terrace structure, at the base of the Sierra San Marcos y Pinos, is a possible spring location and source of hydrothermal water.

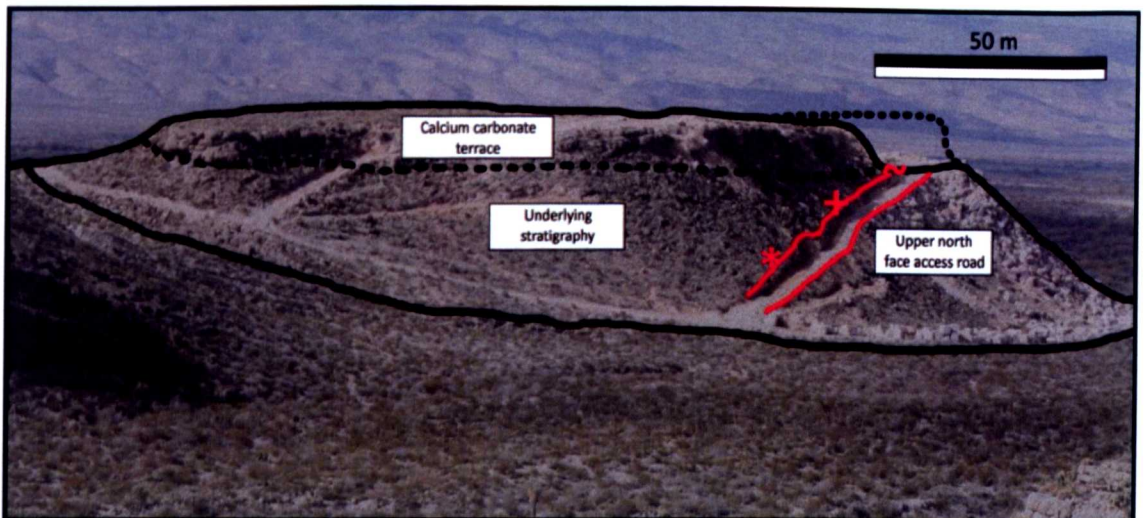


Figure 3.13. Annotated photograph of the perched terrace north face. The black dashed line shows the extent of the flat terrace top before quarrying began. The parallel red lines show the exposed studied section through the underlying stratigraphy due to the construction of the upper north face access road. * shows the location of figure 3.14. + shows the location of figure 3.15. ~ shows the location of figure 3.16.

Overlaying, unconformably to the laminated Cretaceous limestone, is a 20 m layer of conglomerate. The clasts consist of sub-rounded to rounded limestone, medium sandstone and laminated limestone, ranging from 1 cm to 30 cm. The conglomerate is not well consolidated with random sorting of clasts in a caliche

(calcium carbonate cement [e.g. Zhou and Chafetz, 2009]) matrix, no apparent grading is present and also no channels appear to be present within this conglomerate layer.



Figure 3.14. Red colouration suggesting hot fluid circulation and deposition of FeO within the laminated limestone bedrock.

The conglomerate lying unconformably on top of the limestone suggests possible flash floods, debris flows or hyperconcentrated flows. 'Jigsaw puzzle' clasts [e.g. Fulop, 2001] are characteristic of hyperconcentrated flows and are observed within the conglomerate layer (Fig. 3.15). Towards the top of the conglomerate bed is a 4 m 'lens' of calcium carbonate containing rounded clasts of limestone, similar to those of the conglomerate bed. The calcium carbonate 'lens' is below a second bed of conglomerate indicating the calcium carbonate deposition was contemporaneous with the conglomerate deposition, suggesting the possibility of a fluvatile meteogene tufa [Pedley *et al.*, 2003; Ortiz *et al.*, 2009].

The second conglomerate bed is approximately 6 m thick and leads into the 10 m thick calcium carbonate cap on the sequence. Like the calcium carbonate 'lens' lower in the sequence, the second conglomerate inter-beds with the overlying calcium carbonate terrace, forming incised channels into the underling laminated calcium carbonate and containing sub-rounded to rounded clasts (Fig. 3.16).

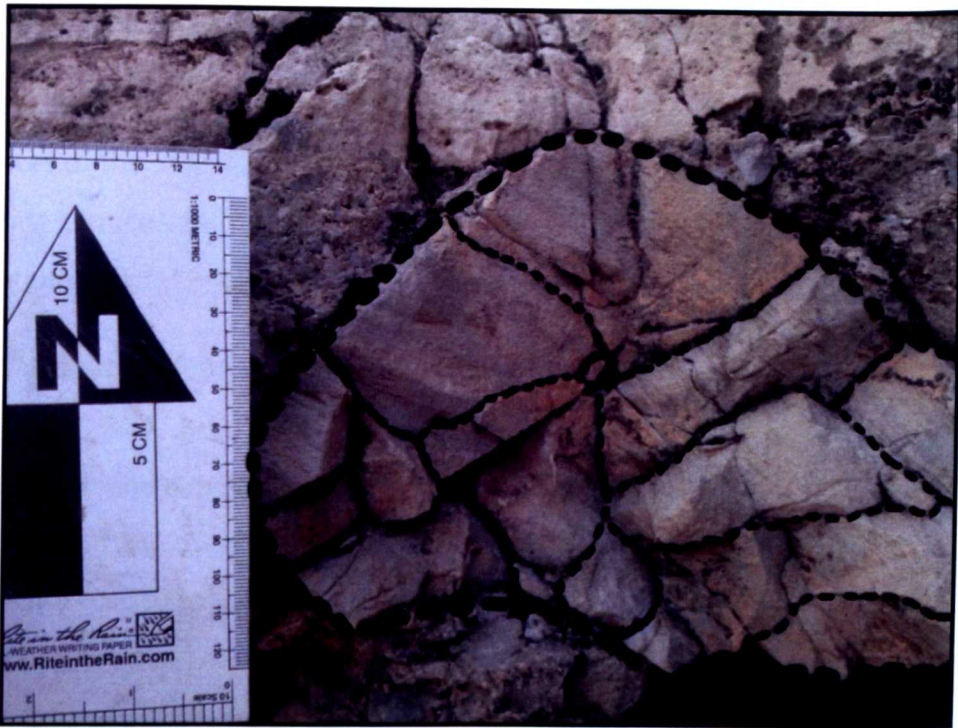


Figure 3.15. Photograph of 'jigsaw puzzle' clast observed in the perched terrace conglomerate. The clast maintains its sub-rounded shape despite extensive fracturing.

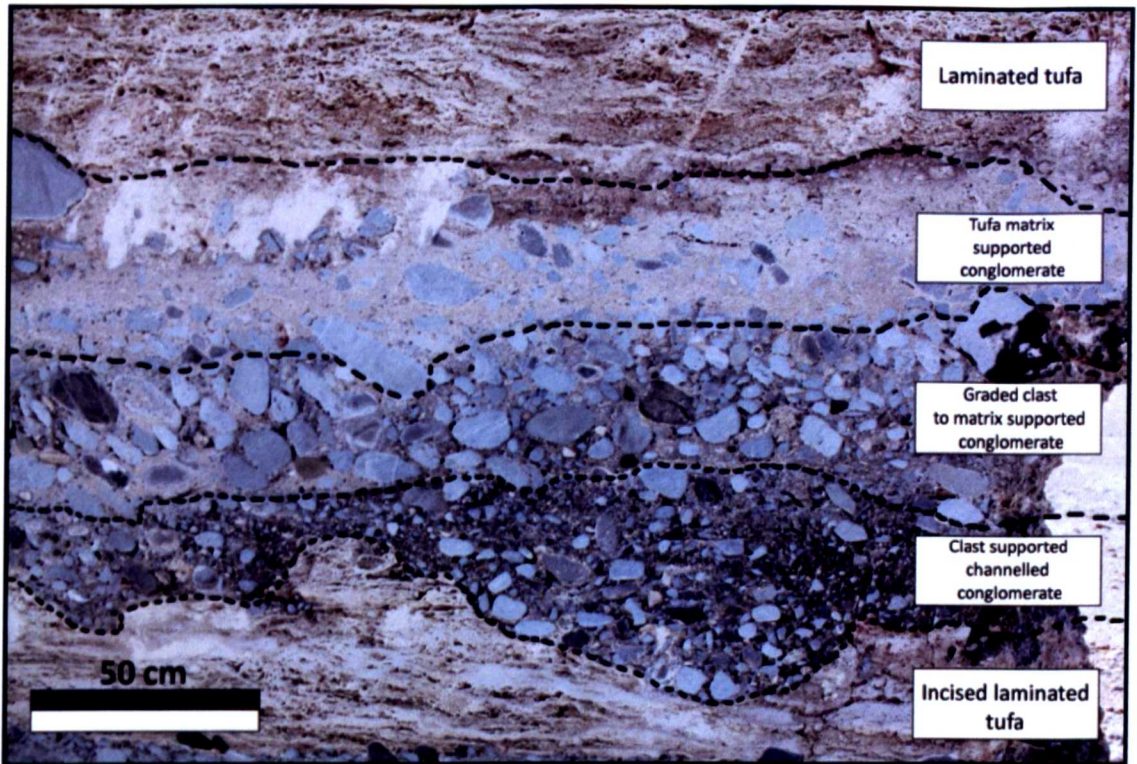


Figure 3.16. Annotated photograph of inter-bedded conglomerate and laminated calcium carbonate. Incised laminated tufa and poorly sorted, sub-rounded conglomerate at the base suggest fluvial/flash flood deposition. A change from clast supported to tufa matrix supported conglomerate up the section suggests intermittent fluvial and spring activity at the perched terrace.

b) South and west faces

A series of eight detailed stratigraphic logs were measured on the south and west faces of the perched terrace to investigate the depositional history of the calcium carbonate terrace cap (Figs. 3.10, 3.17, 3.18, 3.19, 3.20, 3.21; for detailed stratigraphic descriptions see appendix 1.2).

All stratigraphic logs from the south face of the perched terrace – logs 1, 2, 3, 7 and 8 (Figs. 3.17 and 3.18) - display inter-bedded conglomerates and laminated calcium carbonate deposits at the base. Conglomerate beds at the base of logs 1, 2 and 3 are overlain by laminated calcium carbonate beds displaying horizontal bedding planes. The basal conglomerate beds, particularly in logs 1, 2 and 3 (Figs. 3.18 and appendix 1.2), contain imbricated gravel channels, suggesting intermittent fluvial activity between calcium carbonate deposition. Moving along the E-W axis of the perched terrace (from log 1 to log 8 (Figs. 3.17 and 3.18)), channelling of the conglomerate beds becomes less prominent, particularly in log 7, with deposition in sheets displaying reverse grading, characteristic of hyperconcentrated flows. Despite the observed horizontal bedding planes within the calcium carbonate units there appears to be little to no lateral continuity, particularly between logs 2, 3, 7 and 8, suggesting complex spatial deposition of both the laminated calcium carbonates and conglomerates. Section h of log 1, section a of log 2 and sections a, b, c of log 3 (Fig. 3.18) display some lateral continuity, although the calcium carbonate units in logs 2 and 3 contain vugs and solution fractures respectively, not observed in Log 1, again highlighting the lack of spatial continuity within the laminated calcium carbonate units. Section b of log 7 can be tentatively matched with log 3 as both contain mottled sand and solution fractured calcium carbonate, however, conglomerates in log 3 display evidence of channelling that is not evident in section b of log 7. The observed complex spatial deposition of the perched terrace is possibly as a result of apparent braided channelling (Fig. 3.16) and vegetation growth, observed as micrite filled vugs (Fig. 3.18, appendix 1.2). These observations are characteristic of fluvial and paludal facies meteogene tufa deposition [e.g. Pedley *et al.*, 2003].

No major hiatuses are observed within the 10 – 12 m calcium carbonate sequence at the top of the perched terrace (Figs. 3.19, 3.20, 3.21 and appendix 1.2)

suggesting no major interruptions in deposition. Large hydrofracture structures are observed in logs 4 and 5 (Figs. 3.19, 3.20 and appendix 1.2) suggesting the fluid circulation observed in the north face limestone (Fig. 3.14) may have been of a thermal nature and possibly the source for the laminated calcium carbonate deposits observed throughout the whole sequence. Bryophytic and macrophytic crusts can be seen throughout the sequence with submergent *Chara* and *Typha* species the most prominent macrophytes, forming a cascade type feature on the west face of the perched terrace (Figs. 3.22 and 3.23) as well as large fossil palm frond encrustations abundantly well preserved at the base of the calcium carbonate sequence (Fig. 3.24).

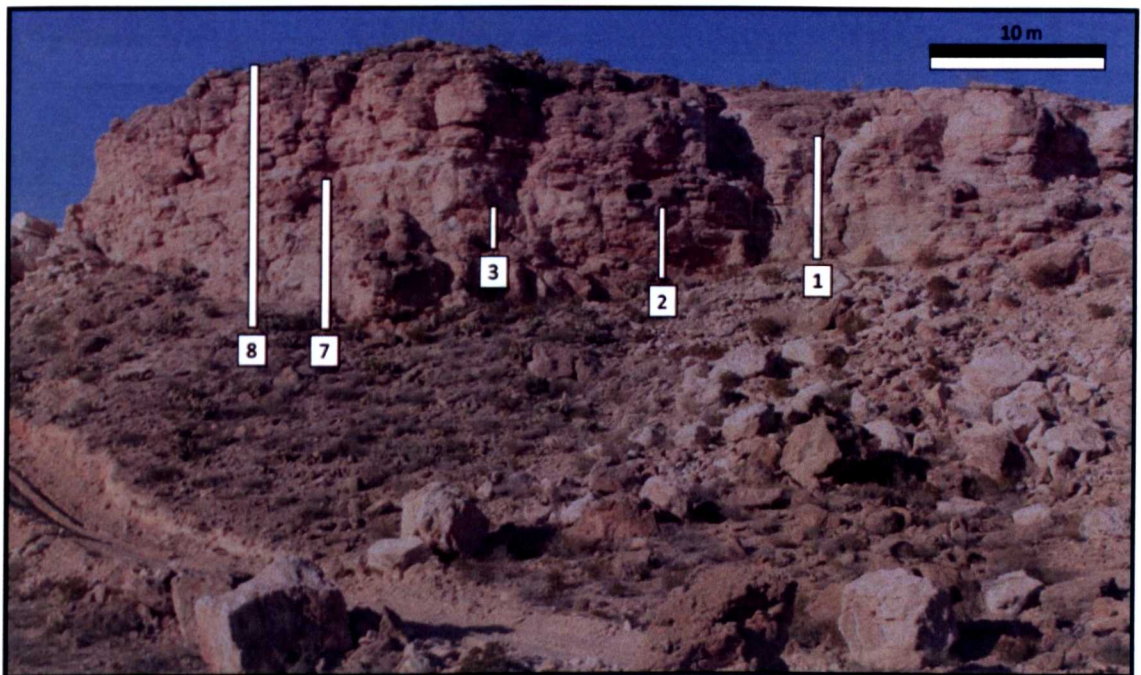


Figure 3.17. Annotated photograph showing the locations of measured stratigraphic logs 1, 2, 3, 7 and 8 (Fig. 3.18).

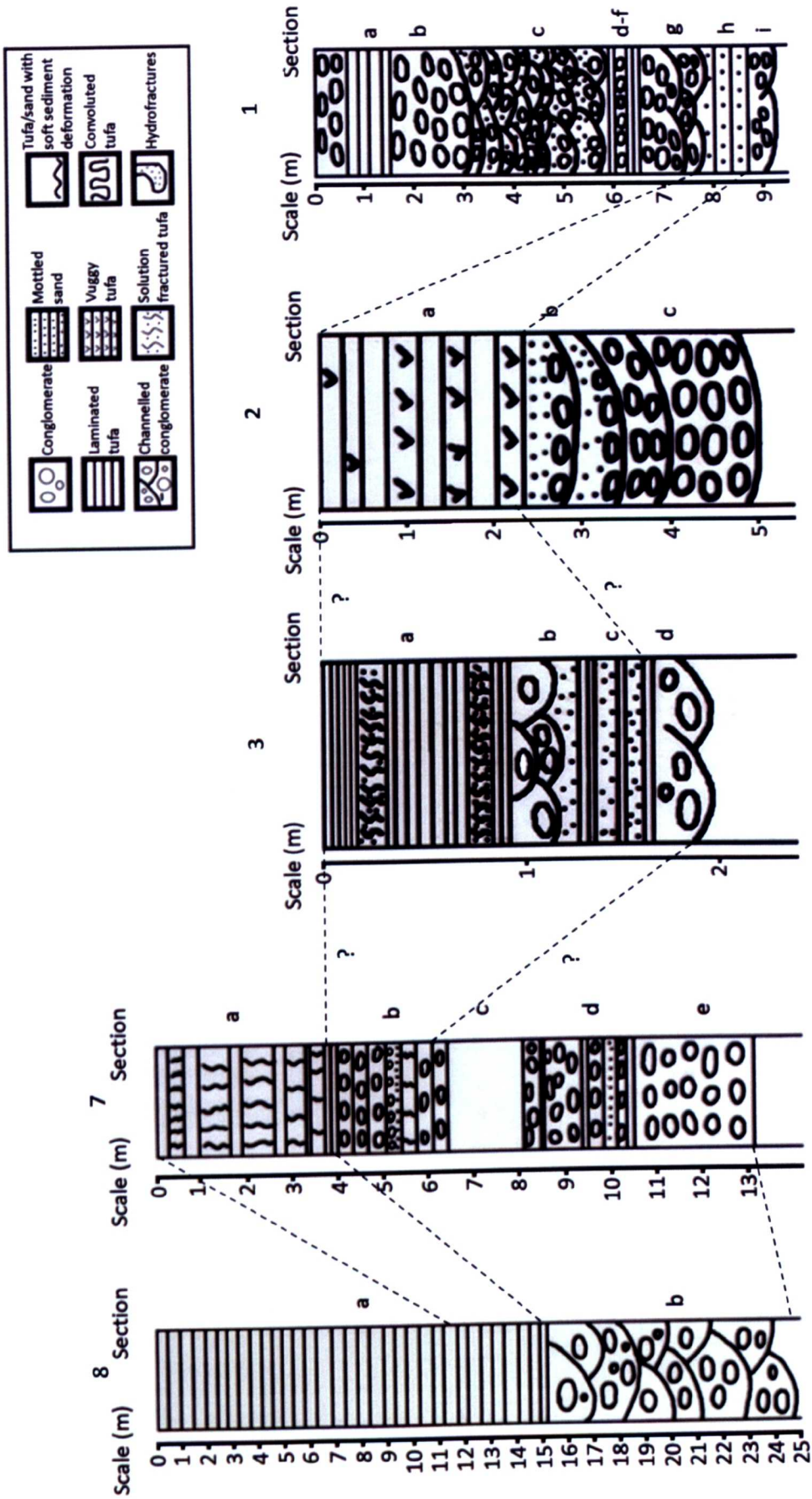


Figure 3.18. Stratigraphic logs 1, 2, 3, 7 and 8. Location of the stratigraphic logs can be seen in Figures 3.10 and 3.17. Full stratigraphic descriptions can be seen in appendix 1.2.

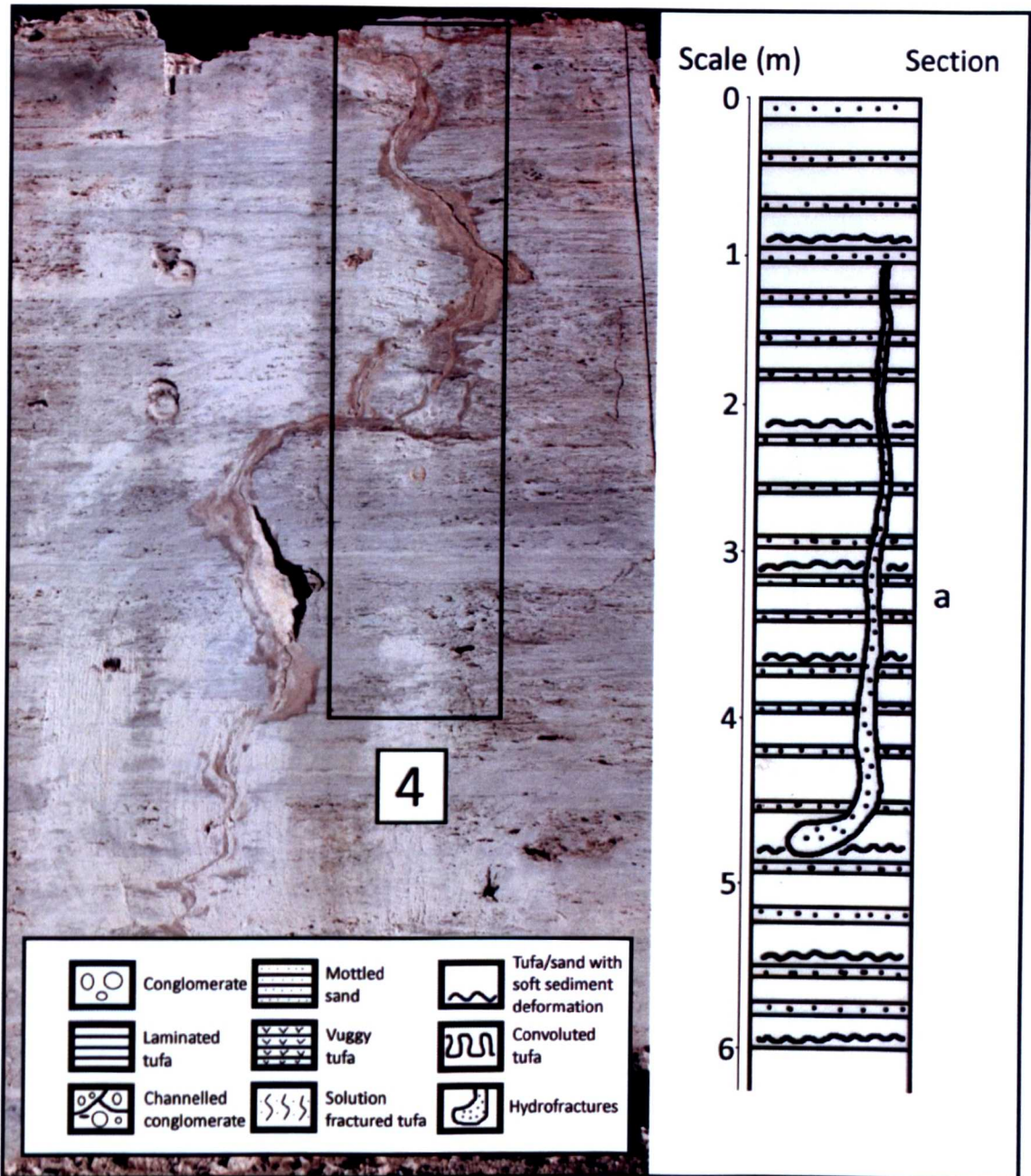


Figure 3.19. Stratigraphic log 4 presented alongside an annotated photograph of the logged section. Full stratigraphic descriptions can be seen in appendix 1.2. See Figure 3.10 for exact log location.

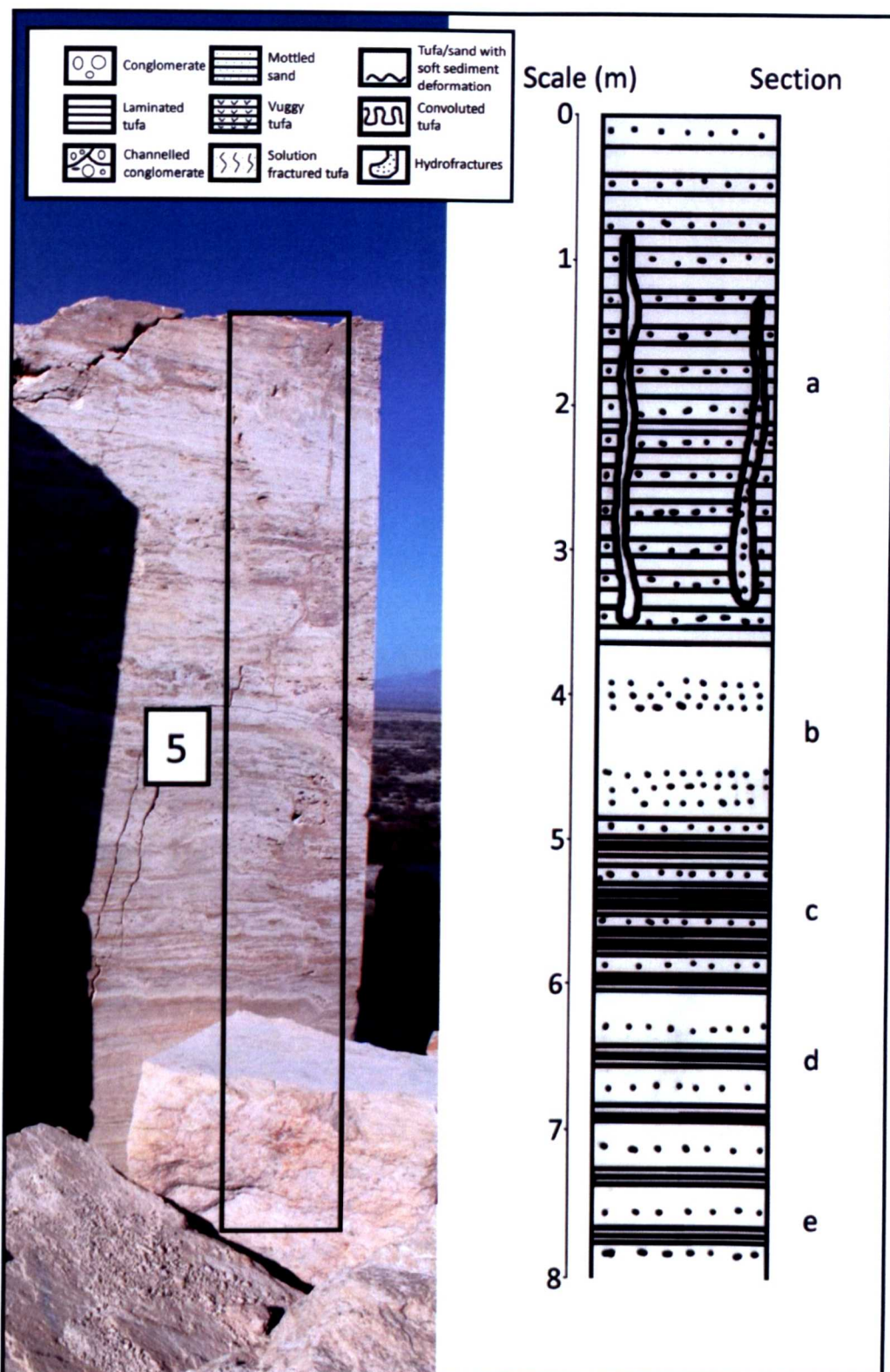


Figure 3.20. Stratigraphic log 5 presented alongside an annotated photograph of the logged section. Full stratigraphic descriptions can be seen in appendix 1.2. See Figure 3.10 for exact log location.

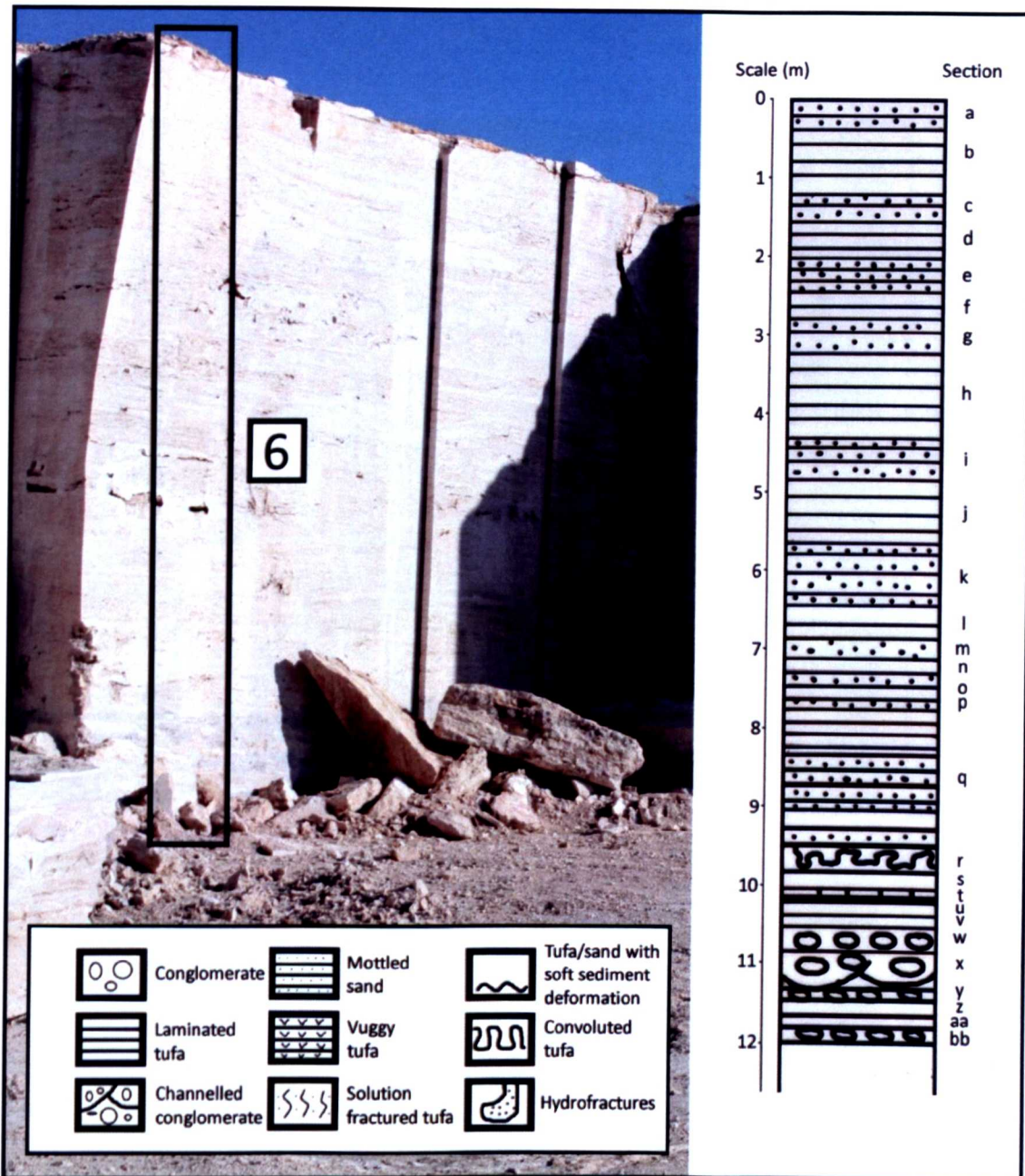


Figure 3.21. Stratigraphic log 6 presented alongside an annotated photograph of the logged section. Full stratigraphic descriptions can be seen in appendix 1.2. See Figure 3.10 for exact log location.

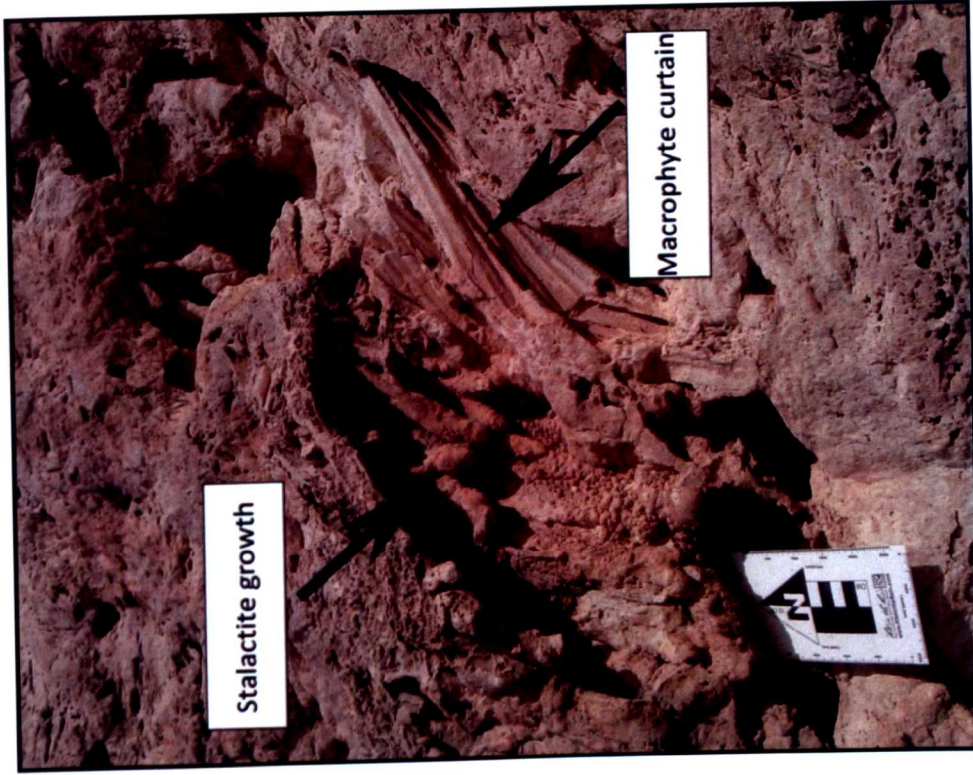


Figure 3.23. Enlarged photograph of figure 3.22. Steeply dipping macrophytic stem structures with subsequent stalactite growth. Stalactite growth is indicative of a waterfall type structure.

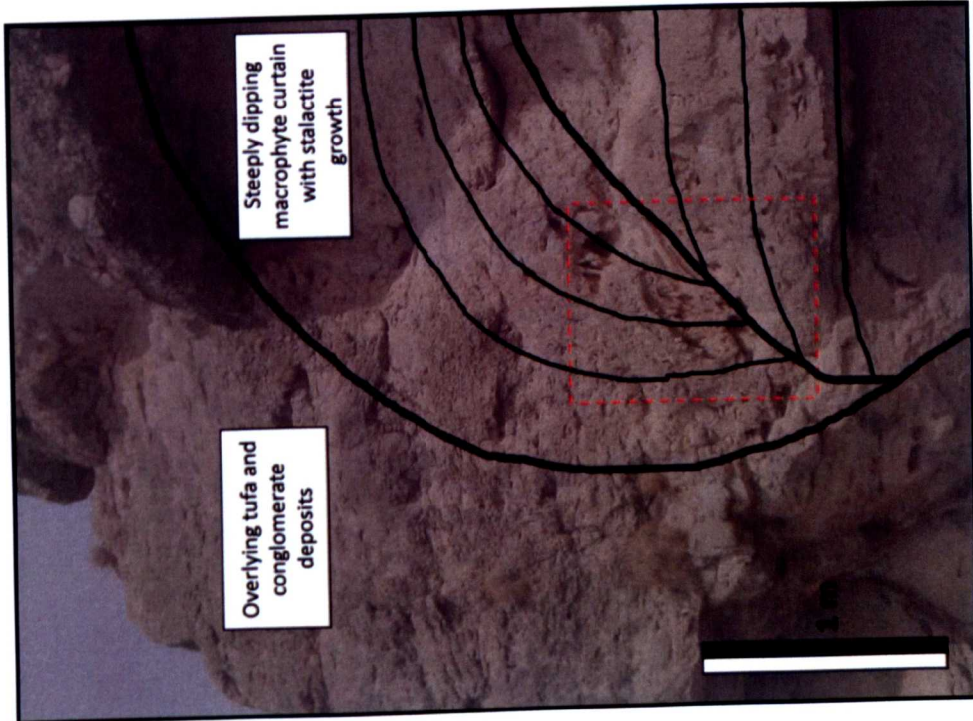


Figure 3.22. Annotated photograph showing the steeply dipping macrophyte curtain on the front (west face) of the perched terrace. The red box is enlarged in figure 3.23.



Figure 3.24. Abundant palm frond impressions towards the base of the tufa sequence, hammer is presented as scale.

Preliminary $\delta^{18}\text{O}_{\text{CARB}}$ and $\delta^{13}\text{C}_{\text{DIC}}$ isotope results

A total of 16 samples were taken from a 10 m section in alternating biogenic – non-biogenic layers (Fig. 3.25). For the full methodology used see chapter 5.

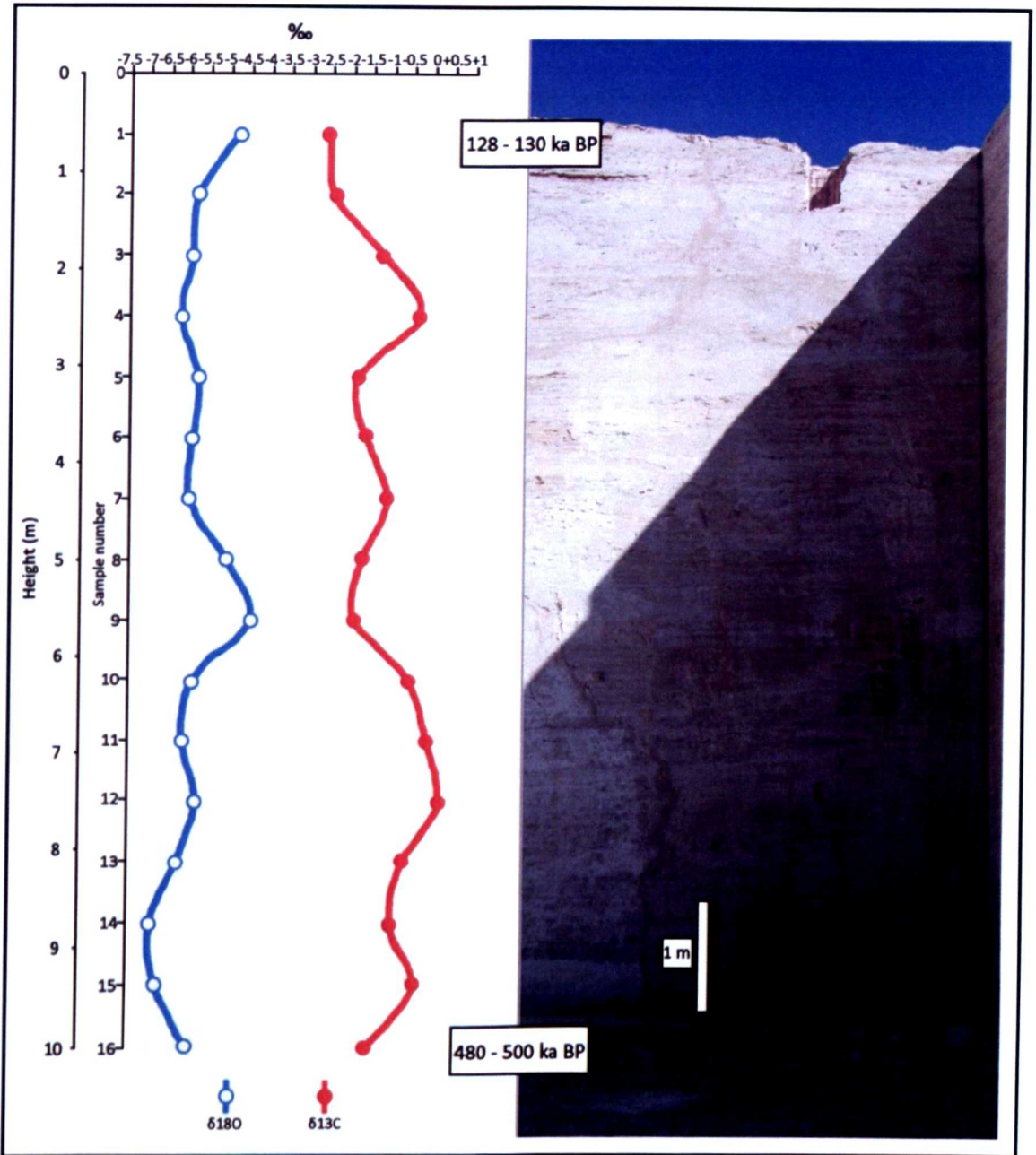


Figure 3.25. Preliminary $\delta^{18}\text{O}_{\text{CARB}}$ and $\delta^{13}\text{C}_{\text{DIC}}$ isotopes for the perched tufa terrace. Samples were taken at 16 intervals down the sequence. Photograph of the sampled section is also presented alongside isotopic data.

The $\delta^{18}\text{O}$ isotope value of the carbonate remained relatively constant throughout the section but observed an overall increase from -6‰ to -4.9‰ . The lowest $\delta^{18}\text{O}$ isotope value of -6.9‰ is observed at sample 14 at approx. 9 m depth. The $\delta^{18}\text{O}$ isotope value of the carbonate sequence, until this point, is gradually

decreasing, but becomes more constant after ranging between -5.8‰ and -6.2‰ . The largest increase in the $\delta^{18}\text{O}$ sequence occurs between samples 10 and 9 (approx. 6.5 m to 5.85 m) where $\delta^{18}\text{O}$ shifts from -5.9‰ to -4.4‰ , an increase of $+1.5\text{‰}$. The $\delta^{18}\text{O}$ isotope value of the carbonate decreases after this shift with the largest decrease from -4.4‰ to -5.1‰ ($+0.7\text{‰}$), before becoming more constant with values ranging between -5.8‰ and -6.2‰ , similar to those seen earlier in the sequence. A similar increase is again observed between approx. 65 cm and 0 cm (samples 2 and 1), where a 0.9‰ shift from -5.8‰ to -4.9‰ is observed.

The $\delta^{13}\text{C}$ isotope values of the carbonate display a gradual decrease through the sequence from -1.5‰ to -2.6‰ . The highest $\delta^{13}\text{C}$ isotope value of $+0.2\text{‰}$ (sample 12) is observed at approx. 7.8 m after a gradual increase from -1.5‰ at sample 16 (approx. 10 m). A recurring pattern follows the highest $\delta^{13}\text{C}$ isotope value where a large decrease from -0.5‰ to -1.9‰ (-1.4‰) at approx. 567 cm (samples 10 to 9) is observed before increasing to -1.1‰ at approx. 441 cm (sample 7) and decreasing again to -1.8‰ at approx. 315 cm (sample 5). The largest increase in the $\delta^{13}\text{C}$ value of the carbonate (-1.8‰ to -0.3‰ ($+1.5\text{‰}$)) is observed between approx. 315 cm and 252 cm (samples 5 and 4) before values decrease gradually to the lowest $\delta^{13}\text{C}$ value of the sequence: -2.6‰ at 0 cm (sample 1). Both $\delta^{18}\text{O}_{\text{CARB}}$ and $\delta^{13}\text{C}_{\text{DIC}}$ isotope values appear to display a recurring pattern throughout the carbonate sequence.

Tufa samples from the top and base of the sequence were sent to Dr. Gilbert Price (The University of Queensland) for preliminary U-series dating. Dates of 128 – 130 ka BP and 480 – 500 ka BP were obtained for the top and bottom of the tufa sequence respectively (Fig. 3.25). However, any interpretation must be made with caution since these dates suggest the sequence spans a time period of 350 – 372 kyr. Up to c.23 kyr may have elapsed between each sample, where deposition of calcium carbonate may not have been continuous, containing unknown hiatuses, and large increases or decreases in the isotope values of the carbonate may not be seen, in the current data set.

3.3 Discussion

Hydrology is very important for determining the mechanisms of calcium carbonate deposition within the CCB. Modern day reconnaissance hydrology of the CCB has been discussed in chapter 2 and, combined with the data presented in this chapter; two models of calcium carbonate deposition will be proposed and discussed:

- 1) Calcium carbonate deposition during the Mid-Late Holocene and study sites within the modern hydrological system: Tierra Blanca spring mound, the rim-stone pool/dam complex and the fissure ridge complex.
- 2) Calcium carbonate deposition away from the modern hydrological system, during the Late Pleistocene: the perched terrace.

3.3.1 Calcium carbonate deposition within the modern hydrological system

The main hydrological through-flow system, discussed in chapter 2, originates to the west of the CCB before flowing to the east. The close proximity of the spring mound, fissure ridge complex and rim-stone pool/dam complex (Fig. 3.26) and the location of all three within the hydrologic through-flow system suggest that calcium carbonate deposition and increased hydrostatic head pressure may have occurred at similar times at all locations. Tierra Blanca spring mound has a minimum age of 7.24 ka BP, based on U-series dating of the footprint horizon (see chapter 4), placing its hydrologic activity within the Mid Holocene. Thus, a Mid-Holocene age is inferred for all of the calcium carbonate formations located within the modern hydrological main through-flow system for the CCB (see chapter 2) as the 7.24 ka BP spring mound is located within close proximity to the fissure ridge complex and rim-stone pool/dam complex. The presence of the inactive calcium carbonate formations within this system suggests a synchronous period of greater hydrostatic pressure and possibly climatically wetter conditions when active [Pentecost, 2005], similar to calcium carbonate deposition seen in Pamukkale, Turkey [Altunel and Hancock, 1993].

The relatively constant $\delta^{13}\text{C}_{\text{DIC}}$ isotope values of -1.1‰ to -0.4‰ (see chapter 4) of the Tierra Blanca calcium carbonate fall within the known range of thermogene travertine, however, the comparatively high $\delta^{13}\text{C}_{\text{DIC}}$ of the surrounding limestone mountains ($+2\text{‰}$ to $+4\text{‰}$ [Bralower *et al.*, 1999]) suggests that increased water-rock reactions, expected in the source water for thermogene travertine deposition, are not

occurring as $\delta^{13}\text{C}_{\text{DIC}}$ values would be expected to be higher than those observed in the Tierra Blanca calcium carbonate. The fenestral microfabric as well as the $\delta^{13}\text{C}_{\text{DIC}}$ of the Tierra Blanca spring mound calcium carbonate suggests the source water was of a heated meteoric origin, incorporating some $\delta^{13}\text{C}_{\text{DIC}}$ from the surrounding limestone bedrock, before depositing superambient meteogene tufa [Pentecost, 2005; Sharp, 2007; see chapter 4 for a more detailed discussion] adding to the hypothesis that increased precipitation on the high peaks of the surrounding mountains increased hydrostatic head pressure, causing geothermally heated meteoric water to surface and deposit meteogene tufa as a spring mound structure.

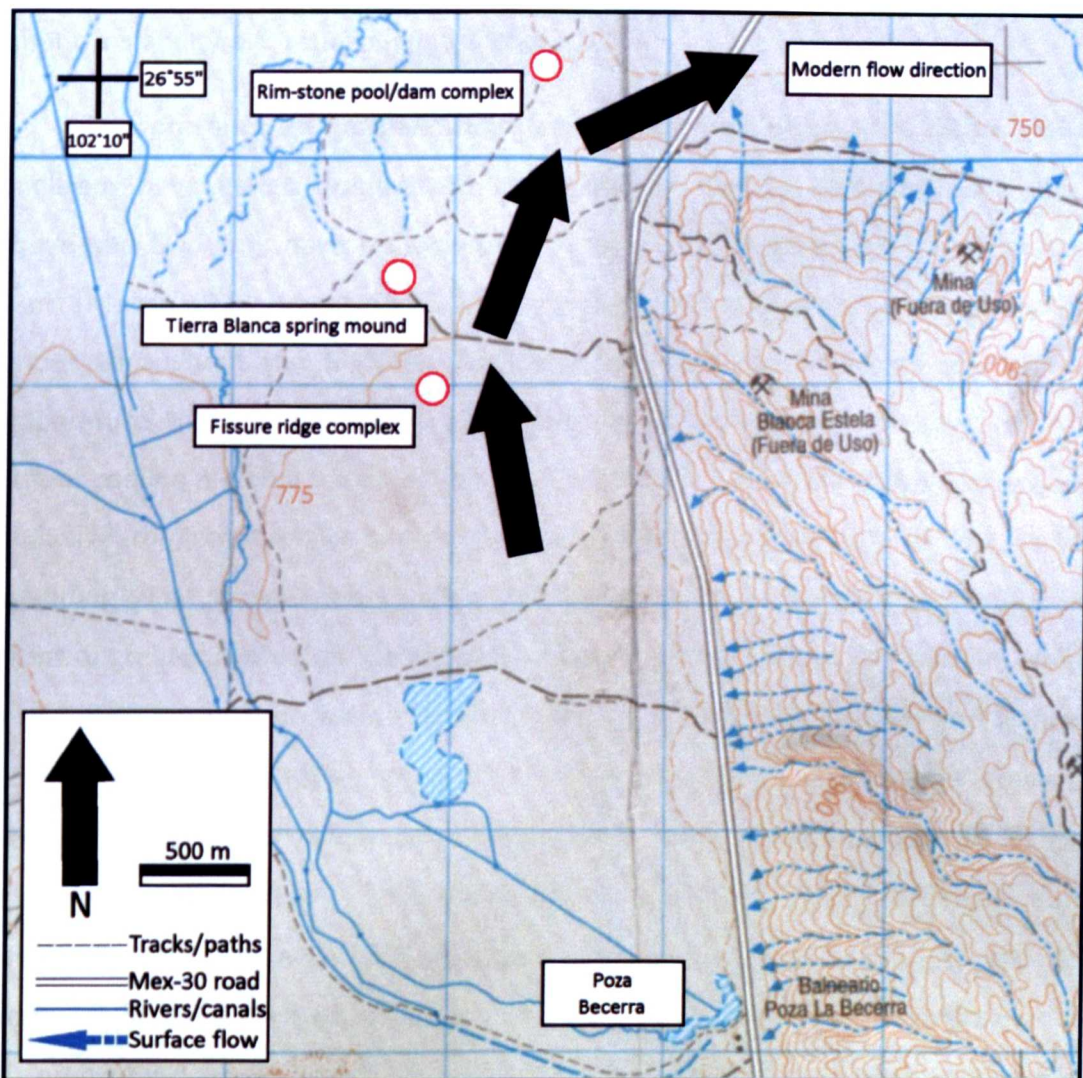


Figure 3.26. Annotated map of the locations of the three tufa areas and their proximity to each other. Red circles show the locations of each area. Black arrows show the modern surface water flow direction within the main through-flow system in the CCB (see chapter 2).

Further to the isotopic data, vegetation preserved within the tufa of the rim-stone pool (see section 3.2.1) and fissure ridge complexes (see appendix 1.1) – *Typha*

sp., and *Dasyilirion sp.* - are species that form in the modern day aquatic ecosystem [Badino *et al.*, 2004]. *Agave* and *Opuntia* pollen preserved in the tufa of Tierra Blanca spring mound [see chapter 4] are also species currently growing in the modern day terrestrial ecosystem suggesting the environment of the CCB has remained relatively unchanged since at least 7.24 ka BP and possibly up to 30 ka BP. This hypothesis of long-term environmental stability was first proposed by Minckley [1969] and furthered by Meyer [1973] and Badino *et al.* [2004]. The floral and faunal endemism observed within the CCB [Minckley, 1969; Meyer, 1973; Minckley and Jackson, 2008] is an important factor in the determination of climatic conditions, as to be endemic suggests a long period of biogeographic isolation and/or climatic stability or moderation of climatic instability e.g. refugia [Fjeldså *et al.*, 1999].

The presence of inactive tufa facies does not necessarily mean climatic conditions have varied dramatically as vegetation species, including xeric species (*Agave* and *Opuntia*), have remained the same. Previous studies of the Chihuahuan desert [Meyer, 1973; Bryant, 1977, 1985; Metcalfe, 1997] have noted wetter and drier periods throughout the Mid-Late Holocene but none have inferred any dramatic temperature shifts in the region suggesting increased regional effective moisture, without cooling regional temperatures. Wetter climatic conditions in the CCB would be conducive to geothermally heated source waters depositing tufa at the surface, expanding what is now the modern hydrologic through-flow system, through the means of greater hydrostatic head pressure causing fissure ridges and artesian wells in close proximity to fault zones. Studies at Pamukkale, Turkey [Altunel and Hancock, 1993; Dilsiz *et al.*, 2004] have shown five modes of thermogene travertine precipitation, three of which are similar to the three discussed here, all in close proximity to each other. Travertine precipitation at Pamukkale increases during climatically wetter periods due to greater mixing of cold groundwater and deep thermal fluid whilst the hydrogeology of the area remains the same. A similar model of tufa precipitation could be applied to the CCB: the modern hydrologic system produces hot springs and pools ($\geq 35^{\circ}\text{C}$), precipitating tufa, whilst the past hydrologic system appears to have precipitated tufa on a larger scale due to higher hydrostatic head pressure from increased effective moisture. Like Pamukkale, the CCB hydrogeology may have remained the same, precipitating tufa in episodes through wet and dry

shifts, leading to these now inactive tufa facies being located within the modern main through-flow system. Both the CCB and Pamukkale are now semi-arid regions and precipitate tufa on a relatively small scale whilst episodic wet transitions have produced larger scale tufa formation in the past.

3.3.2 Calcium carbonate deposition away from the modern hydrological system

3.3.2.1 Perched tufa terrace of fluvial, spring and paludal origin

The location of the perched terrace indicates it is not within the modern active hydrologic system (Fig. 3.3) and can be considered to not be directly related to the other three inactive tufa facies. The location coupled with the $\delta^{13}\text{C}_{\text{CARB}}$ isotope values between -2.6‰ and $+0.2\text{‰}$ (Fig. 3.25) suggest that the source water is of a superambient meteoric origin, depositing meteogene tufa [Pentecost, 2005].

The preserved vegetation impressions within the 10 - 12 m tufa sequence are mainly those of the modern environment - *Typha sp.* and bryophyte (mosses) crusts - but toward the base of the sequence there are large well preserved palm frond encrustations (Fig. 3.24). The species of palm appears to be that of *Acoelorrhaphe wrightii* or *Serenoa repens*, both of which do not currently grow in the CCB. *Acoelorrhaphe wrightii* is the most probable species as it is native to the flooded areas or swamps of Central America and SE Mexico, consistent with the spatial discontinuity observed in the horizontal laminated tufas (Fig. 3.18) and microbially deposited tufa indicative of a paludal (swamp) environment [Pedley *et al.*, 2003]. *Serenoa repens* is endemic to SE United States and is indicative of woodland areas so is unlikely to be the fossilized species. *Acoelorrhaphe wrightii* is an indicator of a more humid, equatorial climate in the CCB and is located in the sequence above a conglomerate bed that is interbedded with tufa. Preliminary U-series dating at the base of the tufa sequence suggests an age of 480 to 500 ka BP. At this point in the sequence (sample 16, Fig. 3.25) the $\delta^{18}\text{O}_{\text{CARB}}$ value is at -6‰ before a gradual shift to the lowest $\delta^{18}\text{O}_{\text{CARB}}$ value of the sequence (-6.9‰) at 8.7 m (sample 14, Fig. 3.25), possibly indicating a shift to wetter climatic conditions with increased ^{16}O input from fresh water. The proposed wetter climate in the CCB around 480 to 500 ka BP coincides with the onset of glacial conditions in MIS 12 where regional cooling and wetting is observed in Nevada [Winograd *et al.*, 1992] and New Mexico [Fawcett *et al.*, 2011]. The presence of the

conglomerates and palm frond impressions at the suggested climatically wettest part of the sequence could indicate flash flooding events or fluvial activity resulting in fluvial tufa formation [Pedley *et al.*, 2003; Pentecost, 2005; Ortiz *et al.*, 2009]. The conglomerate forms incised channels within the tufa (Fig. 3.16) suggesting they are of a fluvial origin at this point. There is no observable evidence of channels in the conglomerate lower down the terrace stratigraphy and, lying unconformably, suggests these conglomerates are of possible flash flood origin as opposed to the later fluvial conglomerates. A prolonged period of increased effective moisture could have resulted in palm growth and a fluvial/swamp environment as well as increasing hydrostatic head pressure in faults located in the Sierra San Marcos y Pinos, resulting in spring activity. Red colouration of the Cretaceous limestone underlying the perched terrace (Fig. 3.14) suggests FeO deposition by circulation of thermal fluids and large hydrofractures observed within the calcium carbonate sequence (Figs. 3.19, 3.20 and appendix 1.2) also corroborate the theory of hydrothermal spring activity. A series of episodic rivers originating from a large canyon to the east of the terrace and spring activity from the Sierra San Marcos y Pinos faults [Dickinson and Lawton, 1999; Badino *et al.*, 2004] could have created a perched tufa terrace sequence within the CCB like those observed in Spain [Ortiz *et al.*, 2009].

However, it is worth noting that spring activity is highly dependent on groundwater flow and regional climate [Pentecost, 2005]. For such a long depositional period – c.370 kya – it is expected that spring/river activity would cease in drier climatic periods creating a hiatus, although no obvious hiatuses appear to occur in the perched terrace structure. It is also hard to determine the length of time any spring has been activity depositing tufa. Observed erosion in the CCB is seen as large alluvial fans at the base of canyons [Badino *et al.*, 2004] suggesting a wet climate is needed for erosion to occur. It is acknowledged that although during dry periods wind and gravitational soil erosion is likely in the CCB, the effects of this would be minimal as is seen in other arid regions around the world [Belnap and Gillette, 1998; Fécan *et al.* 1998; Enzel *et al.* 2012], however, spring activity in the CCB is directly linked to wetter climate so heavy erosion during spring inactivity is unlikely. It is suggested here that the possibility of depositional hiatuses within the perched terrace would not be easily identifiable, while erosional hiatuses would be. Due to the height (off the basin floor)

and location (away from the main hydrological through-flow system) of the perched terrace it is unlikely large erosional periods would occur, creating a hiatus, in periods of spring inactivity due to an arid climate but the possibility of a depositional hiatus is more plausible. Haynes and Agogino [1966] and later Haynes [2008] report similar depositional hiatus features in Clovis, New Mexico although the chronology is much shorter than that of the CCB.

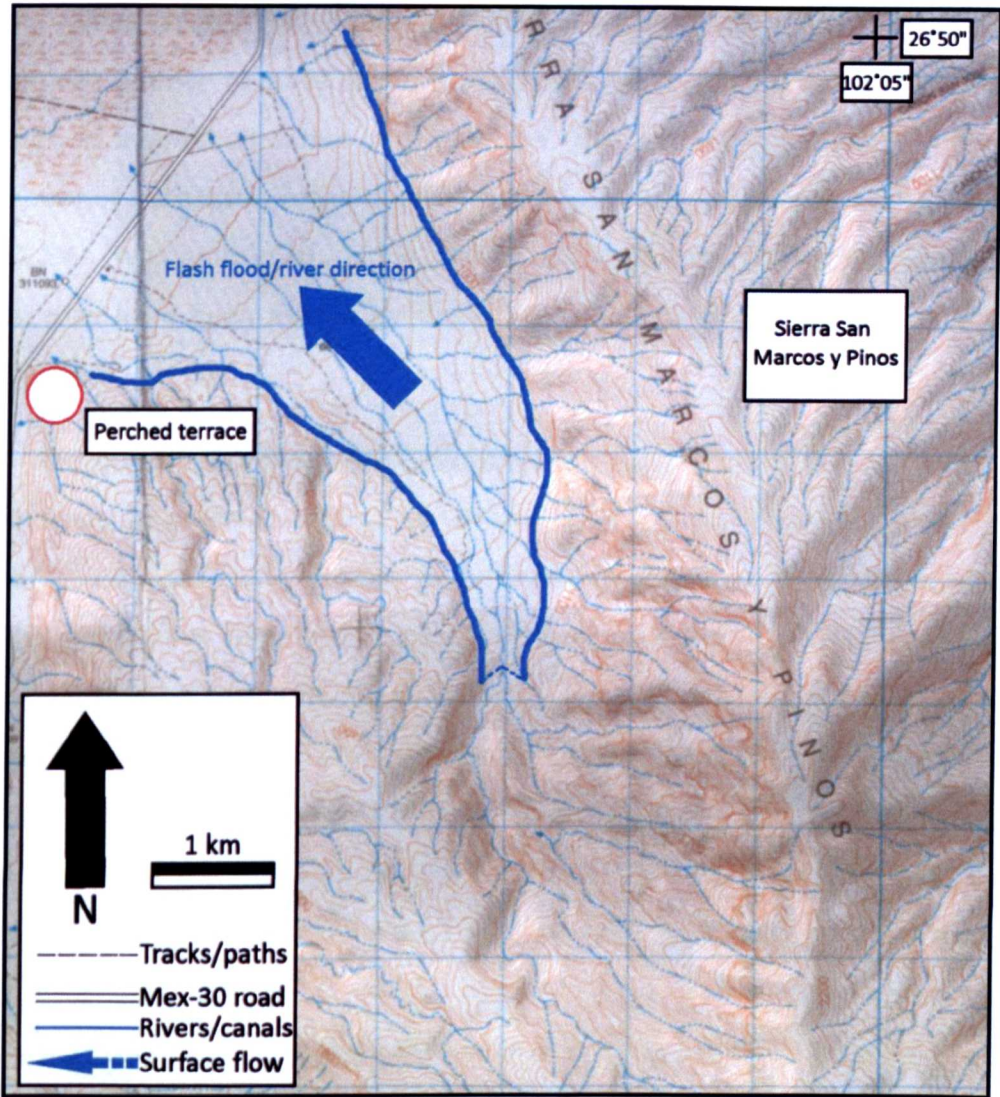


Figure 3.27. Possible direction of water flow from rivers or flash floods originating at the peak of the Sierra San Marcos y Pinos. The combination of this and local faulting could have resulted in episodic river/spring tufa precipitation during the Pleistocene.

3.3.2.2 Raised pluvial lake shoreline

As discussed previously, preliminary U-series dating places the depositional period of the perched tufa terrace between 480-500 ka BP and 128-130 ka BP. The proposed depositional period and cyclical nature of the $\delta^{18}\text{O}_{\text{CARB}}$ isotopic values (Fig. 3.25) could be an indicator of a long climatic sequence preserved within the tufa. The apparent cyclicity could be representative of glacial/inter-glacial cycles although the isotopic values range from -6.9‰ to -4.4‰ with the largest positive shift of $+1.5\text{‰}$ and do not appear to have large enough isotopic shifts for this to be the case. However, as mentioned earlier in this chapter, the lack of larger isotopic shifts in the data does not necessarily mean they did not occur, as larger positive or negative shifts e.g. $\pm 2.1\text{‰}$ [Winograd *et al.*, 1992], characteristic of onset or termination of glacial events, may have been missed by the coarse sampling resolution used in this pilot investigation.

The possible cyclicity observed within the $\delta^{18}\text{O}$ value of the carbonate could also indicate another terrestrial carbonate environment associated with terrace structures. An alternating pluvial lake/closed basin system, as first suggested by Minckley [1969], has been proposed by Wolaver *et al.* [2008]. Previous hydrological work conducted by Rodriguez *et al.* [2005] suggests a catchment area to the CCB of 3030 km^2 , providing regional groundwater flow surfacing at the CCB. However, Echelle and Echelle [1998] hypothesized a larger surface hydraulic connection between the Río Grande, CCB and Río Nazas as part of an extensive pluvial lake system in the Late Holocene. Extensive Palaeo-lakes have been previously documented in the Chihuahuan desert [Metcalf, 1997, 2002; Echelle and Echelle, 1998] including Laguna Mayrán, which existed up until the late 1900s. The surface connection no longer exists to the CCB though the vast Cupido-Aurora aquifer is thought to be a remnant of this large surface system [Rodriguez *et al.*, 2005; Wolaver, 2008].

Evidence of this possible pluvial lake system exists in the CCB in the form of raised alluvial fans to east of the Sierra San Marcos y Pinos as well as large river cut canyons to the far-east/north east of the basin, thought to be former drainage channels. The rounded clasts and braided channels present within the perched tufa terrace do suggest they are of a fluvial origin as earlier mentioned but instead of

episodic flash flooding events, a more sustained fluvial system could have been possible. Rodriguez *et al.* [2005] ¹⁴C dated the perched tufa terrace to 17 ka BP, although the exact sample location is not stated, conflicting directly with the new U-series dates obtained here of 128-130 ka BP and 480-500 ka BP for the top and bottom of the sequence respectively. The conflicting dates and techniques used make comparing the data difficult, although the post LGM (Last Glacial Maximum) date of 17 ka BP would suggest the presence of a pluvial lake system in the CCB, at this time, is unlikely as studies have shown that the climate in NE Mexico and Trans-Pecos became progressively more arid during this time [Metcalf, 1997, 2002; Musgrove *et al.*, 2001]. Increased moisture at this time, however, is possible. Melt water influx from the Laurentide ice sheet has been noted in the Gulf of Mexico and increased speleothem growth on the Edwards Plateau, Texas between 15 and 12 ka BP [Kennett and Shackleton, 1975; Musgrove *et al.*, 2001]. This influx event is a possible source of water for a pluvial lake environment at this time although it is noted that regional climate would more likely have become increasingly arid due to a northward shift of the ITCZ and a change to summer atmospheric moisture source [Peterson *et al.* 2000; Clark *et al.* 2001; Escobar *et al.* 2012].

Wolaver *et al.* [2008] suggests, further to geomorphological evidence, evidence for a huge thickness of cobbles and limestone clasts, similar to those at the perched terrace, underlying the CCB floor alluvium. The underlying cobbles, overlain by various marl facies and alluvium of at least 15 m depth, suggest an extensive pluvial lake system may have existed in the CCB. However, the raised elevation of the perched terrace from the basin floor (+50 m) would suggest either uplift of the terrace occurred or a pluvial lake of enormous magnitude existed. The location of local faulting, behind the terrace, could have resulted in uplift although palaeomagnetic studies by González-Naranjo *et al.* [2008] suggest that no uplift in the region surrounding and incorporating the CCB has occurred since at least 44 Mya, as well as there being no observable evidence of recent fault movement at the perched terrace itself.

3.3.3 Complexity of the CCB hydrology

A pluvial lake in the CCB would have had approximately 1400 km² surface area and up to 40 m depth, if no uplift of the terrace occurred, and would be expected to

have a remnant shoreline comprising beach deposits, similar to lakes King and Sacramento in the Trans-Pecos region of the Chihuahuan desert [Hawley, 1993]. No such deposits exist in the CCB [Badino *et al.*, 2004; Rodriguez *et al.*, 2005; Wolaver *et al.*, 2008] although the location of the now ancestral Laguna Grande could have provided an area for a playa lake. Large gypsum deposits now occupy the playa flats (Fig. 3.28), the location of Laguna Grande, indicating the presence of a once large playa lake. Large hyper-saline lakes also suggest former playa lake systems existed on the east side of the CCB although no gypsum deposits exist to indicate a major drying event like Laguna Grande to the west. This, however, could be the result of the through-flow nature of the CCB hydrology (see chapter 2) which, as suggested earlier in this chapter, would have become a larger scale through-flow system in climatically wetter periods whilst maintaining the same brine evolution system.

Laguna Grande may, formerly, have been a playa lake fed by fluvial outflow from surrounding canyons but onset of more arid conditions led to the lake being fed by surface flow from springs. As discussed in chapter 2, before the complete drying in 2009, Laguna Grande was fed by surface flow from Poza Churince (Chapter 2, Fig. 2.32b), which itself is a hydrothermal spring, highlighting the lateral and stratigraphic complexity of the CCB. Lateral geomorphologic characteristics of the CCB can change substantially over short distances (<10 m) meaning sampling strategies have to be carefully planned. Limestone cobbles and conglomerates found underlying the desert alluvium [Wolaver *et al.*, 2008] may not be present in all directions creating the possibility of misinterpretation of what is believed to be pluvial lake data.

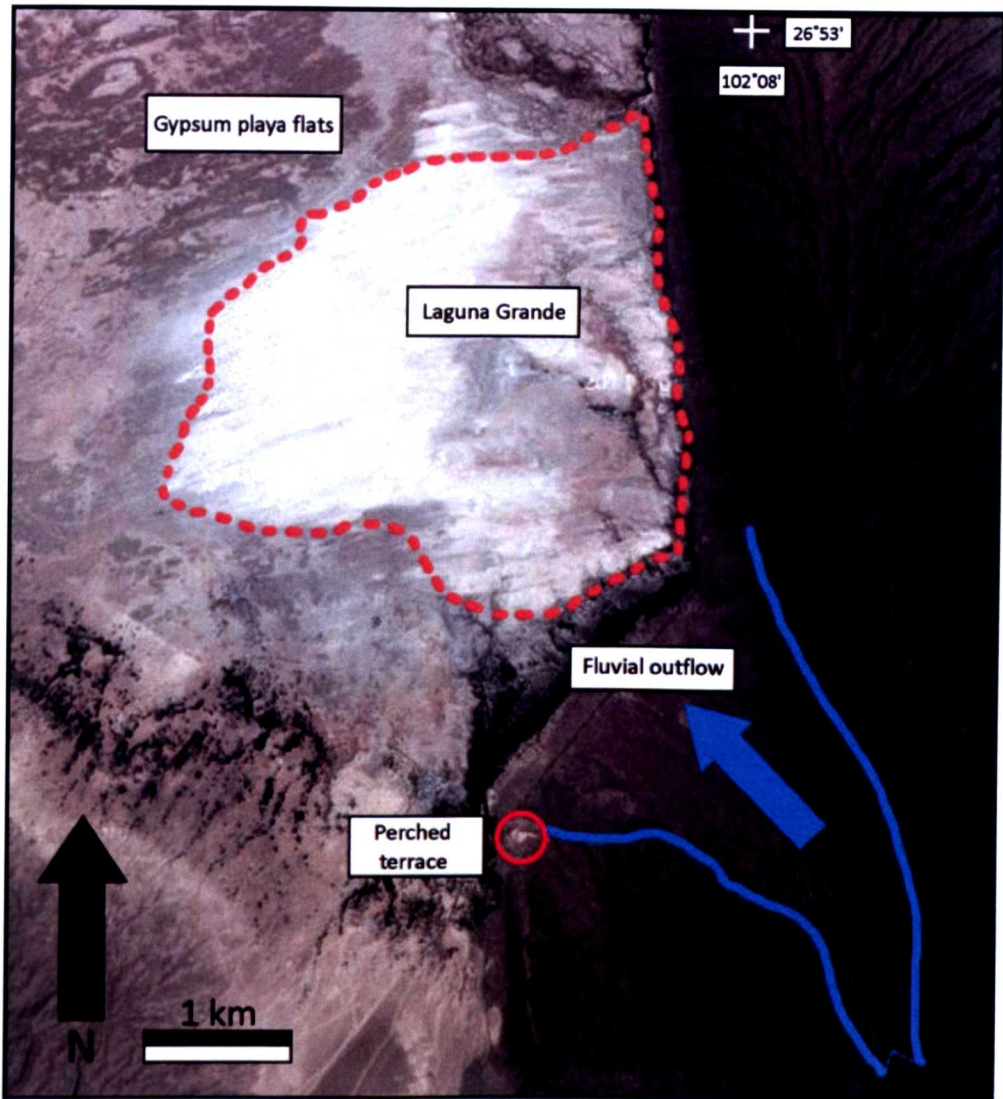


Figure 3.28. Possible direction of fluvial outflow from Sierra San Marcos y Pinos into Laguna Grande. Red line highlights the position of the gypsum playa flats. The aerial photo was taken in 2008 and shows the final location of Laguna Grande before complete drying up in 2009 [image from google.co.uk/earth].

3.4 Conclusions and future work

The CCB has a complex depositional system and based on observations and the data available, two separate episodes of increased effective moisture are suggested to have influenced the hydrology and consequent calcium carbonate formation within the CCB.

The first episode, associated with the perched tufa terrace, appears to be unrelated to the modern day hydrology of the CCB. New evidence presented within the chapter suggests two possible origins for the perched terrace:

- 1) Alternating fluvial/spring line deposition of the terrace with fluvial outflow into a playa lake, possibly Laguna Grande.
- 2) Pluvial lake deposition as first suggested by Minckley [1969] and later Wolaver *et al.* [2008], where geomorphologic evidence preserved in canyons in the CCB suggests the occurrence of a vast pluvial lake system.

Preliminary $\delta^{18}\text{O}_{\text{CARB}}$ and $\delta^{13}\text{C}_{\text{DIC}}$ isotopic data from this study suggests the perched terrace is of a meteoric origin and the preservation of vegetation and apparent continuous deposition of the calcium carbonate sequence may represent a climate record to at least 120 ka BP and possibly back to 500 ka BP. The cause of the isotopic variability through the perched terrace section is hard to identify based on the limited data points available, however, the perched calcium carbonate terrace has the potential to contain a valuable climatic archive for this region which, based on preliminary U-series dates presented, may contain glacial and interglacial cycles. Fluvial/flash flood conglomerates inter-bedded with tufa and palm frond impressions at the base of the large calcium carbonate sequence, containing no apparent hiatuses, suggest a sustained fluvial/spring sequence. Stratigraphic logging of the perched terrace sequence also suggests the conglomerates are channelled, cutting incised channels into underlying tufa deposits, further corroborating fluvial influences.

However, the raised elevation of the perched terrace sequence from the CCB floor as well as large geomorphological features observed by Minckley [1969] and Wolaver *et al.*, [2008] suggest a vast pluvial lake system. There has been no tectonic uplift in the CCB since at least 44 Mya to account for the perched terraces elevation of the CCB floor and there is also no clear evidence of lake shore lines or wave cut terraces. It is proposed here that a fluvial/spring sequence is a more likely origin for the perched tufa terrace, although a higher resolution $\delta^{18}\text{O}$ and $\delta^{13}\text{C}$ climate study coupled with further detailed stratigraphic logging, thin section tufa characterisation and a detailed U-series chronology is needed to permit definitive conclusions.

The second episode of increased effective moisture appears to have directly affected what is now the modern hydrology without changing the hydrogeology. The 7.24 ka BP age of the spring mound and its close proximity to both the rim-stone pool/dam complex and fissure ridge complex, within the modern hydrological through-

flow system suggests the climate was much wetter during the Late Pleistocene/Early Holocene whilst preserved vegetation suggests that the wetland environment remained relatively similar. The data discussed in this chapter indicates the hydrogeology has remained the same from the past to the present but has fluctuated between hydrologically open and (modern) closed basin systematics.

During wetter periods, the modern hydrologic system observed in the CCB (chapter 2) appears to have become larger scale due to increased hydrostatic head pressure from increased atmospheric moisture, possibly causing playa lakes in parts of the CCB. The work conducted within the palaeoenvironmental reconstruction chapter can better help understand the exact timing and dynamics of tufa deposition during wetter and drier periods. The preservation of *in situ* human footprints in what is suggested to be a wetter period also indicates the importance of palaeoenvironmental controls on tufa deposition in the CCB and the affect this may have had on the earliest human populations.

Chapter 4: Human occupation in the CCB and the depositional context for the *in situ* human footprint trackway

4.1 Introduction

This chapter aims to provide an overview of the Coahuilan Indian cultural tradition and to link the archaeology with the palaeoenvironment in which the Coahuilan Indians were living. This chapter provides a study of an *in situ* human footprint trackway that utilizes new preliminary stable isotope and pollen data and U-series dating methods to investigate changing climate and its impact on human populations in the CCB. These new data will be integrated with a review of available documentary and archaeological evidence of the Coahuilan Indians. This will provide an idea of the environment in which they lived and the subsequent adaptations undertaken in the changing Holocene climate in the NE of Mexico.

In 1961, during the construction of the Mexico Highway 30 just outside the town of Cuatro Ciénegas, two human footprints preserved in tufa were discovered and are currently stored in the Museo del Desierto, Saltillo (Fig. 4.1a) [Gonzalez *et al.*, 2007]. The two unambiguous footprints were put on display in the museum in 1999, by which time, the precise location of discovery had been forgotten. The two footprints are well preserved with mud rims clearly visible between the toe impressions and also between the toes and the ball of the foot. This indicates a soft carbonate surface was present at the time of impression, as can be seen in some modern day rim-stone pools (Fig. 4.1b). A preliminary U-series date of 10.5 ka BP was obtained for the footprints [Gonzalez *et al.*, 2007]. The approximate location where the footprints were discovered was known by the locals of the town and led to the discovery of a new *in situ* human footprint trackway in 2006 [Gonzalez *et al.*, 2007; 2009].

Figure 4.1. a) The two footprints preserved in tufa currently on display at the Museo del Desierto, Saltillo [Gonzalez *et al.*, 2007]. b) Example of a modern poza where impressions of horse prints can be seen in the centre, preserved under water in the fine carbonate sediment.

4.1.1 Human occupation and the CCB cultural tradition

Throughout the Late Pleistocene, into and during the Holocene, humans occupied Northern Mexico and Southern USA. The Coahuilan Indians of the CCB are known to have been nomadic hunter-gatherers but conditions were wetter during the Late Pleistocene into the Holocene in these now arid/semi-arid areas making living conditions more favourable, leading to long periods of human occupation and producing well stratified archaeological cave deposits in the Cuatro Ciénegas Basin [Palmer, 1882; Taylor, 1956, 1964, 1966, 1968, 2003; Terry *et al.*, 2006]. The unique desert ecosystem and a wide range of flora and fauna in the basin made it an ideal place to hunt and live. Caves and rock shelters in the surrounding mountains were used as habitation sites, mortuary caves and ritual sites, most with expansive views of the basin. 'Frightful Cave' [Fig. 4.2], first discovered by Walter Taylor in the 1940s, is the most extensively studied cave with roughly 50% of the cave floor having been excavated producing hundreds of sandals, stone points, vegetal fibre artefacts and human hair that have been used to produce a base chronological sequence throughout what he outlined as three major cultural complexes for the Coahuilan Indians:

1. Ciénegas Complex (10 ka BP to 7 ka BP) – this is the first of Taylor's archaeological complexes and encompasses the most ancient phases of the Coahuilan Indians. The most common artefacts associated with this complex include human hair, sandals, snake rattles and, more interestingly, the presence of animal bones consisting of grizzly bear (*Ursus arctos horribilis*), elk

(*Cervus canadensis*) and buffalo (*Bison bison*) [Gilmore, 1947]. The species present within this complex suggest a cooler, wetter climate than today.

2. Coahuila Complex (7.5 ka BP to 1 ka BP) – the second, and most important complex identified by Taylor. The most common artefacts include lithic arrow points, wooden clubs and vegetal fibre artefacts, such as sandals and ‘combs’ used for scarification. Interestingly, within this complex, the use of seed and nut grindstones and the presence of chewed vegetal fibre (‘quids’) suggests a shift to more harsh, arid conditions where collection and storage of foods was necessary together with the use of cacti [Taylor, 1966].
3. Jora Complex (1 ka BP to 0.4 ka BP) – the most recent cultural complex. The presence of smaller lithic tips, for use with bows, and lithic scrapers suggests closer relations with nomadic groups from other areas of Coahuila and possibly the Trans-Pecos region of the USA-Mexico border. In particular, close ties with the Comarca Lagunera people have been suggested, represented by the human burials of Cueva de la Candelaria (Fig. 4.2).

Taylor concluded that the three cultural complexes shared one common cultural tradition that became modified throughout the course of the Holocene [Taylor, 2003]. Taylor’s conclusion of the modification of one common cultural tradition throughout the three cultural complexes relates to the suggested constant presence of water. Taylor [1964] suggested the hypotheses of ‘tethered nomadism’ and ‘water territoriality’, in that exploitation of different resources was undertaken radially from a water source, resulting in reduced cycles of nomadism and the need to regularly return to the initial water source, effectively tethering the Coahuilan Indians to the CCB. Taylor also suggests that a type of social control may have been in place on water sources, particularly as the environment became more arid. Occupation sites tend to be on the lower slopes of the mountains suggesting these were the more favourable locations; within close range of basin floor water sources and woodland vegetation at higher elevation up the mountain canyons [Badino *et al.*, 2004].

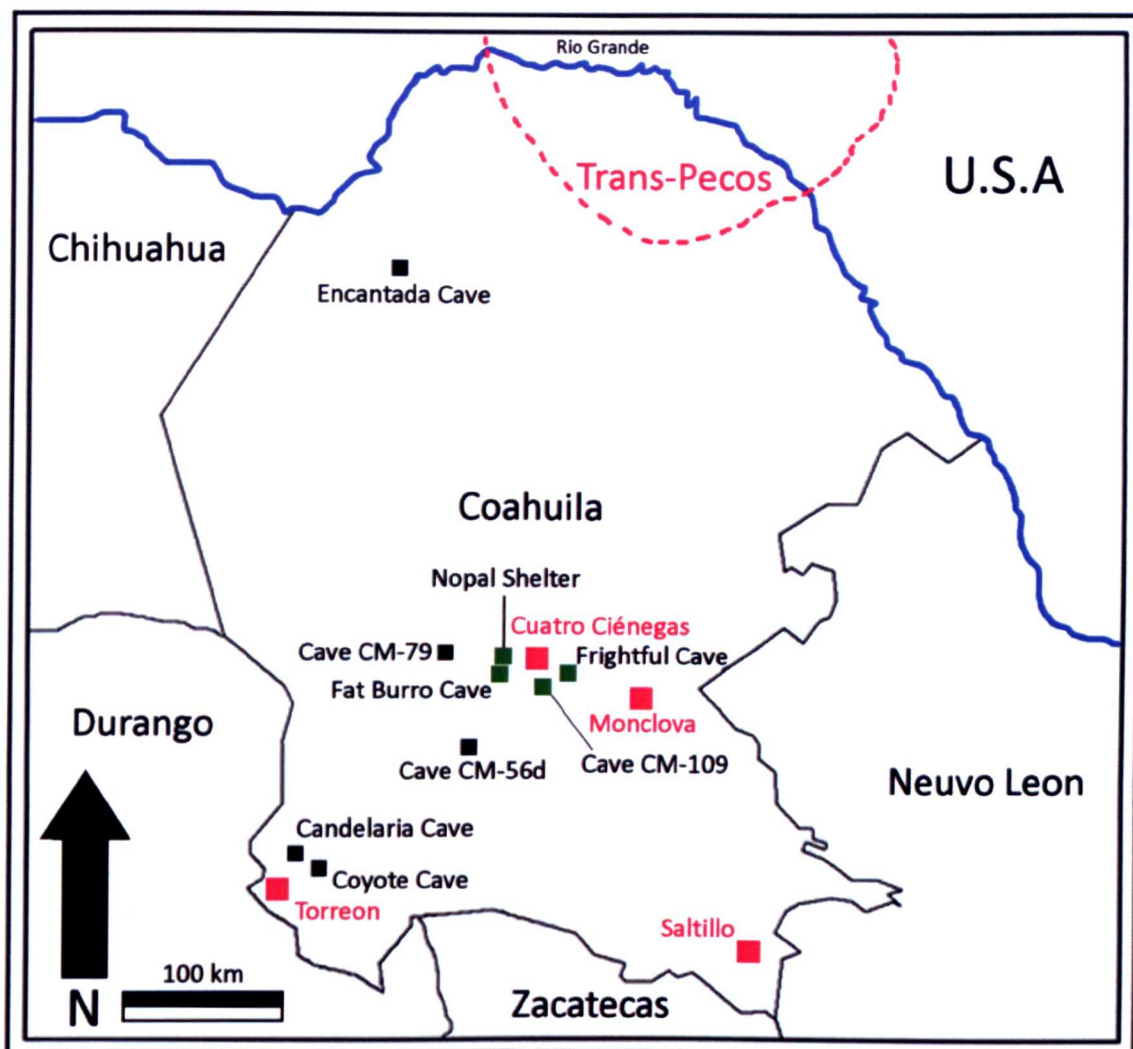


Figure 4.2. Locations of archaeological cave sites in Coahuila state, in particular within the Cuatro Ciénegas Basin shown by green squares. Red squares represent towns and cities and black squares represent cave localities.

Toward the end of the Coahuila complex, Taylor notes the progressive change of tools and vegetal items such as sandals indicated reduced social stability as the progressive disappearance of post-glacial woodland and animals led the Coahuilan Indians to become more reliant on the xeric succulents, such as the prickly pear cactus (*Opuntia sp.*) [Taylor, 1972].

The vegetation of the CCB appears to have provided the majority of vegetal fibre used in sandal, basket, net and mat production throughout all the cultural complexes. This has subsequently provided an excellent material culture chronology for the Coahuilan Indians [Taylor, 1956, 2003; Turpin, 2003]. However, very little chronological work has been performed directly on human material; the only direct dating of human samples in the CCB is provided by a ^{14}C AMS date of 5.3 ka BP from

bone collagen of an individual found in cave CM-109 (Fig. 4.2). After considering the additional U-series date of 10.5 ka BP on the museum human footprints [Gonzalez *et al.*, 2007] with the 5.3 ka BP date on bone collagen, there is still very little direct dating evidence of human occupation in the CCB making this report on the new *in situ* footprint trackway important for future studies of the Coahuilan Indian chronology.

4.2 Study site

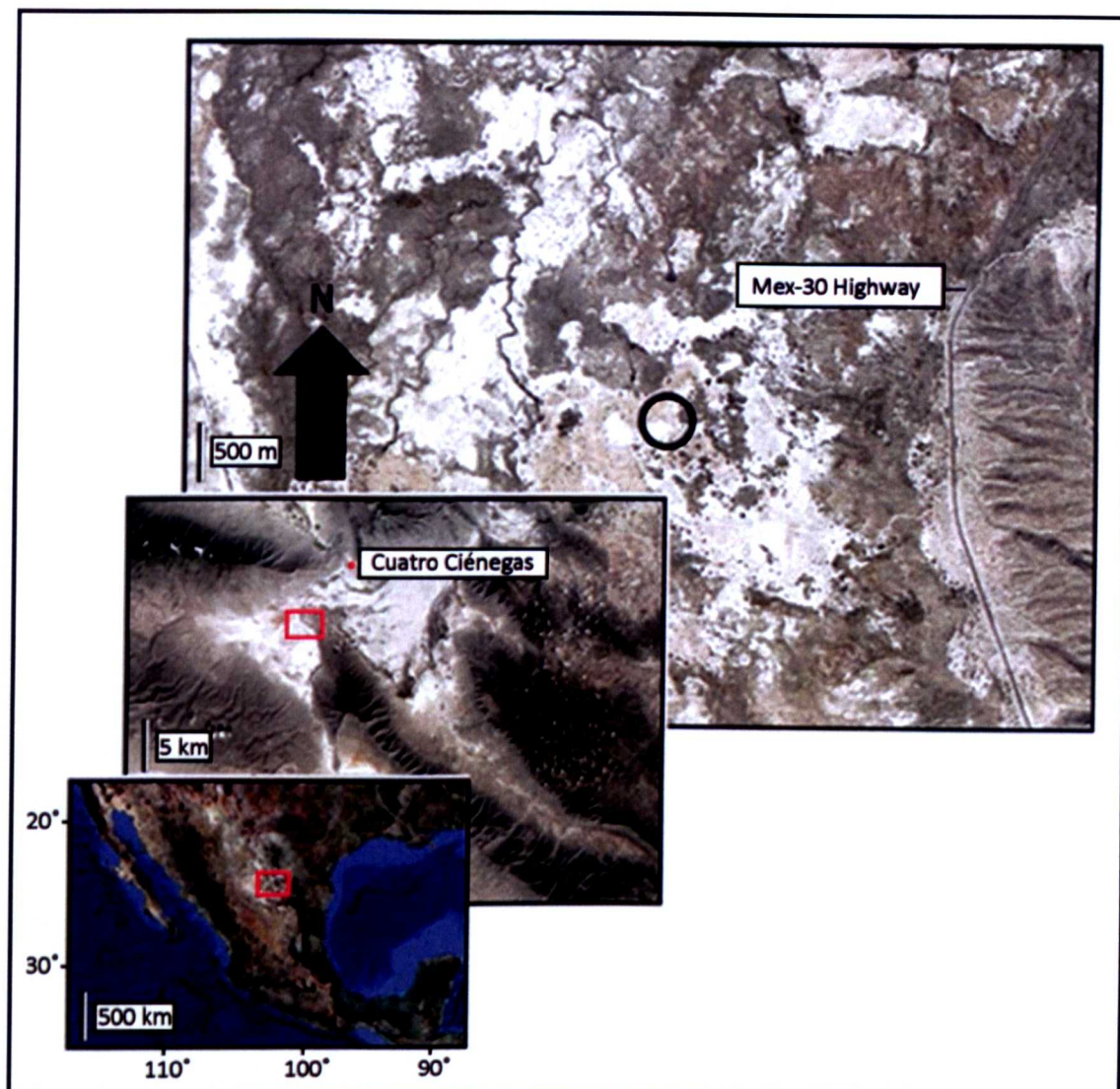


Figure 4.3. Location of the *in situ* human footprint trackway in the Tierra Blanca quarry within the Cuatro Ciénegas Basin and proximity to the Mex-30 highway where the museum footprints were discovered [image from google.co.uk/earth].

The footprint trackway is located at the Tierra Blanca quarry approximately 500 m west of the piedmont of the Sierra San Marcos y Pinos and Mex-30 highway (Grid reference: N. 26°54.526, W. 102°09.117) (Fig. 4.3). The site is located on an ancient spring mound in the centre of the main hydrological through-flow system in the CCB [see chapter 2] and approximately 100 m from the sediment core location [see chapter 5].

4.2.1 Tierra Blanca spring mound

Spring mounds are the most commonly occurring tufa formations, documented around the world, most notably in Iran [Damm, 1968]. Varying facies of spring mounds have also been documented in New Mexico, Wyoming (Mammoth Hot Springs), Slovakia and Australia [Harrington, 1948; Scheuer and Schweitzer, 1985; Ponder, 1986; Pentecost, 2005].

Spring mounds are formed when heated source water exits at the surface under large hydrostatic pressure, depositing calcium carbonate [Pentecost, 2005]. The calcium carbonate forms a dome at the surface which can range from <1m to >100m in height, dependent on determining factors such as local topography, flow rate at the surface, head pressure and degree of carbonate supersaturation. High carbonate saturation will result in a steep sided mound where CO₂ equilibration with the atmosphere and calcium carbonate deposition will be quicker and low carbonate saturation will result in a more shallow relief as CO₂ equilibration with the atmosphere will be less therefore resulting in slower calcium carbonate deposition [Pentecost, 2005].

Spring mounds require a constant hydrostatic head pressure of considerable force - often as much as 7kg cm⁻² - and this pressure is realised in artesian systems (Fig. 4.4) [Pentecost, 2005]. Artesian systems occur as a result of faulting, allowing water to rise up through the fracture to the surface. Divergence of the artesian well from the fault is realised if the fault does not reach the surface or reaches an impermeable body of rock or sediment, known as an aquiclude [Neuman and Gardner, 1989; Pentecost, 2005]. Head pressure is provided by gravity whereby precipitation on higher ground is forced down through the bedrock, creating a pressure great enough to force groundwater out at the surface as a spring. Many mounds have a low relief consisting

of sheet like layers of alternating micritic and sparry tufas, mantling the surrounding topography (Fig. 4.4), often creating irregular shapes and 'shorelines' [Ford and Pedley, 1996; Pedley *et al.*, 2003; Pentecost, 2005].

Figure 4.4. Schematic showing development of a spring mound. a-d) Growth of a mound where alternating (yellow and brown) layers of calcium carbonate are deposited, initially down slope before the mound builds to a higher elevation, depositing calcium carbonate upslope also; f) example of Tierra Blanca spring mound – a fault controlled flowing artesian spring; g) Tierra Blanca spring mound facies [modified after Pentecost, 2005].

4.3 Description of *in situ* human footprint trackway

The footprints were discovered *in situ* at Tierra Blanca quarry, the site of an ancient spring mound, after quarrying activity had exposed but not damaged them. In total, five footprints are well preserved in the tufa whilst six are less well preserved, having been either partially or completely eroded away. A 3D laser scanning technique

has been applied by Prof. Matthew Bennett of Bournemouth University, to the *in situ* track to record and preserve it in a digital format for future studies (Fig. 4.4).

Figure 4.5. 3D Laser scanned map of the *in situ* human footprint trackway located at Tierra Blanca. Well preserved prints are designated 1-5 on the diagram whilst eroded prints are not numbered. Three prints (L-R-L sequence) are missing between prints 1 and 2 and a further three (R-L-R sequence) are missing after print 5 [image courtesy of Prof. Matthew Bennett, Bournemouth University, UK].

The preservation of the *in situ* footprint track way is very similar to that of the two footprints stored in the museum. Mud rims can be clearly seen around the toe impressions and also between the toes and the ball of the foot (prints 1-5, Fig. 4.5), the heel is also clear on three of the prints (1, 2 and 5, Fig. 4.5) where the longitudinal arch of the foot during walking can also be seen. Footprints preserved in the *in situ* trackway average 27cm in length, an approximate modern equivalent of a size 8.5. Print 1 is that of a right foot and has a very well defined 'ball' of the foot and also a very well defined heel impression. The toe impressions of print 1 are not well defined but are preserved enough to be visible. A three metre gap follows print 1 where three prints in a left-right-left sequence are missing, if step length is to be assumed equal the three metre gap leads to an average step of 75cm up to print 2 [Gonzalez *et al.*, 2009]. Print 2 is that of a right foot and is the least well preserved of the five prints in figure 4.5. The toes are not visible and the ball of the foot is heavily eroded but still visible,

the heel of print 2 however is clearly visible and very well preserved. The next footprint in the sequence is named print 4 although it is the 3rd 'visible' print in the sequence. Print 4 is that of a left foot and is in an excellent state of preservation – four clearly defined toe impressions with only the 5th (little) toe not visible. The ball of the foot is also very well preserved across the width of the foot. The heel of print 4 is not the best preserved in the sequence but an outline of the heel impression is visible despite the shallow depth of the impression. Like print 4, the next footprint in the sequence is named print 3, when it is actually the 4th print in the sequence. Print 3 is that of a right foot where four toes are clearly visible and well preserved with the exception of the 5th (little) toe. The instep of print 3 is also well preserved leading from the ball of the foot through to the heel which, despite having a shallow impression, is clearly visible. The last visible print in the sequence is print 5 and is that of a left foot. Print 5 is the best preserved with the complete impression of the foot including toes 1-5. The 1st and 2nd toes are very well preserved with deeper impressions showing as red in colour on the elevation scale, toes 3-5 do not show on the elevation scale but are visible to the eye as shallow impressions. The ball of the foot has a shallow impression but both the in and out-step leading from the ball of the foot to the heel are present and the heel itself is very well preserved with a deep impression preserved. The remaining three prints in the trackway are in a right-left-right sequence and have an average step of 72cm [Gonzalez *et al.*, 2009].

The overall average step (including both visible and eroded prints) of the *in situ* human footprint trackway is 74.57cm ($n = 11$) - based on an average step of 75cm (1-4), 76.7cm (5-7) and 72cm (8-11) [Gonzalez *et al.*, 2009].

4.4 Methods

4.4.1 Tufa sample description

A total of 14 tufa samples for U-series dating, stable $\delta^{18}\text{O}_{\text{CARB}}$ and $\delta^{13}\text{C}_{\text{CARB}}$, and pollen analysis were extracted from a small pit located 5 m from the footprint trackway but containing the same stratigraphic layers. The tufas are petrologically very pure comprising filamentous clusters of CaCO_3 crystals around organic matter (Fig. 4.6a). XRF analysis indicates the tufas comprise 52% CaO, 42% organic matter (LOI), 6% SO_3 with traces of other oxides suggesting the tufas contain very little detrital Thorium. However, contamination can be seen across the surface of the upper most tufa layer (Fig. 4.6b) by <0.1 mm black granules. This contamination continues up to 5 mm below the surface of the tufa and could be linked to modern heavy industry and extraction of coal in the nearby city of Monclova.

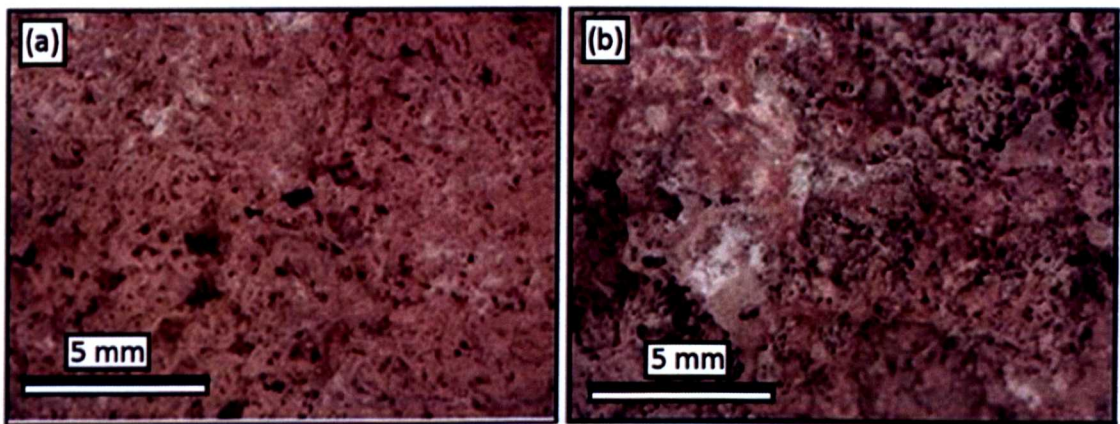


Figure 4.6. Examples of the footprint trackway tufa a) Filamentous structure observed within the tufa where the carbonate can be seen formed around organic matter (dark areas are true pore spaces). b) Black surface contamination observed in the upper most layer of the sampled footprint tufa [images courtesy of Steve Noble, NIGL].

4.4.2 U-series dating

The dating was performed at the NERC Isotope Geoscience Laboratory (NIGL), Nottingham. Between 0.8 and 1.5 g of tufa carbonate was analysed per sample (~ 1 g) which provides enough Uranium and Thorium for analysis. Samples were dissolved in Teflon-distilled HNO_3 . Trace HNO_3 -insoluble detritus was removed by centrifuging, and the dissolved carbonate spiked with a $^{229}\text{Th}/^{236}\text{U}$ tracer calibrated against gravimetric solutions prepared from Ames high-purity Th and CRM 112a U metal pieces. The tracer and sample were equilibrated and then Th and U co-precipitated with FeOH [Edwards *et al.*, 1988] and purified using a two column chromatography procedure following

Potter *et al.*, [2005]. Uranium isotope ratio measurements were performed by thermal ionization mass spectrometry (TIMS) on a Triton mass spectrometer using an RPQ high abundance sensitivity filter and a combination of a Mascom ion-counting secondary electron multiplier (SEM) and multicollector Faraday detectors. Sample uranium was loaded onto zone-refined Re filaments and analysed in double-filament mode. Mass fractionation was negligible based on the measured $^{235}\text{U}/^{238}\text{U}$ ratios in both samples and the CRM 112a and U500 standards analysed during the period when the tufa samples were measured. Th was analysed on the Nu HR multicollector ICP mass spectrometer using simultaneous ion-counting on three ETP SEM's. Intercalibration of the relative gains and mass fractionation was monitored using an in-house $^{229}\text{Th} - ^{230}\text{Th} - ^{232}\text{Th}$ solution calibrated on the Nu HR in multicollector Faraday mode. During the Th solution calibrations mass fractionation was corrected by simultaneous measurement of the $^{235}\text{U}/^{238}\text{U}$ ratio from admixed CRM 112a. All data were processed following Ludwig [2003a] and plotted using in-built functions and graphics routines in Isoplot 3.0 [Ludwig, 2003b] using the decay constants of Cheng *et al.*, [2000]. All ages and errors on isotope ratios are quoted at the 2σ level.

4.4.3 Stable isotopes

The tufa sample material was ground in agate and equivalent of 10 mg of carbonates was reacted with anhydrous phosphoric acid *in vacuo* overnight at a constant 25°C . The CO_2 liberated was separated from water vapour under vacuum and collected for analysis. Measurements were made on a VG Optima mass spectrometer. Overall analytical reproducibility for these samples is normally better than 0.2‰ for $\delta^{13}\text{C}$ and $\delta^{18}\text{O}$ (2σ). Isotope values ($\delta^{13}\text{C}$, $\delta^{18}\text{O}$) are reported as per mil (‰) deviations of the isotopic ratios ($^{13}\text{C}/^{12}\text{C}$, $^{18}\text{O}/^{16}\text{O}$) calculated to the VPDB scale using a within-run laboratory standard calibrated against NBS standards.

4.4.4 Pollen

Tufas for pollen analysis were prepped by Dr. Bruce Albert (University of Durham) and were first pulverized in a mortar-and-pestle before *Lycopodium* tablets (spores = 13,911) being added to large (20-50 cc) tufa samples. Samples were then dissolved in large (1,000-2,500ml) volumes of 20% HCl (Hydrochloric acid) for 48 hours prior to a light (3 min.) H_2SO_4 (Sulphuric acid) based hot acetolysis controlled by glacial

acetic acid. No KOH (Potassium hydroxide) was employed as no humus was detected, although where gypsum was detected, this was dissolved in a hot 0.2 m EDTA (Edetic acid) salt solution. Care was taken to limit the latter treatment to a minimum because of potential effects on pollen exines of a high pH solution. No HF (Hydrofluoric acid) was employed, as almost all non-organics were removed using EDTA. After cleaning and EtOH (ethanol) based dehydration, samples were dyed in a safranin and alcohol solution and finally mounted in silicone oil for light microscopic (LM) work.

4.5 Results

4.5.1 U-series dating

The U-Th isotope data, calculated ages and initial $^{234}\text{U}/^{238}\text{U}$ activity ratios are listed in Table 4.1. Also listed are two analyses of the McMaster speleothem powder 76001 that give an average age of 47.7 ± 2.3 ka BP, compared to the published TIMS U-Th age of 47.6 ± 2.4 ka BP [Li *et al.*, 1989]. Uranium concentrations in the tufa samples are relatively similar ranging between 1.99 and $2.14 \mu\text{g/g}$. $^{230}\text{Th}/^{232}\text{Th}$ activity ratios for the profiled portions of 036521-7 and the upper surfaces of pieces 036521-4 and 036521-5 range from 13.4 to 44.1 which falls within the range for accurate single sample ages. $^{230}\text{Th}/^{232}\text{Th}$ activity ratio is a monitor of the amount of non-radiogenic Th contamination (“detrital” Th) in any given sample. Activity ratios above ~ 20 indicate that correction for the detrital Th is small and has \pm little effect on the calculated age and so the single sample ages are robust. Ratios below this level (~ 20) indicate that a relatively large correction is required and in these cases an isochron approach to

Sample	Uranium ($\mu\text{g/g}$)	^{232}Th ($\mu\text{g/g}$)	Initial $^{234}\text{U}/^{238}\text{U}$	$^{230}\text{Th}/^{232}\text{Th}$	Age (ka BP)	Figure
036521-4 (Top surface)	2.08	0.0177	1.916 ± 0.004	44.1	7.19 ± 0.10	N/A
036521-5 (Top surface)	2.07	0.0273	1.924 ± 0.008	29.3	7.28 ± 0.12	N/A
Top surface coeval date					7.24 ± 0.13	4.6
036521-6 (Top surface)	2.07	0.063	1.933 ± 0.006	16.3	9.49 ± 0.31	N/A
036521-7 (Top surface)	2.14	0.0832	1.932 ± 0.006	13.6	9.80 ± 0.35	N/A
036521-7 (Upper drilled layer)	2.08	0.0233	1.921 ± 0.002	36.9	7.89 ± 0.12	4.6
036521-7 (Middle drilled layer)	2.09	0.0244	1.917 ± 0.002	35.8	7.97 ± 0.13	4.6
036521-7 (Lower drilled layer)	1.99	0.0207	1.924 ± 0.002	42.5	8.46 ± 0.12	4.6
036521-8 (Top surface)	2	0.0793	1.931 ± 0.005	13.4	9.86 ± 0.52	N/A
McMaster 76001-12	0.77	0.0068	2.062 ± 0.008	246.9	48.56 ± 0.30	N/A
McMaster 76001-13	0.79	0.0069	2.060 ± 0.004	243.2	46.91 ± 0.36	N/A

Table 4.1. U-Th isotope data, calculated ages and initial $^{234}\text{U}/^{238}\text{U}$ activity ratios for the *in situ* footprint trackway.

dating the samples is more appropriate and accurate. Subsequently samples 036521-6, 036521-7 and 036521-8 (Top surface) were omitted from the top surface coeval date. The age of the top surface of the tufa, which contains the *in situ* footprint trackway, is 7.24 ± 0.13 ka BP based on the average of the two upper surface ages. The depth profiling analyses indicate that the various layers preserved in tufa piece 036521-7 have a range of ages that increase with depth, with the base layers being older than the surface and uppermost layers as expected. The near-surface porous layer is dated at 7.89 ± 0.12 ka BP, an intermediate porous layer at 7.97 ± 0.13 ka BP, and the lowermost layer at 8.46 ± 0.12 ka BP (Fig. 4.7).

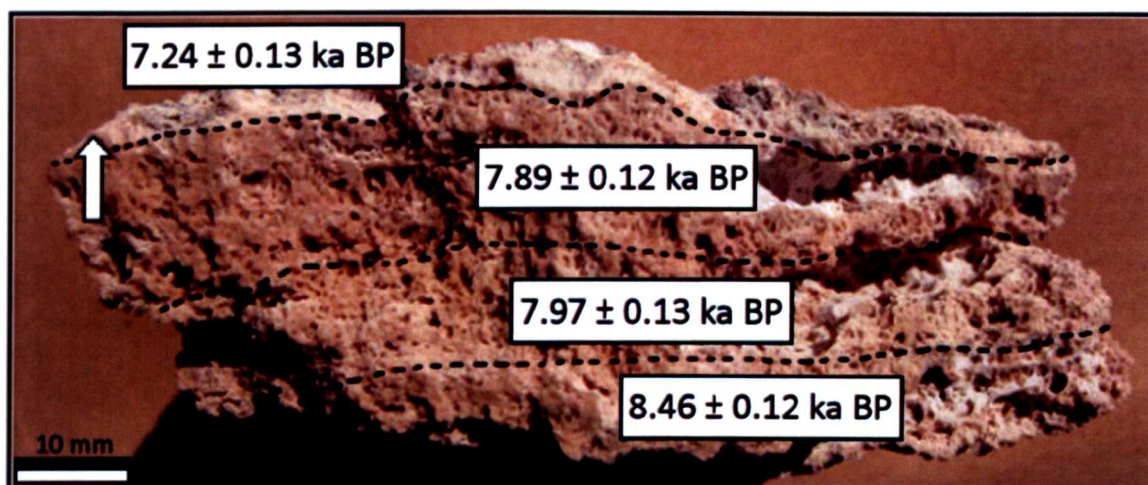


Figure 4.7. Alternating porous/non-porous layers sampled for age profiling within tufa sample 036521-7 with $^{230}\text{Th}/\text{U}$ ages representative of adjacent layer [image courtesy of Steve Noble, NI GL]. Arrow indicates orientation of the sample - base to surface.

4.5.2 $\delta^{13}\text{C}_{\text{DIC}}$ and $\delta^{18}\text{O}_{\text{CARB}}$ isotopes

$\delta^{13}\text{C}_{\text{DIC}}$ and $\delta^{18}\text{O}_{\text{CARB}}$ isotope analysis has been conducted on the Tierra Blanca footprint stratigraphy (Fig. 4.8). 14 layers were identified in the section by their alternating porous – non-porous layers, indicative of a calm ciénega (paludal) spring mound environment (Fig. 4.9) [Tucker and Wright, 1992; Pedley *et al.*, 2003; Pentecost, 2005]. $\delta^{13}\text{C}$ and $\delta^{18}\text{O}$ isotope values were taken at 10 intervals throughout the section (Fig. 4.8). The $\delta^{13}\text{C}$ isotope value of the carbonate remained relatively constant throughout the section with the highest value of -0.4‰ occurring at three depths: 24.5-27cm (B), 23-24.5cm and 0-9cm. The lowest $\delta^{13}\text{C}$ value of -1.1‰ occurs at 24.5-27cm (A) (Fig. 4.8). The $\delta^{18}\text{O}$ isotope value of the carbonate gradually

decreases from -2.9‰ to -6.2‰ suggesting a slight shift to a wetter climate towards the top of the unit. A -2‰ shift is observed between 9-15cm and the surface tufa indicating a more sudden shift towards a wetter climate towards the top of the sequence after previously being a more gradual shift.

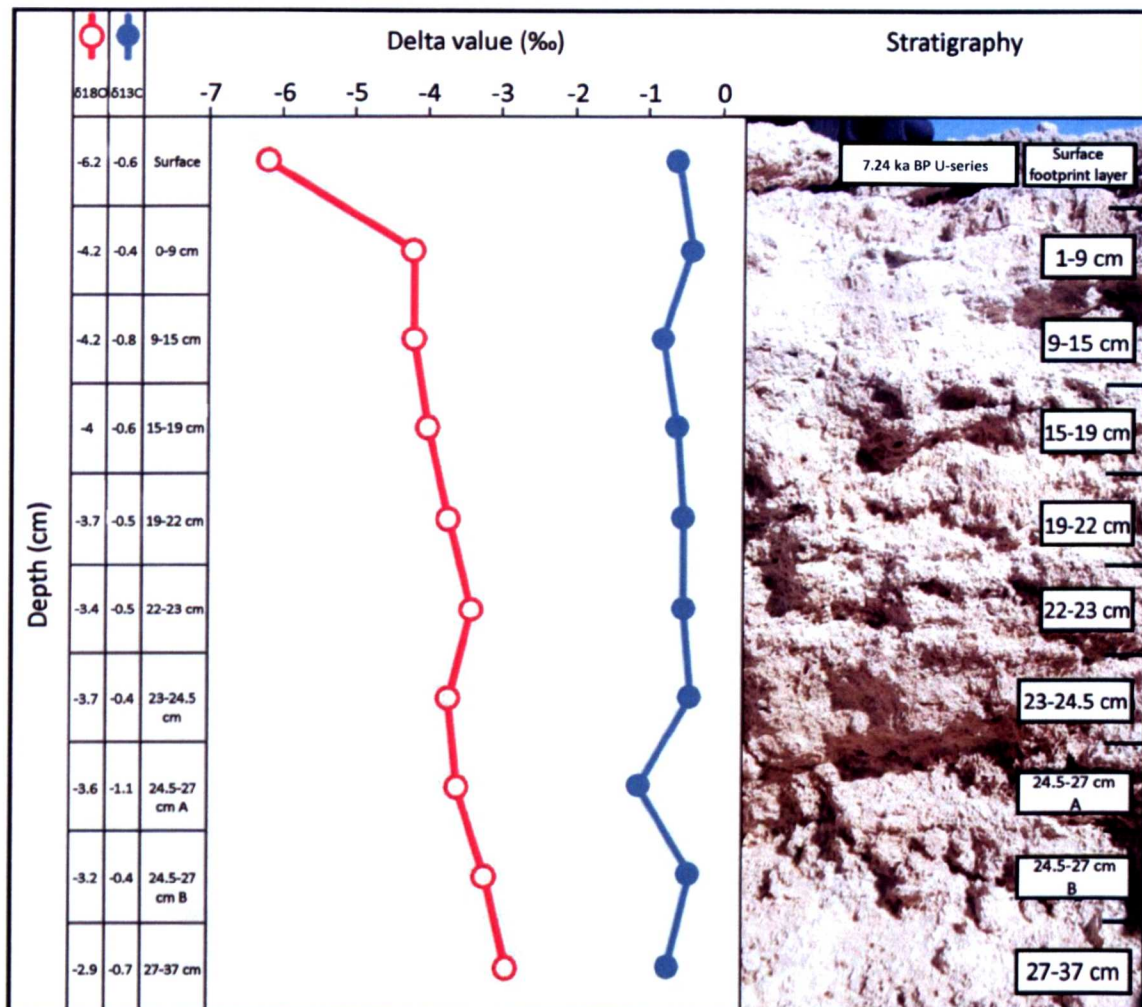


Figure 4.8. $\delta^{18}\text{O}_{\text{CARB}}$ and $\delta^{13}\text{C}_{\text{DIC}}$ isotope values for Tierra Blanca tufa samples. Pit stratigraphy is presented in the photograph with depths. Samples for pollen analysis were taken from the surface and 0-9cm levels.

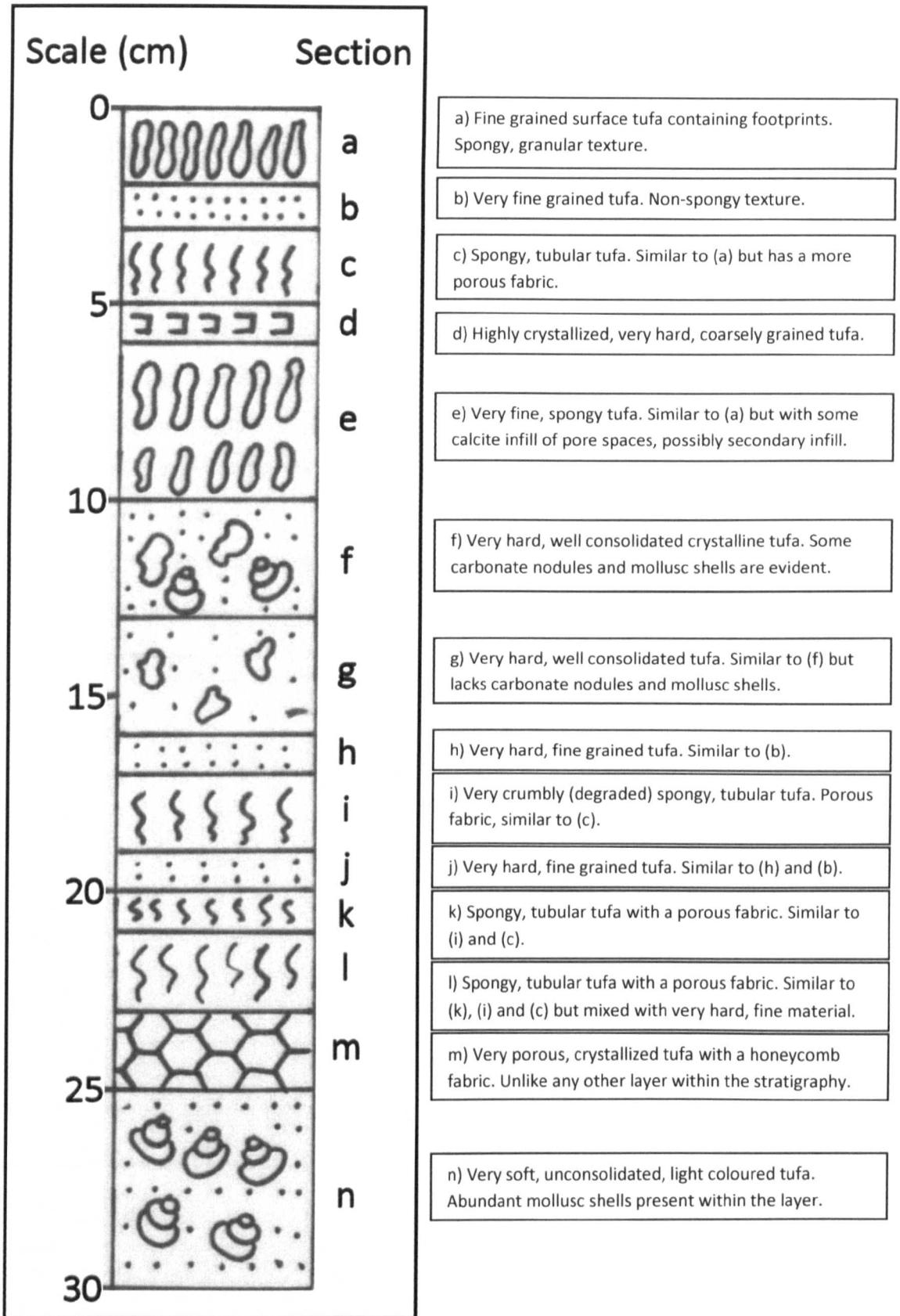


Figure 4.9. Annotated stratigraphic log of the Tierra Blanca footprint site tufa. The log was taken at N 26°54'52.60" W 102°09'11.70 in a small pit 5 m from the footprint locality.

4.5.3 Pollen

Preliminary pollen samples from the Tierra Blanca footprint locality are designated here as TB Print 1 (0 cm) and TB 1-9 cm (excavated pit). These contain a similar range of pollen taxa, including more commonly *Pinus*, *Cupressae*, *Quercus*, *Carya*, *Poacea*, *Chenopodiaceae*, *Asteraceae*, *Ambrosia*, *Ephedra* and *Leguminosae*. Also notable here are less common pollen types such as *Potamogeton*, *Cyperaceae*, *Rhus*, *Myrica*, *Salix*, *Alnus*, *Acacia*, *Centaurea*, *Geranium*, *Agave*, *Opuntia* (fragmentary) and an indeterminate trizonocolporate type (*Leguminosae*). Preliminary pollen data (Fig. 4.10) suggest a wet shift toward the top of the Tierra Blanca tufa sequence (9cm-surface). Regional upland taxa – *Pinus* and *Quercus* – increase from 20 to 254 grains/cc and 13 to 22 grains/cc respectively whereas grasses (*Poaceae*) are seen to decrease from 17 to 6 grains/cc. CCB floor taxa such as *Poaceae* and *Cheno-Ams* can be misleading however, as observed by Meyer [1973], abundance data can indicate local rather than regional pollen rain.

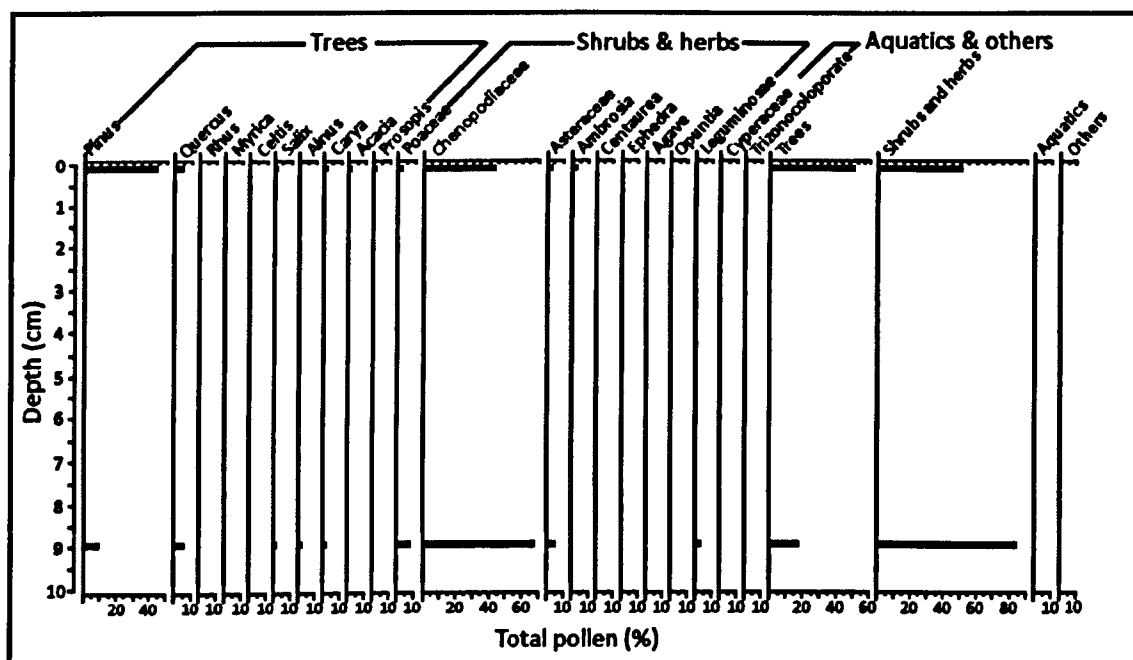


Figure 4.10. Preliminary pollen data for Tierra Blanca tufa stratigraphy. TB Print 1 was taken at the surface so is plotted at 0 cm and 1-9 cm is plotted at 9 cm to accentuate the stratigraphic change in pollen with such a low resolution (two samples).

4.6 Discussion

4.6.1 Palaeoenvironment

Stable isotopes

The relatively constant $\delta^{13}\text{C}_{\text{DIC}}$ values throughout the tufa sequence at Tierra Blanca quarry (Fig. 4.8), as discussed in chapter 3, suggests the calcium carbonate deposited was subject to the hard water effect from the surrounding Cretaceous limestone, the source water containing the dissolved CO_2 was of a thermogene origin or the source water was of a heated meteoric origin [Pentecost, 2005]. False ^{14}C dates obtained for living molluscs of 26.31 ± 1.7 ka BP from Poza Becerra [Silvia Gonzalez, personal comms.] indicate that old carbonate contamination from the surrounding Cretaceous limestone does occur in the CCB, although modern water samples [see chapter 2] display $\delta^{13}\text{C}_{\text{DIC}}$ values between -21.6‰ and -9.2‰ suggesting little or no ^{13}C is sourced from the local Cretaceous limestone bedrock that has much more positive $\delta^{13}\text{C}_{\text{DIC}}$ values between $+2\text{‰}$ and $+4\text{‰}$ [Bralower *et al.*, 1999]. However, unlike Poza Becerra, the Tierra Blanca locality does not form part of the modern day through-flow system and is currently not actively depositing calcium carbonate, suggesting the Tierra Blanca tufas were formed by a different process, possibly through the means of an artesian well surfacing as a spring mound (see section 4.2.1). Source waters from an artesian well would originate as meteoric water in the surrounding mountains before percolating down through the bedrock deep below the surface, reducing the influence of atmospheric and soil CO_2 in percolation water – the main contributors to $\delta^{13}\text{C}_{\text{DIC}}$ values of CCB water between -21.6‰ and -9.2‰ . Less influence of atmospheric and soil CO_2 (the more negative $\delta^{13}\text{C}_{\text{DIC}}$ pool) would in theory increase the influence of water-rock reactions that would result in positive $\delta^{13}\text{C}_{\text{DIC}}$ from the limestone bedrock [Pentecost, 2005].

Any CaCO_3 deposited by this method when CO_2 degasses at the surface would still contain some carbon sourced from the Cretaceous limestone surrounding the CCB and some degree soil zone CO_2 , although the $\delta^{13}\text{C}_{\text{DIC}}$ values of the Tierra Blanca calcium carbonate suggest this may be limited with some CO_2 invasion from the atmospheric CO_2 [Ford and Pedley, 1996; Pentecost, 2005; Baldini *et al.*, 2006].

The presence of a tufa spring mound suggests that at 7.24 ± 0.13 ka BP the CCB was substantially wetter than present as no such active spring mounds exist in the present climate. Increased 'head pressure' is required to drive the flow of water from deep below the surface, through increased precipitation at higher elevations, to discharge at ground level. Pollen and diatom records [Van Devender, 1985; Anderson and Van Devender, 1995; Metcalfe, 1997] from northern Mexico suggest that modern day climate was established sometime after 4 ka BP although large gaps in the record exist between c. 9.5 ka BP and 5 ka BP, particularly in the Bolson de Mapimi [Metcalfe, 1997], where diatom data are sparse indicating a drier climate. However, Van Devender [1985] suggests the Chihuahuan desert experienced significant increases in temperature and summer precipitation after 9 ka BP, increasing effective moisture over the north of Mexico. The preliminary $\delta^{18}\text{O}$ values of the Tierra Blanca tufas corroborate Van Devender's theory of a wetter climate c.9 ka BP as a gradual decrease from -2.9‰ to -6.2‰ is observed from the base of the sequence (Fig. 4.8) with a larger decrease of -2‰ observed between 9cm and the surface. Interestingly a date of 8.46 ± 0.12 ka BP (Table 4.1, Fig. 4.7) was obtained for the lower drilled layer of sample 036521-7 which corresponds to 0-9cm on figure 4.8 and subsequently the onset of a more dramatic wet shift through to the surface and a date of 7.24 ± 0.13 ka BP. After this point, the tufa forming process appears to end at Tierra Blanca suggesting a change in hydrology and reduced effective moisture driving the head pressure that formed the spring mound [Gonzalez *et al.*, 2009]. Spaulding [1991, page 432] suggests "aridity greater than that of the present between ca. 7000 and 5000 yr BP" in the Mojave Desert, N. America which when coupled with data from the Bolson de Mapimi [Metcalfe, 1997] and this study indicates a drier period from c. 7 ka BP to the establishment of the modern climate c. 4 ka BP in Northern Mexico.

Pollen

Vegetation growing at high altitudes, or upland vegetation taxa, in arid regions e.g. *Pinus*, *Quercus* and *Cupressaceae* are considered the most important for regional climate change due to their limited range of environmental tolerances, thus higher sensitivity to climatic instability, and pollen rain over large areas. As opposed to lowland taxa (*Poaceae*, *Cheno-Ams* etc.) which tend to have a broad range of environmental tolerances, thus lower sensitivity to climatic instability, and local pollen

rain [Minckley and Jackson, 2008]. *Pinus* values, which approximate 50% in TB Print 1 and only 8% in TB 1-9cm, increase toward the surface of the Tierra Blanca tufa sequence. It could be assumed that an event such as a fire, or a sustained period of drier climate (or both) suppressed *Pinus* values in the latter sample (Fig. 4.10). Gonzalez *et al.*, [2009] report large amounts of charcoal in the layer 9-15 cm, just before the suppressed *Pinus* values perhaps indicating burning of human origins or a lightning strike causing dried vegetation to burn, as has been reported for the CCB during the recent eight year drought period [APFFCC]. However, with only two *Pinus* pollen samples that could represent a regional pollen rain, an inference of a human burning event or drier climate is speculative. Pollen spectra from Northern Mexico and Southwest Texas [Van Devender, 1985; Anderson and Van Devender, 1995; Bryant, 1977; Bryant and Holloway, 1985] suggest late glacial woodland and parkland was regionally declining c. 10 – 7 ka BP. Bryant and Holloway [1985] note, in the Lower Pecos region of Texas in particular, that decreasing levels of *Pinus* in Hind's Cave and Bonfire Shelter [Bryant, 1977] coincide with increasing levels of grasses and interestingly *Opuntia* and *Agave* – used at this time by palaeoindian hunter-gatherers. Bryant and Holloway do, however, mention that *Pinus* pollen collected in cave locations in the Lower Pecos was sufficient to suggest upland areas or sheltered river canyons were acting as refugia for more temperate species.

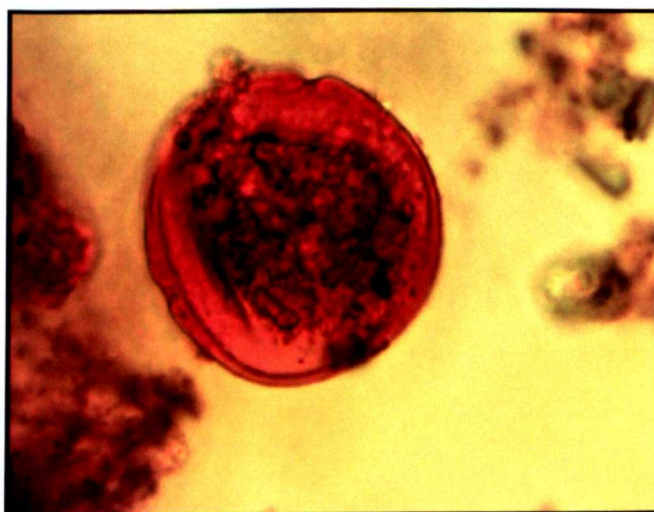


Figure 4.11. Example of *Carya* (Hickory/Pecan) pollen present in the Tierra Blanca footprint top level tufa.

The last remaining temperate species of flora and insects are recorded c. 8.7 ka BP [Van Devender, 1990] in the Lower Pecos around the same time *Pinus* appears to

increase in the CCB (Fig. 4.10). With increased water availability from the Cupido-Aurora aquifer and high (3020m) mountains surrounding the CCB it may have become a desert refuge around this time until c. 7 ka BP when drier conditions took hold. *Carya* (Hickory/Pecan (Fig. 4.11)) and *Salix* (Willow *sp.*) pollen are present, although in low numbers of 5 and 4 grains respectively, in the footprint trackway tufa at Tierra Blanca suggesting this theory may have substance as these are temperate, deciduous species that will have grown at the side of the water bodies in the CCB.

4.6.2 Southward migration and activity of hunter-gatherers

Human footprints have been well documented in the Americas - Chile, Nicaragua, California and Argentina [Dillehay, 2000; Williams, 1952; Rector, 1999; Bayón and Politis, 1996, respectively after Gonzalez *et al.*, 2009] - and, with the exception of 12.5 ka BP prints in Chile, are dated to between 6 and 7 ka BP. With these and the 10.5 ka BP museum footprints from the CCB, very sparse data is provided for an area incorporating Meso and South America of over 20,000,000 km².

The CCB appears to have provided a desert refuge with plentiful water and vegetation rich in desert succulents and fruit bearing trees. The possible shift to wetter climatic conditions, suggested by decreased $\delta^{18}\text{O}_{\text{CARB}}$ values and an increased regional *Pinus* pollen spectra at 7.24 ka BP, places the *in situ* human footprint trackway within the boundaries of Walter Taylor's [1956, 1966, 2003] 'Ciénegas complex' (10 – 7 ka BP) and 'Coahuila complex' (7.5 – 1 ka BP) in which he notes a markedly wetter climate - with remains of grizzly bear, elk and buffalo identified during cave excavations in the 1940s [Gilmore, 1947] - gradually changing to a warmer, drier climate; a climatic shift identified with the concept of changing craftsmanship and tool technology in light of no environmental or climatic data. In this early work, Taylor [1964] suggests that in a dry period water would become increasingly scarce, thus subsistence would become less secure with a decline in craftsmanship in light of increased nomadism. During the wetter 'Cienegas complex', hunting and skilled craftsmanship are seen with spatulate bone awls, animal fur and bifaced stone tools. Technology that needed specialised technique for multiple use in hunting [Taylor, 1966]. The transition into the 'Coahuila complex' sees an increased focus on unifaced stone tool technology that had multiple techniques for single use and an increase in the use of wood and fibre cordage [Taylor,

1966]. This observed shift from craftsmanship and hunting, indicative of a settled culture, to single use tools and reliance on wood and fibre cordage, due to the cultural stresses of an increasingly dry climate and aridity, seen in the well stratified archaeological deposits is a good indicator of drying climate during the transition of these complexes. However, Taylor [1964] acknowledges the limitation of the 'tethered nomadism' hypothesis in light of limited empirical evidence. Although it is an interesting hypothesis, the 'tethered nomadism' argument clearly needs refining with new studies and chronologies.

The presence of both *Opuntia* and *Agave* species in the footprint tufa layer (Fig. 4.10) allude to this transitional environment in the CCB showing more xeric species establishing themselves alongside temperate *Carya* and *Salix* species. *Opuntia* or the 'prickly pear cactus' is a fruit bearing desert succulent, consumed by the Coahuilan nomads [Bryant, 1975; Taylor, 1966, 2003; Badino *et al.*, 2004], flowering in late spring/early summer. The presence of the pollen in the footprint tufa suggests hunting and gathering activities occurred at this time of year along with cave occupation - coprolites from Frightful Cave show the presence of *Opuntia* pollen between 9.5 ka BP and 7 ka BP along with a variety of other fruits, leaves, bulbs and seeds [Bryant, 1975]. The presence of grindstones [Taylor, 1966] found in the same cave site further indicates the reliance of grinding seeds and nuts (*Carya* and *Pinus*) of which there would have been supply, if limited, both locally and regionally [Bryant, 1975, 1977].

The local and regional presence of *Agave* plants at 7.24 ka BP would have been important for providing vegetal fibres necessary for the production of sandals, baskets and ropes (amongst other technologies) [Taylor, 1966; Badino *et al.*, 2004]. *Agave* typically grows in the bajada, or 'monte', part of the CCB which is often near to canyon mouths and cave sites inhabited by the ancient hunter gatherers for their favourable location – both close to vegetal resources (i.e. *Agave*) and to water sources [Taylor, 1956]. The signs of drying climate around 7.24 ka BP appear to mark the beginning of Taylor's longest 'Coahuila complex'. In this complex Taylor [1966] notes extended nomadism in the CCB as local resources became harder to come by, hunter-gatherers expanded their search, becoming more dependent on fibrous plants and the water

sources available whilst changing point technology indicated shifts in hunting practice, possibly toward fish and aquatic fauna.

The footprint trackway is located on a raised spring mound structure which is indicative of a calm ciénega environment [Tucker and Wright, 1990]. With an average (contemporary) foot size of 8.5 and step of 74.57cm it can be assumed the footprints are that of an adult human. Taking the average step into account, the stride length for this particular hunter-gatherer is 149.14 cm and when placed into Alexander's [1989] stride length vs. speed equation gives a speed of 1.7 m/s or 3.8 mph (Fig. 4.12). The average adult walking speed is between 2.8 and 2.95 mph [Knoblauch *et al.*, 1996] indicating that this individual was travelling faster than average and potentially hunting a large animal such as a cervid (deer), of which hoof prints occur near-by the *in situ* trackway [Gonzalez *et al.*, 2009].

Figure 4.12. Stride length against speed for adult humans (circle), dogs (square) and camels (triangle). Red line represents data for the human footprint trackway in the CCB [modified after Alexander, 1989].

4.7 Conclusions and future work

With at least two different human footprint levels identified at 10.5 ka BP and 7.24 ka BP (from this study) in age, the Cuatro Ciéneas Basin (CCB) has a long period of basin floor human occupation. The tufas sampled were sufficiently pure as to yield accurate U-series dates at a young age for this dating method. The pure tufas and reduced karst influence of the CCB waters suggest that, although preliminary, the isotopic sequence studied is accurate, and may provide a valuable climatic data archive, able to be cross referenced with other archaeological sites in the Americas, in particular the Trans-Pecos region of the USA and NE Mexico. The isotopic and pollen study presented in this chapter has allowed a preliminary Mid-Holocene climate pattern of the CCB to be inferred, providing a basis for further work with the CCB tufas. The isotope and pollen data suggest that despite the warming regional climate, the CCB appears to have provided an area of unique refuge for Late Pleistocene/Early Holocene human populations from North America who would be migrating south away from the tundra conditions of N. America. There was a favourable, temperate climate providing food and water in the CCB since at least 10.5 ka BP. As the ancient nomads adapted to the increasingly hostile dry desert conditions, changing technologies and hunting activities allowed these people to expand their ability to find resources leading to longer cycles of nomadism and possibly the expansion of their unique desert culture into the regions surrounding the CCB until the arrival of the Spanish.

More extensive and detailed archaeological excavations are proposed for cave and basin floor sites in the CCB. Thorough excavations would allow for the footprint locality to be better placed into the CCB human occupation chronology whilst also placing them within a detailed environmental phase. If environmental determinations can be made they could then be collated with local and regional records allowing for possible migratory routes and hunter-gatherer activity to be determined.

The presence of the Tierra Blanca spring mound certainly suggests the CCB was substantially wetter around 7.24 ka BP. The U-series dates suggest that further dating of the Tierra Blanca tufas could yield a more accurate chronology throughout the Holocene tufa sequence, which could then allow the environment in which the hunter-gatherers were living to be synthesised into palaeoenvironmental reconstructions of

the CCB. As well as U-series dating techniques, further stable isotopic work is warranted. A good preliminary palaeoenvironmental record has been established, providing an excellent platform on which to base further environmental and hydrological determinations. Synthesis of human activities can then be placed within a regional and global palaeoenvironmental context if the obtained isotopic and hydrological data (from tufas) can be collated.

Chapter 5: Multi-proxy palaeoenvironmental reconstruction of the Cuatro Ciénegas Basin

5.1 Introduction

The main aim of this chapter is to investigate the palaeoenvironment of the CCB using a multi-proxy research approach. $^{18}\text{O}/^{16}\text{O}$ and $^{13}\text{C}/^{12}\text{C}$ isotope ratios were measured to allow the analysis of stable $\delta^{18}\text{O}$ and $\delta^{13}\text{C}$ isotopes alongside pollen samples taken from a 15 m sediment core. A timescale spanning the Late Pleistocene-Holocene in the CCB is investigated. A further aim of this study is to reinvestigate the hypothesis of environmental stability spanning the last 30 ka BP in the CCB, first proposed by Meyer [1973] and later contradicted by Minckley and Jackson [2008]. The contrasting nature of the studies has major implications for the controls of tufa formation, hydrology and human occupation within the CCB.

5.1.1 Climate of the Cuatro Ciénegas Basin

The Cuatro Ciénegas Basin floor today averages 742 m a.s.l and is “in shadow of rain” [Badino *et al.*, 2004], enclosed between the Sierra Madre Occidental to the west and the high peaks of the Sierra Madre Oriental to the east, cutting off the dominant winds and humid air from the Pacific Ocean and Gulf of Mexico (GoM) respectively [Badino *et al.*, 2004] (Fig. 5.1).

The CCB is classed as a semi-arid desert environment. Annual evaporation of >2000 mm/yr exceeds annual precipitation of <250 mm/yr with the majority of rainfall occurring during the summer months [Badino *et al.*, 2004]. Rain falls mainly in September through a mixture of humid air from the GoM and rainout from the North American Monsoon (Fig. 5.2). Individual rainout events can reach up to 40 or 50 mm, although the surrounding mountains play an important role in precipitation patterns in the CCB. Up to 350mm falls in the mountain regions surrounding the CCB due to the mountains forcing ascending movements of air which then cool down with higher altitude, eventually releasing precipitation [Badino *et al.*, 2004].

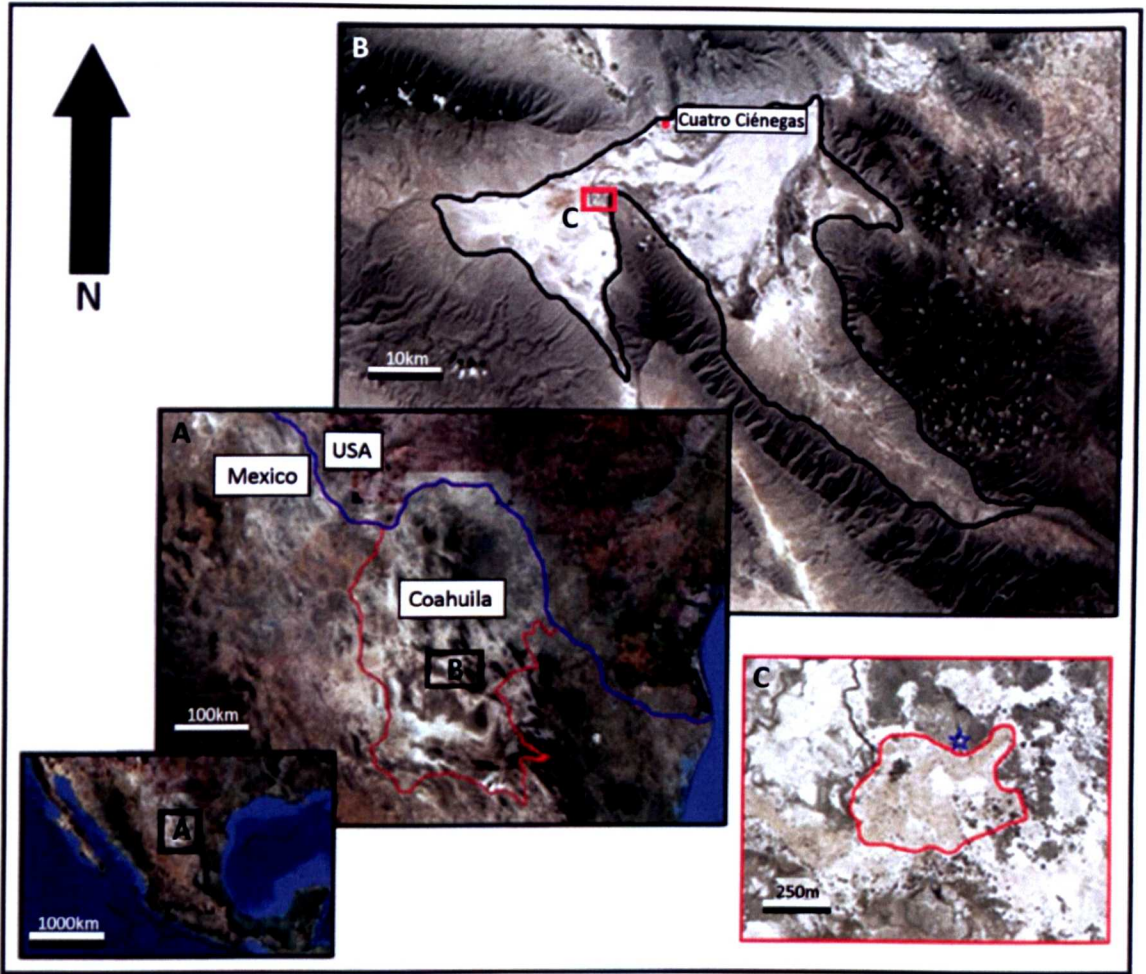


Figure 5.1. Location of the Cuatro Ciénegas Basin in Mexico (A and B) with the Tierra Blanca Quarry site (C). Core Poza Tierra Blanca (PTB) location is marked with a star [image from google.co.uk/earth].

Air temperatures in the CCB have a large range. Average daily temperatures range from $+6.3^{\circ}\text{C}$ to $+24.6^{\circ}\text{C}$ with peaks up to 40°C in June and July and troughs of 0°C during December and January. This gives an average annual temperature of 21.2°C on the CCB floor (742 m a.s.l), 16°C at 1500 m a.s.l and 13°C at 2000 m a.s.l [Badino *et al.*, 2004].

Figure 5.2. The major circulation patterns over Mexico in (a) winter (DJF) and (b) summer (JJA). Dominant seasonal moisture sources are shown with bold arrows. The CCB location is displayed as a red star [modified after Metcalfe *et al.*, 2000].

5.2 Previous palaeoenvironmental studies

Comparatively few palaeoenvironmental studies of northern Mexico have been conducted when compared to the number of studies in central and southern Mexico [Metcalf *et al.*, 2000]. Only two studies have been conducted within the CCB itself, although four important studies focusing around the Chihuahuan Desert and southern United States have been undertaken (Fig. 5.3).

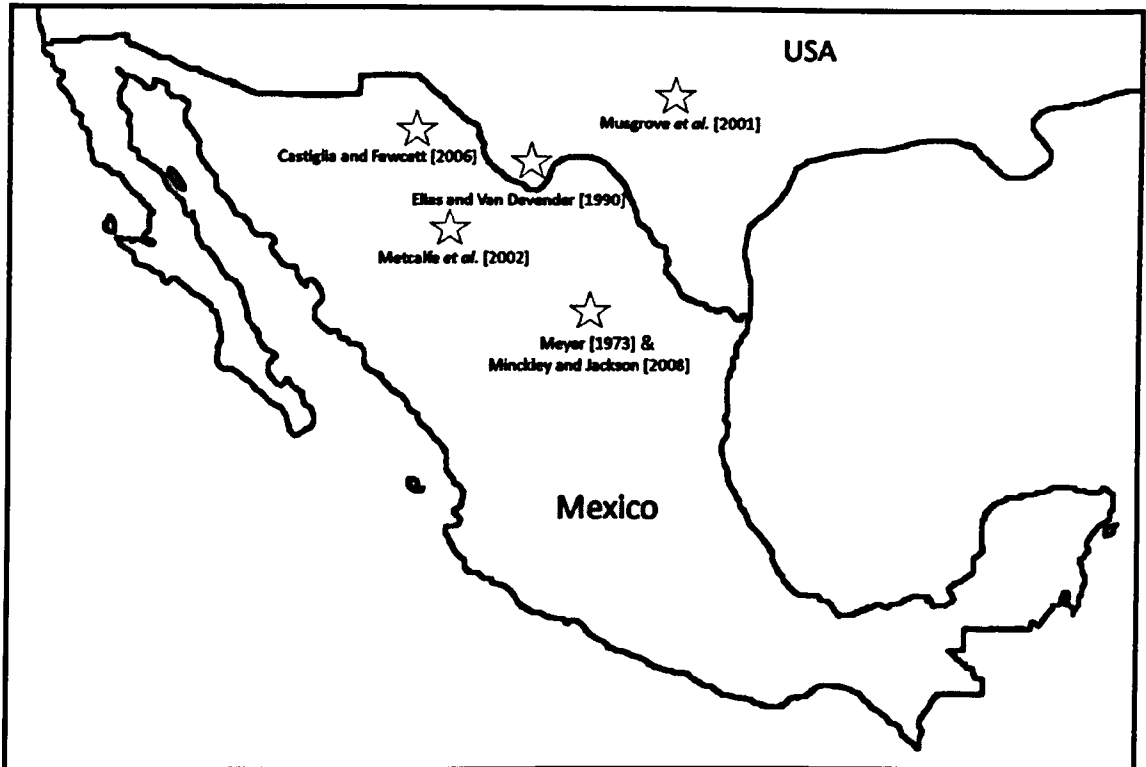


Figure 5.3. Previous palaeoenvironmental studies conducted in the north of Mexico and southern United States.

Meyer [1973] produced the first palaeoenvironmental study of the CCB, studying a 13 m sediment core. The exact location of the sediment core remains unclear although, sedimentologically, several alternating peat/tufa layers were described. Meyer [1973] proposed climate stability in the CCB from 31.4 ka BP to the present through pollen analysis. *Compositae* dominated the sequence (55-83% of total pollen), similar to contemporary CCB floor spectra, supporting the hypothesis of environmental stability. Changes in upland *Pinus* and *Quercus* are noted throughout the pollen sequence, indicating a fluctuating environment, although the expansion of upland vegetation did not progress onto the CCB floor. Inverse ^{14}C dates at the base of the 13 m core – 26.8 ka BP at 13 m and 31.4 ka BP at 11 m – suggest the possibility of

erroneous sampling procedures or pre-sampling contamination, such as re-worked sediment. The apparent errors in the chronology of Meyer's study suggest the final conclusion of environmental stability from 31 ka BP to the present may be incorrect. Although the interpretation of pollen data may be correct indicating vegetational, and therefore environmental, stability over the Late Pleistocene to the present, the inverted dates suggest that the time span of 31 ka BP to the present may be incorrect.

More recently, Minckley and Jackson [2008] studied a fossil packrat midden taken from the Sierra San Marcos y Pinos in the CCB and combined this with a re-investigation of Meyer's [1973] original pollen data. The midden is of glacial age – 16.9 ka BP – showing substantial climatic and ecological changes within the CCB over the Late Pleistocene and Early Holocene. Woodland populated the CCB mountains down to the bajada's (alluvial deposits) at the foot of the mountains from 16.9 ka BP to c. 11 ka BP; migrating upwards as regional climate began to warm into the Holocene.

Metcalf *et al.*, [2002] studied a laminated core taken from Alta Babícora in the Chihuahuan Desert. Using diatom assemblages they found the presence of a deep water lake from at least 65 ka BP to 57 ka BP before shallowing and exhibiting concentrated lake levels at 54.6 ka BP. Between c.55 ka BP and c.30 ka BP a summer precipitation regime dominated the climate, punctuated by high variability in lake levels. Southward displacement of the westerly storm tracks is widely accepted between c.29 ka BP and c.10 ka BP; causing wetter, cooler conditions in the Chihuahuan Desert. This work was a continuation of that by Metcalf *et al.*, [1997] where a diatom record spanning >11 ka BP to 2.5 ka BP was presented. Evidence for a deep water lake in Alta Babícora is indicated prior to 11.06 ± 0.39 ka BP, before a marked shallowing, corresponding to the Younger Dryas c.11.06 ka BP to 9.47 ka BP. The diatom record becomes sparse at that point of the record suggesting a dry mid-Holocene before wet conditions are re-established in the diatom record prior to 2.47 ka BP.

Musgrove *et al.*, [2001] conducted detailed chronologies of four stalagmites in the Edwards Plateau, Trans-Pecos region of Texas. Detailed hydrologic patterns and climate change indications were extracted by studying growth rates of the stalagmites, spanning 71 ka BP to the present. They found three periods of rapid growth – 71 ka BP

to 60 ka BP, 39 ka BP to 33 ka BP and 24 ka BP to 12 ka BP – indicating these periods had significantly increased moisture, corresponding in part with stadial-interstadial cycles. The stalagmites all exhibit a large drop in growth rate between 15 ka BP and 12 ka BP, continuing up to the present, consistent with drying Holocene climate.

Elias and Van Devender [1990] studied a series of 50 packrat middens in the Big Bend region of the Chihuahuan Desert, ranging in age from 36 ka BP to the present. A diverse arthropod fauna was found, substantiating the hypothesis of mesic vegetation of glacial age c.30 ka BP to 12 ka BP, in particular, mid-glacial (c. 30ka BP to 20 ka BP), indicating a temperate, wooded environment. Late glacial (c.20 ka BP to 12 ka BP) fauna were mainly comprised of grassland species indicating a cooler, wetter climate for Chihuahua at that time. After 12 ka BP these temperate species were gradually replaced by desert species up to 6 ka BP, after which species more indicative of severe aridity became abundant, although temperate species were still found in the area up until 2.5 ka BP.

Castiglia and Fawcett [2006] studied Holocene pluvial lake beach deposits in the Chihuahuan Desert. Using ^{14}C AMS dating of beach deposits they found the early, mid and late Holocene was punctuated by periods wet enough to establish pluvial lake systems. Four periods – 8456 ± 97 to 8269 ± 64 yr BP; 6721 ± 68 to 6110 ± 80 yr BP; 4251 ± 59 to 3815 ± 52 yr BP and 221 ± 33 yr BP – were found to be climatically wet enough to support the presence of pluvial lakes.

Meyer's [1973] conclusions of climatic and environmental stability in the CCB are contradicted by the findings of more recent, regional studies of northern Mexico and southern United States. Therefore, the aim of this chapter is to test the following null hypothesis: has the Cuatro Ciénegas Basin (CCB) provided an area of unique desert refuge for flora and fauna, unresponsive to regional climatic and environmental change, from the Late Pleistocene to the present?

The use of stable isotopes ($\delta^{18}\text{O}$, $\delta^{13}\text{C}$) for palaeoenvironmental reconstructions in northern Mexico has been completely neglected up until this point. This study will explore, for the first time in this region, the use of isotopes as proxy environmental indicators by analysing changes in $\delta^{18}\text{O}$ and $\delta^{13}\text{C}$ climate signals. Alongside pollen

samples taken from a 15 m sediment core it should be possible to reconstruct a multi-proxy palaeoenvironmental record for the CCB for the first time.

5.3 Stable isotopes in lacustrine and wetland sediments

Stratigraphic changes in stable isotopic ratios ($^2\text{H}/^1\text{H}$, $^{18}\text{O}/^{16}\text{O}$, $^{13}\text{C}/^{12}\text{C}$) in lacustrine and wetland sediments can be attributed to changes in the steady state composition of the water from which the sediment is being deposited. These changes can be dependent on a number of factors, including temperature, atmospheric moisture source and precipitation/evaporation ratio (E/P) [e.g. Schwalb, 2003; Schwalb *et al.* 1999; Liu *et al.* 2009]. Typically, lakes and wetlands produce primary mineral precipitates which will be authigenic, such as calcite marl [e.g. Dean and Schwalb, 2000], or biogenic, such as ostracod and gastropod shells [e.g. Heaton *et al.* 1995; Escobar *et al.* 2010], from which the stable isotopic ratios can be measured.

5.3.1 Oxygen

Oxygen exists in three isotopic forms - ^{16}O , ^{17}O and ^{18}O – with two of these of importance in palaeoenvironmental studies – ^{16}O and ^{18}O . Oxygen isotopes in carbonate sediments will reflect the environment in which they were precipitated over the course of a stratigraphic sequence [Leng, 2005; Sharp, 2007]. Palaeoclimate studies will often use observed stratigraphic changes in the oxygen isotope composition of biogenic or authigenic carbonate to infer changes in temperature or the oxygen isotope composition of the water, and carbonates have been shown to contain significant archives of palaeoclimatic and palaeoenvironmental information [Andrews *et al.*, 1993, 1997; Yu *et al.*, 1997; Leng *et al.*, 2001; Marshall *et al.*, 2002; Ortiz *et al.*, 2009; Brasier *et al.*, 2010; Holmes *et al.*, 2010 also see Leng, 2005; Sharp, 2007 and Hoefs, 2009 for further discussion].

The oxygen isotopic composition of lacustrine and wetland sediment archives is predictable by thermodynamics in that the oxygen isotope composition of the precipitating mineral is controlled by the temperature and isotopic composition of the source water from which the mineral is precipitated, this is known as equilibrium mineral precipitation [Leng, 2005; Sharp, 2007; Hoefs, 2009]. Precipitation of calcium

carbonate in carbonate sediments is usually an equilibrium reaction, principally caused by the removal of CO₂:



Degassing of source water will occur where waters with high PCO₂ (partial pressure of carbon dioxide) emerge into an area of low PCO₂, consequently the water will equilibrate with the surroundings, typically exchanging with atmospheric CO₂, and precipitate calcium carbonate. Provided it can be shown that a mineral is deposited in equilibrium, fractionation equations (or palaeotemperature equations) can be used to estimate past temperature and any changes of temperature within the sediment archive [Dansgaard, 1964; Shemish *et al.* 2001; Leng and Marshall, 2004; Sharp, 2007].

However, knowledge of what may have affected the isotopic composition of the source water is vital to the interpretation of the oxygen isotope composition of the carbonate; these effects are discussed in detail in chapter 2. Further to the processes affecting the oxygen isotopic composition of the source water are processes that affect the mineral deposition, principally calcite in the case of lacustrine and wetland carbonates [Leng and Marshall, 2004; Leng, 2005; Sharp, 2007; Hoefs, 2009]. Kinetic isotope effects, or disequilibrium effects, are associated with incomplete or modified mineral precipitation. Disequilibrium mineral precipitation affects the δ¹⁸O value contained within the mineral, causing the mineral to have an oxygen isotope composition different to that predicted by thermodynamics, and can be attributed to differing rates of mineral precipitation, pH, speciation controls (known as vital effects) and microenvironmental changes [Leng and Marshall, 2004; Sharp, 2007]. Further to this, disequilibrium processes are often interlinked with each other e.g. air temperature changes will not only affect the oxygen composition of water from which the carbonate is precipitating but will also affect the oxygen composition of rainfall, amount of rainfall, water level and pH. However, disequilibrium processes can be quite systematic e.g. some ostracods display species specific vital effects, between +0.3‰ and +2.5‰ [Holmes and Chivas, 2002]. As the vital offsets are species specific, as long as the factors that offset the isotopic composition from equilibrium are known i.e. pH, these vital effects can be accounted for when interpreting palaeoclimatic information [Leng and Marshall, 2004].

Palaeoclimate studies often rely on the analysis of bulk carbonate, or fine fraction carbonate [Leng and Marshall, 2004]. Unless it can be shown that the carbonate is from a single source component i.e. authigenic, any changes in the oxygen isotopic composition of the carbonate may represent changes in the relative abundance of source components (authigenic vs. biogenic) rather than actual environmental or climatic change e.g. lake eutrophication and photosynthesis by algae leads to a negative shift ($> -3\%$) in the oxygen isotope composition of fine fraction carbonate. This offset can be attributed to increased mineral precipitation rates incorporating more ^{16}O , effectively depleting $\delta^{18}\text{O}$ value of carbonates relative to ones precipitated in equilibrium [Fronval *et al.*, 1995]. However, the change in source component will often be related to a change in water body composition, such as pH, depth etc. which will be a direct response to a change in climate or hydrology.

5.3.2 Inorganic carbon

Carbon exists in three isotopic forms, two of which are stable – ^{12}C and ^{13}C - and one of which is radioactive and unstable - ^{14}C . All three are important for palaeoenvironmental studies with $^{13}\text{C}/^{12}\text{C}$ isotope ratios displaying important environmental changes and variations similar to those seen in $^{18}\text{O}/^{16}\text{O}$ isotope ratios [Drummond *et al.* 1995; Li and Ku, 1997; Leng and Marshall, 2004].

DIC (Dissolved Inorganic Carbon) in waters is a useful proxy in the determination of environmental processes, usually linked to climate change, which may have affected a lake. Inorganic carbon isotopes are mainly derived from HCO_3^- (bicarbonate) and get incorporated into authigenic and biogenic carbonates, and although the direct sensitivity of $\delta^{13}\text{C}_{\text{DIC}}$ as a proxy for temperature change is low, the $\delta^{13}\text{C}_{\text{DIC}}$ isotope value in a sample may represent the depositional environment [Leng, 2005]. There are three processes that control the inorganic carbon isotope composition of lacustrine and wetland sediments:

1. **Composition of inflowing waters** – Plant respiration and production of CO_2 by decaying organic matter in soils is responsible for the majority of carbon in inflow waters. HCO_3^- is the dominant carbon species at pH's between 7 and 10 and in equilibrium with CO_2 , carbonate sediments will have $\delta^{13}\text{C}_{\text{DIC}}$ values up to 10‰ higher than the source water [Leng and Marshall, 2004]

after Romanek *et al.*, 1992]. Terrestrially derived organic matter - C₃ and C₄ plants - have $\delta^{13}\text{C}$ values ranging from -20‰ to -32‰ and -17‰ to -9‰ respectively so based on Romanek *et al.* [1992], ground and river waters have $\delta^{13}\text{C}_{\text{DIC}}$ values that are generally low (-10‰ to -15‰), reflecting the input of soil derived CO₂. However, much higher $\delta^{13}\text{C}_{\text{DIC}}$ (-3‰ to $+3\text{‰}$) can occur in karstic terrain with the dissolution of catchment limestone [e.g. Andrews *et al.*, 1997].

2. ***Interaction of water body with aquatic plants*** – the preferential uptake of ¹²C by aquatic plants and during photosynthesis in periods of high productivity generally leads to increased $\delta^{13}\text{C}_{\text{DIC}}$ values of carbonates. However, the subsequent oxidation of bulk organic matter can lead to $\delta^{13}\text{C}_{\text{DIC}}$ lake water stratification and lower $\delta^{13}\text{C}_{\text{DIC}}$ values at increasing water depth due to a localised availability of ¹²C in CO₂ from respiring sinking organic matter, particularly in shallow lakes [Leng and Marshall, 2004].
3. ***CO₂ exchange of water with the atmosphere*** – the process of CO₂ exchange generally leads to high $\delta^{13}\text{C}_{\text{DIC}}$ in carbonates due to the tendency of water to equilibrate with the atmosphere which has $\delta^{13}\text{C}$ values $\sim 8\text{‰}$ [Leng and Marshall, 2004]. This is particularly noticeable in hydrologically closed systems where $\delta^{13}\text{C}$ will tend to co-vary with $\delta^{18}\text{O}$ due to equilibration with atmospheric CO₂ and preferential evaporation of ¹⁶O respectively [Talbot, 1990].

5.3.3 Carbon isotopes in organic matter

DOC (Dissolved Organic Carbon) occurs in peaty lakes and ground waters and reflects the organic carbon isotope composition ($\delta^{13}\text{C}_{\text{ORGANIC}}$) of the sediments, mainly organic marl and/or peat [Meyers, 1994; Andrews *et al.*, 1998; Meyers and Teranes, 2001; Meyers, 2003; Leng, 2005; Minckley *et al.*, 2009]. DOC is influenced by both initial biomass production and degradation, integrating all the different origins of organic matter, depositional processes, photosynthetic pathways and also preservation. The $\delta^{13}\text{C}_{\text{ORGANIC}}$ value of soil organic matter represents the long term isotopic composition of the standing biomass, consequently the $\delta^{13}\text{C}_{\text{ORGANIC}}$ isotopic composition of carbonates will be distinguishable by the metabolic pathway of carbon fixation in plants [Amundson *et al.*, 1994]:

1. Plants that survive through C₃ carbon fixation thrive in areas where sunlight intensity and temperatures are moderate. These temperate vegetation types represent the majority of the Earth's biomass and are usually deciduous or coniferous woodland plants with $\delta^{13}\text{C}_{\text{ORGANIC}}$ values ranging between -38‰ and -22‰ with a mean of around -27‰ [Deines, 1980; Barbour and Billings, 2000].
2. Plants that survive through C₄ carbon fixation thrive in arid areas due to their efficiency in CO₂ fixation and this efficiency leads to less water and energy loss through photorespiration [Barbour and Billings, 2000]. The most common forms of C₄ plants are desert shrubs, grasses and bushes with $\delta^{13}\text{C}_{\text{ORGANIC}}$ values ranging between -15‰ and -8‰ with a mean of around -12‰ [Deines, 1980].
3. Plants that survive through CAM fixation can thrive in both temperate and arid environments but are more commonly found in arid areas, utilizing specific microenvironments [Barbour and Billings, 2000]. CAM plants have $\delta^{13}\text{C}_{\text{ORGANIC}}$ values that can vary between C₃ and C₄ vegetation, with a range between -30‰ and -13‰ generally accepted to be correct [Osmond *et al.*, 1973; Amundson *et al.*, 1994; Barbour and Billings, 2000].

In theory, higher $\delta^{13}\text{C}_{\text{ORGANIC}}$ values of carbonate indicate increased contribution from C₄ vegetation and a warmer-drier climate and lower $\delta^{13}\text{C}_{\text{ORGANIC}}$ values of carbonate indicate increased contribution from C₃ vegetation and a wetter-colder climate as C₃ favours increased water and/or higher atmospheric CO₂ [Aucour *et al.*, 1994]. However, it has been shown that some C₃ plants can display carbon isotope discrimination when placed under environmental stress, such as increased salinity/aridity [Chaves *et al.* 2009] and altitude [Kohn, 2010; Diefendorf *et al.* 2010]. This discrimination during photosynthesis can increase uptake of ¹³C, thus positively skewing the $\delta^{13}\text{C}_{\text{ORGANIC}}$ values in sediments.

Nitrogen can also be used as a proxy when determining $\delta^{13}\text{C}_{\text{ORGANIC}}$ origin. The use of C/N ratios in sedimentary organic matter has been shown to be useful in distinguishing between the input of terrestrial vegetation and aquatic vegetation/algae [Meyers, 1994; Andrews *et al.*, 1998; Minckley *et al.*, 2009]. Aquatic plants tend to have a greater proportion of N when compared to terrestrial plants so C/N ratios are of great importance; increased C/N (>20) indicates increased terrestrial contributions where decreased C/N (<10) indicates increased aquatic algal contributions [Minckley *et*

al., 2009]. Very little is known about C/N ratios in aquatic vascular plants (macrophytes), but it is thought intermediate C/N values >9 and <20 indicate common macrophytes [Lini *et al.* 2000].

5.4 Study site

During March 2008 a month was spent in the field. Two lake border sediment cores were obtained, using an Acker split spoon corer, in two localities within the Cuatro Ciénegas basin - Core Poza Tierra Blanca (PTB) (N. 26° 54' 65.1, W. 102° 09' 15.8) and Core Cuatro Ciénegas Meyer (CCM) (N. 26° 54' 78.7, W. 102° 07' 72.2) (Fig. 5.4).

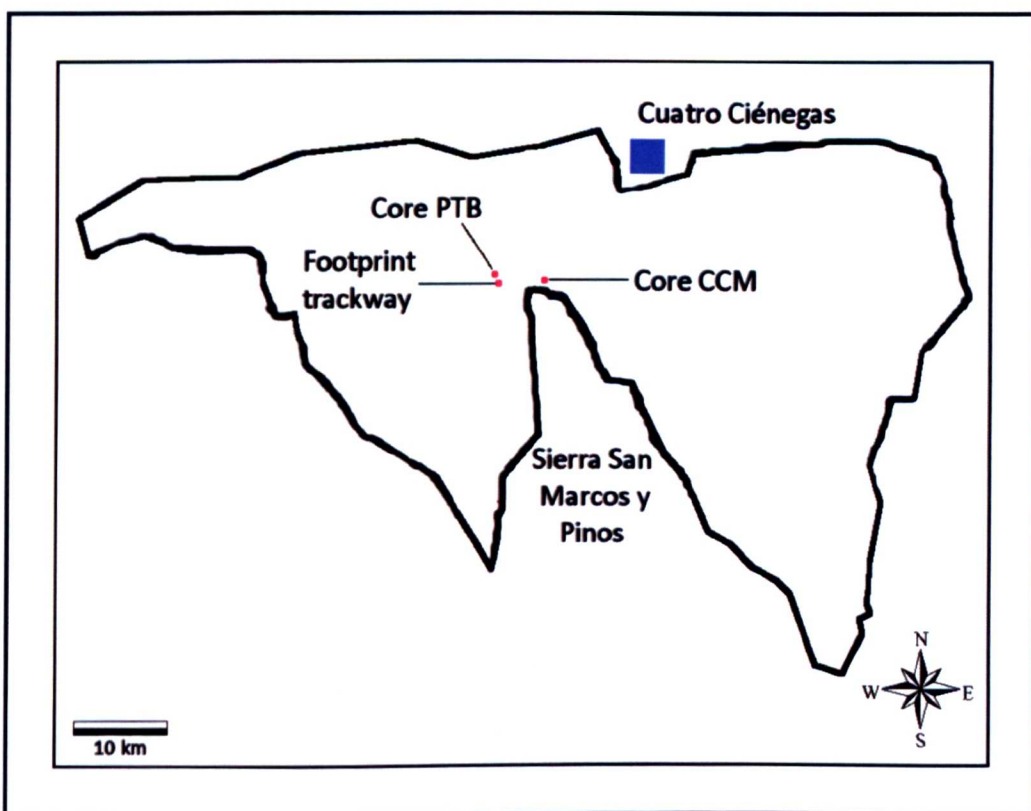


Figure 5.4. Locations of cores PTB and CCM taken within the CCB.

Poza Tierra Blanca (location of core PTB) has an approximate surface area of 50 m², maximum depth of 1 m and is <20°C. The pool is located in the central marsh (ciénega) area of the main through-flow system in the CCB (see chapter 2) and is an open pool with an emergent underground inflow stream entering the pool to the south and an outflow stream exiting to the north, continuing the surface flow throughout the marsh area. The inflow stream of Poza Tierra Blanca emerges from underneath the CCB floor with reconnaissance isotopic data suggesting the pool is

sourced from a mix of cold surface water and warmer Cupido-Aurora aquifer water, however, the exact water source of Poza Tierra Blanca remains unclear due to complex nature of the CCB surface water flow (see chapter 2). Core CCM was taken in the approximate location of Meyer's [1973] sediment core to allow better comparison between sediment descriptions and environmental data.

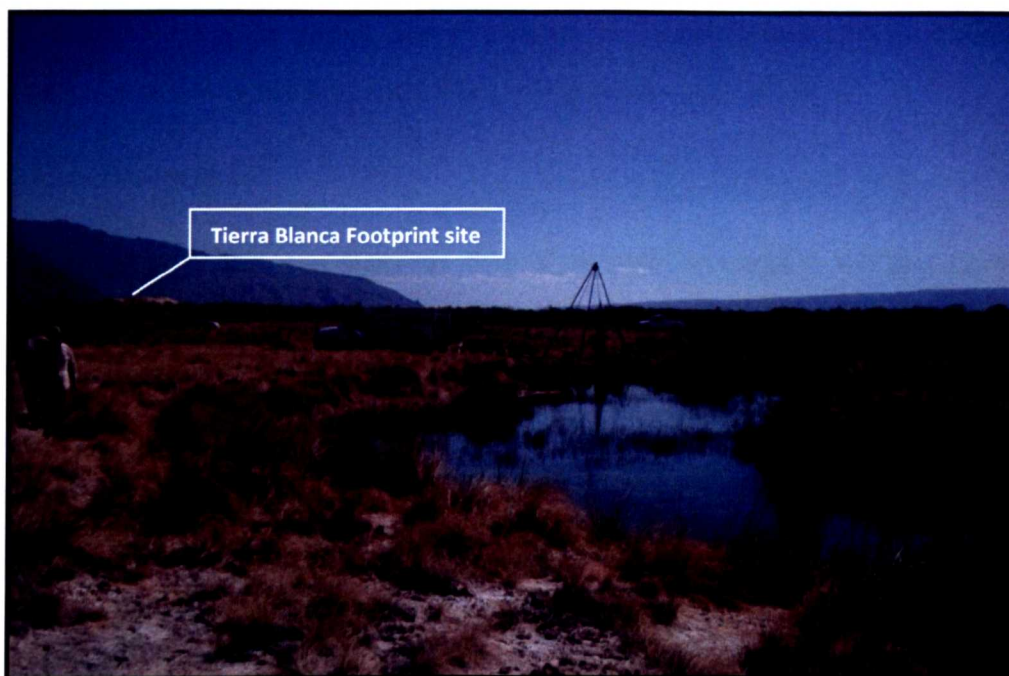


Figure 5.5. The location of core PTB. Poza Tierra Blanca can be seen in the foreground of the photograph. The Tierra Blanca footprint site can also be seen as a small mound to the left of the photograph.

Because the CCB is a natural protected area with National Park status, cores PTB and CCM were taken under very strict limitations from the APFFCC. Core PTB was originally intended to be taken from the centre of Poza Tierra Blanca but, the specific permission granted only allowed the core to be taken on the edge of the pool in what is now a marsh area (Fig. 5.5). The use of a percussion coring device resulted in some sediment loss and re-sampling, so complete core recovery was not possible. Any sediment re-sampling was attributed to the lack of a plug in the end of the split spoon core, resulting in liquefied material at the beginning of each 60 cm core. The presence of unfit (liquefied or re-sampled) sediment was determined in the field and the material disposed of in the field prior to wrapping the remaining sediment for later sub-sampling. The resulting recovery was ~60% from the 1500 cm long core.

Core Cuatro Ciénegas Meyer (CCM) was omitted from all laboratory analyses due to the very fragmented nature and limited recovery of sediments. In total, 421 cm of sediment, from the 900 cm core (46.8%), was missing which meant that analysis of

the core would have been too fragmentary over a relatively short core depth. The core sediments were predominantly marls with varying degrees of organic detritus and lithic fragments, no peat was present throughout the core and although tufa was present at the base (890-897 cm) it was too fragmentary (Fig. 5.6) and therefore too chronologically unreliable to date with U-series. The lack of peat or tufa in core CCM meant that no accurate dating and therefore no chronological control would have been possible and was subsequently discarded from further analysis.

5.5 Laboratory methods

Description and sampling of core PTB was conducted at the Centro de Investigación Científica de Cuatrociénegas. Core stratigraphy was described in detail (see appendix 2.2.1) and samples were comprised of various carbonate facies (marl, clayey marl) and peat (Fig. 5.7). Core PTB also included two sequences of tufa which could possibly be linked to the in situ footprint track way tufa in the Tierra Blanca Quarry. After description of core PTB, it was then sub-sampled contiguously for dating, stable isotopes, pollen and loss on ignition (LOI) analysis at 1 cm intervals to a depth of 358 cm and every 3 cm (alternating for stable isotopes, pollen, LOI analysis) for the remaining 1,142 cm. Pollen subsamples were taken by Dr. Tom Minckley to the University of Wyoming for analysis whilst subsamples for dating, LOI and stable isotope analysis were taken to Liverpool John Moores University.

5.5.1 Stable $\delta^{18}\text{O}_{\text{CARB}}$, $\delta^{13}\text{C}_{\text{DIC}}$ and $\delta^{13}\text{C}_{\text{ORGANIC}}$ analysis

A total of 236 samples taken from core PTB were prepared for $\delta^{18}\text{O}_{\text{CARB}}$, $\delta^{13}\text{C}_{\text{DIC}}$ and $\delta^{13}\text{C}_{\text{ORGANIC}}$ analysis. Two methods of preparation were used (NB, All equipment used during preparation was thoroughly washed with distilled water before being used):

1. Preparation of $\delta^{18}\text{O}_{\text{CARB}}$, $\delta^{13}\text{C}_{\text{DIC}}$ samples removed any unwanted organic fraction within each of the 236 PTB samples, leaving only fine fraction carbonate for analysis. To remove the unwanted organic fraction from each sample, 0.5 cm³ of sample was broken up in a pestle and mortar into <1 mm size and placed in 500ml plastic tri-pour beakers before being immersed in 50 ml (5%) Sodium Hypochlorite (NaOH.Cl) solution. NaOH.Cl was used to digest

the organic fraction of samples. Samples were allowed to dissolve in the NaOH.Cl for 12 hours; if by this time the reaction hadn't finished (an unfinished reaction is identified by the sample fizzing upon the addition of 2 ml NaOH.Cl solution), an additional 10 ml solution was added every hour until the reaction was complete. Samples were then sieved at 80 μm to remove any larger carbonate contaminants e.g. mollusc shells, that are subject to hard water effect, before being decanted three times with distilled water in 500 ml tri-pour beakers to remove any residual NaOH.Cl contamination. Samples were dried overnight at 40°C and ground into fine powder in a pestle and mortar for analysis.

Peat samples contained a small amount of carbonate (LOI 950°C = 0.25% - 12.86%) but this was not analysed because it was likely a contaminant derived from dissolution and re-deposition of calcium carbonate derived from marl sediments further up the sediment column.

2. Preparation of $\delta^{13}\text{C}_{\text{ORGANIC}}$ removed any unwanted carbonate fraction within each of the 236 PTB samples, leaving only organic C for analysis. To remove the unwanted carbonate fraction from each sample 2 cm^3 of sample was broken up in a pestle and mortar into <1 mm size and placed in 500 ml plastic tri-pour beakers before being immersed in 50 ml (pure peat samples) or 100 ml (organic rich marl/tufa) 0.5 M Hydrochloric Acid (HCl) solution. 0.5 M HCl was used to digest the carbonate fraction of samples. Samples were allowed to dissolve in the HCl for 12 hours; if by this time the reaction hadn't finished (an unfinished reaction is identified by the sample fizzing upon the addition of 2 ml HCl solution), an additional 10 ml or 20 ml (for peat and carbonate respectively) solution was added every hour until the reaction was complete. Samples were then sieved at 80 μm to remove any larger contaminants i.e. modern rootlets and seeds, which could alter isotopic ratios and/or ^{14}C AMS dating at a later date. Samples were then decanted three times with distilled water in 500 ml tri-pour beakers to remove any residual HCl contamination. Samples were dried overnight at 40°C and ground into fine powder in a pestle and mortar for analysis.



Figure 5.6. The fragmented basal tufa of core CCM. The fragmented nature of the tufa meant it was unreliable for dating due to the possible mixing of older and younger stratigraphic layers.



Figure 5.7. Alternating peat – marl – tufa stratigraphy of core PTB. Displayed in the photograph is 2.4 m to 1.6 m in the core with well humified peat, marl, organic marl and tufa all present.

5.5.1.1 Organic and carbonate content by loss on ignition (LOI)

Loss on ignition was conducted on the sediments from 236 core PTB samples (see appendix 2.1). The data was primarily used for determining the amount of sample to use (mg) for $\delta^{18}\text{O}_{\text{CARB}}$, $\delta^{13}\text{C}_{\text{CARB}}$ analysis and $\delta^{13}\text{C}_{\text{ORGANIC}}$ mass spectrometric analysis, following the standard three step procedure set out in Lamb [2004; after Dean, 1974]:

1. 1g sediment/sample was weighed and placed in a sterilized crucible of a known weight. Samples were placed in a muffle furnace at 105°C for 12 hours to measure % (g) loss of water per sample. Samples were then cooled to room temperature in desiccators before being reweighed to $\pm 0.1\text{mg}$.
2. The reweighed samples were then placed back into the muffle furnace at 550°C for 2 hours to measure % (g) loss of organics per sample. Samples were then cooled to room temperature in desiccators before being reweighed to $\pm 0.1\text{mg}$.
3. Samples were returned to the muffle furnace and heated to 950°C for 4 hours to determine CO_2 evolved from carbonate minerals, giving an approximation of carbonate content (g). Samples were cooled to room temperature in desiccators and reweighed to $\pm 0.1\text{mg}$.

After these three steps have been followed the following equations can then be applied to calculate; a) Organic content of the sample (%); b) CO_2 content of the sample (%); c) Carbonate (CO_3) content of the sample (%); and d) Calcium carbonate (CaCO_3) content of the sample (%) [for more detail of the methods see Dean, 1974; Lamb, 2004]:

a) $\text{LOI}_{550} = (\text{DW}_{105} - \text{DW}_{550})/\text{DW}_{105} * 100$

LOI_{550} represents LOI at 550°C (as a percentage), DW_{105} represents the dry weight of the sample before combustion and DW_{550} represents the dry weight of the sample after heating to 550°C (both in g). The weight loss should be proportional to the amount of organic carbon contained in the sample.

b) $\text{LOI}_{950} = (\text{DW}_{550} - \text{DW}_{950})/\text{DW}_{105} * 100$

LOI_{950} represents LOI at 950°C (as a percentage), DW_{550} is the dry weight of the sample after combustion of organic matter at 550°C, DW_{950} represents the dry weight of the sample after heating to 950°C and DW_{105} again represents the

dry weight of the sample before any further combustions. The weight loss should be proportional to the amount of CO₂ evolved from the sample.

c) $\text{CO}_{3\text{TOTAL}} = \text{LOI}_{950} * 1.36$

CO_{3TOTAL} represents the weight of carbonate in the sample (as a percentage), LOI₉₅₀ represents LOI at 950°C (as a percentage). Assuming a weight of 44 g mol⁻¹ for CO₂ and 60 g mol⁻¹ for carbonate (CO₃), the weight loss by LOI at 950°C multiplied by 1.36 should equal the weight of the carbonate in the sample.

d) $\text{CaCO}_{3\text{TOTAL}} = \text{LOI}_{950} * 2.27$

CaCO_{3TOTAL} represents the weight of the calcium carbonate in the sample (as a percentage), LOI₉₅₀ represents LOI at 950°C (as a percentage). Assuming a weight of 44 g mol⁻¹ for CO₂ and 100 g mol⁻¹ for calcium carbonate (CaCO₃), the weight loss by LOI at 950°C multiplied by 2.27 should equal the weight of the calcium carbonate in the sample.

5.5.2 U-series dating

A total of five samples for U-series dating were prepared. Core PTB tufas were cut into 1cm slices for ease of storage and sampling. Material for analysis was removed from several tufa pieces using a stainless steel end cutter. Cleaning of the carbonate was conducted under a binocular microscope. Since the tufa pieces were delicate and friable, great care was taken to avoid inadvertent disturbance of the U-Th systematics. As Uranium breaks down into Thorium in a series of half lives (measurements of these half lives provides dates), disturbance of the U-Th systematic can lead to false readings of Uranium and/or Thorium thus producing false dates. Samples were broken down into ≤3mm chunks using a medical scalpel and tweezers, cleaned in distilled water with a fine tipped artists brush to remove contamination from any surfaces and accessible pore spaces before an ultrasonic disintegration technique was applied for one hour to remove any inaccessible contamination.

See chapter 4, section 4.4.2 for the full analytical methodology on U-series dating.

5.5.3 ^{14}C AMS dating

A total of three samples for ^{14}C AMS dating were taken from core PTB. Bulk peat layers were sampled at 36 cm, 160 cm and 368 cm from the most organic rich peat sediments contained within core PTB (see appendix 2.2.1 for peat description). Samples were carefully studied under a binocular microscope to identify any recognisable plant macrofossils such as seeds, roots or leaf matter, however all peat samples were too well humified so did not contain enough macrofossil material for dating. As no macrofossils were evident, 2 g of 'bulk peat matrix' (BPM) was prepared for each of the three samples. Preparation of BPM involved carefully picking out any recognisable contaminants i.e. modern aquatic plant rootlets, with tweezers to ensure only reliable material was sent for dating. The prepared BPM was sent to BETA analytic, Miami, USA for ^{14}C AMS dating.

5.5.4 Pollen

Pollen was extracted from the core material using the standard acid-base-acid digestion procedure set out in Faegri *et al.*, [1989]. Pollen tracers (*Lycopodium*) were added to sediment subsamples to identify if any pollen types were present in unusually high numbers [for details of using pollen tracers see Bryant and Hall, 1993] – in this case, counts of 300 terrestrial pollen grains to 1000 tracers. Pollen counts were conducted for every 1 m of core, giving an initial skeleton examined in more detail plot. Higher density pollen counts were conducted on two sections of core PTB – 691 cm to 576 cm and 576 cm to 372 cm – to increase the resolution of the pollen study, aiding the interpretation to be put alongside stable isotopic data. Pollen data are converted into percentage data only if counts of terrestrial origin reached >100 grains, otherwise data are presented as presence/absence.

5.6 Results

Due to highly complex stratigraphy, plus hiatuses in the sampling (for detailed stratigraphy see appendices 2.2.1 and 2.2.2), subdividing core PTB into units could not be determined solely by changes in the sediment column. Consequently, all data for core PTB is separated into seven units based on qualitative assessment of observed

trends in the $\delta^{18}\text{O}_{\text{CARB}}$ and $\delta^{13}\text{C}_{\text{DIC}}$ isotope values as well as stratigraphic changes, to allow more detailed analysis and interpretation of the 1,500 cm core PTB.

5.6.1 Core PTB chronology

5.6.1.1 Potential problems in age/depth modelling of core PTB

The accumulation history of core PTB, like all sedimentary deposits, will have an imperfect time series that is caused by alternating sediment types, hiatuses, periods of non-deposition, erosion and dating errors [Sadler, 1981; Sommerfield, 2006].

Gaps in the sediment column of core PTB are observed at several intervals throughout the sequence (Appendix 2.2). As discussed previously, these gaps are largely attributed to liquefaction of sediment due to the percussive nature of the Acker coring device [Last and Smol, 2002], leading to the on-site disposal of sediment deemed unfit. However, carbonate deposits are particularly susceptible to secondary processes such as dissolution, particularly in karst terrain [Wohl, 1993; Fritz and Medlock, 1995], like the CCB. Channel incision and conduit formation, linking pools and rivers through subsurface flow, in karst terrain is well documented [Wohl, 1993; Badino *et al.* 2004; Jaillet *et al.* 2004; Becerril *et al.* 2010; Amatya *et al.* 2011] and can create 'voids' within the carbonate sediment column. As well as liquefaction, it is possible that gaps within the sediment core are subsurface voids, as observed in the modern day flow system [Chapter 2, Fig. 2.32a]. These voids within the sediment column can be interpreted as hiatuses, however, it is hard to know what type of sediment is missing and the amount of section missing is not necessarily related to the amount of time missing. A growing sequence of sediment can collapse due to self-weight, a process known as autocompaction, and/or differential sediment compaction, whereby organic and carbonate sediments compact at different rates [Allen, 1999; Sommerfield, 2006; Jones *et al.* 2011].

Compaction of carbonate and organic sediments will have almost certainly occurred in core PTB. However, it is very difficult to quantify compaction rates of peat or carbonate sediments in Late Pleistocene/Holocene lacustrine or wetland sediments [Jones *et al.* 2011]. To be able to quantify compaction rates for any single study site, subsurface geotechnical properties are required alongside a detailed depositional

history from site specific monitoring. The monitoring required to achieve this is unrealistic in terms of both time and money. Compaction rate models have, however, been developed [Kooi and de Vries, 1998; Allen, 1999; Meckel *et al.* 2006], although these models focus on large, clastic sedimentary basins or, in the case of autocompaction, coastal environments. Subsequently, the application of these models to other sedimentary environments is problematic.

Increasing aridity can also create hiatuses in a sediment column whereby the lake sedimentation ceases upon a lake drying out [Thomas, 2011]. This drying is usually marked by a gypsum layer in arid regions [Curtis *et al.* 1996; Thomas, 2011], however, as observed in the CCB [Chapter 2], drying in an arid wetland forms terrestrial peat sediments. The continued sedimentation during arid periods in the CCB reduces the chance of depositional hiatuses within the core PTB sediment archive.

As well as hiatuses and sediment compaction issues, organic lake sediments are widely used for radiocarbon dating of the sediment archive. Organic lake sediments used for radiocarbon dating are susceptible to contamination from old, ^{14}C depleted carbon residues e.g. catchment limestone, carried in the catchment water, a process known as the hard-water effect [Walker, 2005]. The hard-water effect is reflected in the plants and algae that photosynthesise sub-aquatically and can add thousands of years to the apparent age of organic lake sediments [e.g. Shotton, 1972; Child and Werner, 1999]. However, terrestrial plants photosynthesise directly with the atmosphere, so peat formed from terrestrial plants should circumvent the hard-water effect [Bowman, 1990]. Peat formation in the CCB is an indicator of a drying climate and is formed in a semi-terrestrial environment, the sampled peat from core PTB was carefully checked for aquatic plant macrofossils and any unsuitable material removed.

5.6.1.2 ^{14}C AMS and U-series dating

Thin section analysis of the core PTB tufas indicated very little organic contamination or secondary calcite precipitation before cleaning and preparation (Fig. 5.8). Any organic detritus (Fig. 5.8b) was removed during the ultrasonic disintegration technique and possible secondary calcite precipitation (Fig. 5.8f) is not indicated by detrital thorium ratios. All U-series samples obtained 1.5-1.9 ppm U with $^{230}\text{Th}/^{232}\text{Th}$ activity between 77 and 594 (reliable $^{230}\text{Th}/^{232}\text{Th}$ is accepted to be >20) and are

displayed in table 5.1 alongside ^{14}C AMS dates (from peats). All samples for ^{14}C AMS analysis contained sufficient uncontaminated material to produce reliable dates.

Conventional ^{14}C AMS dates for PTB36, PTB160 and PTB368 (Table 5.1) were calibrated using Calib 6.0 and IntCal09 [www.calib.qub.ac.uk]. Calib 6.0 is a ^{14}C calibration program based on the datasets outlined in Stuiver and Reimer [1993] and Reimer *et al.*, [2009]. U-series dating does not require further calibration from the conventional ages produced, providing activity ratios are acceptable, and can be used alongside calibrated ^{14}C dating techniques to produce an age/depth model [for further discussion of U-series and ^{14}C calibration see Reimer *et al.*, 2004; van der Plicht *et al.*, 2004; Fairbanks *et al.*, 2005; Blaauw, 2010].

In total, eight dates were obtained for core PTB (Table 5.1). All the dates are in a good chronological order with the exception of four paired U-series dates – PTB317-318, 321-322, 339-341 and 355-356 – that appear to be mixed. However, these four dates are within range of each other's 2σ calibration which is positive as further refinement is still required on the U-series procedure. A coeval age of $22,150 \pm 880$ cal yr BP is obtained for the four U-series dates which gives a good paired date with the underlying ^{14}C AMS date of $28,051 \pm 417$ cal yr BP obtained from bulk peat. The coeval age of $22,150 \pm 880$ cal yr BP for the 317-357 tufa in core PTB, combined with the four additional dates of core PTB, provides a reasonable chronology in order to base a palaeoenvironmental interpretation to the core PTB sequence.

Lab	Lab code	Sample depth	Material dated	Technique employed	Conventional age (yr BP)	± 2 sigma calibration (yr BP)	Mid Calibrated age (cal. Yr. BP)
BETA	PTB36	36 cm	Bulk Peat	¹⁴ C AMS	70±40	215-267	241 ± 26
BETA	PTB160	160 cm	Bulk Peat	¹⁴ C AMS	8440±50	9399-9535	9467 ± 68
NIGL	PTB317-318	317-318 cm	CaCO ₃	U-series	22710±910	21800-23620	22710 ± 910
NIGL	PTB321-322	321-322 cm	CaCO ₃	U-series	23250±930	22320-24180	23250 ± 930
NIGL	PTB339-341	339-341 cm	CaCO ₃	U-series	22150±890	21260-23040	22150 ± 890
NIGL	PTB355-356	355-356 cm	CaCO ₃	U-series	20400±820	19580-21220	20400 ± 820
BETA	PTB368	368 cm	Bulk Peat	¹⁴ C AMS	23130±130	27634-28469	28051 ± 417
NIGL	PTB1013-1020	1013-1020 cm	CaCO ₃	U-series	56180±2250	53930-58430	56180 ± 2250

Table 5.1. U-series and ¹⁴C AMS dates obtained for core PTB. #PTB 317-318, 321-322, 339-341 and 355-356 give an average age of 22130 ± 880 cal yr BP for the 317-356 tufa within core PTB which is used as a minimum age for this tufa.

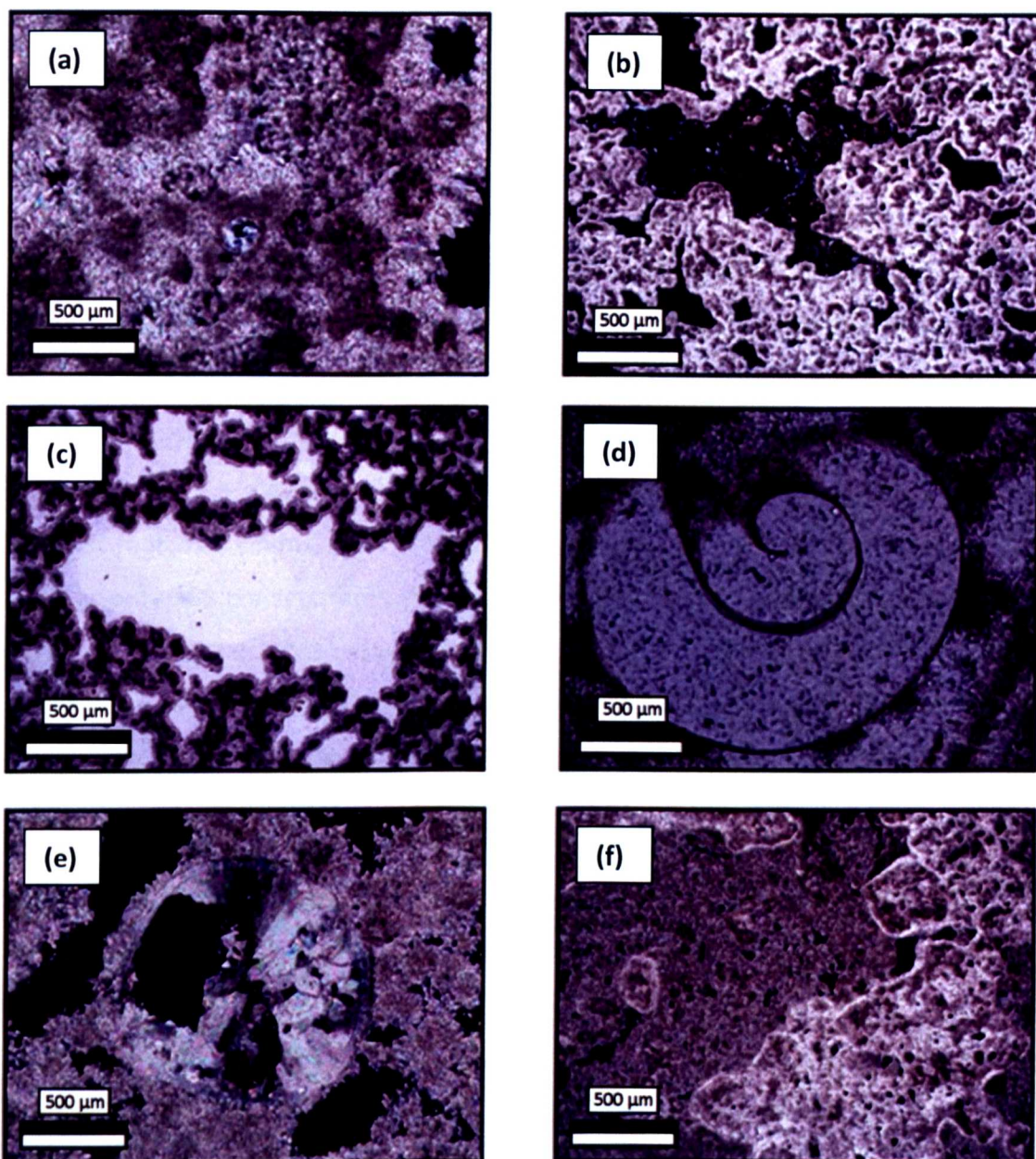


Figure 5.8. Thin sections of tufas from core PTB (taken at x40 magnification under bright field illumination). Showing: (a) PTB 317-318 - Quartz grain in the centre of the slide (b) PTB 317-318 - True pore space in-filled with organic detritus (c) PTB 339-341 - True pore space where calcite crystals can be seen surrounding organic carbonate matter (d) PTB 355-356 - Mollusc sp. where no detrital calcite can be seen (e) PTB 355-356 - Possible pollen grain where organic matter has been replaced by calcite during tufa formation (f) Possible contamination where darker carbonate has in-filled tufa pore space.

5.6.1.3 Linear interpolation

Using only the ^{14}C AMS dates – 241 ± 26 cal yr BP (36 cm), $9,467 \pm 68$ cal yr BP (160 cm) and $28,051 \pm 417$ cal yr BP (368 cm) – a very good linear age/depth model is produced (Fig. 5.9). However, with the stratigraphic hiatuses (see appendices 2.2.1 and 2.2.2), gaps of up to 208 cm between ^{14}C AMS dates and maximum depth of 368 cm for the ^{14}C AMS dates, interpolation of linear age/depth through the entire 15 m

sequence of core PTB, using only three ^{14}C AMS dates for the top 368 cm of core PTB, should be conducted with extreme caution, as outlined previously, and is thus rejected.

With the addition of the U-series dates – $22,130 \pm 880$ cal yr BP (317-356 cm) and $56,180 \pm 2,250$ cal yr BP (1013-1020 cm) – to the age/depth model (Fig. 5.10), the linear relationship remains good ($R^2 = 0.97$). Although a strong linear relationship is indicated between the ^{14}C AMS and U-series dates ($R^2 = 0.97$), the regression only passes through one data point ($9,467 \pm 68$ cal yr BP at 160 cm depth (Fig. 5.10)) suggesting there is a degree of error based on the distance between the data points. The first four data points, up to 368 cm ($28,051 \pm 417$ cal yr BP) are stratigraphically close as only 368 cm separates them, before a 645 cm gap to the final data point at 1,013 cm ($56,180 \pm 2,250$ cal yr BP). This large gap between data points could form part of the apparent error observed in the linear relationship, along with the subsequent gap from 1,013 cm to the base of core PTB at 1,500 cm.

However, criteria for linear age/depth model rejection were based on having such large gaps between dates as well as stratigraphic hiatuses in core PTB. Interpolation of any proposed linear age/depth model lacks precision, as suggested by figures 5.9, 5.10. Changes in sediment type, sediment accumulation rates and compaction of sediment [e.g. Sommerfield, 2006] result in the use of large assumptions between known ages and depths in the core. When constructing chronologies using different methods for different periods of time, in this case ^{14}C AMS and U-series, drastic increases or decreases in accumulation rate can occur due to the way time is compressed in older sections with missing units (thus slower averages result) compared to recent sediments, which often show higher accumulation rates. Recent sediments are stratigraphically more complete than older sections which may contain hiatuses, like in core PTB. Sediment types i.e. marl, peat and tufa, also deposit at differing rates to each other, based on pH, water temperature etc. which can lead to apparent increases or decreases in sediment accumulation rates. However, as discussed previously, this is hard to quantify.

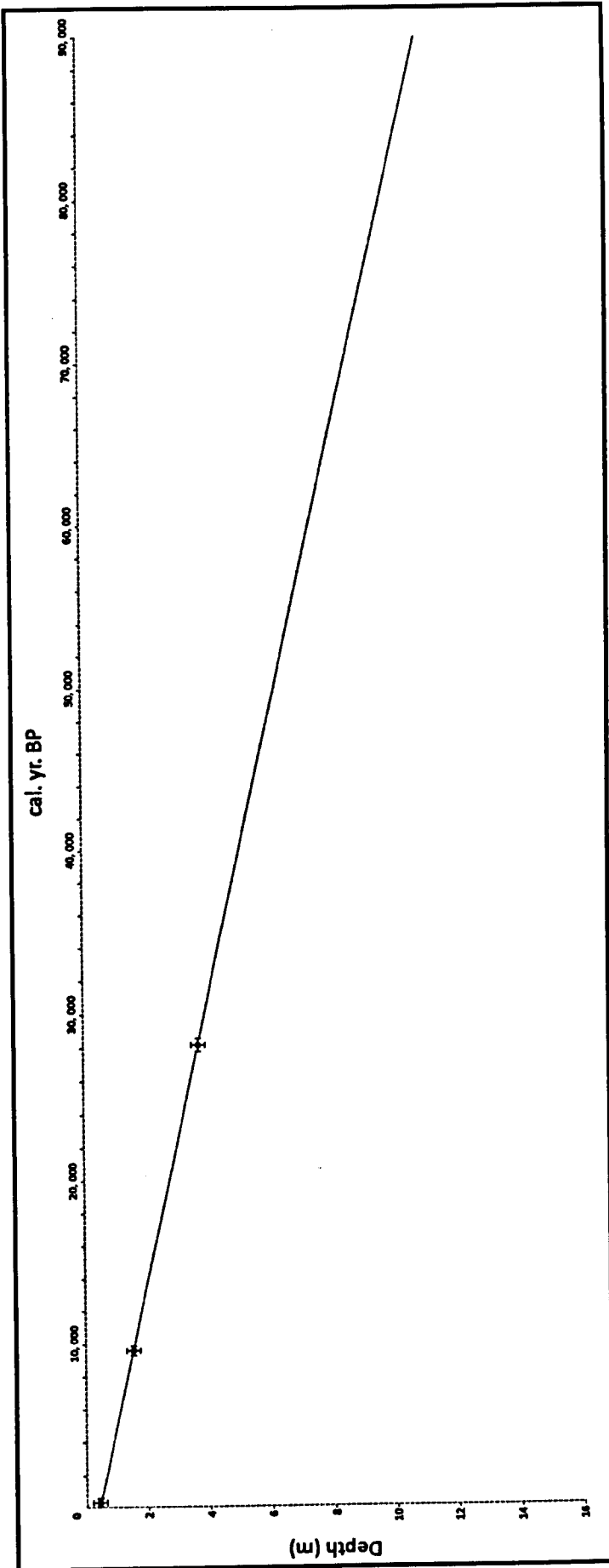


Figure 5.9. Linear age/depth model constructed using only the ¹⁴C AMS dates – 241 ± 26 cal yr BP (36 cm), 9,467 ± 68 cal yr BP (160 cm) and 28,051 ± 417 cal yr BP (368 cm).

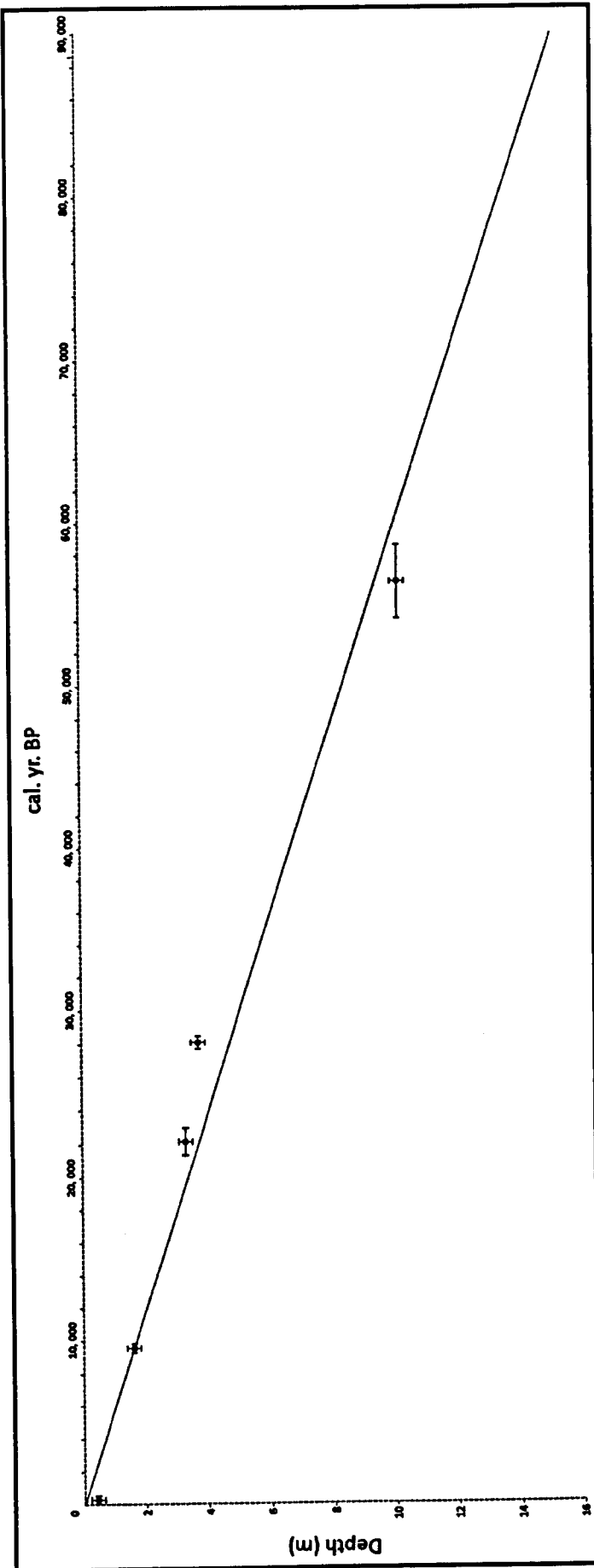


Figure 5.10. Linear age/depth model constructed using the ^{14}C AMS dates – 241 \pm 26 cal yr BP (36 cm), 9,467 \pm 68 cal yr BP (160 cm) and 28,051 \pm 417 cal yr BP (368 cm) – and U-series dates – 22130 \pm 880 cal yr BP (317-356 cm) and 56180 \pm 2250 cal yr BP (1013-1020 cm).

5.6.1.4 Smooth spline interpolation using 'classical' age modelling (CLAM)

The core PTB chronology is shown in figure 5.11 and is based on cm scale age/depth points generated from the three ^{14}C AMS and two U-series dates (the coeval date of $22,130 \pm 880$ cal. yr. BP was used for the upper U-series date) from core PTB. Radiocarbon dates were calibrated using IntCal09 at 2-sigma analytical uncertainty and the age model is based on a smooth spline regression that includes the underlying non-Gaussian uncertainty in the calibrated age probability distribution.

Due to linear interpolation assuming abrupt changes in accumulation rate occur exactly at the dated depths, as shown previously, this method of age/depth modelling is rejected. A proposed alternative to linear interpolation is Bayesian or piecewise linear age modelling. This modelling technique constantly updates the probability of the age/depth model based on new information gained on a point by point basis, at known calibrated ages [Blaauw, 2010]. This is generally accepted to produce very reliable age/depth models when using a high resolution sampling strategy [e.g. Blaauw and Christen, 2005], however, based on the low resolution dating procedure (five dates through core PTB), this type of modelling was not chosen as it would not have been able to model the gaps within the core PTB sediment sequence accurately. A spline regression was chosen for the CLAM model as, through repeated sampling of the calibrated age distributions, an approximation of the cores accumulation history is built up based on the dated depths and their uncertainties through subsets of the data (between, and including, dated depths).

Confidence intervals (95%) were estimated via 10,000 iterations of the smooth spline age model using 'classical' age modelling (CLAM) [Blaauw, 2010].

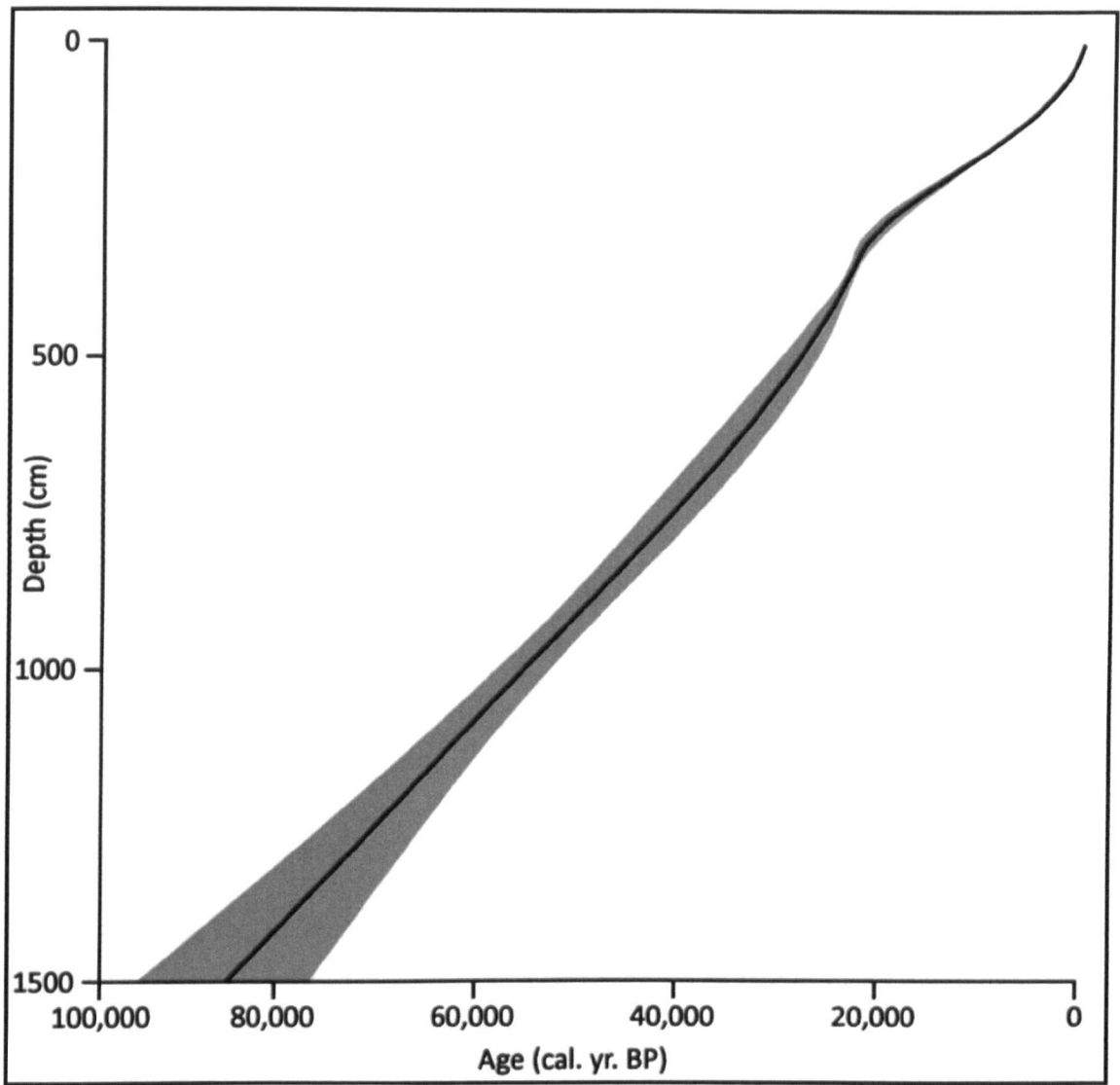


Figure 5.11. Calibrated ^{14}C AMS and U-series dates versus depth using CLAM [Blaauw, 2010]. Black line represents best mid-calibrated age and the grey shaded areas represent a 95% confidence interval range.

The age model indicates a linear sedimentation rate of 0.017 ± 0.002 cm/yr between 1,500 cm (~ 84.9 cal ka BP) and 570 cm (~ 31.1 cal ka BP) with a small increase of sedimentation rate to 0.02 ± 0.001 cm/yr between 694 cm (~ 37.4 cal ka BP) and 570 cm (~ 31.1 cal ka BP). An increase in sedimentation rate to 0.06 ± 0.03 cm/yr or a hiatus is suggested between 570 cm (~ 31.1 cal ka BP) and 372 cm (~ 28 cal ka BP), although a hiatus is unlikely due to the change being gradual through this section. A sharp decrease to 0.01 ± 0.001 cm/yr is observed during the last glaciation between 372 cm (~ 28 cal ka BP) and 200 cm (~ 12.1 cal ka BP). Sedimentation rate then returns to 0.017 ± 0.001 cm/yr to the top of core PTB.

Although age extrapolation beyond the oldest dated interval in an age model is inadvisable [Blaauw *et al.* 2007; Blaauw, 2010], in this case below 1,020 cm, CLAM produces multiple point age estimates through the model, so the spline curve applied through unknown points will provide a reliable basal age approximation [Blaauw, 2010]. It is noteworthy that basal ages from this method should not be regarded as the 'truth' without much more substantial dating evidence. Interpolation of the spline regression gives core PTB a maximum basal age of $84,900 \pm 8,500$ cal yr BP, however, this and all other estimated dates through core PTB cannot be regarded as the 'truth' as the age model created using CLAM is in a large part driven by the uneven interval of the ^{14}C AMS and U-series dating points. However, the error bound ages provide a reliable age estimate based on the weighted means of point age estimates through the model. Thus, stratigraphic consistency of the multi-proxy environmental data is maintained regardless of the inherent possibility of substantial uncertainty and error in the age model.

5.6.2 Stable $\delta^{18}\text{O}_{\text{CARB}}$ and $\delta^{13}\text{C}_{\text{ORGANIC}}$ isotopes and stratigraphy

Stable $\delta^{18}\text{O}_{\text{CARB}}$ and $\delta^{13}\text{C}_{\text{ORGANIC}}$ isotope data for core PTB are presented in figures 5.12, 5.13, 5.14, 5.15, 5.16, 5.17, 5.18 and appendix 2.2.2 along with core depth (cm), stratigraphy, chronology (^{14}C AMS and U-series), C/N ratios, and organic and CaCO_3 content (% determined by LOI) primarily used to support the isotopic interpretation. Data are analysed throughout the core across seven highlighted units. Data units are structured qualitatively by isotopic ranges (‰) and trends in the $\delta^{18}\text{O}_{\text{CARB}}$ and $\delta^{13}\text{C}_{\text{DIC}}$ isotope values (see appendix 2.2.2). Missing or compressed areas of core PTB will not be described within the results section. They are possibly a result of the karst terrain where underground channelling can cause apparent gaps within a core sequence or, more likely, a result of incomplete core recovery as mentioned in section 5.4.

NB. Due to the low organic content of the marl sediments (LOI 550°C = 1.27%-12.98%) a total of 92 $\delta^{13}\text{C}_{\text{ORGANIC}}$ data points are available. C/N ratios are described in section 5.6.3 so will not be described in this section.

Unit 1, 1500 cm – 1020 cm (Fig. 5.12)

$\delta^{18}\text{O}_{\text{CARB}}$ - Data in this unit are extremely fragmentary and highly variable with the lowest delta value of -14.3‰ at 1451 cm increasing to the highest delta value of -0.1‰ at 1425 cm. Immediately following this isotopic value increase is an isotopic value decrease to -8.9‰ , seen at 1422 cm. Throughout the unit, $\delta^{18}\text{O}_{\text{CARB}}$ values do not exhibit any prolonged stable periods although a small, relatively stable period can be seen between 1354 cm and 1321 cm where isotope values of the carbonate range from -7.4‰ to -9.6‰ with a mean value of -8.2‰ . However, despite fragmentary data an overall trend can be observed through the unit where a mean gradual increase from -10.3‰ ($n = 15$, 1500 cm – 1451 cm) to -6.2‰ ($n = 15$, 1129 cm - 1084 cm) is seen – a total mean increase of $+4.1\text{‰}$ over the course of the unit.

$\delta^{13}\text{C}_{\text{ORGANIC}}$ - 14 data points are available in this unit. $\delta^{13}\text{C}_{\text{ORGANIC}}$ values across the 14 data points range from -13.2‰ to -21.7‰ . Through the unit, $\delta^{13}\text{C}_{\text{ORGANIC}}$ values gradually decrease from -13.2‰ to -21.7‰ reflecting an overall negative shift. $\delta^{13}\text{C}_{\text{ORGANIC}}$ isotope values follow the $\delta^{18}\text{O}_{\text{CARB}}$ trend in this unit.

Lithology – Unit 1 is dominated by organic marl, organic banded marl and carbonate marl sediments. The most isotopically negative data points are associated with organic banded marl where dark brown, organic rich sediments are finely inter-bedded with much lighter brown, carbonate marl sediments. Between 1,469 cm and 1,451 cm, where the lowest $\delta^{18}\text{O}_{\text{CARB}}$ values between -14.3‰ and -12.7‰ are observed, is organic banded marl sediments. However, organic content (%) of the bulk organic banded and organic rich marl sediments is still very low, between 1.7% and 12.9%, which may indicate a short lived nature to any organic rich time periods.

Unit 2, 1020 cm – 986 cm (Fig. 5.13)

$\delta^{18}\text{O}_{\text{CARB}}$ – Isotopic values in this unit remain stable within a small range of -7.4‰ to -7.7‰ before a large negative shift of -6.1‰ to the lowest isotope value of the carbonate observed in the unit, -13.5‰ , between 989 cm and 986 cm.

$\delta^{13}\text{C}_{\text{ORGANIC}}$ – Only four data points are available in this unit with the highest delta value of -22.8‰ at 1020 cm before gradually decreasing to -24.7‰ at 995 cm. A sharp

increase from -24.7‰ to -23.2‰ is seen between 995 cm and 989 cm, coinciding with the negative shift observed in the $\delta^{18}\text{O}_{\text{CARB}}$ isotope data.

Lithology – Unit 2 is comprised of tufa and mollusc rich carbonate marl sediments with 3 cm of organic rich marl between 989 cm and 986 cm. The tufa and mollusc rich sediments are calcium carbonate rich (LOI 950°C = 83.4% to 84.6%) and coincide with the constant $\delta^{18}\text{O}_{\text{CARB}}$ isotope values. It is interesting to note that a negative $\delta^{18}\text{O}_{\text{CARB}}$ isotopic shift is associated with the change in sediment type to organic rich marl at 989 cm.

Unit 3, 986 cm – 694 cm (Fig. 5.14)

$\delta^{18}\text{O}_{\text{CARB}}$ – This unit contains the most isotopically negative values of the whole sequence, ranging from -14.9‰ at 883 cm to -6.0‰ towards the end of the unit at 718 cm. After an initial increase from -13.5‰ to -8.5‰ at the beginning of the unit, isotopic values of the carbonate begin to decrease from 943 cm to the most isotopically negative data point of -14.9‰ at 883 cm. After this point isotopic values of the carbonate steadily increase, although fluctuating, up to the highest delta value of -6.0‰ at 718 cm before the transition into unit four. An overall trend for the unit can again be observed where, after an initial increase and decrease, oxygen isotope values of the carbonate can be seen to steadily increase from a mean $\delta^{18}\text{O}_{\text{CARB}}$ value of -11.2‰ ($n = 15$, 986 cm – 895 cm) to -8.1‰ ($n = 15$, 751 cm – 694 cm) – a total mean increase of $+3.1\text{‰}$ over the course of the unit.

$\delta^{13}\text{C}_{\text{ORGANIC}}$ – Only four data points are available in unit 3. The highest $\delta^{13}\text{C}_{\text{ORGANIC}}$ isotope value is -12.8‰ ranging to the most negative $\delta^{13}\text{C}_{\text{ORGANIC}}$ value of -15.2‰ . At two depths – 889 cm and 883 cm – $\delta^{13}\text{C}_{\text{ORGANIC}}$ isotope values are higher than $\delta^{18}\text{O}_{\text{CARB}}$ isotope values, where $\delta^{13}\text{C}_{\text{ORGANIC}} = -12.8\text{‰}$; $\delta^{18}\text{O}_{\text{CARB}} = -14.2\text{‰}$ and $\delta^{13}\text{C}_{\text{ORGANIC}} = -14.8\text{‰}$; $\delta^{18}\text{O}_{\text{CARB}} = -14.9\text{‰}$ respectively.

Lithology – Unit 3 is sedimentologically the most variable, comprising of carbonate marl, fragmented marl, mollusc rich marl, organic banded marl and organic rich marl. Again, variable sediment type appears to coincide with highly variable $\delta^{18}\text{O}_{\text{CARB}}$ isotope values with the more negative delta values associated with organic rich and organic banded sediments, particularly between 900 cm and 880 cm. Organic content remains

low throughout the unit (LOI 550°C = 1.3% to 4.4%) although CaCO₃ content is highly variable, peaking between 21.8% and 85% (LOI 950°C) in carbonate rich and mollusc rich marl sediments, with the highest $\delta^{18}\text{O}_{\text{CARB}}$ isotope values associated with these sediments.

Unit 4, 694 cm – 570 cm (Fig. 5.15)

$\delta^{18}\text{O}_{\text{CARB}}$ – This unit is the first prolonged isotopically stable period in the sequence. Oxygen isotope values of the carbonate range from –5.5‰ to –6.3‰ throughout the unit, before 570 cm, where the $\delta^{18}\text{O}_{\text{CARB}}$ value rapidly decreases to –7.9‰. Excluding the final data point at 570 cm, the mean $\delta^{18}\text{O}_{\text{CARB}}$ value for the unit is –5.76‰ ($n = 27$, 691 cm – 573 cm).

$\delta^{13}\text{C}_{\text{ORGANIC}}$ – Data points mirror those of $\delta^{18}\text{O}_{\text{CARB}}$ where the delta values remain relatively constant. The highest $\delta^{13}\text{C}_{\text{ORGANIC}}$ value in the unit is –19.5‰ at 573 cm ranging to the lowest delta value, –21.9‰ at 640 cm. $\delta^{13}\text{C}_{\text{ORGANIC}}$ values in this unit decrease slightly at 688 cm – 679 cm, before stabilizing through the centre of the unit and increasing to the highest $\delta^{13}\text{C}_{\text{ORGANIC}}$ value of the unit at 573 cm.

Lithology – Unit 4 is the only unit within the core PTB sequence where sediment type remains the same and is comprised of mollusc rich marl only. Unit 4 is sedimentologically very similar to unit 2 (as it is largely comprised of mollusc rich marl), and this is reflected in the similar $\delta^{18}\text{O}_{\text{CARB}}$ isotope values and high CaCO₃ content (LOI 950°C 81.8% to 87.4%) of the sediments.

Unit 5, 570 cm - 372 cm (Fig. 5.16)

$\delta^{18}\text{O}_{\text{CARB}}$ – This unit contains a comparatively small data set when compared to unit size. Oxygen isotope values of the carbonate range from the highest of –2‰ at 525 cm to the lowest of –13‰ at 380 cm but are highly variable throughout the unit, beginning on –5.9‰ at 540 cm, decreasing to –8.8‰ at 537 cm before a positive isotopic shift to –2‰ at 528 cm. $\delta^{18}\text{O}_{\text{CARB}}$ values gradually decrease after 528 cm to –7.1‰ at 513 cm where after, delta values remain relatively constant between 510 cm and 471 cm (ranging between –6.7‰ to –5.5‰). A large negative shift to –13‰, the lowest delta value of the unit, at 380 cm follows a large gap from 471 cm.

$\delta^{13}\text{C}_{\text{ORGANIC}}$ – Only two $\delta^{13}\text{C}_{\text{ORGANIC}}$ values of the carbonate are available for this unit, -19.8‰ and -16.7‰ at 534 cm and 471 cm respectively.

Lithology – Unit 5 is largely comprised of mollusc rich marl sediment with a 5 cm band of organic rich marl between 470 cm and 465 cm. Interestingly, and opposed to the relatively stable CaCO_3 content and $\delta^{18}\text{O}_{\text{CARB}}$ isotopic values observed for this sediment type in units 2 and 4, $\delta^{18}\text{O}_{\text{CARB}}$ isotope values and CaCO_3 content of the mollusc rich marl is highly variable in unit 5. The negative $\delta^{18}\text{O}_{\text{CARB}}$ isotopic shift at 537 cm is mirrored by low CaCO_3 content (LOI 950°C = 9%), followed by a positive $\delta^{18}\text{O}_{\text{CARB}}$ isotopic shift at 528 cm mirrored by higher CaCO_3 content (LOI 950°C = 65.9%). However, the unchanging sediment type suggests this shift may have been over a relatively short time period.

Unit 6, 372 cm – 200 cm (Fig. 5.17)

$\delta^{18}\text{O}_{\text{CARB}}$ – This unit comprises the longest isotopically ‘stable’ sequence in core PTB. Delta values range between the lowest value of -7.5‰ at 215 cm and the highest value of -4.9‰ at 200 cm. Between 356 cm and 317 cm oxygen isotope values of the carbonate remain within a $\pm 0.7\text{‰}$ range, the lowest delta value being -6.6‰ and the highest delta value being -5.9‰ , giving a mean value of -6.17‰ ($n=28$, 356 cm – 317 cm). A 77 cm gap follows this stable period before 240 cm, where $\delta^{18}\text{O}_{\text{CARB}}$ values appear to maintain stability. A small isotopic negative shift from -6.5‰ at 240 cm to -7.5‰ at 215 cm is followed by a gradual increase in $\delta^{18}\text{O}_{\text{CARB}}$ isotope values to -5.3‰ at 190 cm.

$\delta^{13}\text{C}_{\text{ORGANIC}}$ – The most complete $\delta^{13}\text{C}_{\text{ORGANIC}}$ sequence throughout core PTB is displayed in this unit. Delta values gradually decrease from -20.2‰ to -23.7‰ (the lowest $\delta^{13}\text{C}_{\text{ORGANIC}}$ value of the unit) between 372 cm and 317 cm, a total decrease of -3.5‰ for this section of unit 6. After the 77 cm gap, $\delta^{13}\text{C}_{\text{ORGANIC}}$ isotope values become more variable. The highest delta value of the unit is -15.7‰ at 197 cm, occurring just before the largest negative isotopic shift (-4.7‰) to -20.4‰ at 195 cm. The fluctuating values in this part of the unit (240 cm – 190 cm) mirror the variable nature of the $\delta^{18}\text{O}_{\text{CARB}}$ isotope values at the same points.

Lithology – Unit 6 is largely comprised of tufa, fragmented marl and carbonate marl with 5 cm of peat at the beginning of the unit between 370 cm and 365 cm. Oxygen and carbon isotope values of the carbonate, and organic and CaCO₃ content remain relatively unchanged in the tufa and fragmented marl sediments but become more variable within the carbonate marl sediments. Increasing organic content from 1.1% to 13.3% (LOI 550°C) is mirrored by decreasing CaCO₃ content from 93.8% to 33% (LOI 950°C) and a negative shift in $\delta^{18}\text{O}_{\text{CARB}}$ isotope values between 240 cm and 200 cm.

Unit 7, 200 cm – 0 cm (Fig. 5.18)

$\delta^{18}\text{O}_{\text{CARB}}$ – Delta values at the beginning of this unit (190 cm – 177 cm) remain relatively constant, ranging between –5.3‰ and –4.4‰ ($\pm 0.9\%$). A sharp ‘spike’ occurs at 186 cm when the $\delta^{18}\text{O}_{\text{CARB}}$ isotope value decreases from –5.1‰ to –7.8‰ before increasing to –5.2‰ at 185 cm. $\delta^{18}\text{O}_{\text{CARB}}$ isotope values in this unit are the highest, most constant sequence throughout core PTB. $\delta^{18}\text{O}_{\text{CARB}}$ isotope values begin to decrease at 112 cm to –5.9‰ before becoming the most isotopically negative in the unit (–10.6‰) at 16 cm.

$\delta^{13}\text{C}_{\text{ORGANIC}}$ – Data points through unit 7 are variable. $\delta^{13}\text{C}_{\text{ORGANIC}}$ isotope values decrease at the beginning of the unit from the highest delta value of –17.8‰ at 179 cm to –23.4‰ at 173 cm before steadily increasing back to –20.4‰ at 162 cm. A sharp negative isotopic shift of 4‰ is observed between 175 cm and 173 cm. A large positive isotopic shift from –24.4‰ at 119 cm to –19.7‰ at 115 cm is observed before a steady decrease to –24.9‰ at 24 cm.

Lithology – Unit 7 is the most organic rich unit of the core PTB sequence. The unit is comprised of peat, peaty marl and organic rich marl with some carbonate marl at the beginning of the unit. The peat is well humified and has high organic content between 31.4% and 87.8% (LOI 550°C) and low CaCO₃ content between 0.24% and 5.1% (LOI 950°C). The organic rich and peaty marl sediments are disturbed by modern day vegetation rootlet growth and have low CaCO₃ and organic content of <20% (LOI 950°C) and <10% (LOI 550°C) respectively.

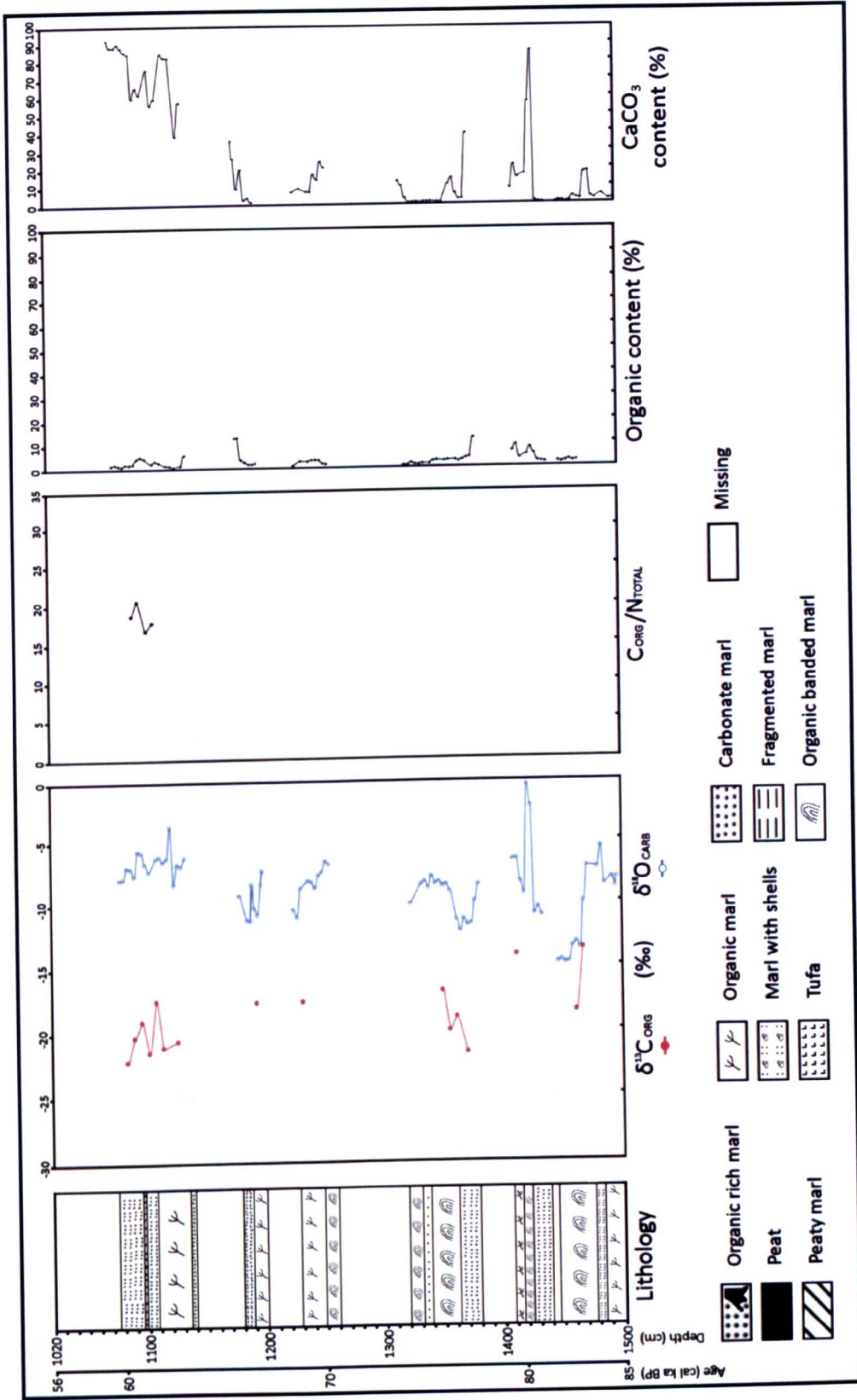


Figure 5.12. Enlarged view of unit 1 $\delta^{13}\text{C}_{\text{ORGANIC}}$ and $\delta^{18}\text{O}_{\text{CARB}}$ isotope trends with C/N ratios, and organic content and CaCO_3 content by LOI (see appendix 2.2.2).

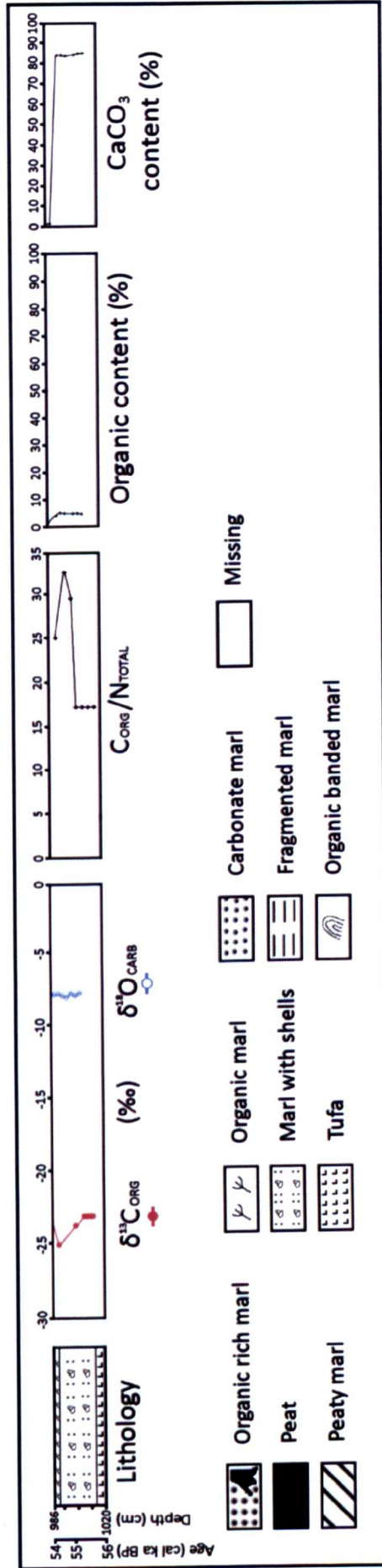


Figure 5.13. Enlarged view of unit 2 $\delta^{13}\text{C}_{\text{ORGANIC}}$ and $\delta^{18}\text{O}_{\text{CARB}}$ isotope trends with C/N ratios, and organic content and CaCO_3 content by LOI (see appendix 2.2.2).

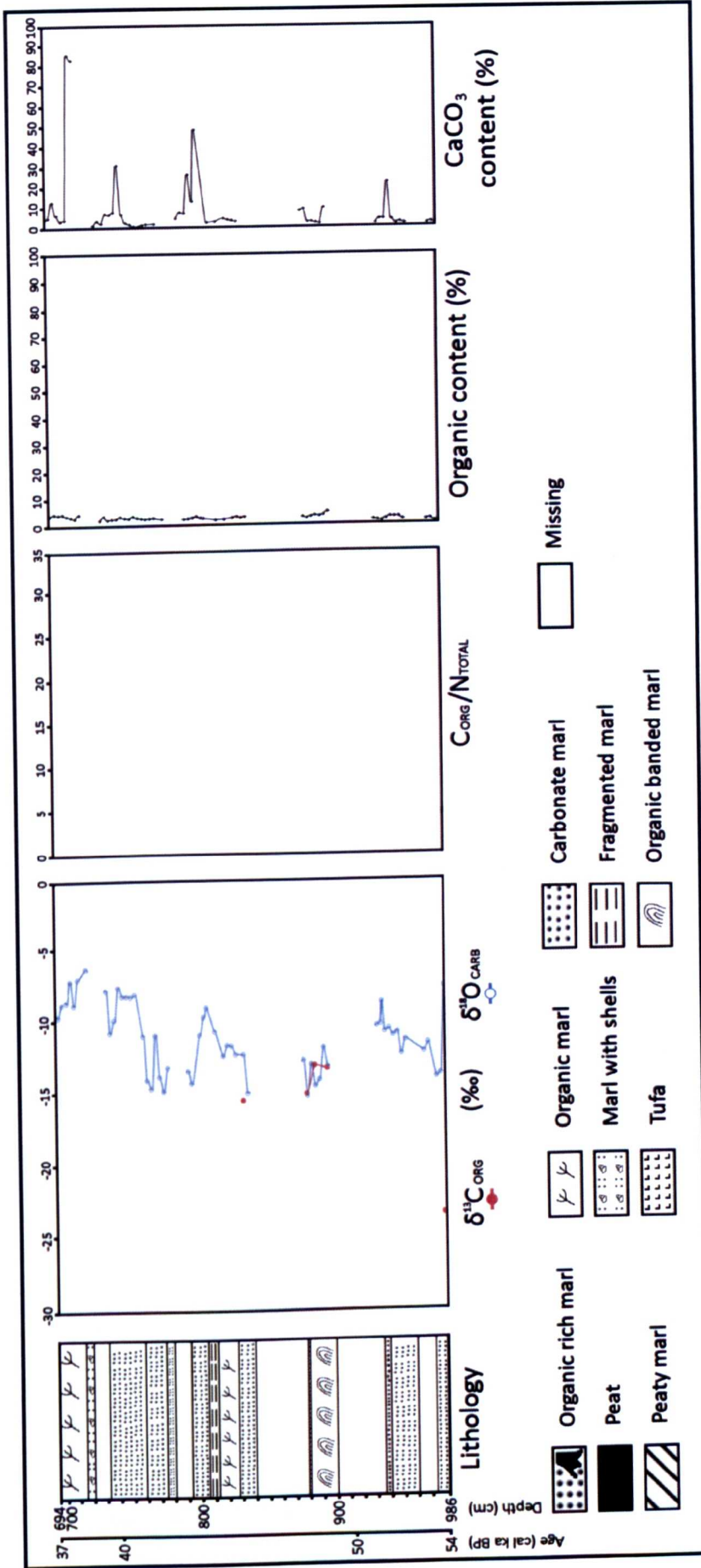


Figure 5.14. Enlarged view of unit 3 $\delta^{13}\text{C}_{\text{ORG}}$ and $\delta^{18}\text{O}_{\text{CARB}}$ isotope trends with C/N ratios, and organic content and CaCO_3 content by LOI (see appendix 2.2.2).

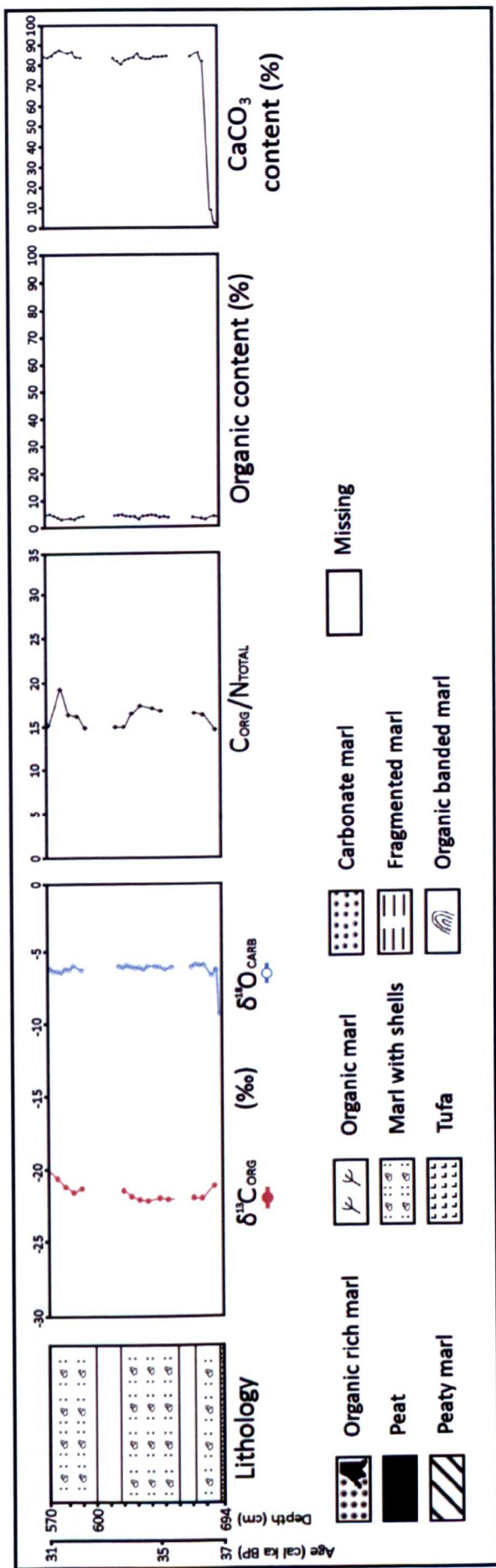


Figure 5.15. Enlarged view of unit 4 $\delta^{13}\text{C}_{\text{ORGANIC}}$ and $\delta^{18}\text{O}_{\text{CARB}}$ isotope trends with C/N ratios, and organic content and CaCO_3 content by LOI (see appendix 2.2.2).

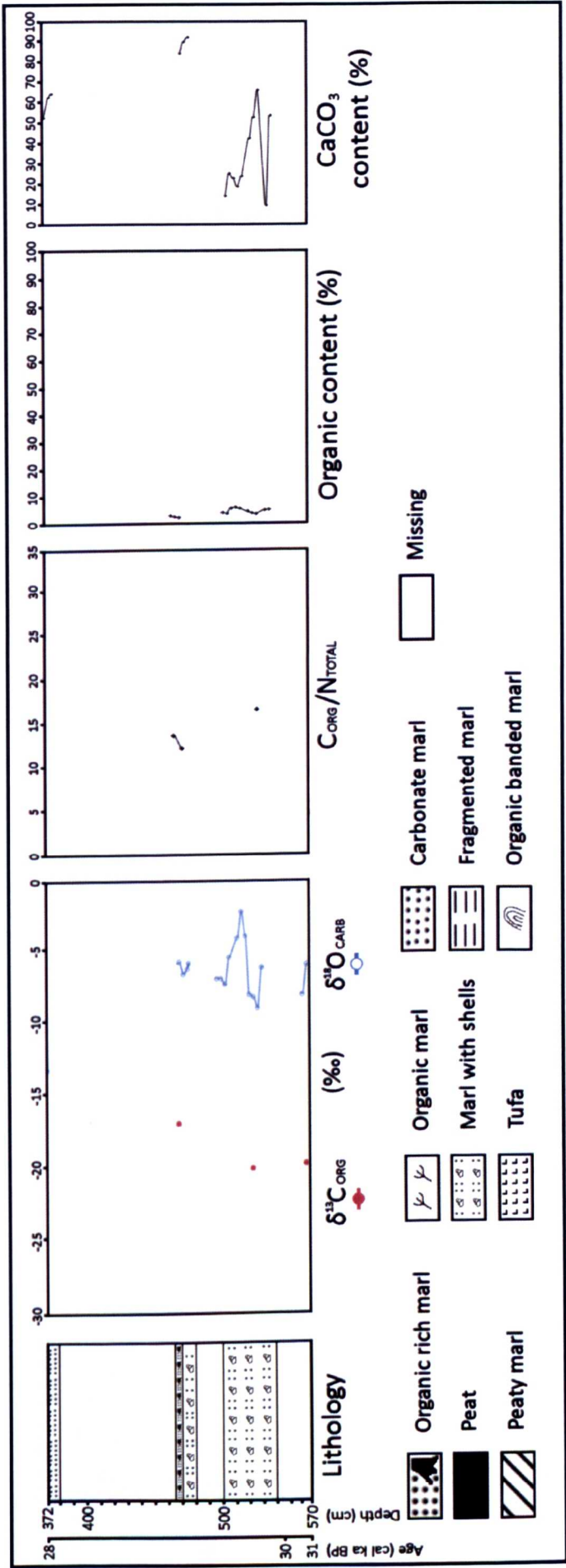


Figure 5.16. Enlarged view of unit 5 $\delta^{13}\text{C}_{\text{ORGANIC}}$ and $\delta^{18}\text{O}_{\text{CARBS}}$ isotope trends with C/N ratios, and organic content and CaCO_3 content by LOI (see appendix 2.2.2).

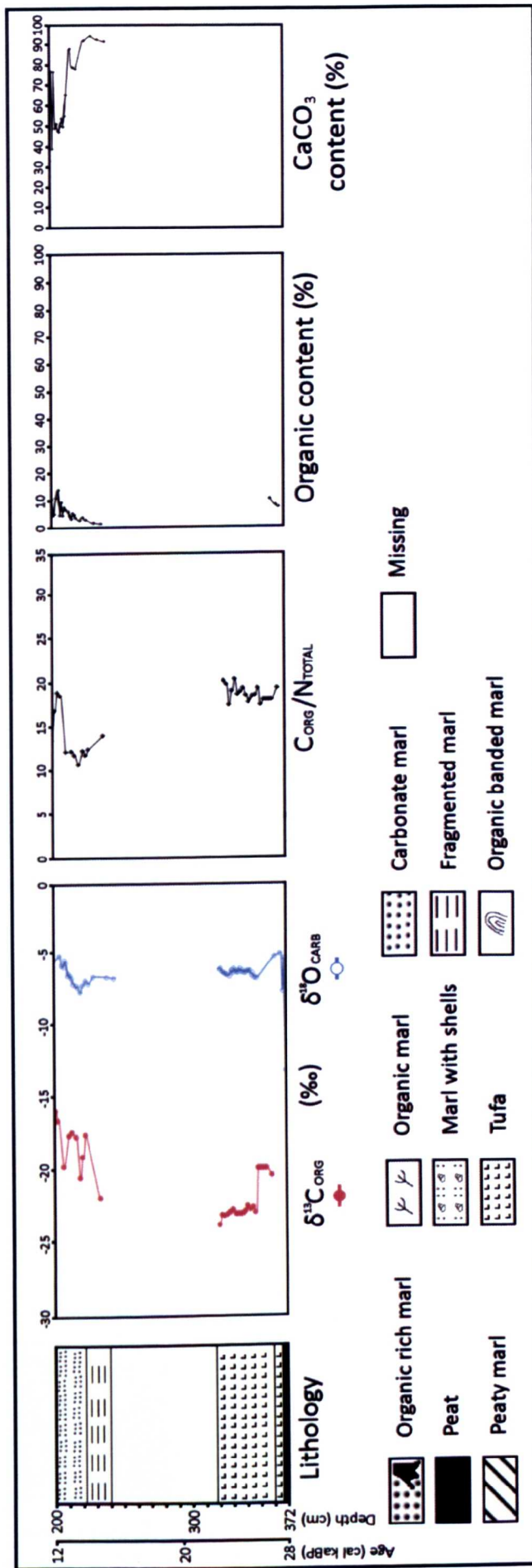


Figure 5.17. Enlarged view of unit 6 $\delta^{13}\text{C}_{\text{ORG}}$ and $\delta^{18}\text{O}_{\text{CARBS}}$ isotope trends with C/N ratios, and organic content and CaCO_3 content by LOI (see appendix 2.2.2).

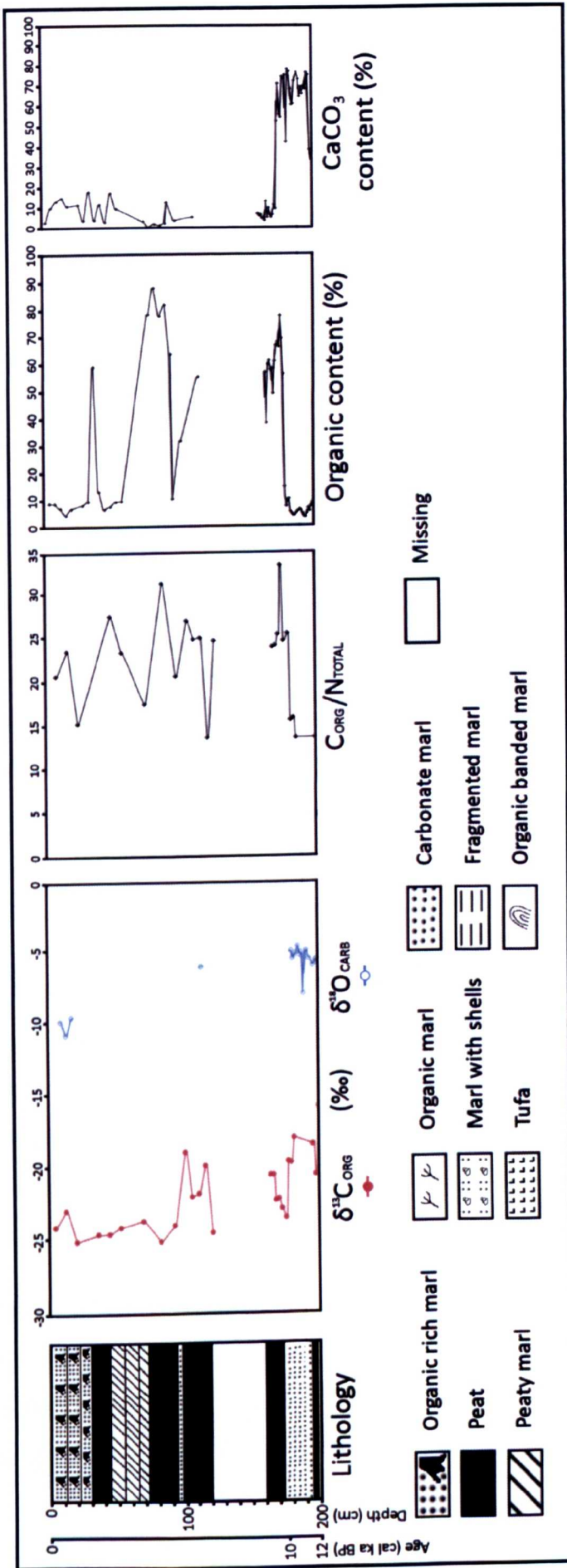


Figure 5.18. Enlarged view of unit 7 $\delta^{13}\text{C}_{\text{ORGANIC}}$ and $\delta^{18}\text{O}_{\text{CARB}}$ isotope trends with C/N ratios, and organic content and CaCO_3 content by LOI (see appendix 2.2.2).

5.6.3 $\delta^{13}\text{C}_{\text{DIC}}$ vs. C/N ratios

Figure 5.19 shows $\delta^{13}\text{C}_{\text{DIC}}$ isotope values and C/N ratios for sediments in core PTB. For unit 3 no C/N ratios are available as low %C in the organic sediments, between 0.11% and 0.57% (mean = 0.23%, $n = 24$), meant that the C/N ratio determination was not possible for this unit.

$\delta^{13}\text{C}_{\text{DIC}}$ isotope values in unit 1 range from -15.3‰ to -0.5‰ with a mean of -9.6‰ ($n = 75$). Values are highly variable within the unit suggesting carbon sources are wide ranging, displaying $\delta^{13}\text{C}_{\text{DIC}}$ values similar to modern day water bodies within the CCB (see chapter 2). Only four C/N values are available for unit 1, ranging between 15.3 and 19.1 which, when compared with $\delta^{13}\text{C}_{\text{DIC}}$ values between -4.3‰ and -1.2‰ at the same depths (1,108 cm – 1,090 cm) suggests a higher component of aquatic vegetation.

Unit 2 $\delta^{13}\text{C}_{\text{DIC}}$ isotope values range between -2‰ and -0.2‰ , with sediments comprising of tufa and carbonate rich marl, similar to the Tierra Blanca tufas (see chapter 4). C/N ratios in unit 2 remain at a constant 17.1 before a sudden spike to much higher values between 24.9 and 33.1. These shifts occur in the stratigraphic section where $\delta^{13}\text{C}_{\text{DIC}}$ values are at their lowest in the unit which may suggest a less prominent groundwater carbon source at these points.

Unit 3 $\delta^{13}\text{C}_{\text{DIC}}$ values range between -15.6‰ and -0.8‰ with a mean of -12.6‰ ($n = 56$). Like unit 1, the $\delta^{13}\text{C}_{\text{DIC}}$ isotope values are within the range defined for modern day water bodies within the CCB suggesting the carbon is sourced from predominantly from soil respired and atmospheric CO_2 with some possible influence from aquifer sourced carbon toward the top of the unit where $\delta^{13}\text{C}_{\text{DIC}}$ values are highest for the unit, -0.8‰ at 718 cm.

Unit 4 $\delta^{13}\text{C}_{\text{DIC}}$ isotope values range between -3.1‰ and -0.3‰ with a mean of -0.8‰ ($n = 28$), high values that are similar to unit 2. C/N ratios range between 14.5 and 19.3 for unit 2 which is consistent with aquatic vegetation. Carbonate rich marl with mollusc shells is a similar lithology to unit 2 also, possibly suggesting higher water levels.

Unit 5 $\delta^{13}\text{C}_{\text{DIC}}$ isotope values range between -14.5‰ and $+0.4\text{‰}$ with a mean of -4.6‰ ($n = 21$). Like units 1 and 3, $\delta^{13}\text{C}_{\text{DIC}}$ values are highly variable suggesting mixed sources of carbon from soil CO_2 in the very low delta values to aquifer sourced CO_2 in the higher delta values. Only three C/N ratios are available for unit 5 due to gaps in the stratigraphy, however, it is interesting to note that the two lowest C/N ratios – 12.07 at 474 cm and 13.5 at 471 cm – suggest aquatic vegetation, corresponding with high $\delta^{13}\text{C}_{\text{DIC}}$ values of $+0.4\text{‰}$ and -1.2‰ respectively. As suggested in previous units, high $\delta^{13}\text{C}_{\text{DIC}}$ values appear to correspond with low C/N ratios which may indicate higher water levels and increased input of aquifer derived CO_2 .

Unit 6 $\delta^{13}\text{C}_{\text{DIC}}$ values begin with a very constant range of -1.1‰ to $+0.2\text{‰}$ (mean -0.56‰ , $n = 28$) between 365 cm and 317 cm. $\delta^{13}\text{C}_{\text{DIC}}$ values become slightly more negative after this point ranging from -6.3‰ to -0.5‰ (mean -2.6‰ , $n = 23$) between 240 cm and 190 cm. C/N ratios are relatively constant from 365 cm to 317 cm, ranging between 17.3 and 20.06 suggesting a mix of aquatic and terrestrial vegetation. A larger range of C/N ratios – 10.6 to 18.88 – between 240 cm and 190 cm is consistent with a larger range of $\delta^{13}\text{C}_{\text{DIC}}$ values toward the top of unit 6 possibly suggesting fluctuating lake levels.

Unit 7 $\delta^{13}\text{C}_{\text{DIC}}$ values are very fragmentary with 11 of the 15 data points between 188 cm and 177 cm. The range of $\delta^{13}\text{C}_{\text{DIC}}$ values, between -13.4‰ and $+0.3\text{‰}$, is highly variable and is reflected by the changing marl and peat sediment types and highly variable C/N ratios, ranging between 13.38 and 33.13. Higher $\delta^{13}\text{C}_{\text{DIC}}$ isotope values again correspond to low C/N ratios and marl sediments with lower $\delta^{13}\text{C}_{\text{DIC}}$ isotope values and high C/N ratios corresponding to organic sediments, possibly due to substrate change from marl to peat and terrestrial vegetation types populating the peat sediments.

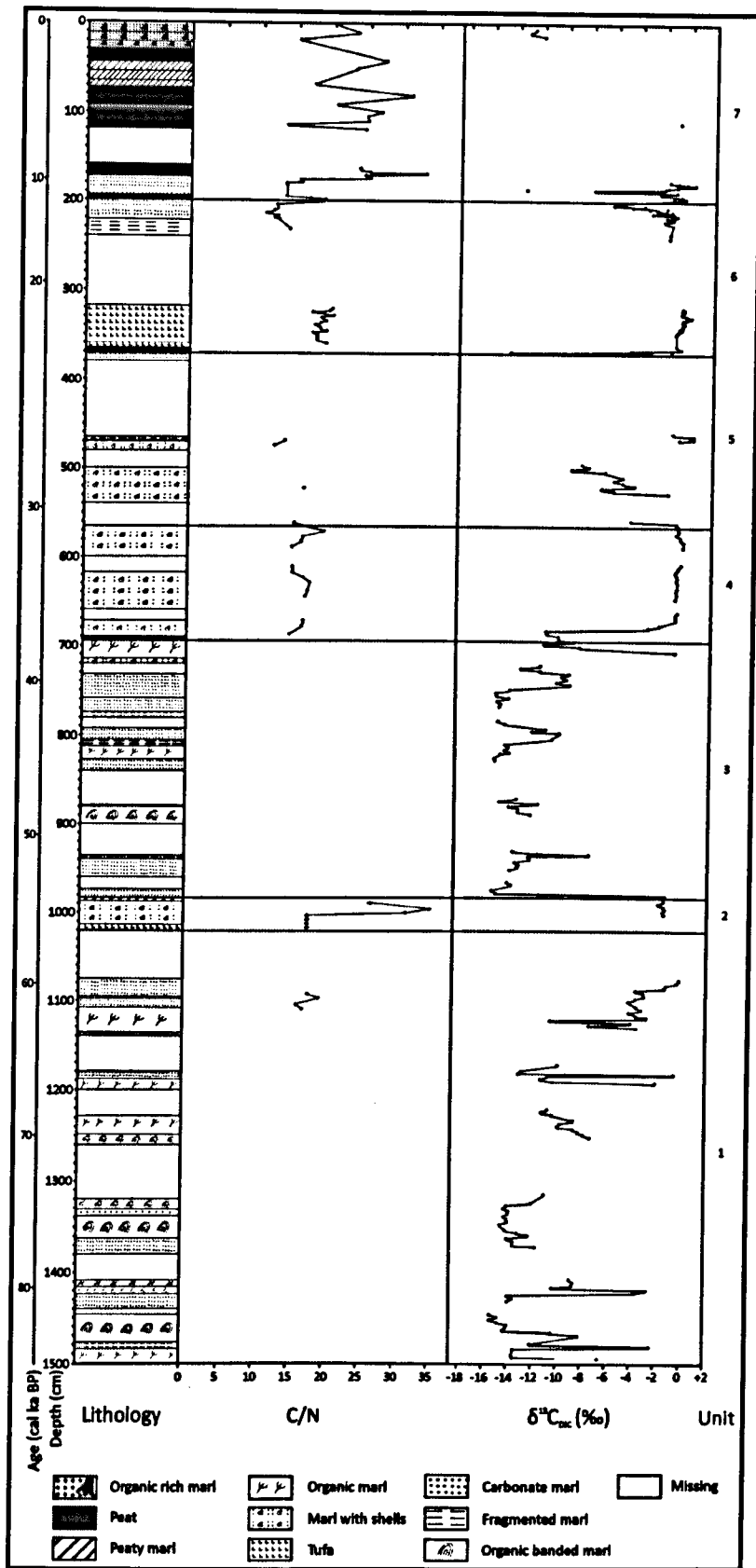


Figure 5.19. Variations in C/N ratios and $\delta^{13}\text{C}_{\text{DIC}}$ values in the core PTB sediment column. Changes in sediment type to carbonate rich marl or tufa appears to coincide with higher $\delta^{13}\text{C}_{\text{DIC}}$ values with organic rich sediments coinciding with much lower $\delta^{13}\text{C}_{\text{DIC}}$ values.

5.6.4 $\delta^{13}\text{C}_{\text{ORGANIC}}$ vs. C/N ratios

Figure 5.20 displays $\delta^{13}\text{C}_{\text{ORGANIC}}$ vs. C/N ratios of the organic sediments in core PTB. To allow better interpretation of the data, each of the core PTB units (1-7) have been plotted individually, with the exception of unit 3 where no C/N ratios were available for the samples. Low %C in the organic sediments of unit 3, ranging between 0.11% and 0.57% (mean = 0.23%, $n = 24$), meant that the C/N ratio determination was not possible for this unit.

All samples ($n = 76$) fall within the ranges of C_3 , CAM and aquatic (algal and macrophyte) vegetation. Unit 1 ($n = 4$) plots within the boundaries of aquatic and low C/N CAM vegetation types suggesting the organic matter is of algal and macrophytic origin. Unit 2 ($n = 4$) plot within low range C_3 and high range CAM terrestrial vegetation with the exception of one sample ($\delta^{13}\text{C}_{\text{ORGANIC}} = -22.8\text{‰}$, C/N = 17.1) that plots within the macrophyte range. Unit 4 ($n = 14$) plots within the aquatic vegetation and on the boundary of CAM vegetation suggesting the organic matter in this unit is predominantly sourced from macrophytes. Unit 5 ($n = 2$) contains the fewest samples and plots similarly to unit 4 between marginal aquatic and CAM vegetation types, possibly suggesting a terrestrial rich organic matter source. The lower $\delta^{13}\text{C}_{\text{ORGANIC}}$ in the unit 5 samples suggests they may be sourced from predominantly CAM origins. Unit 6 ($n = 29$) all lie within C_3 and aquatic vegetation ranges with the exception of five samples, three of which plot within CAM with the final two plotting between CAM and C_4 vegetation types. The three samples plotting within the CAM range also fall within the aquatic range suggesting these may be macrophyte in origin, however, the two samples ranging between CAM and C_4 suggest both aquatic and terrestrial organic matter sources. Unit 7 ($n = 23$) predominantly plots within the low C_3 and high CAM ranges suggesting the organic matter is largely of terrestrial origin. Four samples plot solely within the aquatic vegetation range suggesting unit 7 has some organic matter sourced directly from marginal aquatic plants.

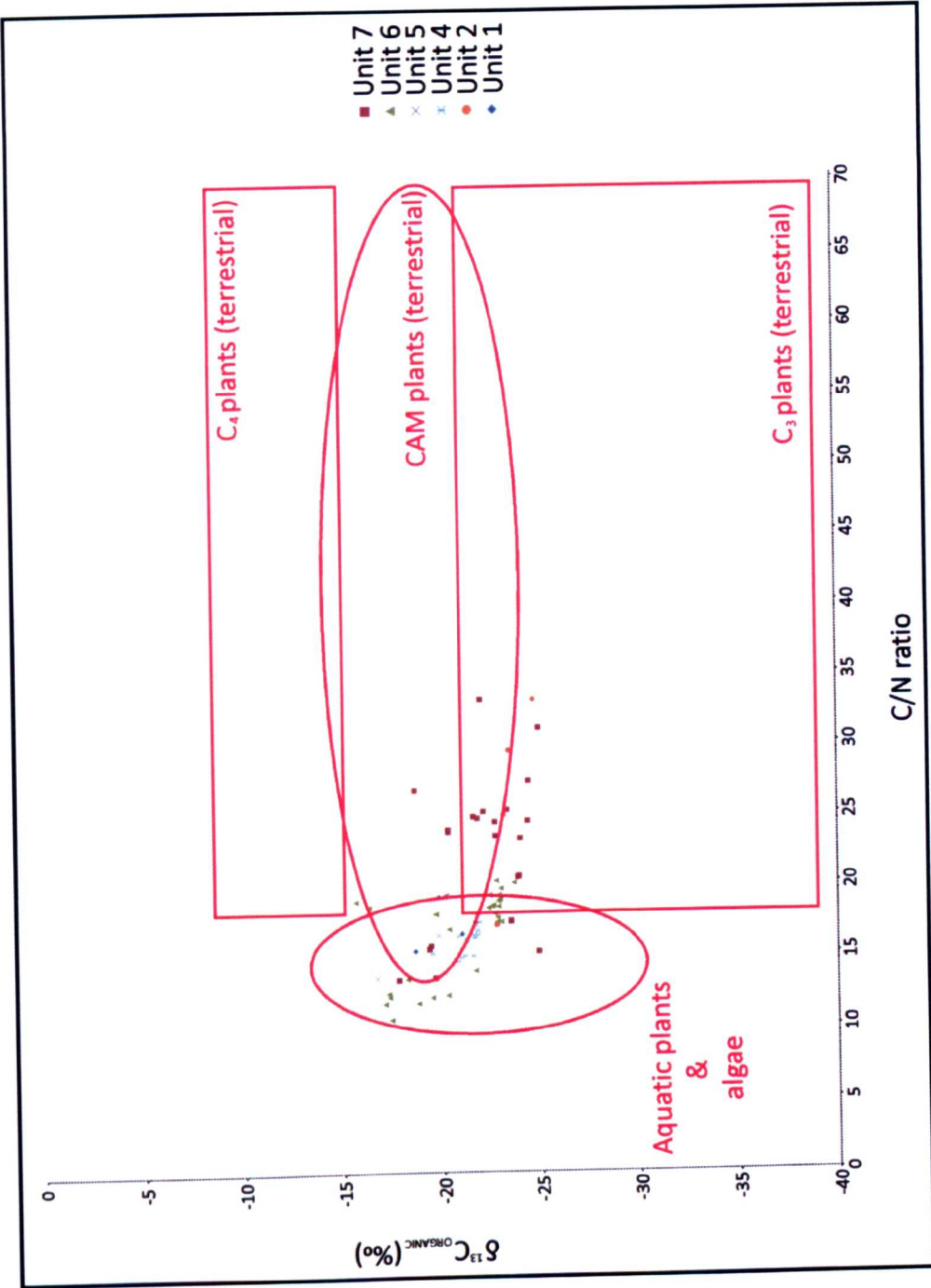


Figure 5.20. $\delta^{13}C_{ORGANIC}$ vs. C/N ratios of organic sediments in core PTB. Ranges of the four major $\delta^{13}C$ contributors – C₄, C₃, CAM and aquatic – are set according to Leng [2005] and Minckley *et al.* [2009] after Meyers [1994].

5.6.5 $\delta^{18}\text{O}_{\text{CARB}}$ and $\delta^{13}\text{C}_{\text{DIC}}$ isotopic covariance

Unidirectional isotopic transitions, known as oxygen-carbon covariance, can often be attributed to simultaneous evaporative drawdown and CO_2 degassing in hydrologically closed arid-region lakes [Talbot, 1994; Drummond *et al.* 1995]. Each of the core PTB units (1-7) has been plotted individually to allow investigation of any linear isotopic covariance (Fig. 5.21), with R^2 data, to allow inter-unit comparison as well as pollen, $\delta^{18}\text{O}_{\text{CARB}}$ and $\delta^{13}\text{C}_{\text{ORGANIC}}$ data comparison. Figure 5.22 displays units 1-7 plotted together with linear regression through the data showing a good correlation ($R^2 = 0.667$, $n = 258$).

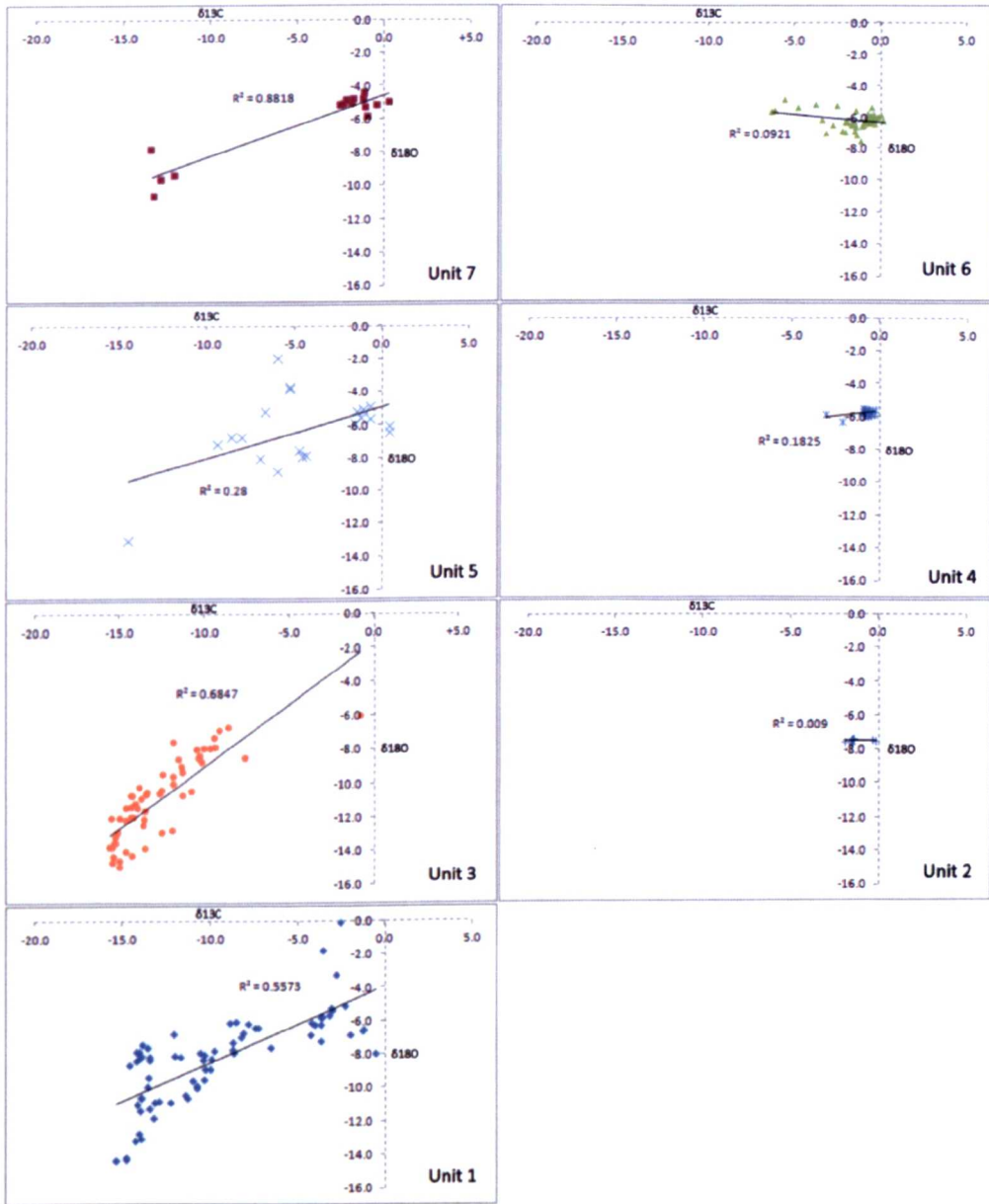


Figure 5.21. Units 1 to 7 $\delta^{18}\text{O}_{\text{CARB}}$ and $\delta^{13}\text{C}_{\text{DIC}}$ isotope data for core PTB with R^2 covariance displayed. Linear regression is shown by a trend line through the data.

Unit 1 data show a moderately high correlation ($R^2 = 0.557$, $n = 76$) before the transition into unit 2 where a drop to the lowest correlation of the seven units ($R^2 = 0.01$, $n = 10$) is observed. Unit 3 shows a high correlation in the data ($R^2 = 0.685$, $n = 57$) which is the most similar R^2 value to the overall data trend across the seven units. Unit 4 shows a drop to low correlation ($R^2 = 0.182$, $n = 28$) before unit 5 shows a rise to a moderate to low correlation ($R^2 = 0.28$, $n = 21$). Unit 6 data display low correlation ($R^2 = 0.092$, $n = 51$) before an increase into the final, unit 7 where linear correlation is at its highest ($R^2 = 0.882$, $n = 15$) throughout the entire sequence. Despite a moderately high correlation of the seven units ($R^2 = 0.667$, $n = 258$), when the units are analysed individually an alternating high-low covariance pattern is observed. Units 1, 3, 5 and 7 show moderate to high correlation of (R^2) 0.557, 0.685, 0.28 and 0.882 respectively where units 2, 4 and 6 show low covariance of (R^2) 0.01, 0.182 and 0.092 respectively.

Units 2, 4 and 6 display very low $\delta^{18}\text{O}_{\text{CARB}}$ and $\delta^{13}\text{C}_{\text{DIC}}$ co-variance and are interpreted as open-basin conditions for Poza Tierra Blanca. Unit 7 displays high $\delta^{18}\text{O}_{\text{CARB}}$ and $\delta^{13}\text{C}_{\text{DIC}}$ co-variance and is interpreted as closed-basin conditions for Poza Tierra Blanca. Units 1, 3 and 5 display moderate to high $\delta^{18}\text{O}_{\text{CARB}}$ and $\delta^{13}\text{C}_{\text{DIC}}$ co-variance and are interpreted as closed-basin conditions punctuated by periodic open-basin conditions [e.g. Johnson *et al.* 1991 (where $R^2 = 0.45$ was interpreted as closed-basin conditions)]. During units 1, 3 and 5 Poza Tierra Blanca may not display high co-variation due to the pool not experiencing closure over a prolonged period of time [e.g. Drummond *et al.* 1995; Li and Ku, 1997].

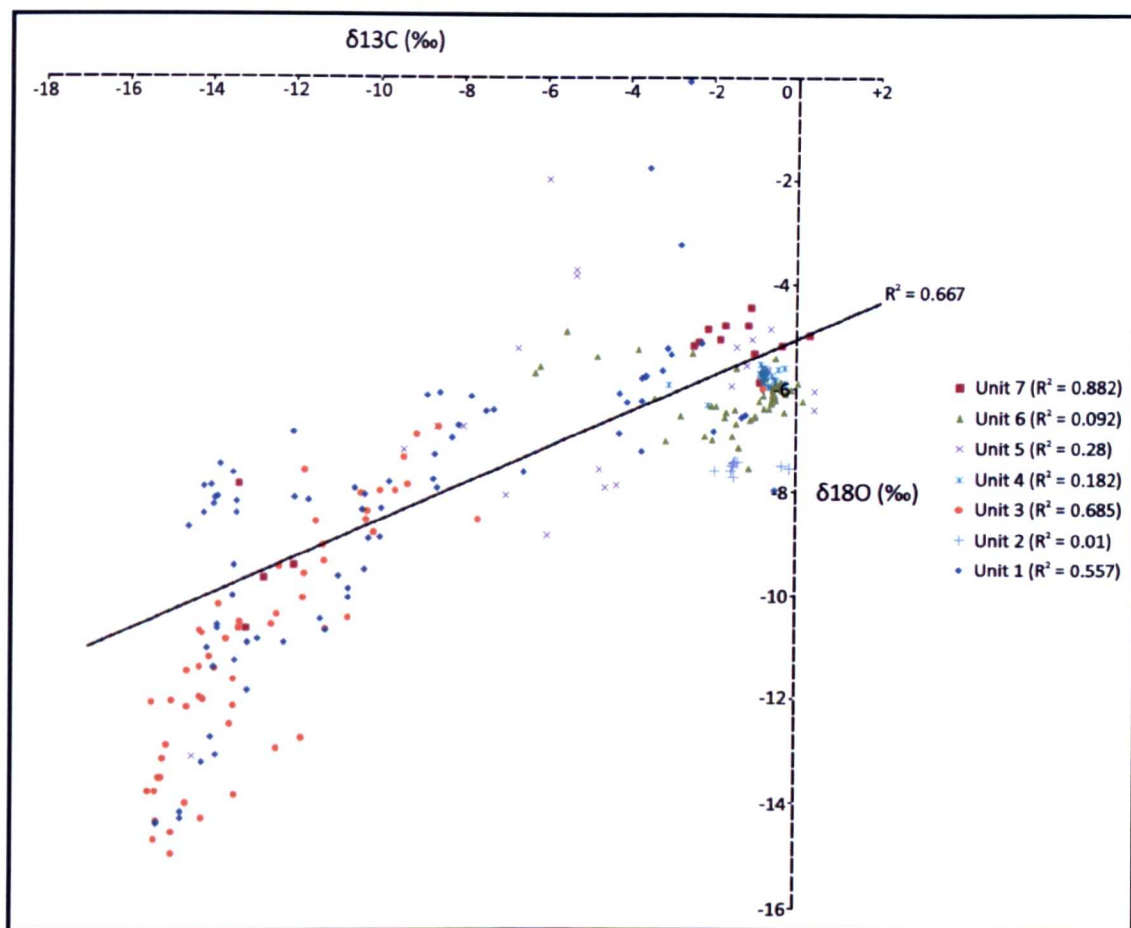


Figure 5.22. $\delta^{18}\text{O}_{\text{CARB}}$ and $\delta^{13}\text{C}_{\text{DIC}}$ isotope data for core PTB with R^2 covariance displayed. Overall R^2 covariance is shown by linear regression through the data. Unit specific linear regressions have been omitted from the data graph for ease of analysis although unit specific R^2 covariance is shown.

5.6.6 Pollen

All pollen data is presented in figures 5.23 and 5.24. Figure 5.23 displays presence (+) of key upland wooded taxa alongside stable $\delta^{18}\text{O}_{\text{CARB}}$ and $\delta^{13}\text{C}_{\text{ORGANIC}}$ data. Upland taxa have been isolated due to being more accurate indicators of local and regional vegetation change, and therefore climate change [Minckley and Jackson, 2008]. Mesic (temperate indicators), xeric (dry indicators) and continual species have been used to complement the stable isotope results. Figure 5.24 is to be used as a reference point for specific data trends observed in figure 5.23, as discussing percentage abundance as a singular proxy of particular pollen taxa can be misleading, particularly in arid environments, creating false interpretations e.g. Meyer [1973] used an unchanging percentage abundance of desert floor pollen taxa *Compositae* to infer arid climatic stability in the CCB. However, when increases in percentage abundance of

upland pollen taxa - *Pinus* and *Quercus* – were considered, climatic instability could be inferred [Minckley and Jackson, 2008].

Unit 1

There is very little pollen preservation within this unit, consequently; sampling of the unit was low resolution (50 cm intervals). The only presence of non-continuous pollen taxa is *Fraxinus* (Ash) at 14 m depth (Fig. 5.23). No pollen percentage data is available for unit 1 due to poor pollen preservation.

Unit 2

Stratigraphically the smallest of the seven units, unit 2 contains more prominent mesic (temperate) and wetland species throughout. *Picea* (Spruce), *Carya* (Hickory) and *Fraxinus* represent the presence of key upland mesic taxa (Fig. 5.23) along with percentage increases in *Pinus* (Pine) and *Quercus* (Oak) (Fig. 5.24). Wetland taxa also experience an increase in unit 2 where *Aster* (Flowers), *Amaranthaceae* (Chenopods), *Poaceae* (Grasses) and *Cyperaceae* (Sedges) all show large increases (Fig. 5.24). No xeric species are observed within unit 2.

Unit 3

Pollen preservation is poor at the beginning and end of unit 3. *Picea*, *Betula* (Birch) and *Fraxinus* represent the presence of mesic taxa between 895 cm and 770 cm along with the more xeric *Celtus* (Hackberry). *Juniperus* (Juniper), *Quercus* and *Pinus* are also present between these depths in unit 3. A significant spike (>70%) of *Amaranthaceae* is observed within this unit (Fig. 5.24) along with smaller increases of *Aster* and *Poaceae*.

Unit 4

Higher resolution sampling was conducted throughout unit 4 due to excellent pollen preservation. The presence of *Abies* (Fir) within the mesic taxa is important as unit 4 is the only unit containing this species. *Fraxinus*, *Acer* and *Picea* are present in their highest abundances' in unit 4 along with *Quercus* and *Pinus*. Xeric taxa are present alongside mesic taxa but in much lower numbers, *Prosopis* (Mesquite) and *Celtus* are both present toward the beginning of the unit, reducing in numbers toward

the middle (Fig. 5.24) when *Agavaceae* (*Agave*) become present in the unit. Wetland *Typha* (Cattail), *Poaceae* and *Amaranthaceae* all show increases within unit 4, *Typha* in particular is interesting since it grows in open water.

Unit 5

Before the missing section toward the top of unit 5, pollen preservation is good. A reduction of both mesic and xeric taxa is observed with the disappearance of *Abies*, *Carya* and *Celtus*. *Picea*, *Quercus*, *Pinus* and *Aster* are all present in high numbers before a sharp drop at approximately 500 cm, just before the missing section. *Amaranthaceae* and *Cyperaceae* reach their highest abundances of the whole sequence in unit 5, with values dropping toward the top of the unit. *Typha* is also present in small numbers within unit 5, both at the bottom and top of the unit.

Unit 6

Unit 6 contains very little preserved pollen. Mesic taxa are best represented with *Betula*, *Carya* and *Celtus* present at the beginning of the unit along with the continual *Juniperus*, *Quercus* and *Pinus*. At approximately 210 cm *Picea* and *Carya* are again present along with the greater presence of xeric taxa - *Prosopis*, *Agavaceae* and *Celtus*. Large abundance drops of *Pinus* and wetland *Poaceae* are observed toward the top of the sequence along with a small spike of *Typha*.

Unit 7

Fraxinus is the only mesic taxa present in unit 7, occurring alongside *Celtus* at the beginning of the unit. Mesic species disappear from the sequence at 100 cm with xeric taxa – *Prosopis*, *Agavaceae* and *Celtus* – establishing larger numbers toward the top of the unit. *Pinus* and *Quercus* also increase in numbers toward the top of the unit. Upland and wetland species of *Aster* drop in numbers at 100 cm also, alongside *Cyperaceae* although *Typha* increase in numbers at this point.

5.7 Interpretation and discussion

Variations in core PTB carbonate $\delta^{18}\text{O}$ and $\delta^{13}\text{C}$ are coupled with changes in sediment lithology, such that higher delta values correspond with carbonate-rich layers and lower delta values correspond with organic-rich layers. A simple explanation of these variations is that they are responding to fluctuating climate change and changes in water volume. However, as discussed in chapter 2, water in the CCB is derived from at least two sources: 1) hydrothermal groundwater sources (Cupido-Aurora aquifer) and, 2) recharge in the surrounding mountains, both with water residence times of approximately 20-1500 years, so carbonate may display weighted average $\delta^{18}\text{O}$ values [Johannesson *et al.*, 2004; Badino *et al.*, 2004].

It is proposed that periods of arid climate are indicated by a decrease in $\delta^{18}\text{O}_{\text{CARB}}$ and $\delta^{13}\text{C}_{\text{DIC}}$ values in the organic rich sediments, as these shifts are mirrored by a positive shift in the $\delta^{13}\text{C}_{\text{ORGANIC}}$ values and increased organic content (Figs. 5.19, 5.22, 5.23 and appendix 2.2.2). A shift to naturally occurring eutrophic lake or marsh conditions is supported by the presence of organic rich banding in the marl sediment of core PTB where conditions would favour terrestrial vegetation and algal growth leading to increased biogenic calcite precipitation by photosynthesis. The kinetic fractionation of photosynthetically precipitated calcite would favour higher carbonate precipitation rates, incorporating more of the lighter ^{16}O and leading to more negative $\delta^{18}\text{O}_{\text{CARB}}$ values [e.g. Fronval *et al.*, 1995]. Lower $\delta^{13}\text{C}_{\text{DIC}}$ in the organic rich sediment in these arid periods is attributed to increased organic matter oxidation in the water column and sediment pore water. During these periods of proposed eutrophication and desiccation it is likely a change in atmospheric circulation would be the driving factor in lake level change. Moisture from the Gulf of Mexico arrives in N. Mexico with lower $\delta^{18}\text{O}$ values (-7‰) [Wassenaar *et al.*, 2009] as well bringing drier atmospheric conditions which may have contributed to any desiccation.

During wetter climate conditions, $\delta^{18}\text{O}_{\text{CARB}}$ and $\delta^{13}\text{C}_{\text{DIC}}$ values increase in the minerogenic sediments and maintain constant values that more closely reflect the $\delta^{18}\text{O}$ values of modern day water in the CCB (see chapter 2) and $\delta^{13}\text{C}_{\text{DIC}}$ values tufa sediments (see chapters 3 and 4). Higher $\delta^{18}\text{O}_{\text{CARB}}$ values in the proposed wetter periods are attributed to increased authigenic calcite in the carbonate sediments and a

shift to atmospheric moisture from the Pacific, bringing sustained and increased rainout on the surrounding mountains and recharging the Cupido-Aurora aquifer in the Bolson de Mapimi with higher $\delta^{18}\text{O}$ values (-6.9‰) [Wassenaar *et al.* 2009]. Isotopic signals of wetland environments [Winter and Rosenberry, 1995; Rosenberry and Winter, 1997; Clotts *et al.*, 2009] show hydrologically open systems maintain constant $\delta^{18}\text{O}$ values due to the hydrologically charged (increased water body) system having lower sensitivity to variation in $\delta^{18}\text{O}$ input. Hydrologically closed systems, however, show highly variable $\delta^{18}\text{O}$ values due to the hydrologically de-charged (decreased water body) system having a higher sensitivity to variations in E/P and atmospheric moisture source, the main controlling factors of closed basin systems. In these wetter periods, Core PTB $\delta^{13}\text{C}_{\text{DIC}}$ exhibits similar values to the Tierra Blanca tufa (see chapter 4) due to increased recharge in the surrounding mountains with higher $\delta^{13}\text{C}_{\text{DIC}}$ values attributed to increased dissolution of the surrounding catchment limestone.

It has been shown [see chapter 2, section 2.4.1] that water bodies in the modern hydrological system do not co-vary with each other suggesting the flow system to be hydrologically open. This open flow system is suggested to occur in a larger, hydrologically closed basin, beginning in the west of the CCB before ending in a series of highly evaporative endorheic pools in the east of the CCB. However, Poza Tierra Blanca (the location of core PTB) is currently hydrologically open, with both inflow and outflow streams. Therefore, a lack of $\delta^{18}\text{O}_{\text{CARB}}$ vs. $\delta^{13}\text{C}_{\text{DIC}}$ covariance from core PTB is interpreted in terms of Poza Tierra Blanca displaying similar, or more extensive, open hydrological conditions, similar to the modern system. Co-variation of the $\delta^{18}\text{O}_{\text{CARB}}$ vs. $\delta^{13}\text{C}_{\text{DIC}}$ isotope values from core PTB is interpreted as Poza Tierra Blanca displaying closed hydrological conditions, indicating a period of aridity and drying of the pool.

If atmospheric temperature was a controlling factor in the $\delta^{18}\text{O}_{\text{CARB}}$ values of core PTB, large shifts ($>10\text{‰}$ e.g. 1431-1422 cm (Fig. 5.12)) would represent unrealistic temperature change of up to 25°C , based on the well established relationship for equilibrium carbonates of a decrease of 0.24‰ for every 1°C increase in temperature [Dansgaard, 1964; Craig, 1965; Kim and O'Neil, 1997; Fricke and O'Neil, 1999; Leng and Marshall, 2004; Bernal *et al.*, 2011]. Such massive temperature fluctuation is an unrealistic possibility in the CCB and is not supported by regional proxy data (discussed

in more detail later in the chapter). Studies have shown the covariance of $\delta^{18}\text{O}_{\text{CARB}}$ vs. $\delta^{13}\text{C}_{\text{DIC}}$ to be an important factor in determining hydrology [Talbot, 1990; Drummond *et al.*, 1995; Li, 1997]. Based on low covariance ($R^2 < 0.7$) indicating hydrologically open conditions and high covariance ($R^2 > 0.7$) indicating hydrologically closed conditions [Talbot, 1990], the seven units of core PTB have been categorised according to their R^2 covariance (Fig. 5.25). However, moderate covariance (R^2 between 0.3 and 0.6) can generally be accepted to indicate transitional periods that have a mix of hydrologically open and closed conditions [Shemish, 2011].

The c. 84 cal ka BP palaeoenvironmental history of the CCB will be interpreted using $\delta^{18}\text{O}_{\text{CARB}}$ vs. $\delta^{13}\text{C}_{\text{DIC}}$ covariance of core PTB as well as varying $\delta^{18}\text{O}$ and $\delta^{13}\text{C}$ isotope values in the carbonate and organic sediments, sediment composition and pollen. The co-variation data is to be used as an indicator of hydrological conditions in the CCB, which can be used as a platform for further interpretation of proxy-data.

Depth (m)	Unit	Unit age (cal yr BP)	Hydrologic system
1	7		Closed $R^2 = 0.882$
2		12,156 ± 411	
3	6		Open $R^2 = 0.092$
4		28,051 ± 417	
5	5		Closed/Open (transitional) $R^2 = 0.28$
6		31,164 $\pm 2,204$	
7	4		Open $R^2 = 0.182$
8		37,466 $\pm 2,528$	
9	3		Closed $R^2 = 0.685$
10		54,356 $\pm 2,464$	
11		56,380 $\pm 2,639$	Open $R^2 = 0.001$
12			
13	1		Closed w/ open periods $R^2 = 0.557$
14			
15		84,905 $\pm 8,449$	

Figure 5.25. Classical age/depth model (CLAM) applied to units 1-7. Top and bottom dates are applied to each unit based on the cm scale age point estimates predicted by CLAM. Hydrology of the CCB (open vs. closed system) is also displayed based on $\delta^{18}\text{O}_{\text{CARB}}$ vs. $\delta^{13}\text{C}_{\text{DIC}}$ linear covariance (Figs. 5.21 and 5.22).

5.7.1 Unit 1. $84,900 \pm 8,500 - 56,400 \pm 2,600$ cal yr BP

The chronology of core PTB can only be accurately constrained to the lower U-series date of $56,180 \pm 2,250$ cal yr BP, making unit 1 chronologically the least reliable from core PTB. However, the extrapolated basal age of $84,900 \pm 8,500$ cal yr BP for core PTB means that it is potentially one of the longest palaeoenvironmental records obtained for N. America, although without accurate chronological control this inference is hard to substantiate.

Covariance data (Figs. 5.22 and 5.25) suggest Poza Tierra Blanca to be largely a closed system with stable $\delta^{18}\text{O}_{\text{CARB}}$ values showing high variability. Sedimentologically, the unit is largely comprised of banded organic marls displaying alternate layers of marl and peat, dubbed 'the marble cake effect' (Fig. 5.26, appendices 2.2.1 and 2.2.2).

With the CCB currently experiencing an 8 year drought [from APFFCC data], peat formation within the CCB is directly observed to be associated with drying events. Within the basin, drying pools create a marsh area, increasing the bulk organic matter before a complete drying of the water body creates a semi-terrestrial peat forming wetland environment (Fig. 5.27) [from my own observations and APFFCC observations]. The alternating marl and peat suggests Poza Tierra Blanca experienced rapid wetting and drying events respectively, supported by the highly variable isotopic results where more negative $\delta^{18}\text{O}_{\text{CARB}}$ values are associated with the more organic rich sediments, particularly between 1,469 cm and 1,451 cm, and where the lowest $\delta^{18}\text{O}_{\text{CARB}}$ values between -14.3‰ and -12.7‰ are observed within organic banded marl sediments. These more negative $\delta^{18}\text{O}_{\text{CARB}}$ values can suggest two possible theories: 1) disequilibrium precipitation of carbonate as a result of a shift to eutrophic conditions [e.g. Fronval *et al.*, 1995]; 2) a change in the atmospheric circulation from Pacific dominated to the Gulf of Mexico (GoM) dominated, where precipitation generally displays more negative $\delta^{18}\text{O}$ values [Wassenaar *et al.*, 2009], rather than short term trends in water influx and evaporation [e.g. Yu *et al.*, 1997]. It is proposed that, rather than $\delta^{18}\text{O}$ values from the moisture influencing the $\delta^{18}\text{O}$ value in the sediment, change in atmospheric moisture source drives a drying climate, creating a peat forming wetland.

Over the course of the unit $\delta^{13}\text{C}_{\text{ORGANIC}}$ values decrease from -13.2‰ (C_4/CAM) to -21.7‰ (CAM/C_3) where $\delta^{18}\text{O}_{\text{CARB}}$ values increase from -10.3‰ to -6.2‰ (Figs. 5.12, 5.20, and 5.23) suggesting a gradual shift from a dry climate toward a wetter climate. Records for the Trans-Pecos and Chihuahuan desert regions suggest substantially wetter conditions than the present between 71 ka BP and 57 ka BP [Musgrove *et al.*, 2001; Metcalfe *et al.*, 2002]. This wetter period begins toward the centre of unit 1 (c.12.5 m, Fig. 5.12) ending at the transition to unit 2. The upper missing section of unit 1 (1,020 cm – 1,076 cm) could possibly contain the majority of this wet period, with unit 2 possibly displaying the final 1 kyr (Figs. 5.12). $\delta^{18}\text{O}_{\text{CARB}}$ values appear to begin to stabilize between 1,140 cm and 1,076 cm again suggesting the missing section could be the beginning of stable, hydrologically open conditions.

The continued presence of juniper, pine and oak (Fig. 5.23) throughout unit 1, although in low numbers, support the hypothesis of open oak and pine woodland in Chihuahua [Metcalfe *et al.*, 2002]. The presence of other mesic species – *Fraxinus*, *Artemisia* and *Aster* – toward the top of unit 1 also indicate a climatic wet shift at this point, corroborated by stabilising $\delta^{18}\text{O}_{\text{CARB}}$ values (Figs. 5.23 and 5.24), adding to the theory of a hydrologically closed to open system transition within the unit.



Figure 5.26. Alternating bands of marl and peat within unit 1 of core PTB. Soft sediment deformation can be seen within the peat banding which is a process of percussion coring.



Figure 5.27. Modern peat formation in a marsh (ciénega) area of the CCB. Peat formation is the product of the drying process whereby grasses and mosses populate the marshland, increasing biomass and creating peat.

5.7.2 Unit 2. $56,400 \pm 2,600 - 54,300 \pm 2,500$ cal yr BP

Sedimentologically, unit 2 is carbonate dominated – carbonate marl and tufa (Fig. 5.13 and appendix 2.2.1 and 2.2.2) - which in itself suggests this unit is climatically wetter as increased precipitation recharge on the surrounding Cretaceous limestone mountains may cause the formation of artesian springs on the CCB floor (see chapters 2 and 4). The presence of tufa suggests an increase in groundwater input into the hydrologic system, increasing spring activity and CaCO_3 dissolution [Ford and Pedley, 1996; Pedley *et al.*, 2003; Pentecost, 2005]. Unit 2 appears to be beyond the 71 ka BP to 57 ka BP wet period for N. Mexico/S. United States, although the uncertainty within the age/depth model and residence time of water discharging from the Cupido-Aurora aquifer could possibly place this unit at the end of this wet period at 1,013 cm.

$\delta^{18}\text{O}_{\text{CARB}}$ values maintain a small range between -7.4‰ and -7.7‰ along with very low R^2 covariance (0.01); suggesting Poza Tierra Blanca in unit 2 is hydrologically open, suggesting increased water in the CCB. It is widely believed that the periods of increased moisture in N. Mexico are caused by the displacement of the westerly storm tracks during glacial periods [Metcalf *et al.*, 2002]. $\delta^{18}\text{O}_{\text{CARB}}$ values in this unit are similar to the modern day $\delta^{18}\text{O}_{\text{LAKEWATER}}$ value of -5.68‰ sampled at Poza Tierra

Blanca (see chapter 2). The modern day pool is situated in the centre of a hydrologically open evaporative through flow system in a larger closed basin system suggesting the $\delta^{18}\text{O}_{\text{CARB}}$ values may indicate a similar flow system to the one observed in the modern environment.

The evidence for increased moisture in the CCB could possibly indicate the presence of a stadial period at this time. Musgrove *et al.*, 2001 suggest that the wet period - 71 ka BP to 57 ka BP – in S. Texas is a process of precessional orbital forcing, increasing the dominance of the Pacific moisture source with increased winter precipitation and maximum soil saturation. This model may also be applicable to the CCB, as cooler temperatures associated with precession favour groundwater recharge due to lower evaporation. It is shown (chapter 2) that Poza Tierra Blanca water, today, is derived from the Cupido-Aurora aquifer that has flowed from the west of the basin, experiencing evaporative effects as it flows. However, a wetter climate in the CCB is thought increase head pressure of groundwater recharging in the local mountain range resulting in the activation of artesian springs [Johannesson *et al.* 2004; chapters 3 and 4]. Tierra Blanca tufa $\delta^{13}\text{C}_{\text{DIC}}$ values range from -1.1‰ to -0.4‰ and unit 2 $\delta^{13}\text{C}_{\text{DIC}}$ values range from -2‰ to -0.2‰ . Thus, the activation of Tierra Blanca spring mound, in close proximity to Poza Tierra Blanca, may have resulted in the pool being sourced from increased local groundwater discharge. The modern day $\delta^{13}\text{C}_{\text{DIC}}$ value of Poza Tierra Blanca is -18‰ suggesting the catchment of the pool is derived more from soil CO_2 and terrestrial plant matter which may indicate the wide carbon sources as the water flows across the CCB floor (see chapter 2). The more positive $\delta^{13}\text{C}_{\text{DIC}}$ values of the carbonate in unit 2 suggest the source water has some influence from the surrounding Cretaceous limestone. Increased dissolution of the Cretaceous limestone from local precipitation would lead to increased bicarbonate in the water, accounting for $>10\text{‰}$ variations in $\delta^{13}\text{C}_{\text{DIC}}$ values in core PTB e.g. Lake Jih Tan [Stuiver, 1975], indicating the possibility of more localised Pacific sourced moisture directly raining out onto the CCB mountains and recharging into the hydrologic system, rather than recharging from the Cupido-Aurora aquifer as is seen today.

The presence of mesic pollen taxa – *Picea*, *Carya* and *Fraxinus* – within unit 2 along with spikes of increased wetland taxa – *Aster*, *Amaranthaceae* and *Poaceae* – also suggests the period 56,993 yr BP to 54,993 yr BP to be wetter.

5.7.3 Unit 3. $54,300 \pm 2,500 - 37,500 \pm 2,500$ cal yr BP

A change in diatom species suggests a shallowing of lake conditions in Chihuahua c.57 ka BP [Metcalf *et al.*, 2002] with a dramatic shift to concentrated lake levels at 54.6 ka BP. Towards the end of unit 2 and into unit 3, c.54 ka BP, a large decrease of -6.1‰ is seen in the $\delta^{18}\text{O}_{\text{CARB}}$ values (Figs. 5.13 and 5.14) which could possibly indicate lake level decrease in the CCB, as is seen more widely in Chihuahua.

After this point, the $\delta^{18}\text{O}_{\text{CARB}}$ isotope record in unit 3 is highly variable but maintains an average of -11.2‰ , slightly lower than the average of unit 1. Covariance of 0.685 (R^2) also suggests Poza Tierra Blanca is hydrologically closed along with the highly variable $\delta^{18}\text{O}_{\text{CARB}}$ values. Periodic desiccation and deflation are reported in Chihuahua between 54.6 ka BP and 38.5 ka BP which is in part supported by the $\delta^{18}\text{O}_{\text{CARB}}$ and $\delta^{13}\text{C}_{\text{ORGANIC}}$ isotopic values, the pollen record and the alternating carbonate marl/peat lithology (Figs. 5.14, 5.24 and appendices 2.2.1 and 2.2.2). Like unit 1, this may suggest a shift to eutrophic lake conditions driven by a change in the dominate moisture source to the GoM, bringing more arid conditions. The presence of key mesic taxa *Picea*, *Fraxinus* and *Betula* at 900 cm, 820 cm and 800 cm respectively alongside spiked isotopic increases in the $\delta^{18}\text{O}_{\text{CARB}}$ values (Fig. 5.23) suggest these three points to be associated with greater groundwater recharge within the CCB and coinciding with periods of deep water in Chihuahua [Metcalf *et al.*, 2002]. Percentage abundance increases of wetland *Aster*, *Amaranthaceae* and *Poaceae* (Figs. 5.14, 5.23 and 5.24) also suggest these three points to be much wetter, despite the unit as a whole displaying generally very negative $\delta^{18}\text{O}_{\text{CARB}}$ isotopic values. The xeric *Celtis* species is only present within the unit at 810 cm, coinciding with a decrease from -10.1‰ to -14.2‰ in the $\delta^{18}\text{O}_{\text{CARB}}$ values (Figs. 5.14 and 5.23). As mentioned previously, $\delta^{18}\text{O}_{\text{CARB}}$ values as low as -14.2‰ are not reasonable values to associate solely with MAT change and atmospheric circulation change. Including the aforementioned two, a number of other factors must contribute to such negative $\delta^{18}\text{O}_{\text{CARB}}$ values, the main one being disequilibrium effects possibly due to eutrophication and preferential uptake of ^{16}O in the mineralization of calcite.

When the $\delta^{13}\text{C}_{\text{ORGANIC}}$ values are within the isotopic range of C_4 vegetation (-12.8‰ at 889 cm) the $\delta^{18}\text{O}_{\text{CARB}}$ values are at their lowest (-14.2‰), again suggesting

decreases within the $\delta^{18}\text{O}_{\text{CARB}}$ values indicate an arid shift and GoM dominated moisture source. Complex interplay between the circulation patterns of the Pacific and Gulf of Mexico due to climate forcing [Musgrove *et al.*, 2001] could be important, as shifts between summer and winter atmospheric patterns change source waters as well as changing lake levels which could lead to periods of eutrophication and desiccation. Isotopically lighter source waters, lower soil saturation and higher evaporation within a summer, GoM climate could create an environment less conducive to groundwater recharge within the pools of the CCB, creating a closed basin system, with periodic episodes of increased water recharge coinciding with changes to winter dominated conditions.

Toward the top of unit 3 $\delta^{18}\text{O}_{\text{CARB}}$ values begin to increase with a transition from an average of -11.2‰ to -8.1‰ observed, suggesting a possible transition into hydrologically open conditions.

5.7.4 Unit 4. $37,500 \pm 2,500 - 31,200 \pm 2,200$ cal yr BP

Musgrove *et al.*, [2001] propose the Trans-Pecos region of Texas experienced a significantly wetter period between 39 ka BP and 33 ka BP. During unit 4, Poza Tierra Blanca exhibits hydrologically open characteristics with R^2 covariance of 0.182 whilst $\delta^{18}\text{O}_{\text{CARB}}$ values maintain a fairly constant range between -5.5‰ and -6.3‰ , encompassing the modern $\delta^{18}\text{O}_{\text{LAKEWATER}}$ value for Poza Tierra Blanca of -5.68‰ . Unit 4 exhibits slightly more positive $\delta^{18}\text{O}_{\text{CARB}}$ values than unit 2 but has similar low $\delta^{18}\text{O}_{\text{CARB}}$ vs. $\delta^{13}\text{C}_{\text{DIC}}$ covariance and mesic pollen taxa. Again, like unit 2 and the Tierra Blanca tufas (see chapter 4), unit 4 displays a limited range of $\delta^{13}\text{C}_{\text{DIC}}$ values between -3.1‰ and -0.4‰ (Fig. 5.19), suggesting the source water to be of a superambient meteoric origin with karst sourced carbon. Interestingly, within unit 4, the carbonate-rich sediment in Poza Tierra Blanca contains an abundance of hydrobiid snails, known to be endemic to the CCB [Hershler, 1984; Hershler and Minckley, 1986; Badino *et al.* 2004]. Studies of these snails within the modern pools of the CCB have shown them to live in thermal pools with temperatures between 29°C and 37.8°C whilst favouring carbonate-rich sediments and waters. The abundance of these snails within the sediment of unit 4 again suggests the water to be of a superambient meteoric origin and may indicate a

hydrologic link to the active Tierra Blanca spring mound during climatically wetter periods.

There is a presence of xeric pollen taxa within unit 4 – *Prosopis* and *Celtus* toward the beginning (700 cm to 550 cm) of the unit before these two species disappear and *Agavaceae* becomes present in small numbers (Fig. 5.24). The disappearance of xeric pollen taxa is consistent with regional vegetation change, where an emergence of mesic taxa as the dominant taxa is seen after 36 ka BP [Elias and Van Devender, 1990]. Unit 4 contains the only presence of the mesic *Abies* species at 670cm and 600cm suggesting these two periods experienced much wetter and more temperate climates, favourable for the growth of *Abies* [Schorn and Wehr, 1986]. $\delta^{13}\text{C}_{\text{ORGANIC}}$ isotope values are between -19.5‰ and -21.9‰ (Figs. 5.15 and 5.23) throughout unit 4 which fall into the low range of C_3 , high range CAM and aquatic macrophyte vegetation suggesting the vegetation between $37,500 \pm 2,500$ cal yr BP and $31,200 \pm 2,200$ cal yr BP was better suited to more temperate and wet conditions. The appearance of marginal aquatic vegetation e.g. *Typha*, and upland mesic vegetation and CAM photosynthesizers e.g. *Prosopis*, in the pollen record corroborate the C/N ratios in the range of aquatic macrophyte and CAM vegetation types (Fig. 5.20). Of the aquatic vegetation in unit 4, *Typha* is present for the first time in core PTB along with higher numbers of *Poaceae* and *Amaranthaceae* suggesting that this period was much wetter than the previous hydrologically open period in unit 2. *Fraxinus*, *Picea*, *Acer*, *Pinus* and *Quercus* all have their highest numbers in this unit also, with the mesic taxa all exhibiting highest numbers toward the beginning and end of the unit, suggesting the middle of unit 4 to be drier, coinciding with an increase in *Prosopis* (Figs. 5.23 and 5.24)

Toward the end of unit 4 and into unit 5 mesic and aquatic pollen taxa all show a rapid decrease in numbers along with a large decrease in *Pinus* abundance, coinciding with negative shift in $\delta^{18}\text{O}_{\text{CARB}}$ values from -5.9‰ to -8.8‰ and a gradual increase in the $\delta^{13}\text{C}_{\text{ORGANIC}}$ values from -21.3‰ to -19.8‰ (Figs. 5.15 and 5.16) suggesting enhanced C_4 vegetation input and drying environment at c. 31 ka BP.

5.7.5 Unit 5. 31,200 ± 2,200 – 28,051 ± 417 cal yr BP

Relatively few data are available for unit 5 although low R^2 covariance of 0.28 suggests Poza Tierra Blanca is largely hydrologically open at this time. Metcalfe *et al.*, [2002] suggest lake levels in Chihuahua to be highly variable up to 29 ka BP which is consistent with very negative $\delta^{18}\text{O}_{\text{CARB}}$ values at the beginning of unit 5 (Fig. 5.16). However, it is suggested [Elias and Van Devender, 1990; Huang *et al.*, 2001] that Chihuahua maintained C_3 vegetation dominance, peaking at 27 ka BP. At 525 cm (Figs. 5.23 and 5.24) a large positive shift in the $\delta^{18}\text{O}$ isotope value of the carbonate is observed (-8.8‰ to -2‰ , $+6.8\text{‰}$) synchronously with a large increase in upland and wetland pollen taxa (Figs. 5.23 and 5.24). Upland mesic species - *Pinus*, *Picea* and *Artemisia* – and wetland species – *Amaranthaceae*, *Poaceae* and *Cyperaceae* – all increase suggesting the presence of a climatically wet period in unit 5. The wet shift observed is not a prolonged event, but is short lived and high magnitude and could possibly be related to the H3 Heinrich event c.30 ka BP [Bond and Lotti, 1995; Vidal *et al.*, 1999; Roche *et al.*, 2004] with a shift to a predominance of westerly storm tracks and cooler and wetter conditions in the north of Mexico. The dumping of glacial water into the N. Atlantic from the H3 event in interstadial conditions may have caused wetter climate to be pushed down to N. Mexico from a much more northerly position, although the timing (ka BP) of the H3 Heinrich event is debateable [Kirby and Andrews, 1999; Grousset *et al.*, 2000].

Rapid carbonate rich sediment accumulation in Poza Tierra Blanca during unit 5 (198 cm deposited in c. 3 kyr) is consistent with higher water level and a climatically wet period in the CCB, with flooding events causing rapid sedimentation as is seen at San Bernadino ciénega in the Sonora Desert [Minckley and Brunelle, 2007]. Again, hydrobiid snails are present within the sediment for unit 5 suggesting that, like unit 4, there may be a hydrologic connection with Tierra Blanca spring.

Toward the top of unit 5 and into unit 6 a 7.5‰ negative shift (from -5.5‰ to -13‰) followed by a 7.8‰ positive shift (from -13‰ to -5.3‰) in $\delta^{18}\text{O}_{\text{CARB}}$ values is observed synchronously with decreases in numbers of mesic and wetland pollen taxa (Figs. 5.16, 5.23 and 5.24). The presence of peat within the stratigraphy at this point, ^{14}C dated to 28,051 cal yr BP, suggests a shift to a closed hydrology and drying of Poza

Tierra Blanca. This could be a process associated with catchment instability seen in Chihuahua [Metcalf *et al.*, 2002] before the onset of full glacial conditions at the Last Glacial Maximum (LGM). A rapid recovery of the hydrology is seen after this drying event, possibly the result of increased displacement of the westerly storm tracks and wetter climatic conditions.

5.7.6 Unit 6. 28,051 ± 417 – 12,200 ± 400 cal yr BP

A much cooler, wetter climate for Chihuahua and Texas is proposed during the LGM [Elias and Van Devender, 1990; Huang *et al.*, 2001; Musgrove *et al.*, 2001; Metcalf *et al.*, 2002]. The presence of the Laurentide ice sheet is generally accepted to be the reason for this with the southward displacement of the westerly storm tracks and the Intertropical Convergence Zone (ITCZ) bringing a dominance of colder, wetter conditions.

The presence of tufa within Poza Tierra Blanca, like unit 2, between 360 cm and 317 cm is a lithological indicator of much wetter conditions the CCB with deposition of tufa over a c.6 kyr period observed (Fig. 5.17). $\delta^{13}\text{C}_{\text{DIC}}$ values of the tufa range from -1.1‰ to +0.2‰ for this period, again supporting a shift to wetter conditions conducive to tufa deposition, similar to Tierra Blanca spring mound (see chapter 4). Sparse pollen data is available at the beginning of the unit due to the presence of tufa but constant $\delta^{18}\text{O}_{\text{CARB}}$ values (between -6.6‰ and -5.9‰) and a low R^2 covariance of 0.092 also support the suggestion that this period is much wetter. $\delta^{13}\text{C}_{\text{ORGANIC}}$ values also remain relatively constant between 360 cm and 317 cm (-23.7‰ and -20.2‰) (Figs. 5.17 and 5.23), with C/N ratios predominantly within low range C_3 and macrophyte vegetation types but with some high range CAM vegetation as well (Fig. 5.20). The continued presence of CAM vegetation species throughout core PTB, however, may be misleading. Shifts from C_3 to C_4 vegetation types, and vice versa, will typically show mixed $\delta^{13}\text{C}_{\text{ORGANIC}}$ isotope values and C/N ratios which may be interpreted as CAM vegetation [Barbour and Billings, 2000; Sharp, 2007]. However, the Chihuahuan Desert, in particular the CCB, does contain large numbers of CAM vegetation types e.g. *Agavaceae* and *Cactaceae*, living in semiarid montane areas [Kemp, 1983; Burgess and Shmida, 1988; Barbour and Billings, 2000; Badino *et al.*, 2004], as can be seen figure 5.24. Kemp [1983] states that C_3 and CAM vegetation

types are less dependent on soil moisture than C₄ vegetation in arid areas with changes in vegetation types more closely linked to temperature rather than moisture availability with mesic microsites e.g. areas of pooled water, able to support C₃ and CAM vegetation in what is otherwise considered an arid area. This can be applied to the CCB but highlights the diversity of the CCB vegetation and the importance of proxy pollen data to support the $\delta^{13}\text{C}_{\text{ORGANIC}}$ isotope data.

A gap in the record after 317 cm up to 240 cm follows the stable hydrologically open period. A 1.1‰ negative shift in the $\delta^{18}\text{O}_{\text{CARB}}$ values between 240 cm and 210 cm (15,900 ± 800 to 13,100 ± 500 cal yr BP) coincides with a regional drying period in Chihuahua c. 15 ka BP to 12 ka BP [Elias and Van Devender, 1990; Huang *et al.*, 2001; Metcalfe *et al.*, 2002]. This regional drying can be attributed to the Bolling-Allerod period where glacial melt water influx to the Gulf of Mexico (GoM) is proposed from c.15 ka BP to c.12 ka BP [Kennett and Shackleton, 1975; Flower *et al.* 2004] which may have caused a change in regional climate in Chihuahua and southern Texas. Reduced sea ice and a northward shift in the ITCZ [Peterson *et al.* 2000; Clark *et al.* 2001; Escobar *et al.* 2012] would have resulted in a shift to a GoM summer precipitation regime causing the North American Monsoon (NAM) and ITCZ to briefly be dominant drivers of climate, resulting in regional drying. A greater presence of xeric pollen taxa – *Prosopis*, *Agavaceae* and *Celtus* – at this time is also a strong indicator of a shift to more arid conditions in the CCB.

5.7.7 Unit 7. 12,200 ± 400 cal yr BP - present

It is widely considered that the onset of arid conditions in the regions surrounding the CCB began around the Pleistocene-Holocene boundary (c.12 ka BP to 10 ka BP) [Bryant, 1977; Bryant and Holloway, 1985; Van Devender, 1985; Elias and Van Devender, 1990; Anderson and Van Devender, 1995; Huang *et al.*, 2001; Musgrove *et al.*, 2001; Metcalfe *et al.*, 2002; Minckley and Jackson, 2008]. Little isotopic data is available for unit 7 although R² covariance of 0.88 (the highest observed throughout the PTB sequence) suggests this unit is hydrologically closed.

Decreasing numbers of regional upland mesic taxa coincides with increasing numbers of xeric species c.10 ka BP to 7 ka BP, although some areas became refugia for more temperate species [Bryant and Holloway, 1985]. Relatively constant $\delta^{18}\text{O}_{\text{CARB}}$

values and persistence of mesic pollen taxa into the beginning of unit 7 (Figs. 5.18 and 5.23) suggests the CCB may have been a desert refuge up to at least 9,470 cal yr BP. Castiglia and Fawcett [2006] add credence to this theory with the suggestion that a period wet enough to support pluvial lakes in Chihuahua existed up to 8.27 ka BP. The presence of a thick peat layer after 9,467 cal yr BP in core PTB suggests that conditions dried dramatically after the possible persistence of increased groundwater recharge.

The predominance of peat within the unit 7 stratigraphy suggests the Holocene to be largely dry although the occurrence of xeric species as the dominant pollen taxa does not occur until the top of the unit, consistent with full onset of arid conditions in Chihuahua between 6 ka BP and 4 ka BP [Van Devender, 1985; Elias and Van Devender, 1990; Anderson and Van Devender, 1995; Huang *et al.*, 2001; Musgrove *et al.*, 2001; Metcalfe *et al.*, 2002; Minckley and Jackson, 2008].

5.8 Regional and global climate change or environmental stability in the CCB?

The time period covered by this study, based on the basal age of $84,900 \pm 8,500$ cal yr BP, encompasses the last glacial period, c.85 ka BP to 11 ka BP, almost in its entirety. Stable isotope and pollen data in units 2, 4 and 6 suggests that these units were hydrologically open and climatically wetter with a dominance of winter conditions. These wet periods, particularly units 2 and 4, coincide with the Tahoe and Tenaya stadial periods of the last glacial period, before the onset of full Laurentide ice sheet conditions (Tioga stadial) in unit 6 [Ehlers and Gibbard, 2004].

It is widely accepted that during the last glacial maximum the presence of the Laurentide ice sheet caused the southward displacement of the ITCZ and a dominance of westerly trade winds, resulting in wetter conditions in central and northern Mexico [Metcalfe *et al.* 2000; Musgrove *et al.* 2001; Stevens *et al.* 2012]. The same climatic mechanism could be applied to the possible stadial periods, coinciding with units 2 and 4, in the CCB to propose the cause of the hydrologically open conditions in the basin at these times. A southward shift of the ITCZ and dominance of westerly trade winds bringing moisture from the Pacific would have caused cooler, wetter conditions in N. Mexico, including the CCB (Fig. 5.2). The timing of this transition has been the focus of much debate [Metcalfe *et al.* 2000] but the possibility of cooler, wetter conditions would allow for expansion of mesic and wetland vegetation species, observed in the

pollen record, as well as increasing groundwater recharge from the Cupido-Aurora aquifer, creating a hydrologically open system. The Cupido-Aurora aquifer originates in the Bolson de Mapimi, in the Sierra Madre Oriental to the west of the CCB. Pacific moisture sources are currently prevented from reaching the CCB because of the presence of the Sierra Madre Occidental and Sierra Madre Oriental [Badino *et al.*, 2004]. During climatically wetter periods, increased rainout from Pacific sourced moisture could occur due to the presence of the mountains, recharging the Cupido-Aurora aquifer and subsequently increasing groundwater flow in the CCB. Coupled with increased groundwater flow, an increased moisture body from the west could also provide rainout in the CCB itself, increasing local precipitation and recharge from the main recharge zone of the Sierra San Marcos y Pinos. However, it is suggested [Stevens *et al.* 2012] that these cooler and wetter conditions did not reach more easterly basins in the central highlands of Mexico. Instead, a temperature depression around the time of the LGM [Lozano-García and Vásquez Salem, 2005] is proposed to have reduced evaporation, thus relating various records of increased wetness to reduced evaporation rather than increased winter precipitation. The timing of the wet season is not clear and precipitation varied seasonally through the Late Pleistocene in the eastern basins making the exact timing of wet/reduced evaporation periods hard to substantiate and translate in to the record from the CCB.

The timing of the negative $\delta^{18}\text{O}_{\text{CARB}}$ shift in core PTB at the top of unit 6 coincides with regional and global records of glacial meltwater dumping in the Gulf of Mexico during the Bolling-Allerod period (~15 to 13 ka BP) [Kennett and Shackleton, 1975; Elias and Van Devender, 1990; Metcalfe *et al.* 2000; Peterson *et al.* 2000; Clark *et al.* 2001; Huang *et al.* 2001; Metcalfe *et al.* 2002; Flower *et al.* 2004; Escobar *et al.* 2012]. It is thought to have caused a northward shift in the ITCZ and a dominance of Gulf of Mexico moisture source, which will have resulted in arid conditions within the CCB.

The possibility of the CCB being controlled by regional cooling and wetting during hydrologically open periods also has major implications for the climate controls during hydrologically closed periods. Highly variable interstadial periods, originally identified in the Greenland and Vostok ice cores [Dansgaard *et al.*, 1993; Petit *et al.*, 1999], are observed within the CCB during units 1, 3, 5 and 7. These hydrologically

variable units display a lot more variability in the $\delta^{18}\text{O}_{\text{CARB}}$ values suggesting changes in regional moisture source and moisture volume, which are controlled by global climate, are reflected in the CCB palaeoenvironment. Small increases and decreases observed in units 1, 3, 5 and 7 (Figs. 5.12, 5.14, 5.16 and 5.18) most likely reflect weighted average annual, decadal or centennial fluctuations in dominant moisture sources and/or *E/P* relationships [Clotts *et al.*, 2009]. However, larger isotopic swings not associated with changes in sediment type could possibly reflect a response to global climate fluctuations as observed in unit 5 ($31,200 \pm 2,200$ to $28,051 \pm 417$ cal yr BP).

5.9 Conclusions and future work

Although core PTB is not chronologically well constrained past 1,013 cm depth, the reliability of the ^{14}C and U-series dates above this depth give a good classical age/depth model. Based on the age/depth model, a maximum age of $84,900 \pm 8,500$ cal yr BP for core PTB is proposed, possibly making this palaeoenvironmental record the oldest in N. Mexico and one of the oldest in N. America.

Stable isotope values ($\delta^{18}\text{O}_{\text{CARB}}$, $\delta^{13}\text{C}_{\text{DIC}}$ and $\delta^{13}\text{C}_{\text{ORGANIC}}$) and pollen in core PTB yielded a multi-proxy record spanning the last ~84 ka, despite gaps in the sediment column. Variations in $\delta^{18}\text{O}$ and $\delta^{13}\text{C}$ values occur with changes in sediment lithology, suggesting these variables responded to changes in CCB hydrology. Carbonate rich sediments i.e. marl and tufa, are marked by higher, narrow ranging $\delta^{18}\text{O}_{\text{CARB}}$ and $\delta^{13}\text{C}_{\text{DIC}}$ values and were deposited under higher water level conditions with an increased input of groundwater sourced from recharge in the high mountains. Organic rich sediments are marked by lower $\delta^{18}\text{O}_{\text{CARB}}$ and $\delta^{13}\text{C}_{\text{DIC}}$ values and were deposited during arid periods where periodic desiccation and low water level created wetland environments.

$\delta^{18}\text{O}_{\text{CARB}}$ and $\delta^{13}\text{C}_{\text{DIC}}$ covariance displayed an alternating pattern of closed/open basin hydrology in the CCB. Three units – 2 (~56 to 54 cal ka BP), 4 (~37 to 31 cal ka BP) and 6 (~28 to 12 cal ka BP) – support the notion of wetter climate conditions, through open hydrologic conditions similar to the through-flow system seen today in the CCB, that correlate well with known stadial periods [Ehlers and Gibbard, 2004]. The isotope record supports regional interpretations of wet climate during stadial conditions where the southerly shift of the ITCZ and predominance of westerly trade winds brought moisture from the north Pacific. In these three periods, proxy pollen, C/N ratios and

$\delta^{13}\text{C}_{\text{ORGANIC}}$ isotope values also suggest a dominance of mesic and wetland vegetation types and montane woodland expansion to the CCB floor. Four units – 1 (~84 to 56 cal ka BP), 3 (~54 to 37 cal ka BP), 5 (~31 to 28 cal ka BP) and 7 (~12 cal ka BP to present) – support the notion of highly variable hydrologic conditions where complex interplay between summer (northerly position of ITCZ) and winter (southerly position of ITCZ) monsoon moisture sources is proposed to have controlled climate. Mid-high $\delta^{18}\text{O}_{\text{CARB}}$ and $\delta^{13}\text{C}_{\text{DIC}}$ covariance suggest Poza Tierra Blanca was highly susceptible to changing hydrologic conditions, with increasingly closed lake conditions marked by periods of desiccation coinciding with organic rich sediment deposition and possible lake eutrophication. In these four periods, proxy pollen, C/N ratios and $\delta^{13}\text{C}_{\text{ORGANIC}}$ isotope values also suggest a dominance of xeric vegetation types and the retreat of montane woodland to the high mountain peaks.

The pollen, lithological and stable isotope data from core PTB suggest the CCB is responsive to global climate change patterns. A high magnitude, short lived $\delta^{18}\text{O}_{\text{CARB}}$ shift in unit 5 (~31 to 28 cal ka BP) coincides with the H3 Heinrich event, whereby much wetter climate is proposed for the CCB due to glacial meltwater pulses causing a southerly shift in the ITCZ and westerly trade winds. A negative shift in the $\delta^{18}\text{O}_{\text{CARB}}$ record in unit 6 is interpreted as the transition from the LGM to the deglacial involving a shift from wet climate, high water discharge conditions to arid climate, low water discharge during the Bolling-Allerod period (~15 to 13 cal ka BP). The palaeoenvironmental record presented in this chapter is in agreement with regional pollen and diatom records obtained from N. Mexico and also with moisture records from the southern USA, suggesting the possibility of stadial-interstadial climate controls [Peterson *et al.* 2000; Clark *et al.* 2001; Musgrove *et al.*, 2001; Metcalfe *et al.*, 2000, 2002]. This suggests both that the stable isotopic and pollen data are accurate and that the CCB climate is in tune with regional climate patterns.

Key upland pollen data supported the $\delta^{18}\text{O}_{\text{CARB}}$ and $\delta^{13}\text{C}_{\text{ORGANIC}}$ data well, adding credibility to the overall moisture balance in the CCB, suggested by the stable isotopic data, and also highlighting the importance of a multi-proxy research approach in a palaeoenvironmentally understudied and complex area.

However, further work on the chronology of core PTB is still warranted, as an absolute age/depth model of the core is still unknown. No tufa carbonate is available at 15 m but, dependent of several parameters, dating of carbonate rich marls could be possible, as shown by Li *et al.*, [1989], Schwarcz [1989] and Torfstein *et al.*, [2009]. Further detailed coring work within the CCB is proposed as the marl and peat sediments contain excellent palaeoenvironmental records that are chronologically containable. It may be necessary to use an alternate coring method as the Acker percussion corer does not line the hole, leading to possible re-sampling of sediment and the nature of percussion coring leads to soft sediment deformation, liquefaction and possible loss of sediment. A complete core sequence could be possible if a combination of a Livingston (or similar) and Acker corer is used. A Livingston coring method would increase the possibility of complete recovery of a core sequence within the soft sediments but would not be able to penetrate the tufas within the sequence. The use of the percussive Acker coring method would result in tufa recovery whilst soft sediment recovery would be achieved with a Livingston coring method. The CCB's response to global climate fluctuations is possibly reflected within the $\delta^{18}\text{O}_{\text{CARB}}$ isotope values. However, large shifts up to 10‰ for both $\delta^{18}\text{O}_{\text{CARB}}$ and $\delta^{13}\text{C}_{\text{DIC}}$ may not be representative of actual environmental change. Disequilibrium effects and changes in lake catchment and source water may be worth investigating in more detail to determine any non-climate related changes in the palaeoenvironmental record. A quantitative approach is needed on the modern day lacustrine sediments in the CCB to identify the mechanisms driving any disequilibrium effects observed in the Palaeo-record i.e. natural eutrophication or lake stratification. This is crucial to interpretation of the proxy data as if disequilibrium effects can be identified and corrected in the isotopic composition of the sediment archive, further more detailed fractionation equations may be possible. This aspect of the CCB palaeoenvironment, particularly during interstadial conditions, warrants further research as a continuous depositional sequence from the CCB could allow a long spanning environmental record to be recorded and integrated within the global context.

As the CCB groundwater flow, the main input of water in the basin, originates predominantly in the Bolson de Mapimi, to the west of the CCB, further work could involve detailed studies of hydrology at the source of the groundwater. Detailed

comparisons can then be made between the Bolson de Mapimi and CCB to determine the full hydrological controls influencing the CCB.

This study has shown that although the CCB appears to have undergone extensive environmental change over the Late Pleistocene/Holocene, contradicting Meyer's [1973] hypothesis of environmental stability, the basin has remained relatively hydrologically stable enabling the high degree of observed endemism. This hydrological stability could be misinterpreted as environmental or climatic stability if a multi-proxy research approach is not adopted, so great care has to be taken when interpreting the palaeoenvironmental record of the CCB. However, further stable isotopic, pollen and chronological work is required to conclusively demonstrate this palaeoenvironmental change in the CCB. An alternate lake coring strategy could be used to obtain a complete stratigraphic sequence which would allow for a complete isotopic and pollen sequence to be obtained. A complete stratigraphic sequence would allow for a more accurate covariance data set also.

Chapter 6: Discussion

This chapter provides an overall discussion of the study. By combining results and common themes from previous chapters, an overall interpretation of palaeoenvironmental change and its subsequent impact on human populations can be determined.

6.1 Hydrology and palaeoenvironment of the Cuatro Ciénegas Basin

Data from modern day water bodies and core PTB sediments suggests the hydrology of the CCB, as well as the environment, has changed considerably over time [see chapters 2 and 5]. Meyer [1973] suggested that pollen assemblages indicated conditions in the CCB from the present up to, and possibly beyond 31 ka BP, were stable. Minckley and Jackson [2008] later suggested that conditions had varied from the Late Pleistocene, c.16 ka BP, to the present day based on pollen data from a pack rat midden. It is also widely accepted that, regionally, wetter climate in the Late Pleistocene/Holocene the north of Mexico is a result of the dominance of westerly storm tracks and southward displacement of the ITCZ caused by the presence of a N. American ice sheet [Metcalf *et al.*, 2000]. The isotopic and palynological record obtained from core PTB [see chapter 5] demonstrated considerable variability within the CCB hydrology and environment, supported by modern hydrological data in chapter 2 and tufa geomorphological observations in chapter 3. The evidence suggests hydrological and environmental changes are climatically driven, an interpretation supported by regional climate reconstructions from both N. Mexico and the Trans-Pecos (USA) (Table 6.1), and contradicting Meyers [1973] original conclusion of environmental stability in the CCB.

Table 6.1. Summary table comparing the palaeoenvironmental interpretation obtained from this study with previous published studies from the Chihuahuan Desert and southern United States region.

Chronology (cal ka BP)	No data	This study	Meyer [1973]	Minckley & Jackson [2008]	Metcalfe <i>et al.</i> , [2002]	Musgrove <i>et al.</i> , [2001]	Elias & Van Devender [1990]	Castiglia & Fawcett [2006]
0								
5		Wet conditions and dominant mesic vegetation suggest the CCB to be a desert refuge up to 9.2 ka BP. Inherent forest sediments indicate onset of aridity c. 9 ka BP and extreme aridity c. 8 ka BP.	High numbers of desert floor taxa - Compositae - dominate the pollen record from 31 ka BP to the present. Environmental stability and climatic homogeneity inferred from the pollen record.	Decreasing numbers of C_3 vegetation taxa indicate a woodland retreat to higher altitudes. Increasing numbers of desert taxa suggest onset of aridity. Chihuahuan montane woodland extended to the CCB valley floor.	Wet conditions re-established c. 24 ka BP. Shallowing thought to be related to the Younger Dryas wet but not high-Holocene. Marked shallowing of All Babiocom between 11 and 9.4 ka BP.	Much drier environment with higher temperatures indicated by a marked slowing of speleothem growth rate.	Complete shift to arid conditions although some temperate species existed up to 6 ka BP in low numbers. Onset of extreme aridity at 6 ka BP.	Four periods - 8.5 to 8.2 ka BP, 6.7 to 6.1 ka BP, 4.2 to 3.8 ka BP and 221 BP - wet enough to support pluvial lake conditions. Highly variable Chihuahuan climate inferred.
10								
15								
20								
25								
30								
35								
40								
45								
50								
55								
60								
65								
70								
75								
80								
85								

6.1.1 Climatically wet environments in the Cuatro Ciénegas Basin

The last known prolonged wet period in N. Mexico was during the LGM (~24 ka BP – 12 ka BP) [Metcalf *et al.*, 2000; Musgrove *et al.* 2001; Metcalfe *et al.* 2002] (Table 6.1). Evidence of this wet period is interpreted within the core PTB record as hydrologically open (wet) conditions, displayed as an isotopically stable period within the $\delta^{18}\text{O}_{\text{CARB}}$ record in unit 6 (~28 to 12 cal yr BP) with low $\delta^{18}\text{O}_{\text{CARB}}$ vs. $\delta^{13}\text{C}_{\text{DIC}}$ covariance (Figs. 5.17 and 5.21, chapter 5). Two other periods – unit 2 (~56 to 54 cal yr BP) and unit 4 (~37 to 31 cal yr BP) – within core PTB demonstrated similar isotopic stability and low covariance (Figs. 5.13, 5.15 and 5.21, chapter 5) suggesting these, like unit 6, may display hydrologically open characteristics with winter monsoon conditions primarily providing the moisture source, possibly indicating stadial conditions in the CCB beyond the LGM (Figs. 6.1 and 6.2; Table 6.1; also see chapter 5).

Figure 6.1. Geology of the Cuatro Ciénegas Basin with transect (A-B) used in Figures 6.2 and 6.3 [modified after Badino *et al.*, 2004; Rodriguez *et al.*, 2005].

Musgrove *et al.* [2001] propose increased moisture in the Trans-Pecos region of the USA without the presence of an ice sheet. The three observed rapid growth periods are mirrored by the apparent hydrologically open (wet) periods and increased discharge in the CCB, displayed in units 2, 4 and 6 (Table 6.1), suggesting that the CCB hydrology is responsive to regional climate change caused by the southward displacement of the ITCZ and increased dominance of westerly trade winds bringing moisture from the Pacific Ocean. The dominant moisture source from the west may

have also been responsible for recharging the Cupido-Aurora aquifer, originating in the Bolson de Mapimi to the west of the CCB [Badino *et al.* 2004; Johannesson *et al.* 2004; Rodriguez *et al.* 2005]. Increased precipitation would increase water volume in the aquifer which in turn would increase groundwater discharge in the CCB, expanding the hydrological system [see chapters 2, 3 and 5]. Increased discharge would create a hydrologically open lake system, similar to that seen in the modern day CCB [see chapter 2], but on a larger scale, suggested from the presence terrestrial carbonate formations and possible playa lake formation [see chapter 3]. Lithological and stable isotope data from core PTB also support this inference as carbonate rich sediments (marl and tufa), particularly in unit 4 (~37 to 31 cal ka BP), containing hydrobiid mollusc shells coincide with higher $\delta^{18}\text{O}_{\text{CARB}}$ and $\delta^{13}\text{C}_{\text{DIC}}$ values (Figs. 5.15 and 5.19, chapter 5) suggesting increased artesian spring activity, depositing tufa at Tierra Blanca spring mound, from a thermal water source [see chapter 4 and 5].

Vegetation type in the CCB appears to be closely linked with the climate and hydrology, particularly during the LGM (unit 6) [see chapter 5]. Because of the unique hydrological conditions and mountainous terrain in the CCB, certain upland vegetation types - *Pinus* (Pine), *Quercus* (Oak), and *Juniperus* (Juniper) - and wetland vegetation types - *Typha* (Cattail) - are consistently present within the palaeoenvironmental record (Figs. 5.23 and 5.24, chapter 5). However, variation in the percentage abundance of these species along with the increased presence of mesic and wetland plant species during units 2, 4 and 6 indicates a much wetter, more temperate climate during these periods. This interpretation is supported by Elias and Van Devender [1990] (Table 6.1), who suggest warm wet conditions prevailed at the beginning of the LGM with insect species showing a propensity to woodland vegetation. Evidence of *Carya* (Hickory) at the Tierra Blanca spring mound [see chapter 4] also suggests the presence of hydrologically open (wet) conditions in the CCB. *Carya* requires a much more temperate climate to grow with and is dependent on a large water resource. Increased moisture input from the dominant winter conditions would increase hydrological flow in the CCB, creating an environment able to sustain *Carya* whilst also increasing wetland vegetation. These data spanning over 50,000 years provide evidence of a broader distribution for many extant coniferous and wetland taxa onto the lower slopes of mountains and CCB floor that, today, are extinct from these lower ranges.

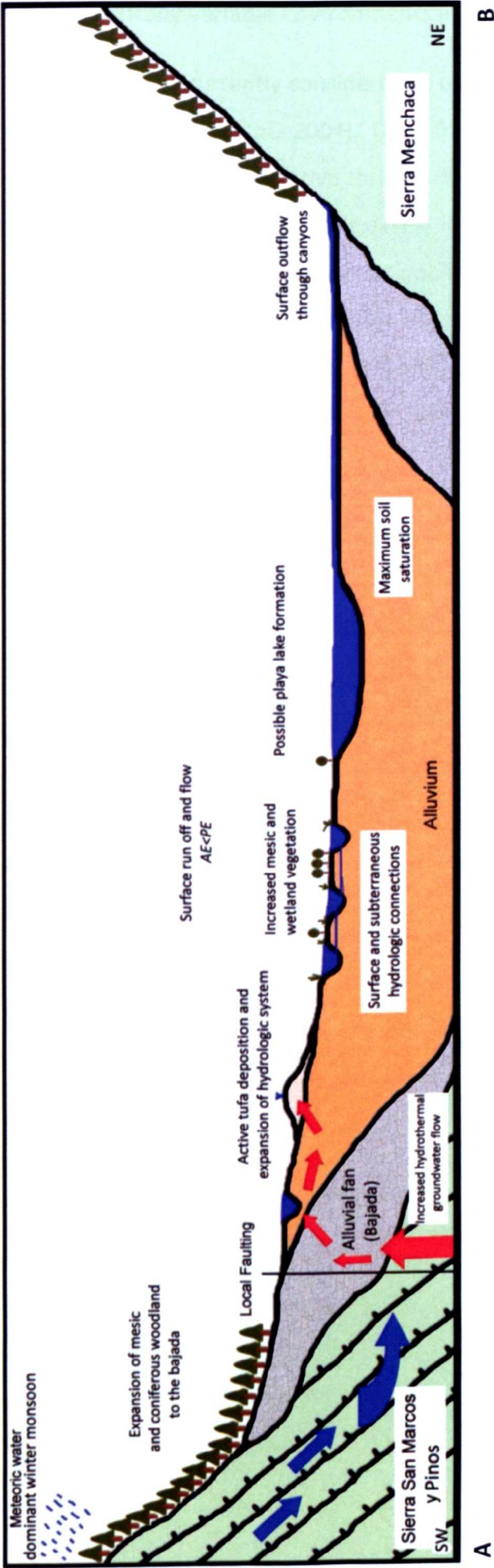


Figure 6.2. Schematic model of stadal conditions in the CCB during units 2, 4 and 6. Dominance of winter monsoon climate with hydrologically open basin characteristics provided a stable basis for woodland expansion down to the bajada level and wetlands suitable for mesic vegetation on the CCB floor.

6.1.2 Climatically variable environments in the Cuatro Ciénegas Basin

The CCB is currently considered to be a hydrologically closed basin [Badino *et al.* 2004; Johannesson *et al.* 2004]. Data from this study [see chapter 2] suggests a hydrologically open evaporative through-flow system, in a larger closed basin, flowing from the west between the pools, lakes, rivers and ciénegas (marshes), before ending in a series of hypersaline, endorheic pools to the east. Inactive terrestrial tufa facies e.g. Tierra Blanca spring mound [see chapters 3 and 4] observed within the modern through-flow system also suggest hydrologically closed conditions, as to be active, increased water discharge and head pressure are needed for tufa deposition to be achieved.

The current closed hydrological regime was established c.4 ka BP, coinciding with evidence of regional drying (unit 7, ~12 cal yr BP to the present, Table 6.1). This sustained period of closed basin hydrology provides an excellent regime from which apply to previous isotopically variable periods identified in the CCB – units 1 (~84 to 56 cal yr BP), 3 (~54 to 37 cal yr BP) and 5 (~31 – 28 cal yr BP) (Figs. 6.1 and 6.3, also see chapter 5). Although high $\delta^{18}\text{O}_{\text{CARB}}$ vs. $\delta^{13}\text{C}_{\text{DIC}}$ covariance data (Fig. 5.21, chapter 5) of these periods suggest the CCB is predominantly closed hydrologically, the low water table and low soil saturation created a highly changeable environment and periodic wetting and desiccation of Poza Tierra Blanca, as indicated by the alternating carbonate/organic rich sediments (Figs. 5.12, 5.14, 5.16 and 5.18, chapter 5). Poza Tierra Blanca, being located at the centre of the evaporative through-flow system and of shallow depth, would be particularly receptive to moisture changes [Shemesh, 2011; Shemesh *et al.* 2001], possibly indicating the presence of climatically variable interstadial conditions, also suggested by regional climate interpretations (Table 6.1). A modern example of climate instability has been observed in the CCB where, as recent as June 2010 [APFFCC], sudden hurricane conditions caused flooding and up to 3 m re-filling of previously dry pools, indicating substantially wet episodes are likely during hydrologically closed periods. Events such as these, assuming regular occurrence, may partly explain isotopic variability in $\delta^{18}\text{O}_{\text{CARB}}$ record during these periods (Figs. 5.12, 5.14, 5.16 and 5.18, chapter 5).

The isotopic variability within core PTB during hydrologically closed basin conditions indicates dry and wet phases are represented $\delta^{18}\text{O}_{\text{CARB}}$ value decreases and increases respectively [see chapter 5]. These results are unusual as dry phases, in semi-arid/arid regions, are usually represented by $\delta^{18}\text{O}$ enrichment due to preferential evaporation of ^{16}O , with wet phases represented by $\delta^{18}\text{O}$ depletion due to preferential rainout of ^{16}O [Leng and Marshall, 2004]. Interestingly however, due the CCB hydrology, the observed negative $\delta^{18}\text{O}_{\text{CARB}}$ shifts appear to represent a disequilibrium effect of increased organic sediment deposition, controlled by increasing aridity from a change in the dominant moisture source to GoM. Increased dominance of xeric pollen taxa e.g. *Prosopis* (Figs. 5.23 and 5.24, chapter 5) and increased $\delta^{13}\text{C}_{\text{ORGANIC}}$ values of organic matter, suggesting increased input of C_4 vegetation [see chapter 5]. It is likely that during times of extreme drought, as is currently being experienced in the CCB, the pools, lakes and rivers never become completely dry, instead the drying of the water body creates a marsh environment, rich in organic matter [see chapter 2]. It is this increase in organic matter and subsequent decomposition that appears to cause the extreme negative shifts in $\delta^{18}\text{O}_{\text{CARB}}$ values during dry periods. The large negative shifts of up to 10‰ (Fig. 5.12, chapter 5) are not representative of actual environmental change but apparent disequilibrium effects caused by a climatically dry phase.

Although evaporative enrichment is observed on surface flow in the modern CCB hydrology, the fractionation effect of evaporation on the $\delta^{18}\text{O}_{\text{LAKEWATER}}$ appears to be minimal until reaching the endorheic, east side of the basin [see chapter 2]. Thus, evaporation of the CCB surface waters does not appear to control the $\delta^{18}\text{O}_{\text{CARB}}$ record during climatically dry periods.

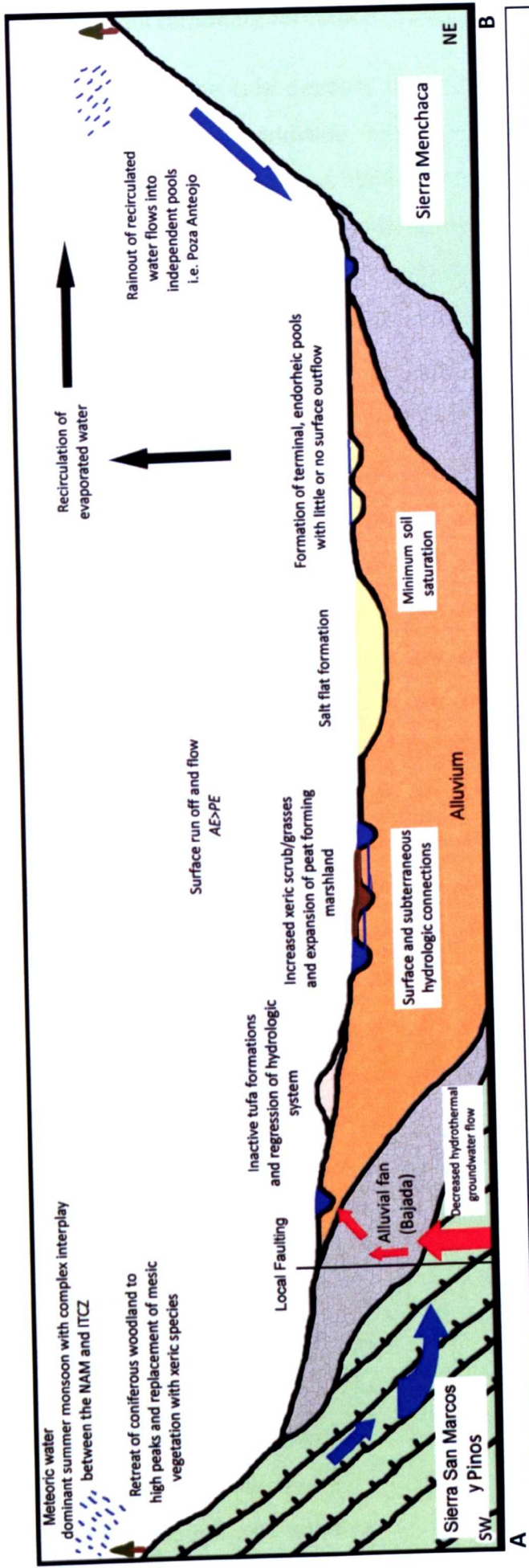


Figure 6.3. Schematic model of possible interstadial, high aridity conditions in the CCB during units 1, 3, 5 and 7. These conditions currently prevail in the CCB. Dominance of summer monsoon climate with hydrologically closed basin characteristics caused by complex interplay between the NAM and ITCZ. Decreased groundwater flow coupled with increased evaporation caused the formation of salt flats and endorheic pools.

6.2 Terrestrial carbonate formation, hydrology and environment

Although the tufa deposits in the CCB have not been previously described, reports and studies worldwide indicate their importance in palaeoenvironmental reconstructions [Andrews *et al.* 1993; Andrews *et al.* 1997; Pedley *et al.* 2003; Ortiz *et al.* 2009; Brasier *et al.* 2010]. The presence of carbonate (tufa) formations in the CCB are, in themselves, an indication of previous episodes of wetter climate and increased hydrological outflow [see chapters 3 and 4]. Tufa in the CCB is deposited in the modern day environment, although on a much smaller scale than previous hydrological regimes, as indicated by inactive tufa facies e.g. the perched tufa terrace [see chapter 3]. In this respect, the CCB is similar to Pamukkale, Turkey [Altunel and Hancock, 1993], where increased tufa deposition is observed during climatically wet periods due to higher rates of carbonate dissolution and increased hydrostatic head pressure. During dry periods, tufa deposition still occurs on a smaller scale as sub-surface hydrogeology remained unchanged. The suggestion of constant groundwater discharge has major implications for the floral and faunal endemism observed in the CCB, as the stable isotopic data in chapter 5 suggests water to be always present despite fluctuations in climate.

The tufas described in the CCB are all located in close proximity to the piedmont of the Sierra San Marcos y Pinos, which is in the centre of the evaporative through-flow system observed in the basin [see chapter 2] and also located close to thrust faulting along the axis of the Sierra San Marcos y Pinos [see chapter 3]. The location of the tufa formations suggests that their occurrence is due to increased local and regional moisture input and the subsequent combination of reactivated fault controlled hydrology and increased surface flow across the CCB. The varying facies of tufa deposition e.g. Tierra Blanca spring mound [see chapter 4] and perched tufa terrace [see chapter 3], are indicators of reactivated fault controlled hydrology. Increased $\delta^{13}\text{C}_{\text{DIC}}$ values of the carbonate, between -2.6‰ and $+0.2\text{‰}$, of these two particular tufa facies have been shown to suggest increased dissolution of the CCB Cretaceous limestone by superambient meteogene water [see chapter 3], supporting fault controlled hydrology [see chapters 3 and 4]. The constant hydrostatic head pressures that are required to deposit the superambient meteogene tufa, which both the spring mound and perched tufa terrace are composed of, are only achievable

through increased precipitation at higher elevations creating enough pressure to force groundwater discharge through faults and fissures, indicating a considerably wetter climate. The wetter climate reactivating fault controlled hydrology also suggests increased surface flow in the CCB; Tierra Blanca spring mound $\delta^{13}\text{C}_{\text{DIC}}$ values of the carbonate, between -1.1‰ and -0.4‰ , are within $\delta^{13}\text{C}_{\text{DIC}}$ value of the carbonate range between -3.1‰ and $+0.2\text{‰}$ in core PTB during proposed hydrologically open (wet) periods (Figs. 5.13, 5.15 and 5.17, chapter 5) providing further supporting evidence.

Extinct rim-stone pool complexes provide further evidence that increased surface flow has existed in the CCB [see chapter 3]. Currently, active pools exist on the fringes of the rim-stone pool complex that, when a larger water body is present, would expand, depositing tufa and creating a series of pools like those seen in the extinct rim-stone pool complex. Although dating of terrestrial tufa formations is limited within the CCB, a date of 7,240 cal yr BP was obtained for the spring mound complex [see chapter 4], placing at least this tufa facies within the Holocene, when regional conditions wet enough to support pluvial lake formation are thought to have existed episodically [Castiglia and Fawcett, 2006; Table 6.1].



Figure 6.4. Photograph displaying abundant *Acoelorrhaphe wrightii* palm frond impressions and encrustations, towards the base of the perched tufa sequence.

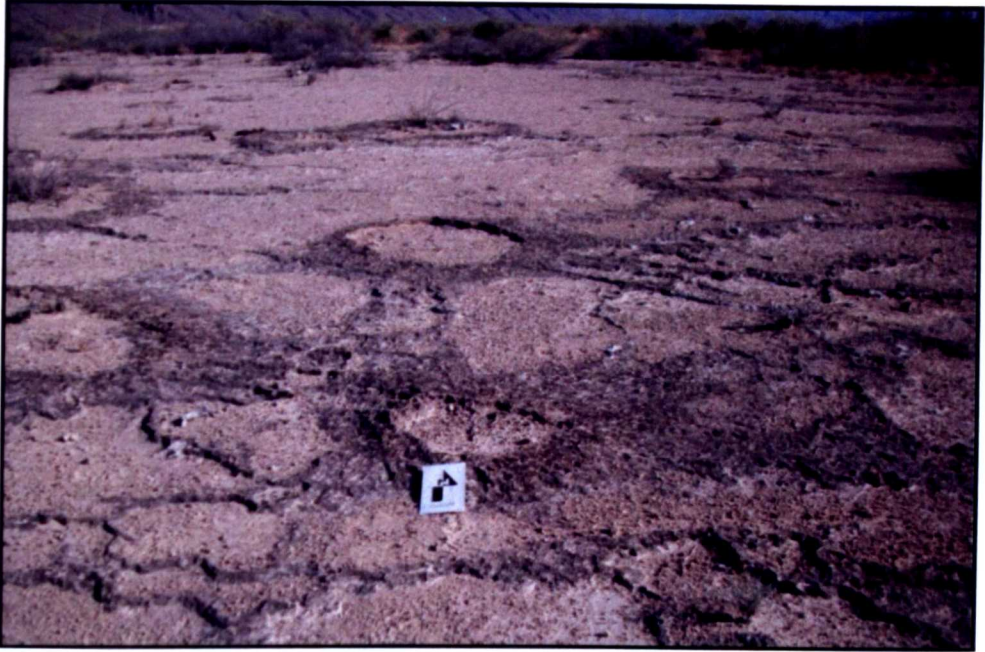


Figure 6.5. Well preserved Sotol grass impressions in what is now a completely dry area in the CCB.

The importance of the CCB tufas as palaeoecological archives is also evident. Preservation of both extinct and extant vegetation types of the CCB is excellent within the tufas (Figs. 6.4 and 6.5) with direct fossil evidence of wetter conditions in what are now completely arid areas of the basin [see chapter 3]. The wetland taxa preserved in the tufa can be seen growing in the modern hydrological system in the CCB, suggesting the hydrologic system of the CCB may have expanded as water volume increased before retracting up to the modern day limit as water volume decreased, similar to expansions and retractions of the hydrologic system observed in Pamukkale, Turkey [Altunel and Hancock, 1993; Dilsiz *et al.* 2004]. In Pamukkale, increased thermal circulation in previously wetter climatic conditions is attested by the existence of calcium carbonate deposits around ancient spring emergences at altitudes of up to 500 m higher than the modern system [Dilsiz *et al.* 2004]. The thermal waters surfacing and mixing with cold, shallow ground water changed the chemistry of the water, facilitating calcium carbonate deposition. During the drying periods, calcium carbonate deposition is suggested to occur at increasing depth below the discharge due to lack of mixing with cold, shallow groundwater. This is observed by a deepening base level of calcium carbonate deposition through time [Altunel and Hancock, 1993; Dilsiz *et al.*

2004]. This expansion and retraction of the Pamukkale hydrologic system suggests there is a multi-layer aquifer system where deep thermal fluids only mix with cold, shallow groundwater when hydraulic pressure is enough to force the thermal fluids to the surface. The presence of inactive tufa facies in the CCB reinforces the theory of the CCB hydrologic system expanding and retracting during wet and dry phases respectively. The current hydrologic system is at lower elevations to the ancient spring emergences, suggesting that there is reduced hydraulic pressure caused by decreased recharge of precipitation at high altitude. The presence of a modern flow system despite the observed reduction in hydraulic pressure from inactive tufa facies, further suggests the CCB benefits from a multi-layer aquifer system [see chapter 2]. The suggested multi-layer aquifer system reduces the likelihood of the CCB completely drying, furthering the implications of endemism being linked to water availability within the basin.

6.3 Palaeoenvironment and archaeology

The survival strategy of the hunter-gatherers of the CCB appears to have been controlled by atmospheric moisture and its subsequent control of water availability and vegetation for food and material production. Excavations and reports by Taylor [1956; 1964; 1966; 1968; 1972 and 2003] suggest the range of human occupation in the basin spans from $9,300 \pm 400$ yr BP to the present over three archaeological complexes; dating evidence from this study both augments and extends this existing chronology for human occupation in the CCB. U-series dates of 10,500 yr BP and 7,240 yr BP for the two footprint sites in the basin extend Taylor's chronology up to the Late Pleistocene-Holocene boundary, long before the onset of contemporary desert conditions c.4 ka BP [Table 6.1].

Taylor [2003] also proposed the theories of 'tethered nomadism' and 'water territoriality' to be key within all three of the CCB's archaeological complexes throughout the Holocene due to the aridity of the Chihuahuan Desert. Whilst records of climate change in the Chihuahuan Desert and Trans-Pecos suggest complete drying and aridity at several stages throughout the Holocene [Table 6.1], the multi-proxy data from this study [see chapters 2, 3 and 5; Table 6.1] suggests the CCB has never completely dried out.

Habitation sites of Coahuilan Indians lie at the juncture between the mouths of canyons and the alluvial fans, mountain regions known as the 'monte' [Taylor, 1964; 1966; 1968; 1972 and 2003]. Indeed, the majority of the well stratified cave deposits associated with the Coahuilan Indians are located in the mountains surrounding the CCB (Fig. 6.6). The main assumption to be made with these habitation sites is their location is such that the nomads were close to both the primary food source – desert succulents – and to a water source. Frightful Cave, Nopal Shelter, Fat Burro Cave and CM-109 contain the most, and oldest, archaeological material including sandals, arrow heads, grinding stones and vegetal fibre. However, in the archaeological record of these habitation sites there is no evidence of vessels for the purpose of carrying water. Dependable water sources and the lack of potable water in conditions of increasing environmental aridity through the Holocene [see chapter 5; Table 6.1], would be the limiting factor in extended cycles of nomadism to the surrounding Chihuahuan Desert in search of food with low nutritional value. However, having a dependable water source suggests the existence of social control assuring the right to pre-emptive use of water [Taylor, 1964].

No society can survive with violent competition for primary resources; the Mayan Civilization is thought to have collapsed due to social unrest in drought conditions [Hodell *et al.* 1995; Curtis *et al.* 1996; Gill, 2000]. The continued, well stratified archaeological record in the CCB habitation sites attests to some form of social control of water resources through times of extreme aridity or low population density. The constant and dependable water sources in the CCB combined with the scarcity of available food sources adds credence to the theory that human occupants were effectively 'tethered' to the basin.

The presence of the Laurentide ice sheet over N. America may have implications for a southward migration of fauna to the CCB from the onset of the LGM c.24 ka BP to at least the first retreat of the ice c.15 ka BP. Stable isotope and pollen data suggest the CCB may have become a Chihuahuan Desert refuge during the LGM with favourable coniferous wooded vegetation and increased, stable moisture availability (Figs. 5.18, 5.23 and 5.24, chapter 5). Archaeological accounts discuss the use of grinding stones and food storage in various localities in the CCB [Taylor, 1966; 1972]. Roasted and chewed agave leaves, or 'quids', are the most commonly found

food resource in the occupation sites of the CCB. Not only was agave used as sustenance, but also the fibrous leaves were utilized as material fibre for netting, sandal production and sacks, suggesting agave to be the most important resource. Caches of xeric vegetation such as mesquite, hackberry, pine and acacia seeds were found in Frightful Cave throughout all three archaeological complexes along with dried fruit, pads and seeds of prickly pear suggesting heavy exploitation of these resources [Taylor, 2003], which will have become more important toward the end of the Holocene when climate became drier and these xeric taxa increased in abundance. Despite stable isotope determination of palaeodiet not being possible on the human remains of the CCB due to lack of access to human skeletal material, pollen data presented from core PTB (Figs. 5.23 and 5.24, chapter 5) indicates the increased presence of nut/seed bearing trees such as hickory (*Carya*), mesquite (*Prosopis*), agave (*Agavaceae*) and pine (*Pinus*) and also the presence of desert succulents such as prickly pear (*Opuntia*) throughout the Holocene (unit 7). Vegetal foods, particularly in the Late Holocene, would most likely have provided the largest proportion of the subsistence strategy of the Coahuilan Indians

Occupation sites have produced a great number of faunal remains, most commonly rabbits, deer and rodents but also megafaunal remains including bison (*Bison bison*) and elk (*Cervus canadensis*) no longer native to the CCB [Gilmore, 1947], indicating these fauna would have been a valuable food resource. It is likely these megafauna existed in the CCB up to the beginning of Taylor's [2003] 'Coahuila complex' c.7.5 kyr BP, after which climate conditions became warmer and drier (Table 6.1). However, it is possible these megafauna may have existed up to the onset of extreme aridity c.4 ka BP as the climate appears to be highly variable up to this point with episodic periods of increased moisture [Elias and Van Devender, 1990; Metcalfe *et al.* 2002; Castiglia and Fawcett, 2006]. Remains of the Columbian mammoth (*Mammuthus columbi*) found in the CCB pools suggest these megafauna may have survived in the CCB along with other megafaunal populations, however, without direct dating evidence of the mammoth specimens found in the CCB, this is hard to substantiate.

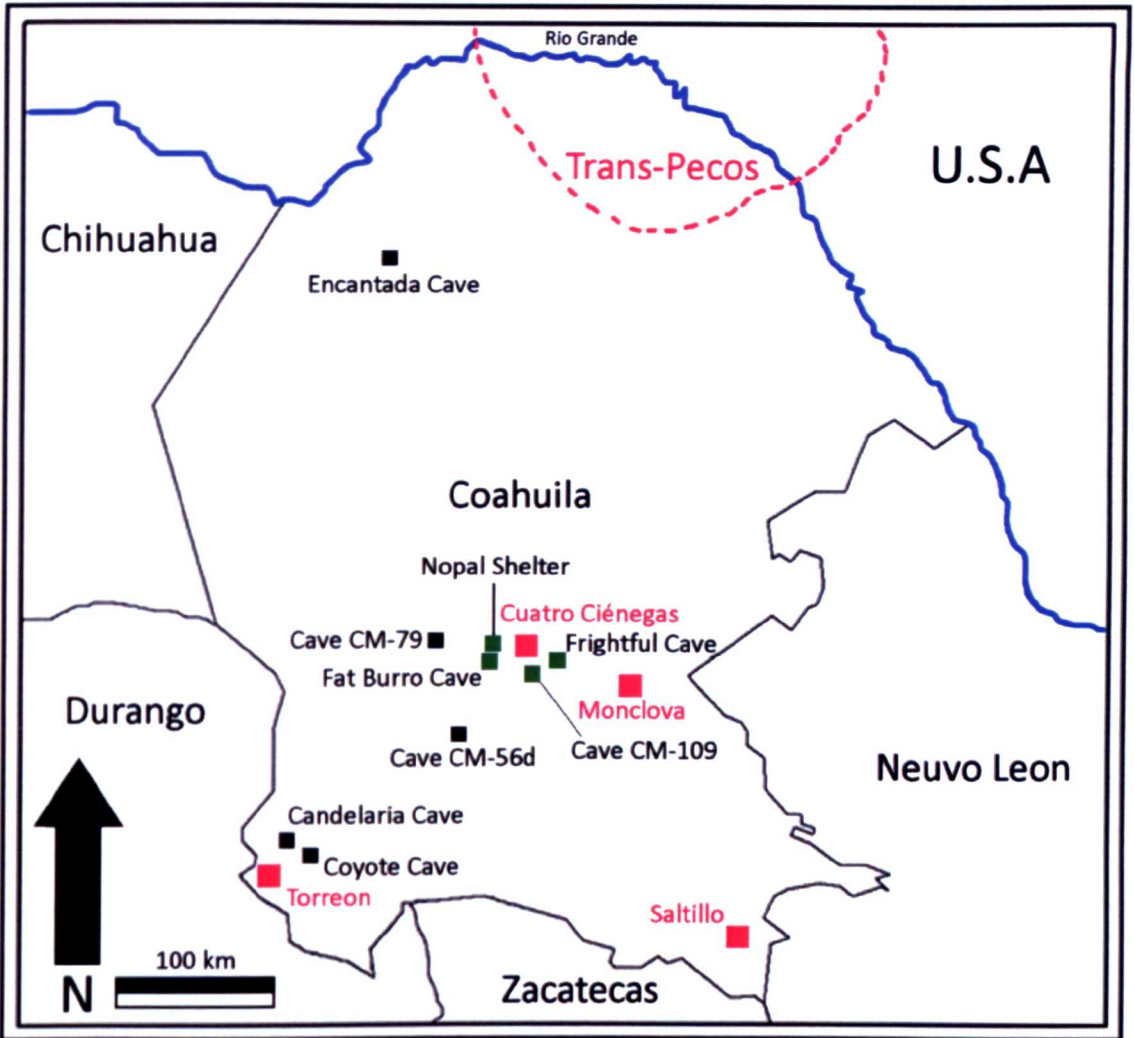


Figure 6.6. Locations of archaeological cave sites in Coahuila state, in particular within the Cuatro Ciénegas Basin (marked with green squares).

Stable isotope and pollen evidence of unit 7 (~12 cal ka BP to present) indicates climate instability (Fig. 5.18, chapter 5). Due to the suggested continual presence of the pools, lakes and rivers throughout the Holocene, resources associated with the aquatic aspect of the environment i.e. fish (*Herichthys minckleyii*), and freshwater shrimp (*Palaemonetes suttkusi*) may have been utilized. Although not mentioned within the archaeological records of the CCB, the *in situ* footprint location on Tierra Blanca spring mound [see chapter 4] suggests some form of hunting and/or gathering may have occurred around the pool location. This valuable food resource is known to have been utilized in the Laguna District of Coahuila – Candelaria Cave and Coyote Cave [Taylor, 1972] (Fig. 6.3) and the shared cultural traditions of Coahuilan Indian tribes suggest that the hunter-gatherers of the CCB may have used aquatic food resources in times of climate change and terrestrial food resource instability.

6.4 Regional and global controls of hydrology and endemism

The stadial-interstadial cycles that are possibly observed within the seven units of core PTB sequence during the last glacial period (c.85 ka BP to 11 ka BP) suggest that the CCB is responsive to regional climate change in the north of Mexico and southern United States and possibly global events, such as the H3 Heinrich (~30 ka BP) and the Bolling-Allerod (~15 to 13 ka BP) (Table 6.1) [also see chapter 5]. This not only carries major implications of environmental change in the CCB but also major implications that floral and faunal endemism observed within the basin is not linked to environmental stability as first proposed [Minckley, 1969; Meyer, 1973] but rather, endemism is linked to constant water availability throughout the stadial-interstadial cycles.

The expansion and retraction of the hydrologic system during hydrologically open (stadial) and hydrologically closed (interstadial) periods respectively, can be observed within the inactive tufa formations e.g. Tierra Blanca spring mound, rimstone pool complex, and contemporary pools, rivers and lakes in the CCB [see chapter 2]. Increased water discharge during the proposed hydrologically open (stadial) periods (Figs. 5.13, 5.15 and 5.17, chapter 5) in the CCB and is supported by the, now, inactive tufa formations observed in arid areas of the basin [see chapter 3]. Increased water head pressure and groundwater discharge would have been required for these tufa formations to be active. The dominant Pacific winter monsoon may have recharged the Cupido-Aurora aquifer in the Bolson de Mapimi, to the west, creating increased groundwater discharge in the CCB whilst increased precipitation in CCB itself would create sufficient head pressure to force the groundwater to the surface.

Decreased water discharge during hydrologically closed (interstadial) periods (Figs. 5.12, 5.14, 5.16 and 5.18, chapter 5), as is currently observed in the CCB, indicates reduced regional moisture input and a dominant summer monsoon regime controlled by the northward shift in the ITCZ and NAM (Metcalf *et al.* 2000; Table 6.1). This reduced aquifer recharge in the Bolson de Mapimi could lead to reduced discharge of groundwater in the CCB, and reduced precipitation of summer monsoon conditions would lead to the formation of terminal, endorheic pools to the east of the CCB. However, the 'reduced' hydrologic flow in the CCB during interstadials does not

cause the complete drying of groundwater fed pools, rivers and lakes, as can be seen in the modern day environment. This may be the result of karst reservoirs and sustained Cupido-Aurora aquifer discharge, with suggested residence times of up to 1500 years [Johannesson *et al.*, 2004], with an inflow volume \geq evaporation volume, effectively propping up the hydrologic system.

The possibility of the CCB having never before become completely dry has major implications for endemism observed in the basin. Currently, over 70 species of flora and fauna are endemic to the CCB; this is widely thought to indicate a large period of biogeographic isolation [Badino *et al.*, 2004] although it has been proposed that a surface hydraulic connection existed at some point during Late Holocene [Echelle and Echelle, 1998]. The suggested continual groundwater source of the CCB, even during times of extreme aridity regionally in the Chihuahuan Desert, will have facilitated a desert refuge since at least $56,180 \pm 2,250$ cal yr BP and possibly as far back as $84,900 \pm 8,500$ cal yr BP. If biogeographic isolation has not occurred for a sufficient period of time to allow species to become endemic, due to surface hydraulic connections, the continual presence of water creating a refuge may be an important reason as to why endemism does occur in the CCB.

Chapter 7: Conclusion

7.1 Aims

The aim of this thesis was to examine the palaeoenvironmental evidence of climate change and associated human responses in the Cuatro Ciénegas Basin (CCB), Coahuila State, NE Mexico from the Late Pleistocene to the present and to obtain a clear picture of the palaeoclimate, hydrology and geoarchaeology. This would be achieved by addressing the following objectives:

- To investigate the palaeoenvironment of the Cuatro Ciénegas Basin from the Late Pleistocene/Holocene to the present through stable isotope and palynological analysis of a 15 m sediment core located in the basin.
- To investigate modern hydrogeology and water flow patterns by stable isotope analysis to obtain a conceptual hydrologic model, applicable to palaeohydrological regimes.
- To explore the relationship between terrestrial tufa formations and previous environmental and hydrological regimes within the Cuatro Ciénegas Basin.
- To explore the relationship between palaeoenvironmental change and consequent human response through integrating archaeological excavations of human footprints with published studies of Coahuilan Indians.

All four of the above objectives have produced results. The work conducted on the modern hydrology of the CCB suggests the basin is currently functioning as a hydrologically closed evaporative through-flow system, providing a useful model from which to identify previous hydrological regimes. Two evaporative through-flow systems have been identified, both surfacing from groundwater discharge on the flanks of the Sierra San Marcos y Pinos before flowing towards the east of the CCB into a series of terminal, endorheic pools. An independent system of evaporation-precipitation fed pools was also identified, suggesting the possibility of re-circulated water from an independent aquifer in the basin. Observations of brine evolution from the west to the east of the CCB corroborate the through-flow system identified from the stable isotope data. Gypsum dunes in the west of the CCB are followed by tufa formation at the piedmont of the Sierra San Marcos y Pinos and salt flats in the east.

The now inactive tufa formations in the centre of the throughflow system also attest to the expansion of previous hydrological regimes in the CCB through increased groundwater recharge.

The palaeoenvironmental work conducted in the CCB has demonstrated the basin contains a long spanning - ~85 kyr - multi-proxy environmental record responsive to both regional and global climate changes. Stable $\delta^{18}\text{O}_{\text{CARB}}$, $\delta^{13}\text{C}_{\text{DIC}}$ and $\delta^{13}\text{C}_{\text{ORGANIC}}$ isotopic, palynological and $\delta^{18}\text{O}_{\text{CARB}}$ vs. $\delta^{13}\text{C}_{\text{DIC}}$ covariance data complemented each other well suggesting the environment of the CCB has changed substantially from as early as $84,900 \pm 8,500$ cal yr BP to the present. $\delta^{18}\text{O}_{\text{CARB}}$, $\delta^{13}\text{C}_{\text{DIC}}$ and $\delta^{13}\text{C}_{\text{ORGANIC}}$ and $\delta^{18}\text{O}_{\text{CARB}}$ vs. $\delta^{13}\text{C}_{\text{DIC}}$ covariance displayed episodic open/closed hydrology across seven alternating units from the Late Pleistocene, through the Holocene up to the present day. Three hydrologically open periods – $56,400 \pm 2,600$ to $54,300 \pm 2,500$ cal yr BP (unit 2), $37,500 \pm 2,500$ to $31,200 \pm 2,200$ cal yr BP (unit 4) and $28,051 \pm 417$ to $12,200 \pm 400$ cal yr BP (unit 6) - appear to display stable, wetter climate conditions, coinciding with stadial periods of last glaciation, including the LGM (unit 6). Unit 6 is punctuated by a relatively short lived shift to arid conditions between ~15 and 13 ka BP, interpreted as the Bolling-Allerod. These hydrologically open periods were punctuated by down slope expansions of coniferous pine-oak woodlands and expansion of the hydrologic system creating larger wetlands and pools able to sustain mesic and wetland vegetation species such as hickory and typha respectively as well as depositing tufa structures such as rim-stone pools and spring mounds.

Further to the three periods of wetter climate and proposed open hydrology on the CCB floor during the past ~85 cal ka BP, the perched tufa terrace identified away from the modern hydrologic system indicated a substantially wet climate existed in the basin between ~500 ka BP and ~130 ka BP. For the terrace to be deposited, conditions wet enough to support playa and/or pluvial lake systems must have existed to create sufficient hydrostatic head pressure. These wet conditions would have also created flowing rivers in the surrounding canyons leading to the fluvial deposits observed.

Four hydrologically variable periods – $84,900 \pm 8,500$ to $56,400 \pm 2,600$ cal yr BP (unit 1), $54,300 \pm 2,500$ to $37,500 \pm 2,500$ cal yr BP (unit 3), $31,200 \pm 2,200$ to $28,051 \pm 417$ cal yr BP (unit 5) and $12,200 \pm 400$ cal yr BP to the present (unit 7) –

appear to display highly variable conditions coinciding with interstadial periods of the last glaciation characterised by rapid, short lived swings in climate. These may be related to global climate events such as the H3 Heinrich event, at 30 ka BP (unit 5). The hydrologically variable units display a retreat of pine-oak woodland to the high peaks of the surrounding mountains with mesic vegetation species being replaced by xeric species such as prickly pear cactus and agave. The expansion of peat forming wetland environments appears to coincide with drying events in the CCB, replacing deeper water bodies, and causing what appears to be disequilibrium effects on the $\delta^{18}\text{O}_{\text{CARB}}$ values of carbonate lake sediments in core PTB. Any hydrological closure of the CCB may not have been over extended time frames, this is reflected in the weak $\delta^{18}\text{O}_{\text{CARB}}$ and $\delta^{13}\text{C}_{\text{DIC}}$ co-variation in units 1 and, in particular, 5. The modern hydrologically closed basin dynamics proposed for the CCB provides a good model to apply to previous hydrologically closed periods, suggesting the possibility that the CCB has never completely dried.

The survival strategy of the Coahuilan Indians of the CCB since at least 10.5 ka BP appears to have been controlled by atmospheric moisture and its subsequent control of water availability and vegetation for food and material production. The palaeoenvironmental data have demonstrated that climate and water availability fluctuated dramatically throughout the Late Pleistocene and Holocene with episodic drought conditions followed by periods wet enough to support pluvial lake formation, particularly in the Early-Middle Holocene. However, palaeoenvironmental and hydrological data suggest that, despite fluctuations in climate and water availability, the CCB never became completely dry, corroborating Taylor's [1964] hypothesis that tethered nomadism was practised by the Coahuilan Indians. The Coahuilan Indians must have been adaptable to environmental changes and archaeological evidence attests to the importance of exploiting seeds and nuts when climate was wetter and more favourable whilst exploitation of fruiting cactus ('quids') would have been undertaken during times of aridity. The permanent water availability in the CCB would also suggest the exploitation of aquatic flora and fauna throughout the Holocene although with no archaeological evidence this theory, though likely, is hard to substantiate.

7.2 Future work

Further work to gain a complete understanding of the hydrology of the CCB is certainly warranted. More work is required categorising pool, lake and river morphology leading to better understanding of the complex sub-surface water flow observed in the CCB. This study has demonstrated the through-flow nature of the CCB waters but understanding as to the origin and environmental controls of the water for each pool is still largely unknown. Proposed future work includes further detailed sampling of water from pools, lakes and rivers in both the west and east sides of the CCB for $\delta^{18}\text{O}$ analysis to gain a more detailed understanding of surface flow across the basin and, more importantly, sub-surface flow patterns. Establishing an understanding of sub-surface interactions between pools would help identify the source waters (i.e. Cupido-Aurora aquifer) for individual water bodies. Further measurements of pH, temperature, mineralogy and $\delta^{13}\text{C}_{\text{DIC}}$ of source waters, both in the CCB and the Bolson de Mapimi, would also assist in determinations of hydrologic interactions, helping both the identification of original water source and also surface flow patterns through brine evolution. By providing a hydrological framework, determinations of how and where to extract water for industry would help ease the socio-economic problems currently ongoing in the CCB.

The coring work conducted in the CCB has highlighted the potential of the basin for detailed palaeoenvironmental research. An incomplete stratigraphic sequence (resulting from problems with the coring technique) limited the results of this thesis but also indicated that the sediments contained largely uncontaminated material. The possibility of disequilibrium effects on the carbonate sediments of core PTB has limited the conclusions of this thesis; further work in establishing disequilibrium effects is certainly warranted. Understanding any disequilibrium effects i.e. eutrophication, in modern day carbonate sediments is critical, as understanding the factors that have offset the isotopic composition from equilibrium will assist in accounting for these effects when interpreting the Palaeo-record. Changes to the coring techniques utilised are proposed to maximise sediment recovery. More dating work is required to establish an absolute age/depth model by understanding the environmental controls of sedimentation rate of the pools, lakes and rivers. Additional dating techniques are needed to clarify the age/depth profile of the CCB. This study, however, has

demonstrated the possibility of a continuous palaeoenvironmental record spanning ≥ 500 ka BP by combining coring processes with detailed sampling of the perched tufa terrace. Further sampling for $\delta^{18}\text{O}$ and $\delta^{13}\text{C}$ isotopes should further enhance the understanding of local hydrology and possibly regional and global climatic influences in the CCB. This work would be combined with recent regional climate reconstructions i.e. Fawcett *et al.*, [2011] to better understand regional controls of climate in the CCB and northern Mexico during the last glacial-interglacial cycles.

Detailed excavations of cave sites and studies of museum collections are another potential future avenue for new research in the CCB. The last known formal excavations were undertaken in the 1940s with the majority of artefacts now stored in museums, private collections or lost. Further archaeological excavations, particularly in Frightful Cave, would not only allow further insights into the understanding of the material culture of the Coahuilan Indians but also allow for more detailed chronological work, adding constraints to Taylor's [2003] three archaeological complexes [c.12 ka BP to 1 ka BP] and Turpin's [2003] subsequent relative sandal chronology. The proposed sampling of human remains from the CCB, and possibly surrounding areas, would allow for stable isotopic determinations of dietary patterns and possible seasonal utilisation of food resources. The analysis of bone collagen would provide an overall indicator of an individual's diet which could then be applied to segmental analysis of hair keratin. Segmental analysis of hair would involve sectioning the hair into two inch segments, providing possible 'snapshots' of dietary seasonality.

7.3 Concluding remarks

The palaeoenvironmental and geoarchaeological records obtained in the Cuatro Ciénegas Basin (CCB) have provided a valuable source of information in regard to both modern and past climate and its affect on floral, faunal and human populations. The CCB is of great importance to understanding past climate change both regionally and globally and its direct affect in northern Mexico. The CCB provides a unique area in which to study past environments as many parallels can be drawn within the modern environment. Such areas are rare, and as such, the importance of conservation in the CCB is elevated due to the increasing threat of industry and the subsequent over extraction of water brought with it.

This thesis has demonstrated the potential of the Cuatro Ciénegas Basin to contain detailed palaeoenvironmental records, applicable to regional and global records, in a largely unspoiled area of the Chihuahuan Desert. The abundance of pools, rivers and lakes in a large arid wetland area suggests that palaeoenvironmental records definitely up to $56,180 \pm 2,250$ cal yr BP, beyond $84,900 \pm 8,500$ cal yr BP, and up to possibly 500 ka BP are obtainable. The palaeoenvironmental, hydrological and geoarchaeological data within the Cuatro Ciénegas Basin and surrounding areas certainly warrants further research. The conclusions reached in this study suggest that future research in this region could prove important to arid/semi-arid regions, not just on a local or regional scale but also on a global scale.

References

Abdalla, O. A. E. 2009. Groundwater recharge/discharge in semi-arid regions interpreted from isotope and chloride concentrations in north White Nile Rift, Sudan. *Hydrogeology Journal*, 17: 679-692

Aggarwal, P, K., Gat, J. R. and Froehlich, K. (eds.). 2005. *Isotopes in the water cycle: past, present and future of a developing science*. Springer, Berlin.

Alexander, R. M. 1989. *Dynamics of Dinosaurs & other extinct giants*. Columbia University Press, New York

Allen, J. R. L. 1999. Geological impacts on coastal wetland landscapes: some general effects of sediment autocompaction in the Holocene of northwest Europe. *The Holocene*, 9: 1-12

Allison, G. B. 1982. The relationship between ^{18}O and deuterium in water in sand columns undergoing evaporation. *Journal of Hydrology*, 55: 163-169

Allison, G. B. and Barnes, C. J. 1985. Estimation of evaporation from normally "dry" Lake Frome in South Australia. *Journal of Hydrology*, 78: 229-242

Altunel, E. and Hancock, P. L. 1993. Morphology and Structural setting of Quaternary travertines at Pamukkale, Turkey. *Geological Journal*, 28: 335-346

Amatya, D. M. Jha, M., Edwards, A. E., Williams, T. M. and Hitchcock, D. R. 2011. SWAT-based streamflow and embayment modelling of karst-affected Chapel Branch Watershed, South Carolina. American Society of Agriculture and Biological Engineers, 54: 1311-1323

Amundson, R., Franco-Vizcaíno, E., Graham, R. C. and DeNiro, M. 1994. The relationship of precipitation seasonality to the flora and stable isotope chemistry of soils in the Vizcaíno desert, Baja California, Mexico. *Journal of Arid Environments*, 28: 265-279

Anderson, R. S. and Van Devender, T. R. 1995. Vegetation history and paleoclimates of the coastal lowlands of Sonora, Mexico – pollen records from packrat middens. *Journal of Arid Environments*, 30: 295-306

Andrews, J. E. 2006. Palaeoclimatic records from stable isotopes in riverine tufas: Synthesis and review. *Earth-Science Reviews*, 75: 85-104

Andrews, J. E. and Brasier, A. T. 2005. Seasonal records of climatic change in annual laminated tufas: short review and future prospects. *Journal of Quaternary Science*, 20: 411-421

Andrews, J. N., Fontes, J.-C., Aranyossy, J.-F., Dodo, A., Edmunds, W. M., Joseph, A. and Travi, Y. 1994. The evolution of alkaline groundwaters in the Continental Intercalaire aquifer of the Irhazer Plain, Niger. *Water Resource Research*, 30: 45-61

Andrews, J. E., Riding, R. and Dennis, P. F. 1993. Stable isotopic compositions of Recent freshwater cyanobacterial carbonates from the British Isles: local and regional environmental controls. *Sedimentology*, 40: 303-314

Andrews, J. E., Riding, R. and Dennis, P. F. 1997. The stable isotope record of environmental and climatic signals in modern terrestrial microbial carbonates from Europe. *Palaeogeography, Palaeoclimatology, Palaeoecology*, 129: 171-189

Andrews, J. E., Greenaway, A. M. and Dennis, P. F. 1998. Combined carbon isotope and C-N ratios as indicators of source and fate of organic matter in a poorly flushed, tropical estuary: Hunts Bay, Kingston Harbour, Jamaica. *Estuarine Coastal and Shelf Science*, 46: 743-756

APFFCC (Área de Protección de la Flora y Fauna de Cuatro Ciénegas), personal communication

Atekwana, E. A. and Krishnamurthy, R. V. 1998. Seasonal variations of dissolved inorganic carbon and $\delta^{13}\text{C}$ of surface waters: application of a modified gas evolution technique. *Journal of Hydrology*, 205: 265-278

Bade, D. L., Carpenter, S. R., Cole, J. J., Hanson, P. C. And Hesslein, R. H. 2004. Controls of $\delta^{13}\text{C}$ -DIC in lakes: Geochemistry, lake metabolism, and morphometry. *Limnology and Oceanography*, 49: 1160-1172

Badino, G., Bernabei, T., De Vivo, A., Giulivo, I. and Savino, G. (eds.). 2004. Under the Desert: The Mysterious Waters of Cuatro Ciénegas, 1st ed. Associazione Geografica La Venta, Treviso, Italy

Baldini, J. U. L., Baldini, L. M., McDermott, F. and Clipson, N. 2006. Carbon Dioxide Sources, Sinks, and Spatial Variability in Shallow Temperate Zone Caves: Evidence from Ballynamintra Cave, Ireland. *Journal of Cave and Karst Studies*, 68: 4-11

Barbour, M. G. and Billings, W. D. (eds.). 2000. *North American Terrestrial Vegetation (Second Edition)*. University of Cambridge Press, Cambridge.

Barger, K. E. 1978. Geology and thermal history of Mammoth Hot Springs, Yellowstone National Park, Wyoming. *U.S. Geological Survey Bulletin*, 1444: 1-55

Barnes, C. J. and Allison, G. B. 1988. Tracing of water movement in the unsaturated zone using stable isotopes of hydrogen and oxygen. *Journal of Hydrology*, 100: 143-176

Barnes, I. and O'Neil, J. R. 1969. The Relationship between Fluids in Some Fresh Alpine-Type Ultramafics and Possible Modern Serpentinization, Western United States. *Geological Society of America Bulletin*, 80: 1947-1960

Barnes, I. and O'Neil, J. R. 1971. Calcium-magnesium soil solutions from Holocene conglomerate cements and travertines in the Coast Range of California. *Geochimica y Cosmochimica Acta*, 35: 699-717

Bayón, C and Politis, G. 1996. Estado actual de las investigaciones en el sitio Monte Hermoso 1 (Provincia de Buenos Aires). *Arqueología. Revista de la Sección Arqueología. Instituto de Ciencias Antropológicas. Facultad de Filosofía y Letras, Universidad de Buenos Aires*, 6: 83-115

Becerril, J. A. O. Heydt, G. H. and Durán, J. J. 2010. The role sculpted forms alongside Endokarstic active conduits in the development of fluviokarstic Canyons. The Rio Puron Cave Conduit (Spain). Pp 387-392. In: Bartoloné, A., Carrasco, F., Durán, J. J. and LaMoreaux, J. W. (eds). 2010. *Advances in Research in Karst Media*. Springer, London

Belnap, J. and Gillette, D. A. 1998. Vulnerability of desert biological soil crusts to wind erosion: the influences of crust development, soil texture, and disturbance. *Journal of Arid Environments*, 39: 133-142

Bernal, J. P., Lachniet, M., McCulloch, M., Mortimer, G., Morales, P. and Cienfuegos, E. 2011. A speleothem record of Holocene climate variability from southwestern Mexico. *Quaternary Research*, 75: 104-113

Betancourt, J. L., Van Devender, T. R. and Martin, P. S. 1990. *Packrat middens: the last 40,000 years of biotic change*. University of Arizona Press, Tucson

Blasch, K. W., Constantz, J. and Stonestrom, D. A. 2008. *Ground-Water Recharge in the Arid and Semiarid Southwestern United States*. USGS Professional Paper 1703, Appendix-1: 353-375

Blaauw, M. 2010. Methods and code for 'classical' age modelling of radiocarbon sequences. *Quaternary Geochronology*, 5: 512-518

Blaauw, M. and Christen, J. A. 2005. Radiocarbon peat chronologies and environmental change. *Applied Statistics*, 54: 805-816

- Blaauw, M., Christen, J. A., Mauquoy, D., van der Plicht, J. and Bennett, K. D. 2007. Testing the timing of radiocarbon-dated events between proxy archives. *The Holocene*, 17: 283-288
- Bond, G. C. and Lotti, R. 1995. Iceberg Discharges into the North Atlantic on Millennial Time Scales During the Last Glaciation. *Science*, 267: 1005-1010
- Bowman, S. 1990. Radiocarbon Dating. British Museum Press, London
- Bradbury, J. P. 1971. Paleolimnology of Lake Texcoco, Mexico: Evidence from diatoms. *Limnology and Oceanography*, 16: 180-200
- Bradbury, J. P. 1989. Late Quaternary lacustrine palaeoenvironments in the Cuenca de Mexico. *Quaternary Science Reviews*, 8: 75-100
- Bralower, T. J., CoBabe, E., Clement, B., Sliter, W. V., Osburn, C. L. and Longoria, J. 1999. The record of global change in Mid-Cretaceous (Barremian-Albian) sections from the Sierra Madre, north-eastern Mexico. *The Journal of Foraminiferal Research*, 29: 418-437
- Brasier, A. T., Andrews, J. E., Marca-Bell, A. D. and Dennis, P. F. 2010. Depositional continuity of seasonally laminated tufas: Implications for $\delta^{18}\text{O}$ based palaeotemperatures. *Global and Planetary Change*, 71: 160-167

Brook, G. A., Burney, D. A. and Cowart, J. B. 1990. Desert paleoenvironmental data from cave speleothems with examples from the Chihuahuan, Somali-Chalbi, and Kalahari deserts. *Palaeogeography, Palaeoclimatology, Palaeoecology*, 76: 311-329

Brown, R. B. 1985. A summary of late-quaternary pollen records from Mexico west of the Isthmus of Tehuantepec. In: V. M. Bryant, Jr. and R. G. Holloway. *Pollen records of Late-Quaternary North American sediments*. American Association of Stratigraphic Palynologists, Dallas, USA: 71-93

Bryant, V. M., Jr. 1975. Pollen as an indicator of prehistoric diets in Coahuila, Mexico. *Bulletin of the Texas Archaeological Society*, 46: 89-106

Bryant, V. M., Jr. 1977. A 16,000 year pollen record of vegetational change in central Texas. *Palynology*, 1: 143-156

Bryant, V. M., Jr. and Holloway, R. G. 1985. A Late-Quaternary Paleoenvironmental record of Texas: an overview of the pollen evidence. In: V. M. Bryant, Jr. and R. G. Holloway. *Pollen records of Late-Quaternary North American sediments*. American Association of Stratigraphic Palynologists, Dallas, USA: 39-70

Bryant, V. M., Jr. and Hall, S. A. 1993. Archaeological Palynology in the United States: A Critique. *American Antiquity*, 58: 277-286

Burger, D. 1990. The travertine complex of Antalya/Southwest Turkey. *Zeitschrift für Geomorphology. N. F. Supplementary. Bd*, 77: 25-46

Burgess, T. L. and Shmida, A. 1988. Succulent growth forms in arid environments, pp. 383-395. In: Whitehead, E. E., Hutchinson, C. F., Timmermann, B. N. and Varady, R. G. (eds.). Arid lands today and tomorrow. Proceedings of an international research and development conference. Westview Press, Boulder, USA.

Caballero Miranda, M. E. 1997. The last glacial maximum in the Basin of Mexico: the diatom record between 34,000 and 15,000 years BP from Lake Chalco. *Quaternary International*, 43: 125-136

Caballero Miranda, M. E. and Ortega Guerrero, B. 1998. Lake levels since about 40,000 years ago at Lake Chalco, near Mexico City. *Quaternary Research*, 50: 69-79

Carrillo-Rivera, J. J., Clark, I. D. and Fritz, P. 1992. Investigating recharge of shallow and paleo-groundwaters in the Villa de Reyes basin, SLP, Mexico with environmental isotopes. *Applied Hydrogeology*, 4: 35-48

Castiglia, P. J. and Fawcett, P. J. 2006. Large Holocene lakes and climate change in the Chihuahuan Desert. *Geology*, 34: 113-116

Chafetz, H. S. and Folk, R. L. 1984. Travertines; depositional morphology and the bacterially constructed constituents. *Journal of Sedimentary Research*, 54: 289-316

Chaves, M. M., Flexas, J. and Pinheiro, C. 2009. Photosynthesis under drought and salt stress regulation mechanisms from whole plant to cell. *Annals of Botany*, 103: 551-560

Cheng, H., Edwards, R. L., Hoff, J., Gallup, C. D., Richards, D. A. and Asmerom, Y. 2000. The half-lives of uranium-234 and thorium-230. *Chemical Geology*, 169: 17-33

Child, J. K. And Werner, A. 1999. Evidence for a hardwater radiocarbon dating effect, Wonder Lake, Denali National Park and Preserve, Alaska, U.S.A. *Géographie physique et Quaternaire*, 53: 407-411

Clark, I. and Fritz, P. 1997. *Environmental Isotopes in hydrology*. Lewis, Boca Raton, Florida.

Clark, P. U., Marshall, S. J., Clarke, G. K. C., Hostetler, S. W., Licciardi, J. M. and Teller, J. T. 2001. Freshwater forcing of abrupt climate change during the last glaciation. *Science*, 293: 283-287

Clotts, R., Ito, E. and Forester, R. M. 2009. How lakes see climate: Stable isotopic indicators. In: *Proceedings 11th International Palaeolimnology Symposium, 2009*, International Palaeolimnology Association: 79

Cook, P. G. and Herczeg, A. L. (eds.). 2000. *Environmental tracers in subsurface hydrology*. Kluwer, Boston.

Cortés, A., Durazo, J. and Farvolden, R. N. 1997. Studies of isotopic hydrology of the basin of Mexico and vicinity: annotated bibliography and interpretation. *Journal of Hydrology*, 198: 346-376

Craig, H. 1961. Isotopic variations in meteoric waters. *Science*, 133: 1702-1703

Cruz, F. W. Jr., Burns, S. J., Karmann, I., Sharp, W. D., Vuille, M., Cardoso, A. O., Ferrari, J. A., Silva Dias, P. L. and Viana, O. Jr. 2005. Insolation-driven changes in atmospheric circulation over the past 116,000 years in subtropical Brazil. *Nature*, 434: 63-66

Curtis, J. H. Hodell, D. A. and Brenner, M. 1996. Climate Variability on the Yucatan Peninsula (Mexico) during the Past 3500 years, and Implications for Maya Cultural Evolution. *Quaternary Research*, 46: 37-47

Damm, B. 1968. Ein Riesenkegel aus Travertin (NW Iran). *Der Aufschluss*, 19: 323-332

Dansgaard, W. 1964. Stable isotopes in precipitation. *Tellus*, 16: 436-468

Dansgaard, W., Johnsen, S. J., Clausen, H. B., Dahl-Jensen, D., Gundestrup, N. S., Hammer, C. U., Hvidberg, C. S., Steffensen, J. P., Sveinbjörnsdottir, A. E., Jouzel, J. and Bond, G. 1993. Evidence for general instability of past climate from a 250-kyr ice-core record. *Nature*, 364: 218-220

Davis, O. K., Minckley, T., Moutoux, T., Jull, T. and Kalin, B. 2002. The transformation of Sonoran Desert wetlands following the historic decrease of burning. *Journal of Arid Environments*, 50: 393-412

Dean, W. E. 1974. Determination of Carbonate and Organic Matter in Calcareous Sediments and Sedimentary Rocks by Loss on Ignition: Comparison With Other Methods. *Journal of Sedimentary Petrology*, 44: 242-248

Dean, W. E. and Schwab, A. 2000. Holocene environmental and climatic change in the Northern Great Plains as recorded in the geochemistry of sediments in Pickerel Lake, South Dakota. *Quaternary International*, 67: 5-20

Deines, P. 1980. The isotopic composition of reduced organic carbon. In: Fritz, P. and Fontes, J. C. (Eds.). *Handbook of Environmental Isotope Geochemistry*. Elsevier, New York, pp. 329-406

Dickinson, W. R. and Lawton, T. F. 2001. Carboniferous to Cretaceous assembly and fragmentation of Mexico. *Geological Society of America Bulletin*, 113: 1142-1160

Diefendorf, A. F., Mueller, K. E., Wing, S. L., Koch, P. L. and Freeman, K. H. 2010. Global patterns in leaf ^{13}C discrimination and implications for studies of past and future climate. *Proceedings of the National Academy of Science of the United States of America*, 107: 5738-5743

Dillehay, T. D. 2000. *The Settlement of the Americas: A New Prehistory*. Basic Books, New York

Dilsiz, C., Marques, J. M. and Carreira, P. M. M. 2004. The impact of hydrological changes on travertine deposits related to thermal springs in Pamukkale area (SW Turkey). *Environmental Geology*, 45: 808-817

Drummond, C. N., Patterson, W. P. and Walker, J. C. G. 1995. Climatic forcing of carbon-oxygen isotopic covariance in temperate-region marl lakes. *Geology*, 23: 1031-1034

Eakin, T. E. 1966. A regional interbasin ground-water system in the White River area, southeastern Nevada. *Water Resources Research*, 1: 251-271

Echelle, A. A. and Echelle, A. F. 1998. Evolutionary relationships of pupfishes in the *Cyprinodon eximius* complex (Atherinomorpha: Cyprinodontiformes). *Copeia*, 4: 852-865

Edwards, R. L., Chen, J. H. and Wasserburg, G. J. 1988. ^{238}U - ^{234}U - ^{230}Th - ^{232}Th systematic and the precise measurement of time over the past 500,000 years. *Earth and Planetary Science Letters*, 81: 175-192

Ehlers, J. And Gibbard, P. L. (eds.). 2004. Quaternary Glaciations – Extent and Chronology Part II: North America. Elsevier Science, Netherlands

Elias, S. A. and Van Devender, T. R. 1990. Fossil insect evidence for late Quaternary climatic change in the Big Bend region, Chihuahuan Desert, Texas. *Quaternary Research*, 34: 249-261

Enzel, Y., Amit, R., Grodek, T., Ayalon, A., Lekach, J., Porat, N., Bierman, P., Blum, J. D. And Erel, Y. 2012. Late Quaternary weathering, erosion, and deposition in Nahal Yael, Israel. An “impact of climatic change on an arid watershed”? *Geological Society of America Bulletin*, 124: 705-722

Escobar, J., Cortis, J., Brenner, M., Hodell, D. A. and Holmes, J. A. 2010. Isotope measurement of ostracod and gastropod shells for climate reconstruction: evaluation of within-sample variability and determination of sample size. *Journal of Palaeolimnology*, 43: 921-938

Escobar, J., Hodell, D. A., Brenner, M., Curtis, J. H., Gilli, A., Mueller, A. D., Anselmetti, F. S., Ariztegui, D., Grzesik, D. A., Pérez, L., Schwalb, A. and Guilderson, T. P. 2012. A ~43-ka record of paleoenvironmental change in the Central American lowlands inferred from stable isotopes of lacustrine ostracods. *Quaternary Science Reviews*, 37: 92-104

Evans, S. B. 2005. Using Chemical Data to Define Flow systems in Cuatro Ciénegas, Coahuila, Mexico: University of Texas-Austin Dissertation: 114 pp

Fairbanks, R. G., Mortlock, R. A., Chiu, T.-C., Cao, L., Kaplan, A., Guilderson, T. P., Fairbanks, T. W., Bloom, A. L., Grootes, P. M. and Nadeau, M.-J. 2005. Radiocarbon calibration curve spanning 0 to 50,000 years BP based on paired $^{230}\text{Th}/^{234}\text{U}/^{238}\text{U}$ and ^{14}C dates on pristine corals. *Quaternary Science Reviews*, 24: 1781-1796

Fawcett, P. J., Werne, J. P., Anderson, R. S., Heikoop, J. M., Brown, E. T., Berke, M. A., Smith, S. J., Goff, F., Donohoo-Hurley, L., Cisneros-Dozal, L. M., Schouten, S., Sinninghe-Damsté, J. S., Huang, Y., Toney, J., Fessenden, J., WoldeGabriel, G., Atudorei, V., Geissman, J. W. and Allen, C. D. 2011. Extended megadroughts in the southwestern United States during Pleistocene interglacials. *Nature*, 470: 518-521

Fécan, F., Marticorena, B. and Bergametti, G. 1998. Parametrization of the increase of the aeolian erosion threshold wind friction velocity due to soil moisture for arid and semi-arid areas. *Annales Geophysicae*, 17: 149-157

Flower, B. P., Hastings, D. W., Hill, H. W. and Quinn, T. M. 2004. Phasing of deglacial warming and Laurentide Ice Sheet meltwater in the Gulf of Mexico. *Geology*, 32: 597-600

Fjeldså, J., Lambin, E. and Mertens, B. 1999. Correlation between endemism and local ecoclimatic stability documented by comparing Andean bird distributions and remotely sensed land surface data. *Ecography*, 22: 63-78

Fontes, J.-C. 1994. Isotope palaeohydrology and the prediction of long-term repository behaviour. *Terra Review*, 6: 20–36

Fontes, J.-C., Yousfi, M. and Allison, G. B. 1986. Estimation of long-term diffuse groundwater discharge in the northern Sahara using stable isotope profiles in soil water. *Journal of Hydrology*, 86: 315-327

Ford, T. D. and Pedley, H. M. 1996. A review of tufa and travertine deposits of the World. *Earth-Science Reviews*, 41: 117-175

Fricke, H. C. and O'Neil, J. R. 1999. The correlation between $^{18}\text{O}/^{16}\text{O}$ ratios of meteoric water and surface temperature: its use in investigating terrestrial climate change over geologic time. *Earth and Planetary Science Letters*, 170: 181-196

Fritz, P. and Fontes, J.-C. 1980. *Handbook of environmental geochemistry, vol 1: the terrestrial environment*, A. Elsevier, Netherlands.

Fritz, P. and Fontes, J.-C. 1986. *Handbook of environmental geochemistry, vol 2: the terrestrial environment*, B. Elsevier, Netherlands.

Fritz, R. D. And Medlock, P. L. 1995. Sequence Stratigraphy of the Mid-Continent. Tulsa Geological Society, USA

Fronval, T., Jensen, N. B. and Buchardt, B. 1995. Oxygen isotope disequilibrium precipitation of calcite in Lake Arreso, Denmark. *Geology*, 23: 463-466

Fulop, A. 2001. Tuffaceous conglomerates: Syn-eruptive resedimented debris flow and hyperconcentrated flow deposits from the "Rhyodacitic formation", Gutâi Mountains, Eastern Carpathians. *Studia Universitatis Babeş-Bolyai, Geologia*, XLVI, 1: 81-98

Gabrovsek, F. and Dreybrodt, W. 2010. Karstification in unconfined limestone aquifers by mixing of phreatic water with surface water from a local input: A model. *Journal of Hydrology*, 386: 130-141

Gat, J. R. 1995. Stable isotopes of fresh and saline lakes. In: Lerman, A., Imboden, D. and Gat, J. R. (eds.). *Physics and chemistry of lakes*. Springer. Berlin, Heidelberg: 139-162

Gat, J. R. 1996. Oxygen and hydrogen isotopes in the hydrologic cycle. *Annual Review of Earth and Planetary Sciences*, 24: 225-262

Gat, J. R. and Issar, A. 1974. Desert isotope hydrology: water sources of the Sinai Desert. *Geochimica y Cosmochimica Acta*, 38: 1117-1229

Gates, J. S., White, D. E., Stanley, W. D. and Ackermann, H. D. 1980. Availability of slightly saline ground water in the basins of westernmost Texas. Texas Department of Water Resources, Report 256: 108

Gill, R. B. 2000. The Great Maya Droughts: Water, Life and Death. University of New Mexico Press, USA, pp 464

Gilmore, R. M. 1947. Report on a collection of mammal bones from Archaeologic cave-sites in Coahuila, Mexico. *Journal of Mammalogy*, 28: 147-165

Gonzalez, A. H. G., Lockley, M. G., Rojas, C. S., Espinoza, J. L. and Gonzalez, S. 2007. Notes on the re-discovery of a 'lost' hominid footprint site from the Cuatro Ciénegas basin (Coahuila), Mexico. *New Mexico Museum of Natural History and Science Bulletin*, 54: 11-15

Gonzalez, A. H. G., Lockley, M. G., Rojas, C. S., Espinoza, J. L. and Gonzalez, S. 2009. Human Tracks from Quaternary Tufa Deposits, Cuatro Cienegas, Coahuila, Mexico. *Ichnos*, 16: 12-24

González-Naranjo, G. A., Molina-Garza, R. S. and Chávez-Cabello, G. 2008. Paleomagnetic study of Jurassic and Cretaceous rocks north of San Marcos fault, central Coahuila, México. *Geofísica Internacional*, 47: 41-55

González Quintero, L. 1986. Analisis polinicos de los sedimentos. In: J. L. Lorenzo. and L. Mirambell. (eds.). Tlapacoya: 35,000 Años de Historia del Lago de Chalco. Colección Científica, Serie Prehistoria, Instituto Nacional de Anthropologia e Historia

- Grousset, F.E., Pujol, C., Labeyrie, L., Auffret, G. and Boelaert, A. 2000. Were the North Atlantic Heinrich events triggered by the behaviour of the European ice sheets? *Geology*, 28: 123–126
- Guendouz, A., Moulla, A. S., Edmunds, W. M., Zouari, K., Shand, P. and Manou, A. 2003. Hydrogeochemical and isotopic evolution of water in the Complexe Terminal aquifer in the Algerian Sahara. *Hydrogeology Journal*, 11: 483-495
- Guo, L. and Riding, R. 1994. Origin and diagenesis of Quaternary travertine shrub facies, Rapolano Terme, Italy. *Sedimentology*, 41: 499-520
- Guo, L. and Riding, R. 1999. Rapid facies changes in Holocene fissure ridge hot spring travertines, Rapolano Terme, Italy. *Sedimentology*, 46: 1145-1158
- Guzman, A. E. 2001. Exploration and production in Mexico – challenges and opportunities. AAPG, Houston, Texas, August 27-29
- Hammarlund, D., Barnekow, L., Birks, H. J. B., Buchardt, B. and Edwards, T. W. D. 2002. Holocene changes in atmospheric circulation recorded in the oxygen-isotope stratigraphy of lacustrine carbonates from northern Sweden. *Holocene*, 12: 339-351
- Harrington, E. R. 1948. Craters and crater springs of the Rio Salado. *Journal of Geology*, 56: 182-185

Harrington, G. A., Cook, P. G. and Herczeg, A. L. 2002. Spatial and temporal variability of groundwater recharge in central Australia: a tracer approach. *Ground Water*, 40: 518-528

Hawley, J. W. 1993. Geomorphic setting and late Quaternary history of pluvial lake basins in the southern New Mexico region. Open-File Report 391. Socorro, New Mexico: New Mexico Bureau of Mines and Mineral Resources

Haynes, C. V. Jr. and Agogino, G. A. 1966. Prehistoric Springs and Geochronology of the Clovis Site, New Mexico. *American Antiquity*, 31: 812-821

Haynes, C. V. Jr. 2008. Quaternary Cauldron Springs as Paleoecological Archives. In: Stevens, L. E. and Meretsky, V. J. (eds.). *Aridland Springs in North America: Ecology and Conservation*. The University of Arizona Press, Tucson: 76-97

Heaton, T. H. E., Holmes, J. A. and Bridgwater, N. D. 1995. Carbon and oxygen isotope variations among lacustrine ostracods: implications for palaeoclimate studies. *The Holocene*, 5: 428-434

Hendrickson, D. and Minckley, T. A. Personal communication

Herczeg, A. L. and Leaney, F. W. 2011. Review: Environmental tracers in arid-zone hydrology. *Hydrogeology Journal*, 19: 17-29

Hershler, R. 1984. The hydrobiid snails (Gastropoda: Rissoacea) of the Cuatro Ciénegas Basin: Systematic relationships and ecology of a unique fauna. *Journal of the Arizona-Nevada Academy of Science*, 19: 61-76

Hershler, R. and Minckley, W. L. 1986. Microgeographic variation in the banded spring snail (Hydrobiidae: *Mexipyrgus*) from the Cuatro Ciénegas basin, Coahuila, Mexico. *Malacologia*, 27: 357-374

Hibbs, B. J. and Darling, B. K. 2005. Revisiting a classification scheme for U.S.-Mexico alluvial basin-fill aquifers. *Groundwater*, 43: 750-763

Hirsch, R. M., Slack, J. R. and Smith, R. A. 1982. Techniques of Trend Analysis for Monthly Water Quality Data. *Water Resources Research*, 18: 107-121

Hobbs, W. O., Lalonde, S. V., Vinebrooke, R. D., Konhauser, K. O., Weidman, R. P., Graham, M. D. and Wolfe, A. P. 2010. Algal-silica cycling and pigment diagenesis in alpine lake sediments: mechanisms and paleoecological implications. *Journal of Paleolimnology*, 44: 613-628

Hodell, D. A., Curtis, J. H. and Brenner, M. Possible role of climate in the collapse of Classic Maya civilization. *Nature*, 375: 391-394

Hoefs, J. 2009. *Stable Isotope Geochemistry* (6th Edition). Springer, Berlin

Hogan, J. F., Phillips, F. M. and Scanlon, B. R. 2004. Groundwater Recharge in a Desert Environment: The Southwestern United States. American Geophysical Union, Florida, USA

Holmes, J., Arrowsmith, C., Austin, W., Boyle, J., Fisher, E., Holme, R., Marshall, J., Oldfield, F. and van der Post, K. 2010. Climate and atmospheric circulation changes over the past 1000 years reconstructed from oxygen isotopes in lake-sediment carbonate from Ireland. *Holocene*, 20: 1105-1111

Huang, Y., Street-Perrott, F. A., Metcalfe, S. E., Brenner, M., Moreland, M. and Freeman, K. H. 2001. Climate change as the dominant control on glacial-interglacial variations in C₃ and C₄ plant abundance. *Science*, 293: 1647-1651

Humphreys, W. F., Awramik, S. W., and Jebb, M. H. P. 1995. Freshwater biogenic tufa dams in Madang Province, Papua New Guinea. *Journal of the Royal Society of Western Australia*, 78: 43-54

Jaillet, S., Pons-Branchu, E., Brulhet, J. and Hamelin, B. 2004. Karstification as geomorphological evidence of river incision: the karst of Cousance and the Marne Valley (Eastern Paris Basin). *Terra Nova*, 16: 167-172

Johannesson, K. H., Cortés, A. and Kilroy, K. C. 2004. Reconnaissance isotopic and hydrochemical study of Cuatro Ciénegas groundwater, Coahuila, Mexico. *Journal of South American Earth Sciences*, 17: 171-180

Johnson, T. C., Halfman, J. D. and Showers, W. J. 1991. Paleoclimate of the past 4000 years at Lake Turkana, Kenya, based on the isotopic composition of authigenic calcite. *Palaeogeography, Palaeoclimatology, Palaeoecology*, 85: 189-198

Jones, B. and Renaut, R. W. 1995. Noncrystallographic calcite dendrites from hot-spring deposits at Lake Bogoria, Kenya. *Journal of Sedimentary Research*, 65: 154-169

Jones, B. F., Naftz, D. L., Spencer, R. J. and Oviatt, G. C. 2008. Geochemical Evolution of Great Salt Lake, Utah, USA. *Aquatic Geochemistry*, 15: 95-121

Jones, R. T., Marshall, J. D., Fisher, E., Hatton, J., Patrick, C., Anderson, K., Long, B., Bedford, A. and Oldfield, F. 2011. Controls on lake level in the early to mid Holocene, Hawes Water, Lancashire, UK. *The Holocene*, 21: 1061-1072

Kastning, E. H. 1983. Relict caves as evidence of landscape and aquifer evolution in a deeply dissected carbonate terrain: Southwest Edwards Plateau, Texas, USA. *Journal of Hydrology*, 61: 89-112

Kaufmann, G. and Braun, J. 2000. Karst aquifer evolution in fractured, porous rocks. *Water Resources Research*, 36: 1381-139

Kemp, P. R. 1983. Phenological patterns of Chihuahuan Desert plants in relation to the timing of water availability. *Journal of Ecology*, 71: 427-436

Kennett, J. P. and Shackleton, N. J. 1975. Laurentide Ice Sheet Meltwater Recorded in Gulf of Mexico Deep-Sea Cores. *Science*, 188: 147-150

Kent-Corson, M. L., Ritts, B. D., Zhuang, G., Baret, P. M., Graham, S. A. and Chamberlain, C. P. 2009. Stable isotopic constraints on the tectonic, topographic, and climatic evolution of the northern margin of the Tibetan Plateau. *Earth and Planetary Science Letters*, 282: 158-166

Kilic, O. and Kilic, A. M. 2010. Salt crust mineralogy and Geochemical evolution of the Salt Lake (Tuz Gölü), Turkey. *Scientific Research and Essays*, 5: 1317-1324

Kim, S-T. and O'Neil, J. R. 1997. Equilibrium and nonequilibrium oxygen isotope effects in synthetic carbonates. *Geochimica et Cosmochimica Acta*, 61: 3461-3475

Kirby, M.E. and Andrews, J.T. 1999. Mid-Wisconsin Laurentide Ice Sheet growth and decay: Implications for Heinrich events 3 and 4. *Paleoceanography*, 14: 211–223

Knoblauch, R. L., Pietrucha, M. T. and Nitzburg, M. 1996. Field Studies of Pedestrian Walking Speed and Start-Up Time. *Transportation Research Record*, 1538: 27-38

Kohn, M. J. 2010. Carbon isotope compositions of terrestrial C3 plants as indicators of (paleo)ecology and (paleo)climate. *Proceedings of the National Academy of Science of the United States of America*, 107: 19691-19695

Kooi, H. and de Vries, J. J. 1998. Land subsidence and hydrodynamic compaction of sedimentary basins. *Hydrology and Earth System Sciences*, 2: 159-171

Krishnamurthy, R. V. and Epstein, S. 1990. Glacial-interglacial excursion in the concentration of atmospheric CO₂: effect in the ¹³C/¹²C ratio of wood cellulose. *Tellus*, 42: 423-434

Lamb, A. L. 2004. Determination of organic and carbonate content in soils and sediments by loss on ignition (LOI). NERC Isotope Geosciences Laboratory Report, 197

L'Apparent, A.F. de. 1966. Les depots de travertins des montagnes Afghanes à l'ouest de Kabul. *Revue de Géographie physique et de geologie Dynamique*, 8: 351-357

Last, W. M. and Smol, J. P. (eds). 2001. *Tracking Environmental Change Using Lake Sediments. Volume 2: Physical and Geochemical Methods*. Springer, Netherlands, 504 pp

Last, W. M. and Smol, J. P. (eds). 2002. *Tracking Environmental Change Using Lake Sediments. Volume 3: Basin Analysis, Coring and Chronological Techniques*. Springer, Netherlands

Lehmann, C., Osleger, D. A., Montañez, I. P., Sliter, W., Arnaud-Vanneau, A. and Banner, J. 1999. Evolution of the Cupido and Coahuila carbonate platforms, early Cretaceous, north-eastern Mexico. *Geological Society of America Bulletin*, 111: 1010-1029

Leng, M. J. 2005. *Isotopes in Palaeoenvironmental Research (Volume 10)*. Springer, Netherlands

Leng, M. J. and Marshall, J. D. 2004. Palaeoclimate interpretation of stable isotope data from lake sediment archives. *Quaternary Science Reviews*, 23: 811-831

Lerman, A., Imboden, D. and Gat, J. R. (eds.). 1995. *Physics and Chemistry of Lakes*. Springer, New York.

Lesser Jones, H. 1965. Confined freshwater aquifers in limestone, exploited in the north of Mexico with deep wells below sea level. In: *Proceedings Dubrovnik Symposium, 1965, Hydrology of Fractured Rocks*. International Association of Scientific Hydrology, 2: 526-539

Lesser, J. M. and Lesser, G. 1988. Region 9, Sierra Madre Oriental. In: Back, W., Rosenhein, J. S. and Seaber, P. R. (Eds.). *Hydrogeology; The Geology of North America*. Geological Society of America, Boulder, 2: 89-92

Li, H. -C. and Ku, T. -L. 1997. $\delta^{13}\text{C}$ and $\delta^{18}\text{O}$ covariance as a paleohydrological indicator for closed-basin lakes. *Palaeogeography, Palaeoclimatology and Palaeoecology*, 133: 69-80

Li, H. -C., Ku, T. -L., Stott, L. D. and Anderson, R. F. 1997. Stable isotope studies on Mono Lake (California). 1. $\delta^{18}\text{O}$ in lake sediments as proxy for climatic change during the last 150 years. *Limnology and Oceanography*, 42: 230-238

Li, W. -X., Lundberg, J., Dickin, A. P., Ford, D. C., Schwarcz, H. P., McNutt, R. and Williams, D. 1989. High-precision mass-spectrometric uranium-series dating of cave deposits and implications for palaeoclimate studies. *Nature*, 339: 534-536

Lini, A., Levine, S., Howse, R. C. and Ferber, L. 2000. Stable isotope composition of lake biota and sediments as proxy for lake trophic state. International Association of Great Lakes Research, 43rd Conference Program and Abstracts, p. 91

Liu, W., Li, X., Zhang, L, An., Z. and Xu, L. 2009. Evaluation of oxygen isotopes in carbonate as an indicator of lake evolution in arid areas: The modern Qinghai Lake, Qinghai-Tibet Plateau. *Chemical Geology*, 268: 126-136

Love, A. J., Herczeg, A. L., Leaney, F. W., Stadter, M. H., Dighton, J. C. and Armstrong, D. 1994. Groundwater residence time and palaeohydrology in the Olway Basin, South Australia. *Journal of Hydrology*, 153: 157-187

Lowenstein, T. and Risacher, F. 2008. Closed Basin Brine Evolution and the Influence of Ca-Cl Inflow Waters: Death Valley and Bristol Dry Lake California, Qaidam Basin, China, and Salar de Atacama, Chile. *Aquatic Geochemistry*, 15: 71-94

Lozano-García, S. and Vásquez Salem, L. 2005. A high elevation Holocene pollen record from Iztaccihuatl volcano, central Mexico. *The Holocene*, 15: 329-338

Ludwig, K. R. 2003a. Mathematical-statistical treatment of data and errors for ²³⁰Th/U geochronology. In: Uranium-Series Geochemistry (B. Bourdon, G. M. Henderson, C. C. Lundstrom and S. P. Turner, eds.). *Reviews in Mineralogy and Geochemistry*, 52: 631-656

Ludwig, K. R. 2003b. Isoplot 3.00; a geochronological toolkit for Microsoft Excel. Berkeley Geochronological Centre Special Publications, 4

Marshall, J. D., Jones, R. T., Crowley, S. F., Oldfield, F., Nash, S. and Bedford, A. 2002. A high resolution late glacial isotopic record from Hawes Water Northwest England. Climatic oscillations: calibration and comparison of palaeotemperature proxies. *Palaeogeography, Palaeoclimatology, Palaeoecology*, 185: 25-40

Maxey, G. B. 1968. Hydrogeology of desert basins. *Ground Water*, 6: 10-22

McDermott, A. 2004. Palaeo-climate reconstruction from stable isotope variations in speleothems: a review. *Quaternary Science Reviews*, 23: 901-918

McKee, J. W., Jones, N. W. and Long, L. E. 1990. Stratigraphy and provenance of strata along the San Marcos fault, central Coahuila, Mexico. *Geological Society of America Bulletin*, 102: 593-614

Meckel, T. A., ten Brick, U. S. And Williams, S. J. 2006. Current subsidence rates due to compaction of Holocene sediments in Louisiana. *Geophysical Research Letters*, 33: L11403, doi:10.1029/2006GL026300

Metcalf, S. E., Bimpson, A., Courtice, A. J., O'Hara, S. L. and Taylor, D. M. 1997. Climate change at the monsoon/Westerly boundary in Northern Mexico. *Journal of Paleolimnology*, 17: 155-171

Metcalf, S. E., O'Hara, S. L., Caballero, M. and Davies, S. J. 2000. Records of Late Pleistocene-Holocene climatic change in Mexico – a review. *Quaternary Science Reviews*, 19: 699-721

Metcalf, S., Say, A., Black, S., McCulloch, R. and O'Hara, S. 2002. Wet Conditions during the Last Glaciation in the Chihuahuan Desert, Alti Babicora Basin, Mexico. *Quaternary Research*, 57: 91-101

Meyer, E. 1973. Late-Quaternary Paleocology of the Cuatro Ciénegas Basin, Coahuila, Mexico. *Ecology*, 54: 982-995

Meyers, P. A. 1994. Preservation of elemental and isotopic source identification of sedimentary organic matter. *Chemical Geology*, 114: 289-302

Meyers, P. A. 2003. Applications of organic geochemistry to palaeolimnological reconstructions: a summary of examples from the Laurentian Great Lakes. *Organic Geochemistry*, 34: 261-289

Meyers, P. A. and Teranes, J. L. 2001. Sediment organic matter. In: Last, W. M. and Smol, J. P. (eds.). *Tracking Environmental Changes Using Lake Sediments – Volume II: Physical and Chemical Techniques*. Kluwer, Dordrecht: 239-269

Michel, R. L. 1992. Residence times in river basins as determined by analysis of long-term tritium records. *Journal of Hydrology*, 130: 367-378

Minckley, W. L. and Cole, G. A. 1968. Preliminary Limnologic Information on Waters of the Cuatro Ciénegas Basin, Coahuila, Mexico. *The Southwestern Naturalist*, 13: 421-431

Minckley, T. A. and Jackson, S. 2008. Ecological stability in a changing World? Reassessment of the palaeoenvironmental history of Cuatro Ciénegas, Mexico. *Journal of Biogeography*, 35: 188-190

Minckley, T. A. and Brunelle, A. R. 2007. Palaeohydrology and growth of a desert ciénega. *Journal of Arid Environments*, 69: 420-431

Minckley, T. A., Clementz, M. T., Brunelle, A. and Klopfenstein, G. A. 2009. Isotopic analysis of wetland development in the American Southwest. *The Holocene*, 19: 737-745

Minckley, W. L. 1969. Environments of the Bolsón of Cuatro Ciénegas, Coahuila, Mexico, with special reference to the aquatic biota. Texas Western Press, University of Texas El Paso Science Series, 2: 1-65

Minckley, W. L. 1992. Three decades near Cuatro Ciénegas, Mexico: photographic documentation and a plea for area conservation. In: Sommerfield, M. R. and Kubly, D. K. (eds.). *Limnology and aquatic biology of the southwest. Proceedings Special Symposium to Honour G. A. Cole 34th Annual Meeting, Arizona-Nevada Academic Science*, 26: 81-110

Moeyersons, J., Nyssen, J., Poeson, J., Deckers, J. and Haile, M. 2006. Age and backfill/overflow stratigraphy of two tufa dams, Tigray Highlands, Ethiopia: Evidence for Late Pleistocene and Holocene wet conditions. *Palaeogeography, Palaeoclimatology, Palaeoecology*, 230: 165-181

Molina-Garza, R. S., Chávez-Cabello, G., Iriondo, A., Porras-Vásquez, M. A. and Terrazas-Calderón, G. D. 2008. Paleomagnetism, structure and $^{40}\text{Ar}/^{39}\text{Ar}$ geochronology of the Cerro Mercado pluton Coahuila: Implications for the timing of the Laramide orogeny, in northern Mexico. *Revista Mexicana Ciencias Geológicas*, 25: 284-301

Musgrove, M., Banner, J. L., Mack, L. E., Combs, D. M., James, E. W., Cheng, H. and Edwards, R. L. 2001. Geochronology of late Pleistocene to Holocene speleothems from central Texas: Implications for regional paleoclimate. *Geological Society of America Bulletin*, 113: 1532-1543

Neuman, S. P. and Gardner, D. A. 1989. Determination of Aquitard/Aquiclude Hydraulic Properties from Arbitrary Water-Level Fluctuations by Deconvolution. *Ground Water*, 27: 66-76

NOAA (2011) JetStream: Online school for weather. http://www.srh.noaa.gov/jetstream/global/climate_max.htm. November 2011

Omelon, C. R., Pollard, W. H. and Anderson, D. T. 2006. A geochemical evaluation of perennial spring activity and associated mineral precipitates at Expedition Fjord, Axel Heiberg Island, Canadian High Arctic. *Applied Geochemistry*, 21: 1-15

Ordóñez, S., González Martín, J. A. and García del Cura. 1987. Formaciones travertínicas y tobáceas en el valle del Tajo (sector Cifuentes-Trillo): estudio geomorfológico, petrológico y sedimentológico. *Cuaternario y Geomorfología*, 1: 231-245

- Ortiz, J. E., Torres, T., Delgado, A., Reyes, E. and Díaz-Bautista, A. 2009. A review of the Tagus river tufa deposits (central Spain): age and palaeoenvironmental record. *Quaternary Science Reviews*, 28: 947-963
- Osmond, C. B., Allaway, W. G., Sutton, B. G., Troughton, J. H., Queiroz, O., Luttge, U. and Winter, K. 1973. Carbon isotope discrimination in photosynthesis of CAM plants. *Nature*, 246: 41-42
- Palmer, A. N. 1991. Origin and morphology of limestone caves. *Geological Society of America Bulletin*, 103: 1-21
- Palmer, E. 1882. Mexican Caves with Human Remains. *The American Naturalist*, 16: 306-311
- Park, J., Byrne, R., Böhnelt, H., Molina-Garza, R. and Conserva, M. 2010. Holocene climate change and human impact, central Mexico: a record based on maar lake pollen and sediment chemistry. *Quaternary Science Reviews*, 29: 618-632
- Pedley, H. M. 1993. Sedimentology of the late Quaternary barrage tufas in the Wye and Lathkill valleys, north Derbyshire. *Proceedings of the Yorkshire Geological Society*, 49: 197-206
- Pedley, M., Martín, J. A. G., Delgado, S. O. and del Curas, M. A. G. 2003. Sedimentology of Quaternary perched springline and paludal tufas: criteria for recognition, with examples from Guadalajara Province, Spain. *Sedimentology*, 50: 23-44

Pentecost, A. 1995. Quaternary travertine deposits of Europe and Asia Minor. *Quaternary Science Reviews*, 14: 1005-1028

Pentecost, A. 2005. *Travertine*. Springer, Netherlands.

Pentecost, A. and Riding, R. 1986. Calcification in cyanobacteria. In: Leadbeater, B. S. C. and Riding, R. (eds). *Biom mineralization of Lower Plants and Animals*. Clarendon Press, Oxford pp. 73-90

Peterson, L. C., Haug, G. H., Hughen, K. A. and Röhl, U. 2000. Rapid changes in the hydrologic cycle of the tropical Atlantic during the Last Glacial. *Science*, 290: 1947-1951

Petit, J. R., Jouzel, J., Raynaud, D., Barkov, N. I., Barnola, J. M., Basile, I., Bender, M., Chappellaz, J., Davis, M., Delaygue, G., Delmotte, M., Kotlyakov, V. M., Legrand, M., Lipenkov, V. Y., Lorius, C., Pépin, L., Ritz, C., Saltzman, E. and Stievenard, M. 1999. Climate and atmospheric history of the past 420,000 years from the Vostok ice core, Antarctica. *Nature*, 399: 429-436

Pires, V., Silva, Z. S. G., Simão, J. A. R., Galhano, C. and Amaral, P. M. 2010. "Bianco di Asiago" limestone pavement – Degredation and alteration study. *Construction and Building Materials*, 24: 686-694

Ponder, W. F. 1986. Mound springs of the Great Artesian Basin. In: De Dekker, P. and Williams, W. D. (eds.). *Limnology in Australia*, Melbourne: 403-420

Potter, E. K., Stirling, C. H., Anderson, M. B. and Halliday, A. N. 2005. High precision Faraday collector MC-ICPMS thorium isotope ratio determination. *International Journal of Mass Spectrometry*, 247: 10-17

PRONATURA (Pronatura Noreste AC Cuatro Ciénegas), personal communication

Ragab, R. and Prudhomme, C. 2002. Climate change and water resources management in arid and semi-arid regions: prospective and challenges for the 21st century. *Journal of Biosystems Engineering*, 81: 3-34

Rank, D., Völkl, G., Maloszewski, P., Stichler, W. 1992. Flow dynamics in an alpine karst massif studied by means of environmental isotopes. In: *Isotope Techniques in Water Resource Development 1991*, pp. 327–343. IAEA Symposium 319. March 1991, Vienna.

Rector, C. H. 1999. Human and animal trackway at Oro Grande. In: Reynolds, R. (ed.), *Fossil footprints. Proceedings of the 1999 Desert Research Proceedings*. San Bernadino County Museum Association Quarterly, 4: 53-55

Reimer, P. J., Baillie, M. G. L., Bard, E., Bayliss, A., Beck, J. W., Bertrand, C. J. H., Blackwell, P. G., Buck, C. E., Burr, G. S., Cutler, K. B., Damon, P. E., Edwards, R. L., Fairbanks, R. G., Friedrich, M., Guilderson, T. P., Hogg, A. G., Hughen, K. A., Kromer, B., McCormac, G., Manning, S., Ramsey, C. B., Reimer, R. W., Remmele, S., Southon, J. R., Stuiver, M., Talamo, S., Taylor, F. W., van der Plicht, J. and Weyhenmeyer, C. E. 2004. IntCal04 terrestrial radiocarbon age calibration, 0-26 cal. kyr. BP. *Radiocarbon*, 46: 1029-1058

Reimer, P. J., Baillie, M. G. L., Bard, E., Bayliss, A., Beck, J. W., Blackwell, P. G., Bronk Ramsey, C., Buck, C. E., Burr, G. S., Edwards, R. L., Friedrich, M., Grootes, P. M., Guilderson, T. P., Hajdas, I., Heaton, T. J., Hogg, A. G., Hughen, K. A., Kaiser, K. F., Kromer, B., McCormac, F. G., Manning, S. W., Reimer, R. W., Richards, D. A., Southen, J. R., Talamo, S., Turney, C. S. M., van der Plicht, I. and Weyhenmeyer, C. E. 2009. IntCal09 and Marine09 Radiocarbon Age Calibration Curves, 0-50,000 Years cal BP. *Radiocarbon*, 51: 1111-1150

Risacher, F. and Fritz, B. 2008. Origin of Salts and Brine Evolution of Bolivian and Chilean Salars. *Aquatic Geochemistry*, 15: 123-157

Roche, D., Paillard, D. and Cortijo, E. 2004. Duration and iceberg volume of Heinrich event 4 from isotope modelling study. *Nature*, 432: 379-382

Rodríguez, A. A. A., Mijares, F. J. A., Ojeda, C. G., Morales, M. M., Hita, L. G., Zamarrón, G. H, Arellano, I. M., González, M. A. M., Flores, G. O., Almanza, P. G., Sánchez, R. L., López, J. L. P., Arzate, G. R., Fritz, P. and J.R. Espinoza. 2005. Estudio hidrogeológico de los acuíferos el Hundido y Cuatrociénegas, Coahuila. Jiutepec, Morelos, Mexico: Secretaria de Medio Ambiente y Recursos Naturales, Instituto Mexicano de Tecnología del Agua, Comisión Nacional del Agua, Instituto Nacional de Ecología

Romanek, C. S., Grossman, E. L. and Morse, J. W. 1992. Carbon isotopes fractionation in synthetic aragonite and calcite: effects of temperature and precipitation rate. *Geochimica et Cosmochimica Acta*, 56: 419-430

Rosenberry, D. O. and Winter, T. C. 1997. Dynamics of water table fluctuations in an upland between two prairie-pothole wetlands in North Dakota. *Journal of Hydrology*, 191: 266-289

- Sadler, P. M. 1981. Sediment accumulation rates and the completeness of stratigraphic sections. *Journal of Geology*, 89: 569-584
- Scanlon, B. R., Keese, K. E., Flint, A. L., Flint, L. E., Gaye, C. B., Edmunds, W. M. and Simmers, I. 2006. Global synthesis of groundwater recharge in semiarid and arid regions. *Hydrological Processes*, 20: 3335-3370
- Scheuer, G. and Schweitzer, F. 1985. Types and forms of travertine cones. *Föld Közl*, 115: 385-398
- Schorn, H. and Wehr, W. 1986. *Abies milleri*, sp. nov., from the Middle Eocene Klondike Mountain Formation, Republic, Ferry County, Washington. *Burke Museum Contributions in Anthropology and Natural History*, 1: 1-7
- Schwalb, A. 2003. Lacustrine ostracodes as stable isotope recorders of late-glacial and Holocene environmental dynamics and climate. *Journal of Palaeolimnology*, 29: 265-351
- Schwalb, A., Burns, S. and Kelts, K. 1999. Holocene environments from stable isotope stratigraphy of ostracods and authigenic carbonate in Chilean Altiplano Lakes. *Palaeogeography, Palaeoclimatology, Palaeoecology*, 148: 153-168
- Schwarcz, H. P. 1989. Uranium Series Dating of Quaternary Deposits. *Quaternary International*, 1: 7-17

Sharp, Z. 2007. Principles of Stable Isotope Geochemistry. Pearson Prentice Hall, London.

Shemesh, A. 2011. Oxygen and carbon isotopes in lacustrine diatoms: Indicators of regional palaeoclimate. Proceedings of the 5th International Limnogeology Congress, Konstanz, Germany

Shemesh, A., Rosqvist, G., Rietti-Shati, M., Rubensdotter, L., Bigler, C., Yam, R. and Karlen, W. 2001. Holocene climatic change in Swedish Lapland inferred from an oxygen isotope record of biogenic silica. *Holocene*, 11: 447-454

Shimokawara, M., Nishimura, M., Matsuda, T., Akiyama, N., Kawai, T. 2010. Bound forms, compositional features, major sources and diagenesis of long chain alkyl, mid-chain diols in Lake Baikal sediments over the past 28,000 years. *Organic Geochemistry*, 41: 753-766

Shiraishi, F., Reimer, A., Bissett, A., de Boer, D. and Arp, G. 2008. Microbial effects on biofilm calcification, ambient water chemistry and stable isotope records in a highly supersaturated setting (Westerhöfer Bach, Germany). *Palaeogeography, Palaeoclimatology, Palaeoecology*, 262: 91-106

Shotton, F. W. 1972. An example of Hard-Water Error in Radiocarbon Dating of Vegetable Matter. *Nature*, 240: 460-461

Sommerfield, C. K. 2006. On sediment accumulation rates and stratigraphic completeness: Lessons from Holocene ocean margins. *Continental Shelf Research*, 26: 2225-2240

Song, X., Wang, S., Xiao, G., Wang, Z., Liu, X. and Wang, P. 2009. A study of soil water movement combining soil water potential with stable isotopes at two sites of shallow groundwater areas in the North China Plain. *Hydrological Processes*, 23: 1376-1388

Spaulding, W. G. 1991. A middle Holocene vegetation record from the Mojave desert of North America and its paleoclimatic significance. *Quaternary Research*, 35: 427-437

Spencer, R. J., Baedeker, M. J., Eugster, H. P., Forester, R. M., Goldhaber, M. B., Jones, B. F., Kelts, K., McKenzie, J., Madsen, D. B., Rettig, S. L., Ruben, S. L. and Bowser, C. J. 1984. Great Salt Lake and precursors, Utah: The last 30,000 years. *Contributions to Mineralogy and Petrology*, 86: 321-334

Stevens, R. E., Metcalfe, S. E., Leng, M. J., Lamb, A. L., Sloane, H. J., Naranjo, E. and González, S. 2012. Reconstruction of late Pleistocene climate in the Valsequillo Basin (Central Mexico) through isotopic analysis of terrestrial and freshwater snails. *Palaeoclimatology, Palaeogeography, Palaeoecology*, 319-320: 16-27

Straka, H. and Ohngemach, D. 1989. Late Quaternary vegetation history of the Mexican highland. *Plant systematics and Evolution*, 162: 115-132

Stuiver, M. 1975. Climate Versus Change in ^{13}C Content of the Organic Component of Lake Sediments During the Late Quaternary. *Quaternary Research*, 5: 251-262

Stuiver, M. and Reimer, P. J. 1993. Extended (super 14) C data base and revised Calib 3.0 (super 14) C age calibration program. *Radiocarbon*, 35: 215-230

Talbot, M. R. 1990. A review of the palaeohydrological interpretation of carbon and oxygen isotopic ratios in primary lacustrine carbonates. *Chemical Geology (Isotope Geoscience Section)*, 80: 261-279

Taylor, C. B. and Fox, V. J. 1996. An isotopic study of dissolved inorganic carbon in the catchment of the Waimakariri River and deep ground water of North Canterbury plains, New Zealand. *Journal of Hydrology*, 186: 161-190

Taylor, W. W. 1956. Some Implications of the Carbon-14 Dates from a Cave in Coahuila, Mexico. *Journal of the Texas Archaeological Society*, 27: 215-234

Taylor, W. W. 1964. Tethered Nomadism and Water Territoriality: An Hypothesis. *Actas y Memorias*: 197-203

Taylor, W. W. 1966. Archaic Cultures Adjacent to the Northeastern Frontiers of Mesoamerica. In: *Handbook of Middle American Indians*, 4: 59-94. University of Texas Press, USA

Taylor, W. W. 1968. A Burial Bundle from Coahuila, Mexico. In: *Collected Papers in Honor of Lyndon Lane Hargrave*: 23-56. *Papers of the Archaeological Society of New Mexico* 1, Albuquerque

Taylor, W. W. 1972. The Hunter-Gatherer Nomads of Northern Mexico: A Comparison of the Archival and Archaeological Records. *World Archaeology*, 4: 167-178

Taylor, W. W. 2003. Sandals from Coahuila Caves. *Studies in Pre-Columbian Art and Archaeology*, 35: 1-151

Terry, M., Steelman, K. L., Guilderson, T., Dering, P. and Rowe, M. W. 2006. Lower Pecos and Coahuila peyote: new radiocarbon dates. *Journal of Archaeological Science*, 33: 1017-1021

Thomas, D. S. G. 2011. *Arid Zone Geomorphology: Process, Form and Change in Drylands*, 3rd Edition. Wiley-Blackwell, England

Torfstein, A., Haase-Schramm, A., Waldmann, N., Kolodny, Y. and Stein, M. 2009. U-series and oxygen isotope chronology of the mid-Pleistocene Lake Amora (Dead Sea Basin). *Geochimica et Cosmochimica Acta*, 73: 2603-2630

Tucker, M. E. and Wright, V. P. 1990. *Carbonate Sedimentology*. Blackwell Scientific Publications, Cambridge, USA

Turpin, S. A. 2003. Walking the Line: A Preliminary Sandal Chronology From Coahuila and Southwestern Texas. *The Journal of Big Bend Studies*, 15: 27-53

van der Plicht, J., Beck, J. W., Bard, E., Baillie, M. G. L., Blackwell, P. G., Buck, C. E., Friedrich, M., Guilderson, T. P., Hughen, K. A., Kromer, B., McCormac, F. G., Ramsey, C. B., Reimer, P. J., Reimer, R. W., Remmele, S., Richards, D. A., Southen, J. R., Stuiver, M. and Weyhenmeyer, C. E. 2004. NotCal04; comparison/calibration ¹⁴C records 26-50 cal kyr BP. *Radiocarbon*, 46: 1225-1238

Van Devender, T. R. 1990. Late Quaternary vegetation and climate of the Sonoran Desert, United States and Mexico. In: J. Betancourt, T. R. Van Devender and P. S. Martin (eds.), *Packrat Middens. The Last 40,000 Years of Biotic Change*. University of Arizona Press, Tucson: 104-133

Van Devender, T. R. and Burgess, T. L. 1985. Late Pleistocene Woodlands in the Bolson de Mapimi: A Refugium for the Chihuahuan Desert Biota? *Quaternary Research*, 24: 346-353

Vega, M., Pardo, R., Barrado, E. and Debán, L. 1998. Assessment of seasonal and polluting effects on the quality of river water by exploratory data analysis. *Water Research*, 32: 3581-3592

Vidal, L., Schneider, R. R., Marchal, O., Bickert, T., Stocker, T. F. and Wefer, G. 1999. Link between the North and South Atlantic during Heinrich events of the last glacial period. *Climate Dynamics*, 15: 909-919

Walker, M. J. C. 2005. *Quaternary Dating Methods*. Wiley-Blackwell, England

Wassenaar, L. I., Van Wilgenburg, S. L., Larson, K. and Hobson, K. A. 2009. A groundwater isoscape (δD , $\delta^{18}O$) for Mexico. *Journal of Geochemical Exploration*, 102: 123-136

Watts, W. A. and Bradbury, J. P. 1982. Paleoecological studies at Lake Patzcuaro on the west-central Mexican Plateau and at Chalco in the Basin of Mexico. *Quaternary Research*, 17: 56-70

Williams, H. 1952. Geological observations on the ancient human footprints near Managua. *Contributions to American Anthropology and History*, 52: 31

Winograd, I. J., Coplen, T. B., Landwehr, J. M., Riggs, A. C., Ludwig, K. R., Szabo, B. J., Kolesar, P. T. and Revesz, K. M. 1992. Continuous 500,000-Year Climate Record from Vein Calcite in Devils Hole, Nevada. *Science*, 9: 255-260

Winsborough, B. 1990. Some ecological aspects of modern fresh-water stromatolites in lakes and streams of the Cuatro Ciénegas Basin, Coahuila, Mexico: University of Texas-Austin Dissertation, 341 pp

Winter, T. C. and Rosenberry, D. O. 1995. The interaction of groundwater with prairie-pothole wetlands in the Cottonwood Lake area, east-central North Dakota, 1979-1990. *Wetlands*, 15: 193-211

Wohl, E. 1993. Bedrock channel incision along Piccaninny Creek, Australia. *The Journal of Geology*, 101: 749-761

Wolaver, B. D. 2005. Hydrologic Analysis of the Cuatro Ciénegas Basin, Coahuila, Mexico: University of Texas-Austin, Report

Wolaver, B. D., Sharp, J. M. Jr., Rodriguez, J. M. and Flores, J. C. I. 2008. Delineation of Regional Arid Karstic Aquifers: An Integrative Data Approach. *Groundwater*: 1-18

Wright, Jr., H. E., Kutzbach, J. E., Webb III, T., Ruddiman, W. F., Street-Perrott, F. A. and Bartlein, P. J. 1993. Global Climates Since the Last Glacial Maximum. University of Minnesota Press, Minnesota

Xelhuantzi Lopez, M. S. 1994. Determinación palinológica del paleoambiente holoceno en la parte norte del estado de Michoacán. Boletín de la sociedad Botánica de México, 54: 251-265

Yang, C., Telmer, K. and Veizer, J. 1996. Chemical dynamics of the "St. Lawrence" riverine system: δD_{H_2O} , $\delta^{18}O_{H_2O}$, $\delta^{13}C_{DIC}$, $\delta^{34}S_{SULFATE}$, and dissolved $^{13}C/^{86}Sr$. Geochimica y Cosmochimica Acta, 60: 851-866

Yoshimura, K., Liu, Z., Cao, J., Yuan, D., Inokura, Y. and Noto, M. 2004. Deep source CO₂ in natural waters and its role in extensive tufa deposition in the Huanglong Ravines, Sichuan, China. Chemical Geology, 205: 141-153

Yu, Z., McAndrews, J. H. and Eicher, U. 1997. Middle Holocene dry climate caused by change in atmospheric circulation patterns: Evidence from lake levels and stable isotopes. Geology, 25: 251-254

Zhou, J. and Chafetz, H. S. 2009. The genesis of late Quaternary caliche nodules in Mission Bay, Texas: stable isotopic compositions and palaeoenvironmental interpretation. Sedimentology, 56: 1392-1410